

SOME STUDIES ON ARTIFICIAL INTELLIGENCE BASED FRACTIONAL ORDER PID CONTROLLER

A Thesis Submitted in Partial Fulfillment of the Requirement

For the Award of the Degree of

DOCTOR OF PHILOSOPHY

Submitted by

AJENDRA SINGH

Roll No. 2K16/Ph.D./EE/15

Under the Supervision of

Prof. J N Rai



DEPARTMENT OF ELECTRICAL ENGINEERING

Delhi Technological University

Bawana Road Delhi-110042

JULY- 2023

CANDIDATE'S DECLARATION

I hereby certify that the work presented in this thesis entitled “**Some Studies on Artificial Intelligence Based Fractional Order PID Controller,**” submitted in partial fulfillment of the requirement for the award of the degree of Doctor of Philosophy in Electrical Engineering , Delhi Technological University, is an authentic record of my work carried out under the supervision of Prof. J N Rai. The research content in this thesis has not been submitted elsewhere for the award of a degree.

Dated: 05.07.2023

Ajendra Singh
Research Scholar

CERTIFICATE

This is to certify that the thesis entitled “**Some Studies on Artificial Intelligence Based Fractional Order PID Controller**” submitted by Mr. Ajendra Singh, research scholar in Electrical Engineering Department, Delhi Technological University, is a dissertation work carried out by him under my supervision towards the partial fulfillment of the requirement for the award of the degree of Doctor of Philosophy. The work carried out by Mr. Ajendra Singh has not been submitted in part or full in any other University for the award of any degree. All the assistance and help received during this course of study have been duly acknowledged.

I wish him all the best in his endeavors

Dated: 05.07.2023

Prof. J N Rai

Supervisor, EED, DTU

The Ph.D. viva-voce of Mr. Ajendra Singh, research scholar has been held on 05-07-2023.

Prof. J N Rai

Supervisor

Prof. Rachana Garg

Head, Dept of Electrical Engg.

ACKNOWLEDGEMENT

I wish to express my gratitude to **GOD** almighty for giving me the courage and the strength to carry out this project, which opened my doors to knowledge.

The work presented in this thesis has been done in Electrical Engineering Department, Delhi Technological University, under the scientific direction of Professor J N Rai.

I would like to express my profound gratitude and sincere thanks to my research Supervisor, who has given me these valuable ideas and suggestions throughout my research period.

I warmly thank Prof. Madhusudan Singh, who has given me a chance in this research field. My thanks also go to Prof. Narendra Kumar (I), Prof. Uma Nangia, Prof. Narendra Kumar (II), Prof. Pragati Kumar, H.O.D Electrical Engineering Department, and Prof. Vishal Verma for their mental support from time to time.

I extend a special thanks to Prof. Suman Bhomik, Prof. Dheeraj Joshi, Prof. Mukhtiar Singh, Prof. M.M Tripathi, Prof. Ram Bhagat, Dr. D.C Meena, Prof. Vinod Yadav, and Dr. Prem Prakash for inspiring me from time to time for this project. My thanks are also addressed to all my teachers/Professors who have contributed to my study since my first step in the school.

My special thanks go to my friend Prof. Vineet Shekher, my research colleague Dr. Nidhi Gupta, Ms. Neevetika Verma, Brijendra Sanger, and my staff members. Mrs. Shalini Gupta and Mrs. Komal support me from time to time in my research project. I bow down respectfully to my Mother and Father. I express my gratitude and obedience without forgetting to thank all my great family members.

Finally, I cannot forget to give a sign of gratitude and thanks to my wife, Smt. Asha Singh and my sons Mr. Vivek Singh and Krapanshu Panwar, without their sacrifice, this work would never have been born.

At last, I thank all those gentlemen who were always involved in my research project.

Ajendra Singh
Research Scholar

ABSTRACT

Process control in industry is improving gradually with the innovations and implementation of new technology. Different control techniques are being used for process control. Proportional Integral and Derivative (PID) controller is employed in every facet of industrial automation. In any of control application, controller design is the most important part. There are different types of controller architectures available in control literature.

The applications of PID controller span from small industries to high technology industries. Designing a PID controller to meet gain and phase margin specifications is a well-known design technique. If the gain and phase margin are not specified carefully, then the design may not be optimum in the sense that a large phase margin (more robust) that could give better performance.

This research outlines the development and design of an infrared radiation heating profile controller. An attempt has been made to theoretically analyze the system, design of the Controller, their simulation, and real-time implementation of an infrared ceramic heating profile controller. The Controller has been subjected to comparative testing with a proportional control model to observe its performance and validate its effectiveness. PID controllers of this nature that are commercially available either lack the functionality of this unit or are too expensive to implement for research purposes. This unit has been designed with cost-effectiveness in mind but still meets the standards required for an industrial controller. Heating profiles are necessary and useful tools for the proper processing of a host of materials. The Controller developed in this research is able to meet a level of a fair degree of accuracy and track a heating profile.

The results confirm that this programmable control model will be advantageous and a valuable tool in temperature regulation. This means that intensive studies into the effects of infrared radiation on materials are now feasible. Research of this nature could possibly expand the application of infrared as a heating mechanism. Although tests were conducted on this Controller, they are not meant to serve as an exhaustive analysis.

The conclusions of these simulations do reveal the benefit of such a

controller. More rigorous investigation is suggested as a subject for further study. System identification of this nonlinear process is done using black box model, which is identified to be nonlinear and approximated to be a First Order plus Dead Time (FOPDT) model.

In order to obtain an accurate mathematical expression of the IR heater used in this research, a step response test of the IR heater has been completed. This method of testing has been done in accordance with the Ziegler-Nichols, Astrom-Hugglund, and Cohen-Coon methods. Simulation of the obtained transfer function, using Mat Lab software, showed good agreement. Although the transfer function represented a first-order model with transportation lag, the simulated results reflected an acceptable accuracy.

An exhaustive study has been done on different PID controller tuning techniques. The PID controller of the model has been designed using the classical method, and the results have been analyzed. A compromise has been made between robustness and tracking performance of the system in the presence of time delay. The results of the simulation indicate the validity of the study.

Integer order PID controller (IOPID) based on Bode plot and Nyquist plot has been designed. The results illustrate that the IOPID controllers have the capability of minimizing the control objectives better than the previously designed controllers (Ziegler-Nichols, Astrom-Hugglund, and Cohen-Coon method-based Controller). With the change in temperature occurs, the oscillations of the controlled system outputs are eliminated and the output steady state errors become very small. The results demonstrate that the IOPID controller is stable and it suppresses the cost function (Maximum overshoot, Rise Time, Settling time and Peak time) even in case of significant disturbances. IOPID controller has also been designed using Bode plot and Nyquist plot for high gain system. The results have shown that the responses of Ceramic IR heater temperature profile have been reduced to very small value and prove that the IOPID controller is still stable and it suppresses the cost function even if significant disturbances have occurred.

Fuzzy Logic controller-based model reference has been designed. Its implementation indicates that the proposed Controller suppresses the output of the controlled system. The results illustrate that the proposed Controller only slightly

improves the performance of the cost function.

The various AI techniques (GA) and Soft Computing (bio inspired) based algorithm (BFO, ACO) for PID controller offers several advantages. These methods can be used for higher order process models in complex problems. Approximations that are typical to classical tuning rules are not needed. Compared to conventionally tuned system, GA, PSO, BFO and ACO tuned system provides good steady state response and performance indices. The genetic approaches can achieve better temperature control with smaller settling time, overshoot and undershoot, and zero steady error. The control signal changes more frequently and with larger magnitude as the genetic algorithms are stochastic in nature.

The PSO has an additional unique advantage that it adapts any change in system conditions, and obtains different system dynamics accurately in a short time period. It is a random search method but if combined with an artificial intelligence features, it tracks required system dynamics accurately in short time (small number of iterations).

The BFO based Controller has the advantage of a better closed loop time constant, which enables the Controller to act faster with a balanced overshoot and settling time. The response of the conventional Controller is more sluggish than the BFO based Controller. Compared to conventionally tuned system, BFO tuned system has better steady state response and performance indices.

Ant- Colony algorithm (ACO) has no special requirements on the characteristics of optimal designing problems, which has a fairly good universal adaptability and a reliable operation of program with ability of global convergence. Simulation results show the controlled system has satisfactory response and the proposed method has an effective tuning strategy. ACO shows better performance for PID controller parameter tuning of the considered control system. The simulation results show that the proposed method achieve minimum tracking error and estimate the parameter values with high accuracy.

The work presents tuning method for fractional order proportional Integral and derivative controllers (FOPID) for the first order plus time delay (FOPTD) class of systems based on gain and phase margin. Techniques such as fractional order PID controller design and the results of their application to real-world system

have been presented.

A comparative study has been done using different control techniques to analyze the performance of different controllers. First, the conventional PID controller is implemented as primary Controller. The performance of PID, IOPID, Fuzzy Logic Controller, and Artificial Intelligence based PID, Bio inspired based PID controller and FOPID controllers have been examined.

It has been concluded that the overall performance of the FOPID-based Controller is better than other controllers. In real-time implementation, the performance of the process control includes the time required by the heater to be settled on the initial set-up temperature. The rising of temperature is slow due to the resistance heating element used in ceramic infrared heaters. So the settling time is very high.

The results obtained by simulation and real-time implementation with fractional order PID controller show overall better performance(rise time , settling time, peak time and peak overshoot) in comparison with other designed and implemented Controllers embedded with ceramic infrared systems.

Further stability problems of fractional order system with leakage delay and distributed delay with hybrid feedback controller have been solved (with examples) using the Mittag-Leffler function and Lyapunov direct method and proved Global Mittag-Leffler stability of fractional order system of the proposed model which implies faster convergence rate of the network model which represents the stability of the system.

This work performs a small-scale test measuring controller performance so that it serves as a platform for future research efforts leading to the real-life implementation of a Ceramic Infrared Heater Temperature control system.

LIST OF CONTENTS

DECLARATION	I
CERTIFICATE	II
ACKNOWLEDGEMENT	III
ABSTRACT	IV
LIST OF CONTENTS	VIII
LIST OF FIGURES	XIV
LIST OF TABLES	XVII
LIST OF PRINCIPAL / SYMBOLS	XIX
CHAPTER-1 INTRODUCTION	1-24
1.1 Overview	1
1.2 Control strategies	2
1.3 Literature Survey	7
1.4 Motivation	20
1.5 Methodology	23
1.6 Organization of thesis	23
1.7 Conclusion	24
CHAPTER-2 DIFFERENT TYPES OF CONTROLLERS	25-37
2.1 Introduction	25
2.2 Variable representation with Laplace transformation	27
2.2.1 Transfer function	27
2.2.2 Frequency response and Bode diagrams	28

2.3	PID Controller	30
2.4	Fractional Order PID Controller (FOPID)	31
2.4.1	Properties of Fractional Order Differentiations	34
2.5	Tilted Proportional and Integral (TID) Controller	36
2.5.1	Commande Robustee d'ordre Non Entire (CRONE) controller	36
2.6	Conclusion	37
CHAPTER-3	HEATING SYSTEM OF CERAMIC INFRARED HEATER	38-48
3.1	Introduction	38
3.2	Heating process	38
3.2.1	Fuel-Based Process Heating	38
3.2.2	Electric-Based Process Heating	39
3.2.3	Steam-Based Process Heating	39
3.2.4	Electric Infrared Processing	39
3.3	Basic Laws and Definitions	39
3.4	Mathematical Model for Infrared Heater	43
3.4.1	Surface Energy Balance	44
3.4.2	Resistance Wire (Heating Element)	45
3.5	Advantages of Using an Infrared Heater	46
3.6	Features of Ceramic Infrared Heater	47

3.7 Specification and Transfer Function	47
3.8 Application of Infrared Heater	48
3.9 Conclusion	48
CHAPTER-4 CONTROLLERS DESIGN	49-86
4.1 Introduction	49
4.1.1 The Extremes: Instability or No Response	50
4.1.2 Mathematical Criteria- Minimization of Index	51
4.2 Zeigler-Nichols Tuning Methods	52
4.2.1 Zeigler Nichols Open Loop Tuning Method	53
4.2.2 Zeigler Nichols Closed Loop Tuning Method	53
4.3 Cohen-Coon Method	54
4.4 Astrom-Hagglund Method	54
4.5 Simulation Results	56
4.5.1 Zeigler Nichols Open Loop Method	56
4.5.2 Zeigler Nichols Closed Loop Method	56
4.5.3 Cohen-Coon Method	56
4.5.4 Astrom-Hagglund Method	56
4.6 Integer Order PID Design (IOPID)	58
4.6.1 Loop Slope Adjustment	58
4.6.2 Design Specification for IOPID Controller	60
4.7 Fractional Order PID Controller (FOPID)	66
4.7.1 Approximation of Integer Order Fractional Order System	69
4.7.2 Oustloup's Recursive Filter	69

4.8 Design of Fractional Order PID Controller	70
4.8.1 Mathematical Computation for Design of FOPID Controller	73
4.9 Nint Blocks	78
4.9.1 Dialogue nipid GUI	79
4.9.2 Performance Evaluation in the Main Dialogue	80
4.9.3 Simulink in MATLAB	82
4.10 Implementation of Fractional Order PID Controller on Ceramic Infrared Heater Plant	84
4.11 Conclusion	86
CHAPTER-5	ARTIFICIAL INTELLIGENCE TECHNIQUES FOR CONTROLLERS DESIGN
	87-129
5.1 Fuzzy Logic Controller	87
5.1.1 Membership Function	87
5.1.2 Defuzzification	88
5.2 Design of Fuzzy Logic Controller	89
5.2.1 Control Structure of Fuzzy Base PID Controller	89
5.2.2 Fuzzy Logic Toolbox Tools	91
5.2.3 Importing and Exporting from GUI Tools	91
5.2.4 Rule Base Matrix of the PID like FLC	95
5.3 Genetic Algorithm (GA)	98
5.3.1 Conventional Genetic Algorithm	101
5.3.2 Design of PID Controller using Genetic Algorithm	102
5.3.3 Flow Chart of GA for PID Tuning	103

5.3.4	Performing the Genetic Algorithm	103
5.3.5	GA Tuning Parameter	104
5.4	Particle Swarm Optimization (PSO)	106
5.4.1	Parameters and Tuning of PID in PSO	109
5.4.2	Implementation of PSO-PID Controller	110
5.4.3	Flow Chart of PSO for PID Tuning	111
5.4.4	PSO Tuning Parameters	111
5.5	Bacterial Foraging Optimization (BFO)	113
5.5.1	Algorithm for Bacterial Foraging Optimization-Based Design	116
5.6	Ant Colony Optimization (ACO)	121
5.6.1	Ant Colony Optimization-Based PID Implementation	124
5.6.2	ACO Algorithm Flow Chart for PID Tuning	125
5.7	Simulation Result	128
5.8	Conclusion	129
CHAPTER-6	STABILITY ANALYSIS OF FRACTIONAL ORDER FUZZY CELLULAR NEURAL NETWORK WITH LEAKAGE DELAY AND TIME-VARYING DELAYS	130-152
6.1	Introduction	130
6.2	Concept of artificial neural networks	130
6.2.1	Biology inspired by mathematics and technology	134
6.2.2	Hopfield-type neural network	134
6.3	Fractional order definition and preliminaries	137
6.4	Main Results	138
6.5	Stability Problem 1	149

6.6 Stability Problem 2	151
6.7 Conclusion	152
CHAPTER-7 STABILITY ANALYSIS OF FRACTIONAL ORDER FUZZY CELLULAR NEURAL NETWORK WITH DISTRIBUTED DELAYS VIA HYBRID FEEDBACK CONTROLLER	153-181
7.1 Introduction	153
7.2 Global –Mittag-Leffler stability of fractional order systems	154
7.3 Lyapunov approach for stability	154
7.4 Model description and preliminaries	155
7.5 Results and Discussion	178
7.5.1 Stability Problem 1	178
7.5.2 Stability Problem 2	179
7.6 Conclusion	181
CHAPTER-8 CONCLUSION AND FUTURE SCOPE	182
REFERENCES	185
LIST OF PUBLICATIONS	205
BIODATA	206

List of Figures

Figure		Page No.
1.1	Open Loop Control System	1
1.2	Closed Loop Control System	1
2.1	Objective of Control System	25
2.2	Basic block of Feedback control System	26
2.3	Nyquist plot	29
2.4	Phase and gain stability margin	29
2.5	Basic Block of Non-interacting form of PID Controller	31
2.6	Effect of Controller on process variable	31
2.7	Block diagram of FOPID	35
2.8	Generalization of the FOPID controller from point to plane	35
3.1	Electromagnetic wave spectrum	38
3.2	Plank's curve log linear scale	40
3.3	Plank's curve log linear scale	41
3.4	Radiant power vs. wavelength	41
3.5	Absorption, Reflection and Transmission by a finite medium	42
3.6	Rate of Change of wire Temperature	46
3.7	Transfer function approximation using reaction curve method	47
3.8	Reaction Curve method for determination for transfer function	48
4.1	Quarter wave decay	50
4.2	Two Point Method	52
4.3	Constant amplitude oscillations	53
4.4	Effect of Changing the PID parameter on Nyquist plot	54
4.5	Simulation model and Results of output by using different controllers (ZNO, ZNC, CC, AH)	57
4.6	Bode diagrams of amplitude and phase of $L(s)$ for $1/K < 2$	59
4.7	Nyquist and bode plot of ceramic IR plant	65
4.8	Step response of IOPID controller with Ceramic IR heater Plant	66

4.9	Region of stability for the commensurate fractional order system with $0 < \alpha < 1$.	67
4.10	Region of stability for the commensurate fractional order system with $\alpha = 1$	68
4.11	Region of stability for the commensurate fractional order system With $1 < \alpha < 2$	68
4.12	Negative feedback control system	70
4.13	Nyquist plot of system controlled for gain margin	72
4.14	Bode Envelope of a FOPTD plant	73
4.15	The main dialog of ninteger before being filled in	79
4.16	Dialogue nipidGui filled in	81
4.17	The main dialogue displaying a Bode diagram	81
4.18	Simulink library	82
4.19	Dialogue of block Fractional PD	83
4.20	Dialogue of block Fractional PID	83
4.21	Simulink block diagram of Ceramic IR Heater Control Using $PI^\lambda D^\mu$ Controller	84
4.22	Magnitude of T(s) and S(s) for CFOPID (s)G(s)	85
4.23	Step response of the system for CFOPID for phase margin (500) and $\omega_{cp} = 2.75$ rad/sec	86
5.1	A simple fuzzy logic control system block diagram	89
5.2	Basic Control Structure of FLC based PID Controller	89
5.3	Overview of fuzzy toolbox inference system	92
5.4	The FIS Editor	92
5.5	Rule Editor	93
5.6	Rule Viewer	94
5.7	Surface Viewer	94
5.8	Membership function editor	94
5.9	Output response of plant with ZNPID controller for observation of deriving fuzzy control rules.	95
5.10	The Polarity of the Temperature Vector	96
5.11	Implementation of fuzzy logic controller with plant using Simulink	97
5.12	Step response of Fuzzy logic Controller for Ceramic IR Heater	98

5.13	Basic Flow Chart of Genetic Algorithm	101
5.14	Block diagram of PID tuning using GA	102
5.15	Flow chart of GA for PID Tuning	103
5.16	Best Fitness function for parameter by GA method	105
5.17	Simulink model for GA based PID controller	105
5.18	Step response Using GA based PID controller	106
5.19	Flow chart of PSO based PID Controller tuning	111
5.20	Best Fitness function for parameter by PSO method	112
5.21	Simulink model for PSO based PID controller	112
5.22	Step response Using PSO based PID controller	113
5.23	Swim and tumble of a bacterium	114
5.24	BFO flow chart for PID Tuning	119
5.25	Block diagram of BPID to IR Ceramic Thermal Plant	120
5.26	Simulink model for BFO based PID controller	120
5.27	Step response Using BFO based PID controller	121
5.28	Finding by ants path from nest to food source	122
5.29	Flow chart of ACO for PID tuning	126
5.30	Best Fitness function for parameter by ACO method	127
5.31	Simulink model for ACO based PID controller	127
5.32	Step response Using ACO based PID controller	128
6.1	Biological neural system	131
6.2	Conventional architecture of an artificial neural unit	132
6.3	Artificial neural network	134
6.4	Circuit for neuron i in the analog implementation of hopfield DNN	135
6.5	Circuit realization of the tangent hyperbolic	136
7.1	State trajectories of the FCNN system from example 1	180
7.2	State trajectories of the FCNN system from example 2	181

List of Tables

Table		Page No.
3.1	Comparison of different Infrared Heaters	45
3.2	Characteristics of commercially used Infrared Heat Sources	46
4.1	Effect of PID Tuning on System	50
4.2	Ziegler –Nichols open loop Tuning values	53
4.3	Zeigler Nichols closed loop Tuning values	54
4.4	Cohen-Coon Tuning values	54
4.5	Astrom- Hagglund Tuning values	55
4.6	Performance table of different Conventional PID Controller for Ceramic IR heater control	57
4.7	Performance table of IOPID Controller for Ceramic IR Heater	66
4.8	Performance table of FOPID Controller for Ceramic IR heater control	86
5.1	Prototype of fuzzy control rules with term sets	96
5.2	Linguistic variables in fuzzy inference system	97
5.3	IF-THEN Rules base for fuzzy logic controller	97
5.4	Performance table of Fuzzy Logic based Controller for Ceramic IR heater control	98
5.5	GA tuning parameters	104
5.6	Performance table of GA based PID controller for Ceramic IR heater control	106
5.7	PSO tuning parameters	111
5.8	Performance table of PSO based PID controller for Ceramic IR heater control	113
5.9	Specification of the BFO	118

5.10	Performance table of BFO based PID controller for Ceramic IR heater	121
5.11	Performance table of ACO based PID controller for Ceramic IR heater	128
5.12	Performance of PID, IOPID, Fuzzy Logic Controller, Artificial Intelligence based PID, Bio inspired based PID Controller and FOPID controllers	129

List of Principal Symbols

K_p	Proportional gain
K_i	Integral gain
K_d	Derivative gain
T_i	Integral time
T_d	Derivative time
$\lambda=v_i$	Thermal Conductivity
$\mu=v_d$	Mu
K	Gain of the System
P_m	Phase Margin
$g_m=\phi_m$	Gain Margin
$e(\tau)$	Error signal
ρ	Resistivity
ξ	Rate of Degradation
K_{cr}	Ultimate Gain
P_{cr}	Ultimate Period
K_u	Gain Magnitude at the point of intersection on Nyquist Curve
Ψ	Phase of Derivative at ω_0
ω_c	Gain crossover frequency
ω_l	Low frequency range
ω_h	High frequency range
γ	Slope of the magnitude in Bode plot
$P(s)$	Plant
$Y_{m(k)}$	Command input in fuzzy logic PID control
Y_p	Plant output in fuzzy logic PID control

Y'_m	Pre compensated command signal in fuzzy logic PID control
$\gamma(k)$	Correction term
IR	Infrared
ZNO	Zeigler-Nichols Open Loop
ZNC	Zeigler Nichols Closed Loop
A-H	Astrom- Hugglund
CC	Cohen-Coon
IOPID	Integer Order PID Control
FOPID	Fractional Order PID Control
AI	Artificial Intelligence
FLC	Fuzzy Logic Control
GA	Genetic Algorithm
PSO	Particle Swarm Optimization
BFO	Bacterial Foraging Optimization
ACO	Ant Colony Optimization
HFE	Heat Flow experiment
ε	Emissivity
T	Temperature
r	Reflectivity
α	Absorptivity
τ	Transmissivity
a	diffusivity
c	Specific Heat
c_p	Heat Capacity
Q	Energy of Activation

L	Length of resistance wire
R	Resistance
L	Inductor
C	Capacitor
R_e	Element Resistance
l	length
A	Area
V	Volume
h	Plank's Constant
D	Diameter
${}^c D^\alpha$	Caputo's fractional derivative
α	Rate of neurons
(t)	state variable of the i th unit at time 't'
c_{ij}, a_{ij}	feedback template elements
h_{ij}	Feed forward template
$u_{ij}, v_{ij}, P_{ij}, Q_{ij}$	Elements of fuzzy feedback MIN template and fuzzy feedback MAX template
\wedge	Fuzzy AND
\vee	Fuzzy OR
I_i	State, input and bias of the i th neuron
f_i	Activation functions
s	variable in Laplace domain
$R(s)$	Real part of s
$V(t)$	continuous functions
$\Gamma(\cdot)$	Gamma function
Γ	Constant in Lemma
f_j	Lipschitz continuous
F_j	Positive constant

$\vartheta_j(t)$	State variable
u_{1i}, u_{2i}	Hybrid feedback controls
ϕ_i and Ψ_i	Feedback gains
ρ	Constant for Global Mittag Leffler

CHAPTER 1

INTRODUCTION

1.1 Overview

In this world, human is the most valuable living creature; he has been involved to know the phenomenon happening in nature and seeks action according to their requirement. In general life we have many objects to be accomplished. The means of achieving the objective remains to control the input actions and the system. So the study to obtain desired output can be termed as control system Engineering.

The system may be traffic control system, chemical process, robotic system, heat transfer system, missiles system in which human element must be excluded. A system incorporating such equipment is known as an Automatic control system. Control system Engineering has taken the present shape because of the contributions from various other fields of knowledge such as feedback theory, linear system analysis network and communication theory, so control engineering belongs to a wide range of applications; such as aeronautical, chemical, mechanical, environmental, civil and electrical.

In order to represent any system properly, it is necessary to know the cause- effect relationship of each of its components; this may be termed as input –the output relationship. If the output of a system depends on the input, the system is said to be an open-loop system Fig 1.

If input cannot be merely manipulated but made dependent on the actual output of the system. Then it is called feedback closed-loop control system Fig2.

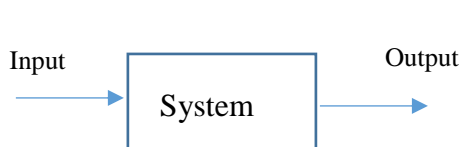


Fig 1. Open Loop Control System

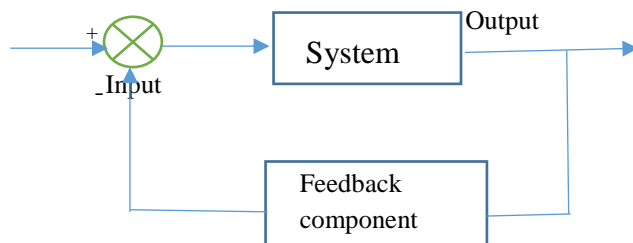


Fig 2. Closed Loop Control system

In open loop control system, the output is quite sensitive to external disturbances and internal variations in the system parameters. On the other hand in case of closed loop control

system in which feedback is inherently present. Feedback system has own effect on the performance characteristics such as stability, bandwidth, overall gain, disturbance and sensitivity.

Feedback control system may be classified based on the method of analysis and design as linear and Non-Linear time varying or time-invariant. It is also classified according to the main purpose of the systems as position – control system and velocity-control system control. Modern control theory encompasses the classical control theory as single –input, single-output (SISO) but with complex system such as airplane and chemical process plant multiple-input, multiple –output(MIMO) systems are taken into consideration which gives as a deeper understanding of control systems dynamics and concepts. A digital computer has proved to a valuable tool that makes possible practical application of modern control theory to the complex engineering systems.

The impact of digital computer provides powerful computing and data handling capacity with high speed digital signal processing makes it extremely useful as an integral operating element and to perform the functions of electronic controllers, data storage, processing and logical operations.

1.2 Control Strategies

It is the ability belonging to monitor and adjust a process to get a desired output, for example, the temperature of a room is kept at a certain point using the heater and a thermometer. So process control technology is so critical and helps manufactures to keep their activities working with in defined limits and to set more specific limits to optimize profitability and guarantee quality and safety. There are several types of process control systems, including SCADA (supervisory control and data acquisition), PLC (Programmable Logic controller) or DCS (Distributed control systems) which function to collect and transmit data acquired during the production process.

There are also four basic concepts of process control systems as regulated variable's desired value, calculated value at a set point to pressure the controlled variable. Process control block (PCB) is a data structure used for storing all the information about a process by computer operating systems. It is also regarded as a descriptor of process. When the process finishes. It returns the PCB to the pool from which new PCBs are drawn. So, a single PCB in each process. A control loop is a corner stone of automatic control for a given phase; a control loop must have a least one sensor, a controller and an aspect of control to which the results

are applied. The effective process control starts with the sensors and measurements must be in suitable positions, and values must be appropriately sized with suitable trimming. The final control components, such as control valves, execute the changes needed to regulate the preferred process parameters, including flow, temperature, pressure level ratio etc.

A controller is a fundamental part of control engineering that attempts to minimize the difference between a system's real value or process variable and the system. Desired value i.e. set point. The function of the controller is to enhance steady-state accuracy by reducing steady state hence stability also improve. They reduces unwanted offsets and noise signals produced by the system controllers can help accelerate an over damped systems slow response. There are mainly two types of controllers: Continuous and discontinuous controllers. The manipulated variable shifts between discrete values in discontinuous controllers. A distinction is made between two positions, three positions and multi positions controls; based on how many different states the manipulated variable may assume. With the comparison of continuous controller, Discontinuous controllers ran on very simple, switching final controlling elements.

In continuous controller, any value within the output range of the controller can be found in the controlled variable. There are three basic modes in the continuous controller theory where the entire control action takes place, which are

1. Proportional controllers
2. Integral controllers
3. Derivative controllers

The combination of these controllers' modes are used in such a way that the process variable is equal to the set point. These modes take a form of given below.

1. Proportional and integral controllers (PI controller)
2. Proportional and Derivative controllers (PD controller)
3. Proportional Integral derivative control (PID controller)

All controllers have a particular case of usage that they are ideally suited to: In any system, we cannot just insert any kind of controller and expect a good result.

For Proportional Controller, two conditions are adopted as:

1. There should not be large deviation between input and output.
2. The deviation should not be abrupt (sudden) in proportional controller, the output is directly proportional error signal; mathematically, expressed as

$$A(t) \propto e(t)$$

Or $A(t) = K_p X_{e(t)}$, K_p is proportional constant

There is a recommendation to keep $K_p > \text{unity} (> 1)$, so that amplifies error signal can be easily detected.

Advantage of proportional controller is to reduce steady state error and to make faster the slow response of over damped system. But we have disadvantage of this controller as: With the presence of this controller some offsets are seen in the system and increase the maximum overshoot of the system.

Integral controller: When we need to return the controlled variable to the exact set point. Then integral controllers are used in which output is directly proportional to the integral of the error signal. It is also called reset controller.

$$A(t) \propto \int_0^{\infty} e(t) dt$$

$$\text{Or } A(t) = K_i \propto \int_0^t e(t) dt$$

K_i is integral constant or controller gain

The drawback of this controller is that it tends to make the system unstable because the produced error responds slowly.

Derivative Controllers: Derivative controllers never used alone because of its presence steady state error improves with the implication of noise signals also so it produces saturation effects:

In a derivative controllers output is directly proportional to the derivative of the error signal, Mathematically

$$A(t) \propto \frac{d e(t)}{dt}$$

$$\text{Or, } A(t) = k_d \frac{d e(t)}{dt}$$

k_d is proportional constant and is called controller gain

A derivative controller's main benefit is that it enhances the systems transient response.

Proportional and Integral controller (PI Controller)

It is a combination of proportional and derivative controller in which output (actuating signal) is equal to the proportional and integral sum of the error signal.

$$A(t) \propto \int_0^t e(t) dt + A(t) \propto e(t)$$

$$\text{Or, } A(t) = k_i \int_0^t e(t) dt + k_p e(t)$$

k_p & k_i are proportional and integral constant.

The main advantage of PI controller is to reduce steady state error so stability also reduces.

Proportional and Derivative controller (PD controller) –

The output or actuating signal is the sum of proportional and derivative of the error signal.

$$A(t) \propto \frac{d e(t)}{dt} + A(t) \propto e(t)$$

$$\text{Or, } A(t) = k_d \frac{d e(t)}{dt} + k_p e(t)$$

k_d & k_p are Derivative and proportional controller.

PD controller improves transient and steady state performance of a control system.

Proportional plus integral plus derivative controller (PID)

PID controller is the combination of proportional integral and derivative controllers.

In 1911, the first PID controller was developed by Elmer Sperry; After that in 1933 Tylor instrument company (TIC) had implemented a pneumatic controller with completely tunable .

In 1942, Ziegler and Nichols developed tuning rules to discover and set the necessary parameters for the Engineers; PID controllers, so (Automatic PID controller was used in industries in the mid of 1950). Finally in the middle of 1950, automatic PID controllers were commonly used in industries. We have seen that the PD controller might add damping to a system, but it does not affect the steady state response. The PI controller improves steady state error and relative stability with increasing the rise time. So PID controller is motivated and may be configured to incorporate the three basic control actions.

The input – output relationship of such a controller is

$$m(t) = k_p e(t) + k_p T_d \frac{d e(t)}{dt} + \frac{K_P}{T_i} \int_0^t e(t) dt$$

and T(s) Transfer function $\frac{M_s}{E_s} = k_p [1 + T_d s + \frac{1}{T_i s}]$

k_p = Proportional sensitivity

T_d = Derivative time

T_i = integral time

The implementation of PID controllers belongs to analog electronic components but now day's, microprocessors are used by PID controllers. The inbuilt PID controller's instructions also have programmable logic controllers. These are traditionally used in process controller applications due to the simplicity and reliability of PID controllers.

Integer order PID controller (IOPID)

When single fractional order pole model representation is considered then IOPID controller design methodology is adopted in which low order inverse integer approximation for fractional order model with keeping the emphasis on dominant poles and zeros. It contains only single design parameters as controller gain. It is clear from simulation results that the proposed IOPID controller shows a satisfactory response to overshoot, setting time and complete variation of the controller in comparison to the classical PID controller.

Fractional order PID controller (FOPID)

The conventional Integer order PID controller is not suitable to control the non-minimum phase processes, and non-linear or process belongs to high dead times so researchers turned their focus on fractional order controllers, which have remarkable performance over classical PID controllers. Many mathematicians have been drawn to fractional calculus since then. The main advantage of fractional derivatives over traditional integer order models is their great memory. When modeling mechanical systems, the advantage of fractional derivatives becomes obvious.

Fractional calculus is being employed in an expanding number of applications. Previously, integer order models were used; the fundamental reason for this was the lack of fractional differential equation solution methods. Because there are numerous methods for approximating fractional derivatives and integration, fractional calculus is now widely employed in modelling and control. The number of FO-PID can be used in real-world scenarios because integer order PID is the most used controller in industry. We have calculated parameters and implemented to get the better results in respect of PID controller. It is also demonstrated that fractional order systems are suited for dynamic system modelling and control.

Stability

The majority of stability research results are from integer-order networks, which has made stability a popular research area. Any dynamical system's performance can be evaluated using the stability problem. Pure mathematics has a very long history of using fractional-order calculus. Fractional calculus, which dates back to the late seventeenth century, is seen as a

generalization of the derivation and integration of arbitrary order. Additionally, fractional-order systems are more likely to be adopted than integer-order ones to explain the majority of real-world behavior since they can deliver more useful information and correct outcomes. Fuzzy cellular neural network stability analysis has received a lot of attention recently from researchers. A stability study of fuzzy cellular neural networks with temporal delay in the leakage term and impulsive disturbance is examined in a finite-time synchronization of delayed fuzzy cellular neural networks with discontinuous activation.

1.3 Literature Survey

Abdollah Homaifar et.al. developed the optimization technique using Genetic Algorithm to solve the problem using Fuzzy Logic. They focused on the development of rule sets or high performance membership functions which are completely computer designed. They have also shown GA's ability to design a robust controller which can work over a wide range of parameters [1].

Amjad J. et.al. adopted a strategy to optimize the gains of PID Controller for positioning control of a pneumatic system. In which the optimization model of E. coli bacterial foraging has been used and the performance index (cost) is based on Integral Square Error (ISE) for obtaining the optimal values of controller parameters [2].

Antonio Visioli adopted fuzzy inference system to determine the value of the weight that multiplies the set point for the proportional action based on the current output error and its time derivative [3].

Anuj Narang, et.al. proposed a strategy based on a reference model whose open loop transfer function is given by Bode's ideal transfer function. The parameters of the controller are estimated by formulating a constrained non-linear optimization problem. They proposed a fractional order PI controller design method for a fractional order plant [4].

B.Nagaraj et.al. shows an optimal tuning of PID controller parameters using GA, EP, PSO and ACO. Soft Computing techniques were used to tune the system to get good steady-state response and performance indices [5][6].

C R Madhuranthakam et.al. presents the synthesis and analysis of optimal tuning of PID parameters for different process system: first order plus time delay(FOPTD), second order plus time delay (SOPTD) and second order plus time delay with lead (SOPTDLD).It was shown

that the controller tuned with the proposed method is highly robust and ensures best achievable controller performance [7].

C.Yeroglu et.al. Presents an optimization strategy to obtain new parameters and other design procedure based on using bode envelops of the control system with parametric uncertainty [8] [10].

Christian Blum presents the first technique for approximate optimization inspired by the collective behavior of social insects. He presents ant colony and hybridizations of ant colony optimization algorithm [9]

Deepyaman Maiti, et.al. Presents the design method for minimizing the integral time absolute error (ITAE) criteria for fractional order plant model [11].

Duarte Valério et.al. presented two sets of tuning rules for fractional PIDs. These rules are quadratic and require the same plant time response data used by the first Ziegler-Nichols tuning rule for (usual, integer) PIDs [12].

Emine Dogru Bolat presents Matlab-SIMULINK based real time temperature control of oven designed as an experiment using a different kind of Auto Tuning PID method (Zeigler – Nichols step response method, Relay method and Integral Square Time error method) are used to control temperature of the experiment set up [13].

Fernando G. Martins presents the minimization of the integral of time-weighted absolute error for a good tuning of PID controller [14].

Hamideh Hamidian et.al. shows a numerical approach for the fractional order proportional integral derivative controller (FOPID) design for the unstable first-order time delay system. He specified that stability region is inversely proportional to the system delay [15].

Hongbo Xin, et.al. present a self-adaptive PID controller based on fuzzy to optimize the control process continuously. The temperature control system has the characteristics of non-linearity, large inertia and time variability. A fuzzy self-adaptive PID controller has good robustness, rapidity and good dynamic performance [16].

HongSheng Li et.al. present a new tuning method of fractional order proportional and derivative (PD μ) or FO-PD controller to ensure the closed loop system is robust and to gain variation. The FOC design method is practical and applicable [17].

Hu Sheng et.al. present the application of Laplace transform in solving differential equations with integer order. But for differential equations with non-integer order, the Laplace transform technique works effectively only for relatively simple equations because of the difficulties of calculating inversion of Laplace transform [18].

Hung-Cheng Chen et.al. present the optimal PID controller design for an Active Magnetic Bearing using Genetic Algorithm [19].

Hung-Ching Lu et.al. present a proportional-integral derivative (PID) estimator that is a parallel ant colony system (para-ACS) to regulate and obtain the precise parameters of PID controller. The framework consists of a main controller that is a PID controller and an para-ACS in which is offline tuned for the parameters of PID. The structure of para-ACS consists of three ACS sets that are parallel. Each ACS set individually estimates the three parameters of a PID controller. The integral of time and absolute error (ITAE) and the tracking error are used in the cost function (Rise Time, Settling Time, Peak Time and Overshoot) of each ACS set to update the pheromone of each ACS set [20].

Huseyin Atakan Varol et.al. present an ant algorithm (AA) which is a new nature-inspired optimization technique in which result are compared with results of Zeigler tuning methods which gives a performance that is at least as good as that of the PID tuning methods mentioned [21].

Hyo-Sung Ahn et.al. present a new strategy to tune a fractional order integral and derivative (ID) controller satisfying gain and phase margins based on Bode's ideal transfer function as a reference model , for temperature profile tracking. He examined the performance of two different fractional-order controllers in temperature profile tracking [22].

I.Santi Prabha et.al. show the performance analysis of conventional PID controller versus fuzzy-based controller for Injection Mould Machine process control [23].

Ibtissem Chiha, et.al. present a tuning method of PID controller method using multi-objective ant colony optimization. The design objective was to apply the ant colony algorithm in the aim of tuning the optimum solution of the PID controllers (K_p , K_i , and K_d) by minimizing the multiobjective function. The potential of using multiobjective ant algorithms is to identify the Pareto optimal solution. The other methods are applied to make comparisons between a classic approach based on the "Ziegler-Nichols" method and a metaheuristic approach based on the genetic algorithms [24].

Ivo Petráš et.al. Present a synthesis of fractional $P I^\lambda D^\mu$ controllers, analysis of their behavior and simulation methods. They point out the non-adequate approximation of non-integer systems by integer-order models and differences in their closed-loop behavior [25].

Jianming Zhang et.al. developed a fuzzy tuning scheme for PID Controller settings of integer plus time delay processes in which a fuzzy rule base reasoning method are utilized online to determine a tuning parameter based on the error and the first change in error of the process. This tuning parameter is used to calculate the PID controller parameters [26].

Jin-Sung Kim et.al. present an optimal control of the Reverse Osmosis plant using the auto-tuning concept in conjunction with PID controller. They propose a control scheme comprising of an auto-tuning stochastic technique based on an improved Genetic Algorithm [27].

Lasse M. Eriksson et.al. present a comparison of five control algorithms that are based on PID, IMC and fuzzy gain scheduling techniques and discusses their performance in varying time-delay systems [28],[29].

Li Xu-zhou et.al. developed particle swarm optimization algorithm to design an online self-tuning framework of PID controller [30].

Liu Yijian et.al. present a novel improved E.Coli foraging optimization algorithm (IEFOA) for parameter tuning of PID controller. IEFOA is presented with three main operators as tumbling, swimming and tracing that at the same time records the optimal position of individual E.Coli in order to update the locations of swarm. Instead of using traditional analysis algorithm, the parameters of the PID controller, such as proportional gain, integral factor, and differential coefficient are selected and optimized by IEFOA. The effectiveness of the proposed optimization algorithm is tested by simulation experiments of the common one-order and two-order industrial models. The IEFOA approach provides an attractive method for the design of PID controller parameters [31].

M Adonis et.al. Present a programmable type industrial style infrared dryer. The load power supplied for each kind of dryer is analyzed. The design and implementation of an infrared radiation controller is also presented. The infrared drying controller contributes to a more energy efficient drying system than the always-on techniques that are employed to fluctuate the heater temperature [32, 33, 41].

Mahmud et.al. show design of a PID Controller using PSO algorithm. The model of a DC motor is used as a plant in this paper. The conventional gain tuning of PID controller (such as the

Ziegler-Nichols (ZN) method) usually produces a big overshoot, and therefore modern heuristics approaches such as genetic algorithm (GA) and particle swarm optimization (PSO) are employed to enhance the capability of traditional techniques. The comparison between PSO-based PID (PSO-PID) performance and the ZN-PID is presented [34].

Marco et.al. proposed different ant colony optimization algorithms. They describe how a generic ACO algorithm is applied to the well-known traveling salesman problem and also give a more formal description of ACO [35].

Mendes N et.al. focus

\

ed on the mathematical model applied to both building thermal analysis and control system design. They show the influence of thermal parameters on the building air temperature, HVAC (Heating, Ventilation, and Air conditioning) system, sensor, heating system performance, energy consumption, and advantage of using Matlab/SIMULINK in building thermal and energy analysis [36, 37].

Mohammad Ali Nekoui et.al. present the optimal design of PID controller based on a particle swarm optimization(PSO) approach for a continuous stirred tank reactor(CSTR) [38].

Muhammet Ünal et.al. present comparison of the performances of genetic algorithm (GA) and ant colony optimization (ACO) algorithm for PID controller tuning on a pressure control process. GA and ACO were used for tuning of the PID controller when predefined trajectory reference signal was applied. Realized pressure process dynamic has nonlinear behavior, thus system was modeled by a nonlinear auto regressive and exogenous input (NARX) type artificial neural network (ANN) approach. PID controller was also tuned by Ziegler-Nichols (Z-N) method to compare the results. A cost function was designed to minimize the error along the defined cubic trajectory for the GA-PID and ACO-PID controller. Then PID controller parameters (K_p , K_i , K_d) were found by GA-PID, ACO-PID algorithms, which were adjusted with their optimal parameters. It was concluded that both ACO and GA algorithms could be used to tune the PID controllers in the pressure process with excellent performance [39].

Nazlia Omar et.al. present the design and development of a real-time temperature and voltage monitoring system. It was developed for the purpose of monitoring and controlling semiconductor component devices which are very heat sensitive in the industry-based

application. The system has been successfully designed, implemented and tested in the working environment [40].

P.Poongodi et.al. proposed a certain novel algebraic schemes for obtaining reduced order models of a higher order linear time invariant system represented in the form of transfer functions[42].

P.Wang and D.P.Kwok presents advanced Genetic Algorithm used to automatically carry out the fine tuning of the parameter settings of classical PID controllers [43].

Podlubny I. et.al. Present notes to some methods used in fractional calculus and application of the fractional calculus to modeling and control of dynamical system [44].

R. Padma Sree and M.Chidambaram propose design of PI controllers for stable inverse response systems with and without delay. The method is based on matching the corresponding coefficient for a servo problem and by specifying the initial (inverse) jump [45].

Ramiro S. Barbosa et.al. present two applications of fractional calculus in the area of closed systems robust to gain variations and fractional order PID controller for the hexapod robot [46].

S R Vaishnav and Z J Khan present design of PID controller using Zeigler-Nichols(ZN) technique for higher order system. A fuzzy logic controller using simple approach and smaller rule set is proposed [47].

S.M.Giriraj Kumar et.al. present optimal tuning of a PID controller used in a high performance drilling system for controlling the output obtained and hence to minimize the integral of absolute errors (IAE) [48].

S.M.GiriRaj Kumar et.al. present an application of an Ant Colony Optimization for PID tuning. Computational Intelligence (CI) an off shoot of Artificial Intelligence relies on heuristic algorithms mainly evolutionary computation. Swarm intelligence (SI) a derivative of CI, describes the collective behavior of decentralized, self-organized systems. Ant behavior was the inspiration for the Meta heuristic optimization technique. The designed controller ability in tracking a given set point is compared with an Internal Model Control (IMC) tuned controller [49].

Saeed Tavakoli and Mahdi Tavakoli present an optimal method for tuning PID controllers for first order plus time delay systems by considering integral square error (ISE) and integral time absolute error(ITAE) performance criteria [50].

Sing-Fu Lee et.al. Presented GA based fuzzy PID control systems. By using GA technique, two crossover operators are used for rule optimization and parameter optimization [51].

Sofiane Bououden et.al. Evaluated parameters of PI controller by Ant Colony Optimization (ACO) using objective function [52][53].

Duan Hai-Bin et.al.presents an example of using the Ant Colony Optimization (ACO) algorithm to improve the design parameters for a nonlinear PID controller.. The ACO algorithm is a novel heuristic bionic algorithm, which is based on the behavior of real ants in nature searching for food. This nonlinear PID controller using the ACO algorithm has high precision of control and quick response [53].

Song Chaohong et.al. Focus on the constraint of complex system optimal problem, a method which solved problems by the combination of genetic algorithm and traditional non-linear or linear programming algorithm. New algorithms decompose the decision variables and associated variable, and then use genetic algorithm and traditional optimal algorithm to optimal independent variables and optimal associated variables respectively [54].

T. Hägglund and K J Åström present an analysis of the Zeigler-Nichols frequency response method for tuning PI controllers, showing that this method has severe limitations. The limitations can be overcome by a simple modification for processes where the time delay is not too short [55] and also proposed an idea of tuning controller based on simple features of the step response based on robust loop shaping [56].

T .Suksri et.al. presents the design temporal controller for small oven process using STM32F103RE,MCU ARM 32 bits microcontroller. The proposed system is based on form of On-Off control devices together with temporal logic algorithm that can provide high precision and accuracy [57].

Truong Nguyen Luan Vu et.al. Lee present a new design method of fractional-order proportional-integral controllers based on fractional calculus and Bode's ideal transfer function for a first-order-plus-dead-time process model. It can be extended to various dynamic models. Tuning rules were analytically derived to cope with both set-point tracking and disturbance rejection problems. Simulations of a broad range of processes are reported with each simulated controller being tuned to have a similar degree of robustness in terms of resonant peak. The proposed controller showed improved performance over other similar controllers and established integer PI controllers [58].

V.Rajinikanth et.al. present an enhanced bacteria foraging optimization (EBFO) algorithm-based Proportional integral derivative (PID) controller tuning for nonlinear process models. The EBFO algorithm is a modified form of standard BFO algorithm. A multiobjective performance index is considered to guide the EBFO algorithm for discovering the best possible value of controller parameters. The efficiency of the proposed scheme has been validated through a comparative study with classical BFO, adaptive BFO, PSO, and GA based controller tuning methods. The proposed algorithm was tested in real time on a nonlinear spherical tank system. The real-time results show that, EBFO tuned PID controller gave a smooth response for setpoint tracking performance [59].

Wael M. Korani et.al. proposed a new algorithm Bacteria Foraging oriented with PSO (BF-PSO) techniques. This algorithm was applied to the problem of PID controller tuning and compared with conveniently Bacterial Foraging algorithm and Particle swarm optimization [60][61].

Y.Jin , Y-Q et.al. discusses fractional order [proportional derivative] controller tuning rules for robustness motion control systems. The controller is designed to satisfying the robustness property with respect to time constant variation and the desired phase margin criteria. A systematic tuning rule is developed for the FO-PD controller for first order plus time delay model with integrator [62].

YangQuan Chen et.al. Present a new practical tuning method for fractional order proportional and integral (FO-PI) controller to determine the best fractional order parameter α and at the same time to determine the best FO-PI gains [63, 64].

Yanhai Chen and Weixing Lin present analysis of the optimization mechanism. A series of measures are taken to improve the classic BFO known as IBFO. In the modified method, search scope and chemotaxis step varies dynamically which can accelerate the convergence and enhances the searching precision. Besides, a variable denoted the overall best value incorporated to guide the bacterial swarm to move to the global optima and replace the role of interaction behavior between bacteria in classic BFO, which is complicated and time-consuming. The superiority of the algorithm proposed is tested over several test functions and parameter estimation of the NARMAX (nonlinear autoregressive moving average with exogenous) model. The simulated result shows that it has high efficiency, rapid speed of convergence and strong capability of global search [65].

Ying Luo et.al. Present two fractional order proportional integral controllers designed to improve the performance and robustness for fractional order systems, which can better model many real systems such as bioengineering systems [66, 67].

Ying Pei et.al. Propose a new ACO algorithm that oriented the multicore computing based on the multicore computing environment. There are many improvements to the ACO algorithm, like the improvements of algorithm in the self-adaptive environment, the improvements of increasing the diversity of various groups, the improvements of enhancing local search, combining with the global optimization algorithm, and combining with a deterministic local optimization algorithm, etc. However, with the developments of the theory and technology in multicore computing, how to implement ACO efficiently and paralleled in a multicore computing environment being a new challenge for all researchers [68].

Ying Tung Hsiao et.al. Present an optimum approach to design PID controllers. At the same time, the transient response is guaranteed by minimizing the maximum overshoot, settling time, rise time of step response. This study proposes a solution algorithm based on the ant colony optimization technique to determine the parameters of the PID controller for getting a good performance for a given plant. Simulation results demonstrate a better control performance can be achieved in comparison with known methods [69].

Yung K.Lee and John M. Watkins present a new method for finding all fractional-order (FO) proportional-integral-derivative (PID) controllers that stabilizes a given system of integer or non-integer order. The stability boundaries of such FO PID controllers are calculated in the frequency domain and are given in terms of the proportional gain K_p , integral gain K_i , and derivative gain K_d . They will be plotted on the (K_p, K_i) , (K_p, K_d) , and (K_i, K_d) planes. A key advantage of this approach is that it provides the stability boundaries even when the transfer function of a system is not available, as long as the frequency response of the system can be obtained [70].

Zaid Amin Abduljabar suggested a computer simulation of temperature control of the heating and cooling water system. The proposed system uses the concept of fuzzy logic, where the fuzzy rule base consists of a collection of fuzzy IF-THEN rules [71].

Zhenyu Yang and Gerulf Pederson present the automatic PID control design for a one-dimensional magnetic levitation system. The PID controller is automatically tuned using the non-dominated sorting genetic algorithm based on a nonlinear system model [72][73].

Zhou Ying et.al. Proposed an adaptive algorithm that adjusts the probabilities of crossover and mutation by IAE and ISE function of the changes of fitness value. GA for tuning the parameter of the nonlinear PID controller is very effective [74].

Deepyaman Maiti et.al. describes an application of PSO to the problem of designing a fractional-order proportional-integral-derivative ($PI^\lambda D^\delta$) controller whose parameters comprise proportionality constant, integral constant, derivative constant, integral order (λ), and derivative order (δ). The presence of five optimizable parameters makes the task of designing a $PI^\lambda D^\delta$ controller more challenging than conventional PID-controller design, the design purpose is to minimize the integral time absolute error (ITAE) criterion [75].

Ying Luo et.al. designed fractional order proportional Integral controller (FO-PI) and fractional order (Proportional Integral) FO [PI] controllers both can satisfy all the three specifications proposed. From the simulation result, it can be seen that both the FOPI and FO [I] controllers [76].

S.M Girijay et.al. presented a stable, robust, and controlled system by tuning the PID controller using a particle swarm optimization (PSO) algorithm. The incurred value is compared with the traditional .Tuning techniques like Ziegler-Nichols and is proved better. Hence the results establishes that tuning the PID controller using PSO technique gives less overshoot, the system is less sluggish and reduces IAE (Integral Absolute Error) [77].

C.Yeroglu et.al. proposed two methods for tuning of $PI^\lambda D^\lambda$ Controller, having one method based on the idea of using Ziegler-Nichols and Astrom. Hagglund method, in which Ziegler-Nichols method is used to compute the parameters K_p and K_i of $PI^\lambda D^\lambda$ controller and K_d, λ and μ have been found from Astrom –Hagglund method using critical point information. Simulation results show that the $PI^\lambda D^\lambda$ Controller has better response than the classical PID controllers. Five design specifications of the Monje-Vinagretal method are used to derive five non-linear equations from satisfying the robust performance of the system [78].

Anuj Narang et.al. is proposed a servo control strategy for tuning of fractional order PI (FO-PI) controllers with and without time delays for satisfactory tuning parameters of the controllers, an iterative optimization method is suggested based on the minimization of a quadrature cost function and defined as the weighted sum of squares of control input moves and sum of the integral squared error (ISE) between the time response of the reference model and the fractional system with the FO-PI controller [79].

B.Nagaraj et.al. Presents soft computing techniques to determine the parameter of the PID controller for position control of a D.C. Motor. The proposed approach has superior features and is compared with Z-N methods whose performance have been compared and analyzed

with intelligent tuning techniques like GA, Evolutionary programming, and PSO. The soft computing method was more efficient in improving the step response characteristics of DC motors [80].

Ying Luo et.al. proposed two fractional-order proportional integral controllers and designed for a class of fractional order system. This proposed scheme offers a practical and systematic way of the controllers design for the simulation and experimental results presented; both of the two designed fractional order controllers work efficiently with improved performance compared with the designed stabilizing integer order PID controller by the observation [81].

Yung K et.al. is proposed the FOPID controller that stabilizes a given system of integer or non-integer order. The stability boundaries of such FOPID controllers are calculated in the frequency domain and are given in the terms of K_p, K_i and K_d . This approach provides stability boundaries even when the transfer function of a system is not available, as long as the frequency response of the system can be obtained and results are compared with integer-order (IO) PID controllers for a sample [82].

Wei Guo et.al. is proposed a novel model Algorithmic controller (MAC) with fractional order PID structure (Called FOPID-MAC), which combines with the advantages of both FOPID and Mac. Through the derivation of algorithm and simulation analysis [83].

Sabtarshi Das et.al. Using a genetic algorithm to improve the Nyquist-based sub-optimal model reduction technique has been proposed, tuning of optimal PID and $PI^\lambda D^\lambda$ Controllers is employed while minimizing an objective function comprising an error index [84].

Manuel A et.al. design a direct fractional order model reference adaptive controller (FOMRAC) is presented to an automatic voltage regulator (AVR) in which controller parameters are adjusted using fractional order differential equations so the improvement of controller behavior and its robustness with respect to model uncertainties [85].

Laura E et.al. explore the evolution of the Mittag-Leffler Theorem from its initial state in 1876 to its final version, published in 1884. Mittag-Lefflers work contributed significantly to Weierstrass' program on the foundations of analysis. His interest in generalizing his results to functions having arbitrarily many essential singularities, however, which led to his research on infinite sets of singular points, attracted him to Georg Cantor's set-theoretic work [86].

Anidya- pakhira et.al. are used the continued fraction expansion (CFE) method for the analog realization of fractional order chitter-integrator with special classes of fractional order controller (FOPID) and several formulations for rational approximations to get equivalent rational transfer function in terms of controller tuning parameters [87].

Lu Liu et.al analyzed the FOPID for oscillatory fractional time delay systems based on the numerical inverse Laplace transform algorithm and applied it to solve the problem caused by the difficulties of searching for an analytical solution to a complicated fractional order differential equation [88].

Abbasali Zamain et.al. is used **an** FOPID controller based on Gases Browniom motion optimization (GBMO) is used to solve the load frequency curve; the performance of the proposed controllers in time domain and robustness verified when compared with other controllers as GBMO based fuzzy controller and PI controller used for load frequency control system in computing with model parameters variations[89].

E.Yumuk et.al is taken inverse of the integer low order approximation of the fractional order model. In this approach by focusing poles and zeros that are dominant. PID parameters are derived directly from fractional order model and simulation results show that the proposed order PID controllers perform comparably in terms of overshoot and settling time in respect of classical integer order PID controllers [90].

A.Tejljkov et.al Tanned PID controllers for an Experiment of a DC Motor platform in which results in leads to equivalent PI^λ or $PI^\lambda D^\lambda$ Control loop because of incorporating fractional-order dynamics in an existing integer-order DC feedback control system [91].

Karima rabah et.al. set a fractional order laws are provided which gives a guarantee asymptotic stability of fractional order chaotic system by considering the Lyapunov stability theorem in which Genesio-Tesi chaotic and modified jerk systems are provided and we get the effectiveness and robustness of control solution industrial control systems are generally used sampled and it is thus important to provide a numerical approximation of the fractional operator several approximation exist depending on temporal or frequency domain [92].

Z.Yakoub et.al. designed FOPID based on the numerical optimization of a frequency domain criterion, any change in the parameter is detected by the proposed algorithm. For a model-based fractional control design. The performances of the proposed algorithm are evaluated with the help of unstable and linear time-varying processes [93].

Sánchez et.al. is used to minimize integrated absolute error for both set point, and load disturbance response has been addressed for a multi-objective optimization problem by considering a first-order-plus dead time process model subject to robustness and maximum sensitivity [94].

Lei Zhang et.al examined uniform stability analysis of fractional-order complex-valued neural network with leakage and discrete delays has been examined with sufficient conditions and

derivations which gives to guarantee the existence, and uniqueness of the unique equilibrium point [95].

Alikeesi et.al. did survey on Recent Results PID Controllers have been mostly popular due to its simplicity and applicability to a wide range of industrial control problems (Astrom and Haggling 2006) optimal performance can be achieved by using the fraction of PI/PID controllers based loops(O'DWYer 2009)advantages of FOPID over IOPID have been seen from both simulations and experiments with real life objects and also potential efforts are reduced in case of using FOPID controllers, the designing of FOPID is based on mostly frequency domain analysis [96].

Henlong Wu et.al are designed a pressurized heavy water reactor model and heating furnace model by tuning procedure of parameters of fractional order PID controller to verify the efficacy of the proposed method and show promising application value and enhance the performance robustness and ability of handling uncertainties of FOPID. FOPID has been used to control the underwater vehicle longitudinal angle for stability problem; considering the transfer function as the investigated subjects [97].

Liping Chen et.al. employed the maximum modulus principle and the spectral radii of matrices, two new delay-independent stability criteria for FO systems with single or multiple delays are proposed. Based on the stability results, a novel stability formulation for FMNN with multiple delays is established [98].

Helem et.al. obtained the primary goal of this work has been to minimize the IAE for either the load disturbance rejection task and the set-point following task with a constraint on the maximum sensitivity [99].

Erdal et.al. obtained the stability regions satisfying specified gain and phase margins for varying integral order for integrating processes with fractional-order PI controller have been obtained. Also shown improved stability and closed loop responses by keeping the value of λ less than 1[100].

T.Verma et.al. is presented based on idea of the Ziegler–Nichols and Cohen Coon for the tuning of PID controller with the optimization techniques depend on initial estimates, Valerio and Costa have introduced some Ziegler-Nichols-type tuning rules for FOPIDs [101].

Ardak et.al. are obtained sufficient condition for the exponential stability of the periodic solutions by constructing Lyapunov functional This study can be extended further by considering FSICNNs with different type of delays such as continuously distributed delays or involving leakage term [102].

Swapnil W et.al are provides brief design procedure of fractional order proportional-integral-derivative (FO-PID) controller through the indirect approach of approximation using constant phase technique. The new modified dynamic particle swarm optimization technique is proposed to find controller parameters. The FO-PID controller is implemented using floating point digital signal processor [103].

M. Syed et.al discussed sufficient conditions are derived to ensure the finite- solution and differential inclusion theory, by using H^∞ older inequality, Gronwall inequality time stability of concerned fractional-order complex-valued memristive neural networks [104].

Hongyun Yan et.al.has investigated the global fractional-order BAM neural network Mittag-Leffler stabilization. To start, a new lemma is put forth by leveraging fundamental inequality to increase the range of possible Lyapunov functions. Additionally, fractional-order BAM neural networks are intended to be stabilized using linear state feedback control techniques. [105].

Jia Jia, et.al. addressed the global stabilization of fractional-order memristor-based neural networks (FMNNs) with time delay. The voltage threshold type memristor model is considered, and the FMNNs are represented by fractional-order differential equations with discontinuous right-hand sides [106].

Ibrahim et.al provides numerical solutions for a general form of fractional delay differential equations with fractional derivatives defined in the Caputo sense. A fractional integration operational matrix, created using a fractional Taylor basis, is applied to solve these fddes [107].

M. Syed Ali et.al. is to establish a new set of sufficient conditions for the uniform stability in mean square of such stochastic fractional-order neural networks with leakage [108].

1.4 Motivation

Practically every aspects of our lives uses a control system, including our homes, workspace, communications/ information technologies etc. more complex control system have been developed as a result of growing issues with non-linear process ties, operating limitations, time delay, uncertainty and other factors. Therefore there is a constant guest for a better methods that can take into account all of these issues give the system stability and offer greater performance.

Practical application of a model has to be taken into consideration before their use in industry. The identified models based on the nature of the relationship can be broadly classified as: linear and nonlinear models. It is well known that a majority of the real world processes are nonlinear

by nature; however, the objective is always to get a reasonably accurate representation of the true process, which at times can be obtained using localized linear models. Also, it is easier to obtain a representation of a process if the process is assumed to be locally linear. System identification methodology in the area of linear models is well-developed. For linear time series models, a wide variety of model structures are available for capturing the dynamics of a system with respect to known inputs and unmeasured disturbances. However, handling time delays in modeling has always been challenging. It is not possible to identify an accurate model of the process because of a number of reasons. In practice, the true model order of the process is not always exactly known and also data length for identification is finite and data contains unmeasured disturbances/noise. In this respect, the stochastic nature of the process makes the identification problem challenging.

The emergence of the industrial revolution necessitated the use of regulated heat sources to boost output and enhance product quality. Since their late 1930s infrared has been employed in the business sector in the light bulbs with exterior reflectors. When IR is compared to these traditional methods, particularly for applications involving surface heating, certain applications using IR are far more effective and efficient and the quality of the finished product is much improved (Howard et.al, 1996). Consequently, the infrared heating process has higher efficiency because of minimum energy loss.

For linear models, discrete-time models are very well researched. However, most often the model parameters for a discrete model have no physical interpretation compared to the continuous-time models. The physical systems are inherently continuous in nature; the use of continuous-time models in controller design and the strong relation between model parameters and the system properties are the major forces for developments in continuous time identification.

Chen (Chen et.al, 2006) has argued that fractional order control is ubiquitous when the dynamic system is of distributed parameter nature (DPS). Whenever material or energy is physically moved in a process or a plant, there is usually a time delay associated with the movement. Apparent time delays may result in the identification exercise when a higher order process (or DPS) is approximated by a lower order model. Both the equation error based and output error based approaches have been explored in the literature for fractional order models. However, none of the studies discuss methods for identification of fractional order system models with time delays.

PID controllers are still widely used in the industry because they are easy to implement and perform well for wide class of processes. It is argued that fractional order systems require much more design than classical PID controllers to achieve good closed loop performance. A fractional-order PID (FOPID) controller is considered as the generalization of the conventional PID controllers (Podlubny et.al, 1999a). Fractional order PID controllers, which provide additional tuning parameters, can provide better closed loop performance and robustness features compared to classical PID controllers. PID controllers in general are not well suited for control of processes with long dead time characteristics as they can cause stability issues for the closed loop systems. The controller designs of these processes are challenging problems.

The main focus from an engineering standpoint is enhancing or optimizing performance. Therefore, our goal is to use fractional-order control (FOC) to improve the performance of the dynamic system control (integer order). The controller is an extension of the classical PID structure with an added advantage of considering the integrator and differentiator of any non-integer order. It is expected that fractional PID will perform better over an integer order PID due to an extra controller parameter to be tuned. A lot of research has gone into developing tuning methods for $PI\lambda D\mu$ controllers.

The focus of this thesis is that identification and control go in hand, and it is equally important to have a high-fidelity and parsimonious model (model with fewer parameters) to design an excellent model-based controller. The objective is to build data-based models (parsimonious models) for integer and fractional order systems which can represent a process sufficiently well and use the model(s) to design controllers (simple PID, Integer order PID, fractional order PID, fuzzy logic, Artificial intelligence based PID controller and Bio inspired based PID Controller etc.) to provide good robustness and closed loop performance or cost function (Rise Time, Peak time, Settling time, Peak Overshoot and performance Indices).

Stability is very important in a research field that has drawn much attention from mathematicians, physicists, and computer scientists. The Lyapunov direct approach and extended Mittag-Leffler stability are established for fractional-order nonlinear dynamic systems. The goal of is to use hybrid feedback controllers to examine the global Mittag-Leffler stability of fractional-order fuzzy cellular neural networks with distributed delays. To guarantee the stability of the concerned fractional order systems, stability requirements are developed by building a suitable Lyapunov functional. The Caputo definition is used. For the synchronization of master and slave systems under consideration, a successful controller is attained. A numerical example is used to demonstrate the accuracy of the suggested procedure.

1.5 Methodology

The presentation and partial contribution that distinguishes it from the other work to be done in this field.

1. Development a model for P-I-D Controller.
2. . Implementing a model of a first-order plant with a delay and fine-tuning a traditional PID controller based on the Zeigler-Nichols open loop, Zeigler-Nichols plus closed loop, and Astrom-Hagglund to calculate and identify various controller parameters.
3. Fractional order controller by an integer order controller lower order system with time delay.
4. Design of fractional order controllers based on frequency domain specifications and calculation of five parameters (K_p , T_i , T_d , λ and μ).
5. Design of fuzzy logic PID controller, based on minimization of the time domain.
6. Design of Artificial Intelligence (GA and PSO) based FOPID controllers.
7. A comparative study of the transient parameters and performance index are performed to determine the better control architecture.
8. By employing the analysis technique, some leakage delay-dependent criteria have been established for checking the global uniform stability of the fractional-order neural networks.
9. Application/Implementation of global Mittag-Leffler stability of fractional order control system for fuzzy cellular neural network using Mittag-Leffler function and Lyapunov function with two examples.
10. Stability criteria has been derived to ensure the stability of the concerned fractional order systems with examples with two examples.

1.6 Organization of Thesis

Chapter 1 contains a basic introduction, a literature survey, and details of the work done.

Chapter 2 covers fundamental PID controller theory, integer order PID

controller theory, and fractional order controller theory that explains traditional PID tuning techniques for both closed-loop and open-loop systems.

Chapter 3 gives an overview and mathematical modeling of the Ceramic Infrared Heater.

Chapter 4 gives an explanation of classical PID tuning methods for open-loop and closed-loop systems, Astrom –Hagglund, Cohen-Coon, Integer order PID Controller and Fractional order PID Controller using frequency analysis, and its implementation is to be used.

Chapter 5 gives an introduction about fuzzy logic and its control application. The basic theory and algorithm about the optimal tuning of controller based on Artificial Intelligence (GA, PSO) and bio-inspired based (BFO, ACO) PID Controller and its problem formulation have been discussed.

Chapter 6 studies of Global Mittag-Leffler stability of fractional order fuzzy cellular neural networks and checks stability based on the hybrid feedback control technique and Lyapunov approach with examples.

Chapter 7, sufficient conditions are established to guarantee the stability for leakage delay and time-varying delay for a generalized Fuzzy cellular fractional-order neural network has been derived by considering the concept of the Lyapunov Function with examples.

Chapter 8 result and conclusion

1.7 Conclusion

Based on an extensive literature review on the temperature control process, it has been felt that new techniques are required to control the temperature in food processing industries, surface heating, certain applications using infrared(IR) heaters are more effective, efficient and the quality of the finished product is much improved (Howard et.al, 1996). Consequently, the infrared heating process is having a higher efficiency due to minimum energy losses.

CHAPTER 2

DIFFERENT TYPES OF CONTROLLERS

2.1 Introduction

In modern time, Control System plays a very important role in the development and advancement of modern civilization and technology. The concepts of control are fundamental and well-mined in every aspect of our life. The trends of the modern civilization have been in the direction of greater control [56][61]. The importance of control has grown tremendously in almost every field of technical endeavor. Thermostats regulate the temperature in air-conditioners, refrigerators, ovens, and furnaces. Numerous Control arrangements find their way into industrial and military applications for the control of position, speed, tension, temperature, humidity, pressure, and flow. Some specific examples are- tension controllers of sheet rolls in paper mills, thickness controllers of sheet metals in rolling mills, pressure controllers in boilers, temperature controllers, Flow controllers, reaction controllers etc. in chemical processes. Radar, sweeping antenna control, food processing, printing heating system, gun director, missile control and control in space, etc.[7] are some of the varied uses of automatic control.

A system is a co-ordinate unit of individual elements performing a specific function. The word control is usually taken to mean regulate, direct and command. The essential ingredients of the Control System can be described in figure 2.1:

- ❖ Objective of control
- ❖ Control system components
- ❖ Results or Output

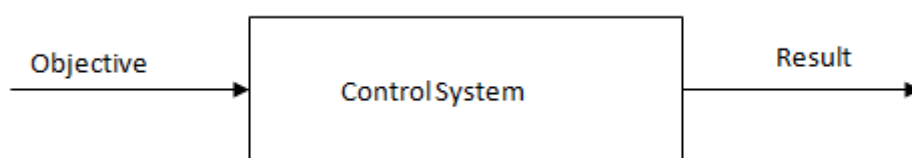


Fig: 2.1 Objective of Control System

The reference input (objective) is essentially a signal or a set of movements in some form that acts upon the system in such a way that the response at the output takes place in a desired manner. Control Systems may be classified into two types, depending on whether the controlled variable affects the actual input to the control system, i.e., whether some feedback is used or not [61].

An industrial control system comprises of an automatic controller, an actuator, a plant, and a sensor (measuring element). The set point controller must be converted to reference input with the same unit as the feedback signal from the sensor element as shown in figure 2.2

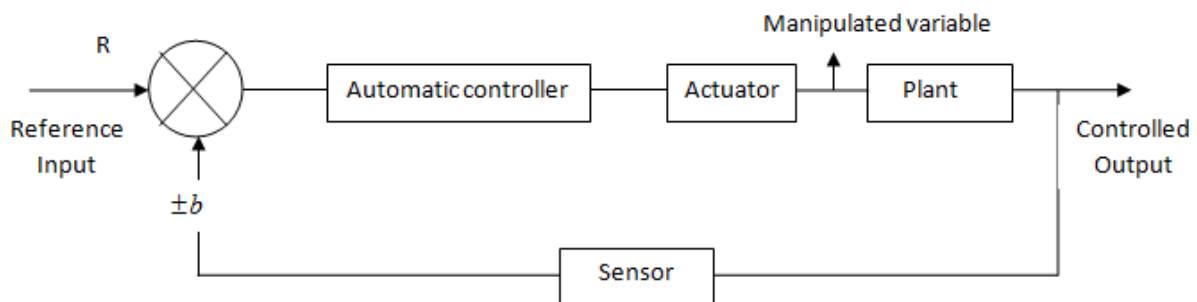


Fig: 2.2 Basic block of Feedback control System

The main components of a SISO Control System are a Transconductor, a Compensator, The Plant, and a Pre-filter. Transconductors are divided in to actuators and sensors, as per shown in figure 2.2.

The following definitions are given

- ❖ A Transconductor is an electrical device that converts one form of energy into another. There are two kinds of transconductor: actuators and sensors.
- ❖ An actuator is a particular transconductor that transforms a signal into action on the plant. It usually receives an input signal from the controller and provides the plant with the necessary action.
- ❖ A Sensor is a particular transconductor that transforms a physical measurement of a plant variable in to an electrical signal. It is mainly used to obtain the feedback signal.
- ❖ A compensator, also known as a controller, is an additional part or circuit put into a control system to make up for subpar performance.
- ❖ An additional component or circuit is added to a control system as a compensator or controller to make up for subpar performance.

2.2 Variable Representation with Laplace Transformation

The variables are expressed in the frequency domain by the Laplace transformation. The operator is defined by the following equation

$$L[f(t)] = F(s) = \int_0^{\infty} f(t) e^{-st} dt \quad (2.1)$$

Where $f(t)$ is a function of time, ' s ' a complex variable, ' L ' is an operational symbol, and $F(s)$ is the Laplace transform of $f(t)$. The Laplace transform method allows solving the algebraic and complicated differential equations in the real variable t into the complex variable ' s '.

The Laplace variable ' s ' is often used differential operator where $s \equiv \frac{d}{dt}$

$$\text{and} \quad \frac{1}{s} \equiv \int_0^t dt$$

2.2.1 Transfer function

Given the definition of the Laplace transformation, we can define the concept of the transfer function as follows.

The ratio of the Laplace transform of the output (also known as the response function) to the Laplace transform of the input (also known as the driving function), under the presumption that all initial conditions are zero, is the transfer function of a linear, time-invariant, differential equation system. (Ogata) 1997, Page 55).

A transfer function expresses the relation between the input and the output of a system regardless of the internal dynamics. It can be defined only for a linear, time-invariant System (LTI). If the System is non-linear or contains non-linear elements, a transfer function cannot be used to describe the process.

A generic transfer function is expressed in the form

$$G(s) = \frac{a_0 s^m + a_1 s^{m-1} + \dots + a_{m-1} s + a_m}{b_0 s^n + b_1 s^{n-1} + \dots + b_{n-1} s + b_n} \quad (2.2)$$

Where m and n are the grades of numerator (m) and denominator (n) and value of n is greater than m . The solutions of the numerator are called zeros of the transfer function and the solutions of the denominator are called poles. The values of zeros and poles are represented in equation (2.2) given below:

$$G(s) = k \frac{(s + Z_1)(s + Z_2) \dots (s + Z_m)}{(s + P_1)(s + P_2) \dots (s + P_n)} \quad (2.3)$$

Where Z_1, \dots, Z_m and P_1, \dots, P_n are the zeros and poles of the transfer function and K is called gain.

2.2.2 Frequency response and Bode diagrams

The frequency response is a representation of the response of the system to sinusoidal input at varying frequencies. The frequency response is defined as the magnitude and phase differences between the input and output sinusoids (Doff, Bishop 2001, and et.al) expressed by the following definition:

“The frequency response of a system is defined as the steady-state response of the system to a sinusoidal input Signal; the output signal for a linear system, as well as all other signals inside the system, is sinusoidal in the steady state and only differs from the input waveform in terms of amplitude and phase angle.

The frequency response can be graphically drawn with a Bode plot or Nyquist plot. The magnitude is expressed in dB where

$$dB = 20 \log_{10} |G(\omega)|$$

The frequency is represented on a logarithmic scale.

Nyquist plot of a feedback system is a plot of the frequency response of the return ratio, with the imaginary part plot against the real part. The Nyquist stability criteria state that if

- The open loop system is asymptotically stable and
- If the Nyquist diagram does not enclose the point “-1”, then the closed-loop system will be asymptotically stable.

The real power of the Nyquist stability criterion is that it allows us to determine the stability of the closed-loop system from the behavior of open loop Nyquist diagram. Gain and phase margin measure how close the Nyquist locus get to -1. The Nyquist diagram shown in figure 2.3 of a system $G(s)$ is plot of the frequency response ($G(j\omega)$) on an Argand diagram. That is; it is a plot of imaginary ($G(j\omega)$) Vs Real($G(j\omega)$).

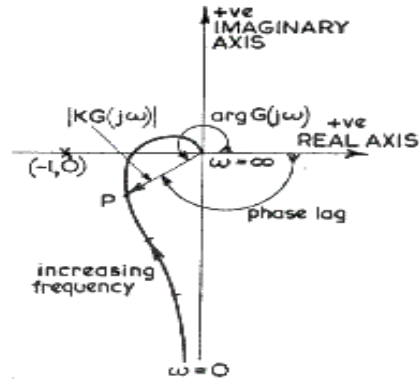


Fig: 2.3 Nyquist plot

This gives the degree of relative stability; in other words, this tells how the system forms the instability region. The formal definitions are provided by

$$P_m = 180^\circ + \arg [G(j\omega_{cg}) + H(j\omega_{cg})] \quad (2.4)$$

$$G_m [dB] = 20 \log \frac{1}{|G(j\omega_{cp})H(j\omega_{cp})|} [dB] \quad (2.5)$$

Where ω_{cg} and ω_{cp} stands for, respectively, the gain and phase crossover frequencies, which obtain from the figure (2.4) as

$$|G(j\omega_{cg})H(j\omega_{cg})| = 1 \Rightarrow \omega_{cg} \quad (2.6)$$

$$\arg [G(j\omega_{cp}) + H(j\omega_{cp})] = 180^\circ \Rightarrow \omega_{cp} \quad (2.7)$$

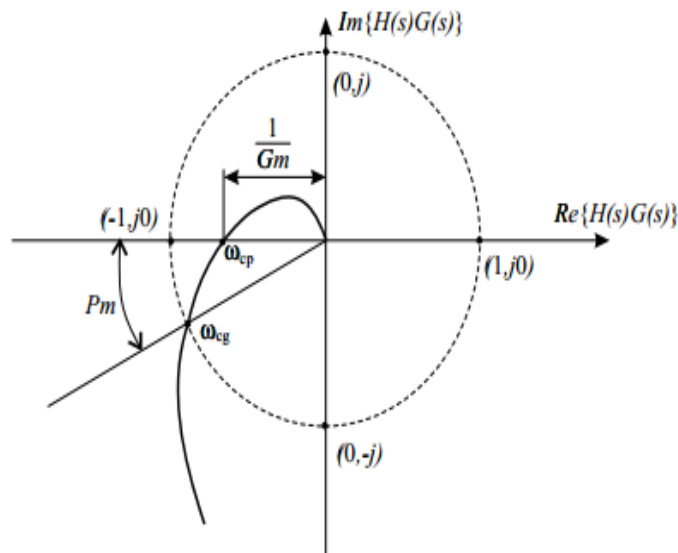


Fig: 2.4 Phase and gain stability margin

2.3 PID Controller

One of the first industrial controllers was the PID controller. It has a lot of benefits: It is affordable, straightforward, durable, and simple to tune. It has been demonstrated that this controller is exceptionally effective at controlling a variety of processes. It can be used for processes whose models are very challenging to drive because it does not require an accurate model [28]. The PID Controller does have some benefits, but there are also some downsides. In certain circumstances, such as:

- Non-linear processes(changing in operating point)
- Time-Varying parameters
- Compensation for strong and rapid disturbances
- Supervision in multivariable control

The following groupings can be used to categorize PID controller tuning rules:

1. Tuning rules based on a measured step response.
2. Tuning rules based on minimizing an appropriate performance criterion.
3. Tuning rules that give a specified closed-loop response.
4. Robust tuning rules

The topology of the PID Controller is widely spread in the industry. More than 90% of all control loops are PID (Astrom,- Hagglund 2001) [56].

A PID Controller's action on a plant can be expressed as follows in the time domain:

$$c(t) = k \left(e(\tau) + \frac{1}{t_i} \int_0^t e(\tau) d\tau + t_d \frac{de(\tau)}{d\tau} \right) \quad (2.8)$$

In the frequency domain, a PID Controller can be expressed by the transfer function as:

$$G_{PID}(s) = K \left(1 + \frac{1}{sT_i} + sT_d \right) \quad (2.9)$$

Equation (2.9) is called the standard or non-interacting form of PID controllers (Åström, Hägglund 1995) and is shown in figure 2.5.

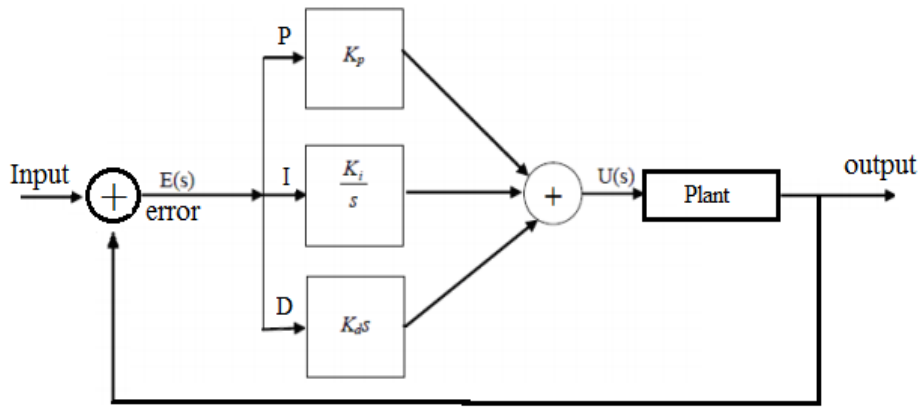


Fig: 2.5 Basic Block of Non-interacting form of PID Controller

The Proportional (P) action is the control action, proportional to the actuating error signal, which is the difference between the input and the feedback signal. The Integral (I) action is the control action which is proportional to the integral of the actuating error signal. Finally, the Derivative (D) action is the control action which is proportional to the derivative of the actuating error signal. The effects of PID controller action on the process variable are shown in figure 2.6.

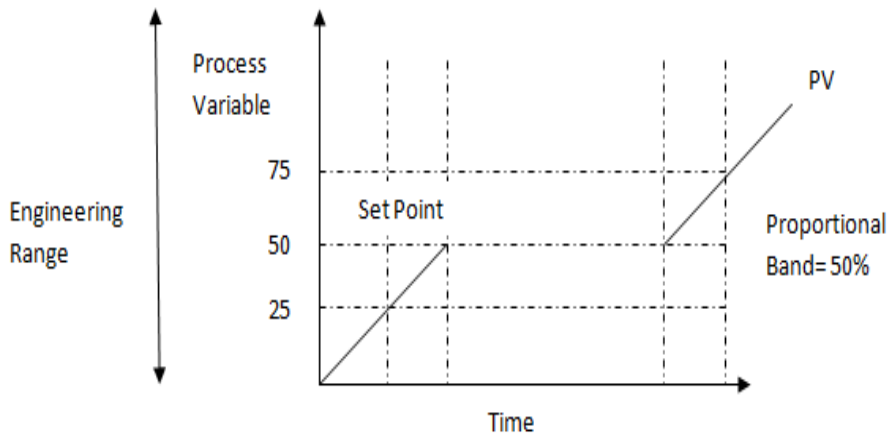


Fig: 2.6 Effect of PID controller on process variable

2.4 Fractional Order PID Controller (FOPID)

Now a day, a better understanding of the potential of fractional calculus and an increasing number of studies related to the applications of fractional order controllers in any area of science and engineering have led to the importance of its studies like analysis, design, tuning, and implementation of these controllers [8].

FOPID controller has received considerable attention both from an academic and industrial point of view. In fact, they provide more flexibility in the controller design with respect to the standard PID Controllers because they have five parameters to select (instead of three). However, this implies that the tuning of the controller can be much more complex.

The different integral operator, ${}_a D_t^q$, is a combination of differentiation and integration operators commonly used in fractional calculus. The definition of this operator, which can be used to take both the fractional derivative and the fractional integral in a single equation, is [18]

$${}_a D_t^q = \left\{ \begin{array}{ll} \frac{d^q}{dt^q} & q > 0 \\ 1 & q = 0 \\ \int_a^t (de)^{-q} & q < 0 \end{array} \right. \quad (2.10)$$

Where q is the fractional order which can be a complex number and a and t are the limits of operation. There are some definitions for fractional derivatives. The commonly used definitions are Grunwald- Letnikov, Riemann- Lowville and Caputo definition (Podlubny, 1999b). The Grunwald- Letnikov definition [18] is given as:

$${}_a D_t^q f(t) = \frac{d^q f(t)}{d(t-a)^q} = \lim_{N \rightarrow \infty} \left[\frac{t-a}{N} \right]^{-q} \sum_{j=0}^{n-1} (-1)^j \binom{q}{j} f \left(t - j \left[\frac{t-a}{N} \right] \right) \quad (2.11)$$

The Riemann- Lowville definition is the simplest and easiest definition to use. This definition is given as:

$${}_a D_t^q f(t) = \frac{d^q f(t)}{d(t-a)^q} = \frac{1}{\Gamma(n-q)} \frac{d^n}{dt^n} \int_0^t (t-z)^{n-q-1} f(z) dz \quad (2.12)$$

Where, ‘n’ is the first integer which is not less than q i.e. $n-1 \leq q < n$ and Γ is the gamma function.

$$\Gamma(z) = \int_0^{\infty} t^{z-1} e^{-t} dt \quad (2.13)$$

For a function $f(t)$ having n continuous derivative for $t \geq 0$ where $n-1 < q < n$, the Grunwald-Letnikov and Riemann- Lowville definitions are equivalent. The Laplace transform of the Riemann- Lowville fractional integral and derivative are given as follows:

$$L\left\{{}_0D_t^q f(t)\right\} = s^q F(s) - \sum_{k=0}^{n-1} s^k {}_0D_t^{q-k-1} f(0) \quad n-1 < q \leq n \in N \quad (2.14)$$

Unfortunately, the Laplace transform technique appears to be inadequate for treating the Riemann-Lowville fractional derivative since it necessitates knowledge of the non-integer order derivatives of the function at $t=0$. The Caputo definition, often known as smooth fractional derivatives in some literature, does not have this issue. The following is the definition of a derivative:

$$d_{a_t}^q f(t) = \left\{ \begin{array}{l} \frac{1}{\Gamma(m-q)} \int_0^t \frac{f^{(m)}(\tau)}{(t-\tau)^{q+1-m}} d\tau \quad m-1 < q < m \\ \frac{d^m}{dt^m} f(t) \quad q = m \end{array} \right\} \quad (2.15)$$

Where the first integer, m , is greater than the second integer, q . By making the assumption that the homogeneous initial conditions hold, it is discovered that the equations with Riemann-Lowville operators are equal to those with Caputo operators. The fractional derivative of Caputo's Laplace transform is given as

$$L\left\{{}_0D_t^q f(t)\right\} = s^q F(s) - \sum_{k=0}^{n-1} s^{q-k-1} f^{(k)}(0) \quad n-1 < q \leq n \in N \quad (2.16)$$

The Laplace transform of the Caputo fractional derivative only exhibits integer order derivatives of function f , in contrast to the Riemann-Lowville fractional derivative's Laplace transform. The aforementioned equation becomes: with a zero initial condition for zero initial condition, the above equation reduces to:

$$L\left[{}_0D_t^q f(t)\right] = s^q F(s) \quad (2.17)$$

2.4.1 Properties of Fractional Order Differentiations

The following characteristics of the fractional order differentiation [22]:

1. The Fractional Order differentiation ${}_0D_t^\alpha f(t)$ with respect to t of an analytic function $f(t)$ is also analytical.
2. The Fractional Order differentiation is exactly the same as integer-order one when $\alpha=n$ is an integer. Also

$${}_0D_t^\alpha f(t) = f(t)$$

3. The Fractional Order differentiation is linear; i.e., for any constants a, b has

$${}_0D_t^\alpha [af(t) + bg(t)] = a {}_0D_t^\alpha f(t) + b {}_0D_t^\alpha g(t)$$

4. Fractional Order differentiation operators satisfy the commutative-law and also satisfy

$${}_0D_t^\alpha [{}_0D_t^\beta f(t)] = {}_0D_t^\beta [{}_0D_t^\alpha f(t)] = {}_0D_t^{\alpha+\beta} f(t)$$

5. The Laplace transform of Fractional Order differentiation is defined as

$$L[{}_0D_t^\alpha f(t)] = s^\alpha L[f(t)] - \sum_{k=1}^{n-1} s^k [{}_0D_t^{\alpha-k-1} f(t)]_{t=0}$$

For a special cases, if the derivatives of the function $f(t)$ are all equal to 0 at $t = 0$,

$$L[{}_0D_t^\alpha f(t)] = s^\alpha L[f(t)]$$

The most common form of a fractional order PID controller is $PI^\lambda D^\mu$ Controller (Podlubny et.al, 1999a), involving an integrator of order λ and a differentiator of order μ , where λ and μ can be any real number—replacing the integer order derivatives and integrals in eq. (2.8) by integral and derivative operators of arbitrary real order provide a fractional order PID.

$$u(t) = K_p e(t) + K_i ({}_a D_t^\lambda e(t)) + K_d ({}_a D_t^\mu e(t))$$

The operator of the form ${}_a D_t^\rho$ shown here is the Grunwald-Letnikov (GL) form of the fractional differ, integral operator, where (a, t) are the terminals. Applying Laplace transform to this equation with null initial conditions, the transfer function of the controller can be expressed by:

$$\frac{U(s)}{E(s)} = C_{FOPID}(s) = K_p + \frac{K_i}{s^\lambda} + K_d s^\mu, (\lambda, \mu > 0) \quad (2.18)$$

Where $C_{FOPID}(s)$ represents the transfer function of the fractional order Controller. For designing a FOPID controller, 3 parameters (K_p, K_i, K_d) and 2 orders (λ, μ) with non-integers should be optimally determined for a given system. The integrator term is $1/s^\lambda$, that is to say, on a semi-logarithmic plane, there is a line slope of -20λ db/decade.

Figure (2.7) is a block diagram configuration of FOPID clearly, selecting $\lambda=1$ and $\mu=1$, an integer order PID Controller (Classical PID) can be recovered. The selections of $\lambda=1, \mu=0$, and $\lambda=0, \mu=1$ correspond to conventional PI and PD Controllers, respectively as shown in figure 2.8.

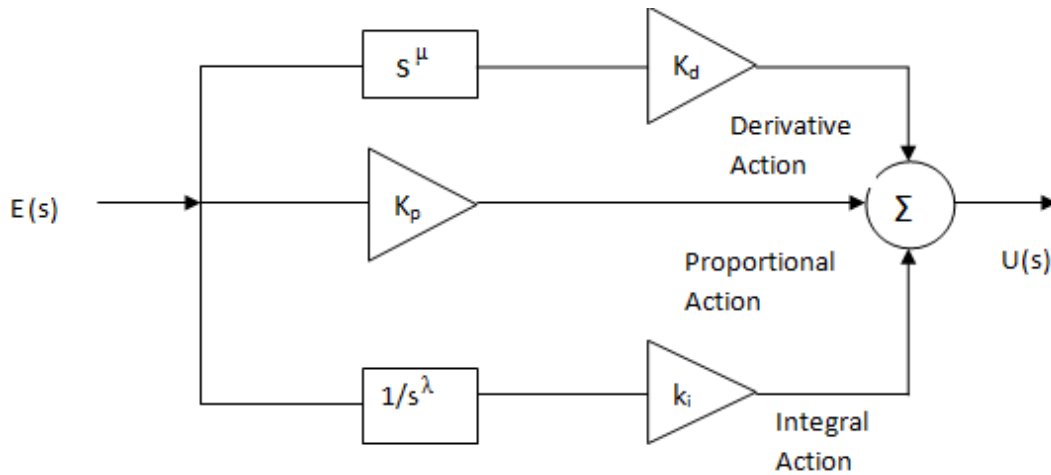


Fig: 2.7 Block diagram of FOPID

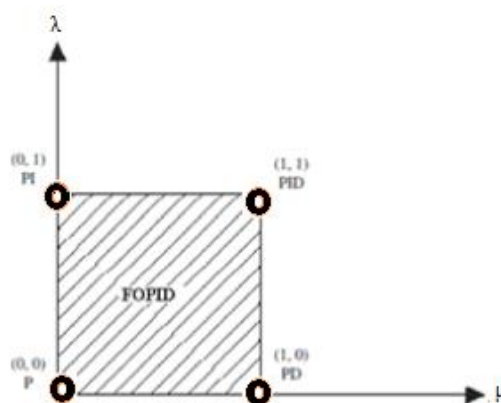


Fig: 2.8 Generalization of the FOPID controller from point to plane

It is reasonable to assume that the PI-D Controller will improve system performance. The better control of dynamic systems, which are modeled by fractional order mathematical equations, is one of the PID Controller's key advantages. Another advantage lies in the fact that is the $PI^\lambda D^\mu$ controllers are less sensitive to change of the parameters of a Controlled System (Xue et.al, 2006) [46][64].

Usually, the four basic approaches to fractional order control, i.e. four different fractional order Controllers, are there, have been overviewed.

2.5 Tilted Proportional and Integral (TID) Controller

First, the TID Controller has the same structure as the classical PID Controller. Still, the proportional gain is replaced with the function $S^{-\alpha}$ where $\alpha \in \mathbb{R}$, which allows wider tuning options and better control behavior compared to the integer order PID Controller.

2.5.1 Commande Robustee d'ordre Non Entire (CRONE) Controller

Next popular controller is CRONE. The abbreviation CRONE stands for French “Commande Robustee d'ordre Non Entire” (Non- integer robust Control) and represents an approach inspired by fractal robustness [44]. Presently, three generations of the CRONE methodology have been developed:

- a) The first generation CRONE Control- “Control of plant with an uncertain magnitude and constant phase with respect to frequency around the desired open loop gain crossover frequency” (real fractional order for Controller definition).
- b) The second generation CRONE Control- “Control of plant with an uncertain magnitude around the desired open gain crossover frequency” (real fractional order for open loop definition).
- c) The third generation CRONE Control- “The most generation CRONE methodology (Complex fractional order (s) for open-loop definition).

Fractional lead-lag Controller- Lead-lag Compensator is also a popular control system design method. The fractional order lead-lag Compensator should be equal to CRONE or $PI^\lambda D^\mu$ controller.

The popular CRONE Mat lab Toolbox is dedicated to fractional order calculus and applies to the original theoretical and mathematical concepts developed by the CRONE research group. The CRONE toolbox has been developed progressively since the nineties.

Presently, there are two versions of the toolbox available – a classical and an object-oriented one. Both of them can be downloaded (after registration) from the internet. The classical version is embellished with a Graphical User Interface (GUI) and contains three main modules:

- Mathematical module – implementation of fractional calculus algorithm
- System identification module – identification of fractional order models in frequency and time domain
- CRONE control module – implementation of fractional order robust control design

The object-oriented version contains various scripts and allows the overloading of some basic mathematical operators and standard Mat lab routines for the fractional order cases. It assumes the user to be familiar with the basics of work with Mat lab.

2.6 Conclusion

This chapter presents the basic terms, and definitions for fractional derivatives explained by Grunvald- Letnikov, Riemann-Lowville and Caputo definitions used in the studies related to the applications of fractional order controllers in many areas of science and engineering like analysis, design, tuning, and implementation of controllers. Different types of controllers are also explained.

CHAPTER 3

HEATING SYSTEM OF CERAMIC INFRARED HEATER

3.1 Introduction

All the materials absorb heat energy, due to which atoms vibrate. Absolute zero (-273) is the temperature at which there is no vibration motion in a bit. The electric and magnetic fields are generated by vibration and heating atoms. Hence electromagnetic wave takes place, and places hot objects radiate electromagnetic wave. These electromagnetic waves may be visible light, microwave radio waves, X-rays, and infrared radiation. The difference between these waves depends upon wavelength and frequency, and they travel equal to the speed of light Figure Shows how the various frequencies and wavelengths of electromagnetic waves. Fig.31.1

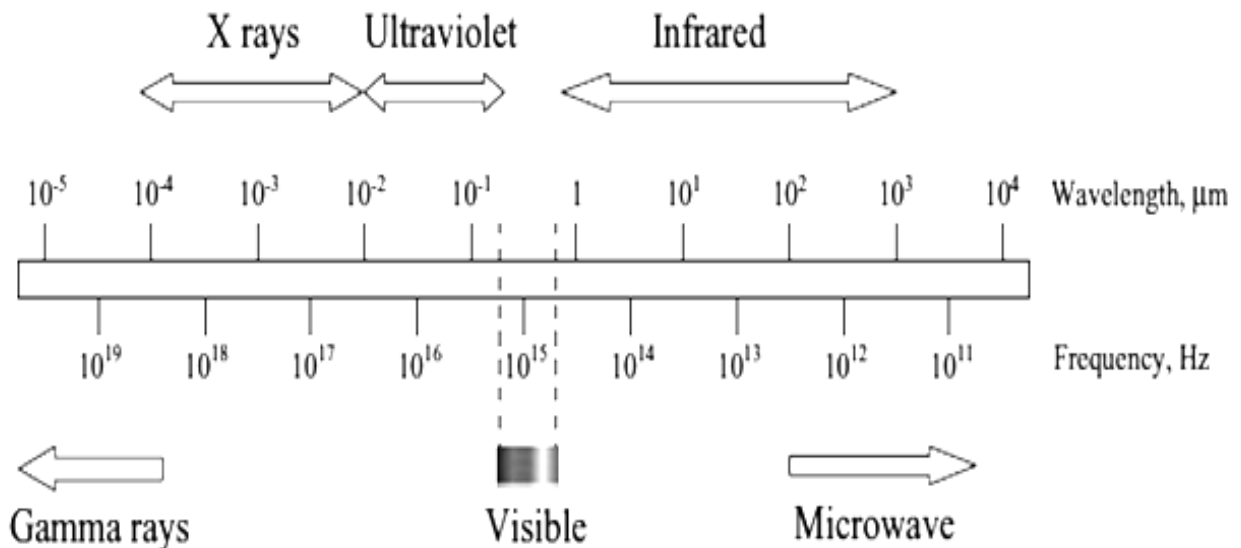


Fig: 3.1 Electromagnetic wave spectrum

3.2 Heating Process

Process heating is essential for food processing industries and other plastic, rubber, concrete glass, and ceramic; these may be categorized as:

3.2.1 Fuel-Based Process Heating: Fuel based heating as furnaces, kilns, and melters, typically, the energy used for the process accounts for 2% to 15% of the total production cost.

3.2.2 Electric-Based Process Heating: In which electric currents or electromagnetic fields are used for heating materials as:

- (i) Electric current passing through the material
- (ii) By using Eddy Currents in the material
- (iii) By Exciting atoms of the materials with Electromagnetic radiation (Microwave)

3.2.3 Steam-Based heating: - Most of the heat contents of steam is collected in the form of the latest heat used in steam turbines of thermal plants.

3.2.4 Electric Infrared Processing: First of all, Ford motor company used the infrared system to cure paint on Auto bodies in the mid-1930 with the invention of new infrared tolerant coatings; electric Infrared was used successfully in the manufacturing sector. The concept of Infrared radiation depends upon the electric current passing through a solid resistor. It is typically employed in applications where precise temperature control is necessary, such as heat surfaces, cure coatings, and dry materials.

3.3 Basic Laws and Definitions

Depending on the type of material used and its thickness, electromagnetic waves that are applied to a body may be absorbed, reflected, or transmitted, depending on whether the surface is opaque, semi-transparent, or clear.

Emissivity E is the property of a black body that absorbs all the incident radiation on its surface regardless of direction and wavelength

$E = (\text{Energy emitted from a real surface} / \text{energy emitted from a black body at the same temperature})$

It varies from $0 \leq E \leq 1$, for black body $E=1$ for polished surfaces $E=0.02$ generally for non-metal as ceramics organic materials $E > 1$, normally emissivity of metals increases with temperature

Specifically, polished metals have low emissivity in infrared. For $\lambda \geq 8 \mu m$, ϵ_λ can be approximated by $0.00365 \sqrt{\rho / \lambda}$ where ρ ohm-cm (resistivity) is and wavelength λ in μm .

At shorter wavelengths, the emissivity increases and, for many metals, has values of 0.4 to 0.8 in the visible range of the spectrum. The emissivity is approximately proportional to the square root of the absolute temperature ($\epsilon_\lambda \propto \sqrt{\rho}$ and $\rho \propto T$) in the far infrared range and temperature insensitive in the near-infrared range.

The emissivity increases as grain-size increases in the range of 1 to 200 μm (Hottel and Sarofim et.al, 1996). The amount of energy radiated by a heater and the wavelengths of this energy is determined by the temperature of the heater. Figures (3.2 and 3.3) are Plank's Curves plotted with various scales.

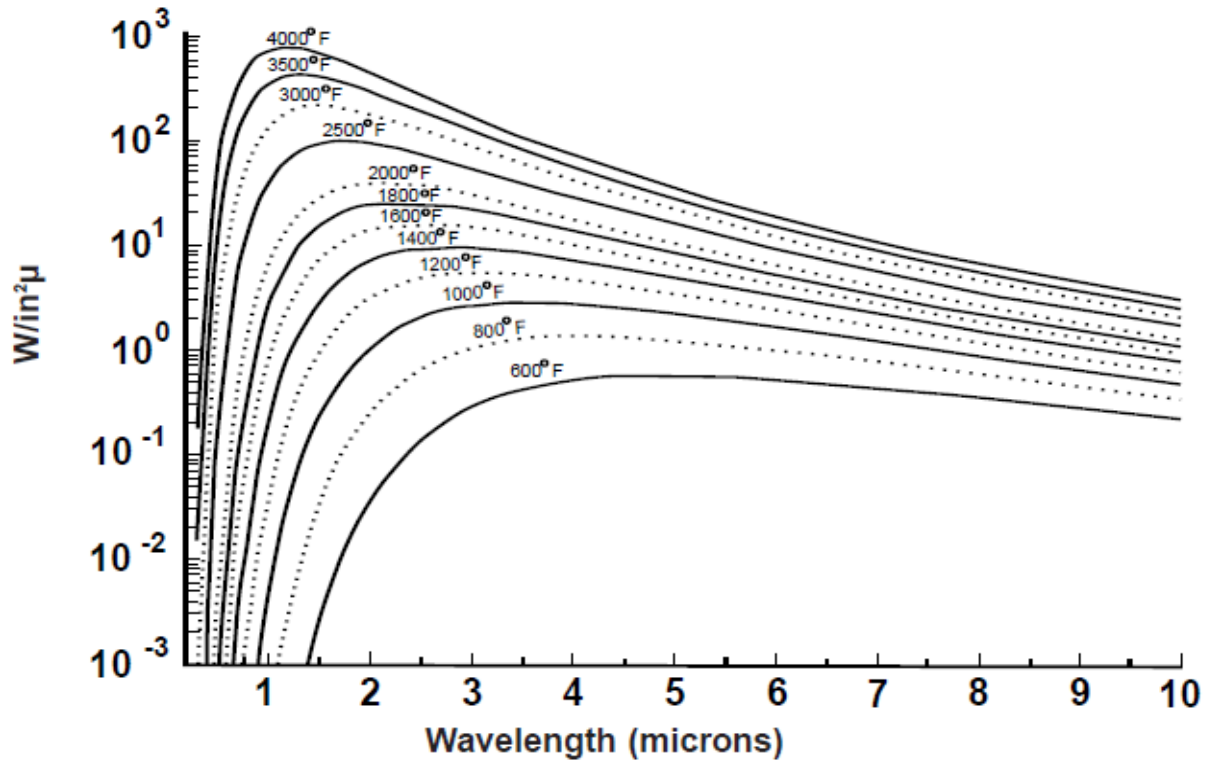


Fig: 3.2 Plank's curve log linear scale

From the Curves in figure 3.4, it can be seen that a heater radiates energy over a broad spectrum of wavelengths. It can be seen that as to heater temperature (T_h) increases:

- ❖ The energy radiated increases (as T_h^4)
- ❖ The “peak” energy wavelength gets shorter
- ❖ For a given heater, more energy is radiated at all wavelengths
- ❖ A higher percentage of the energy is distributed in a narrow wave band

Further, three important physical parameters are considered:

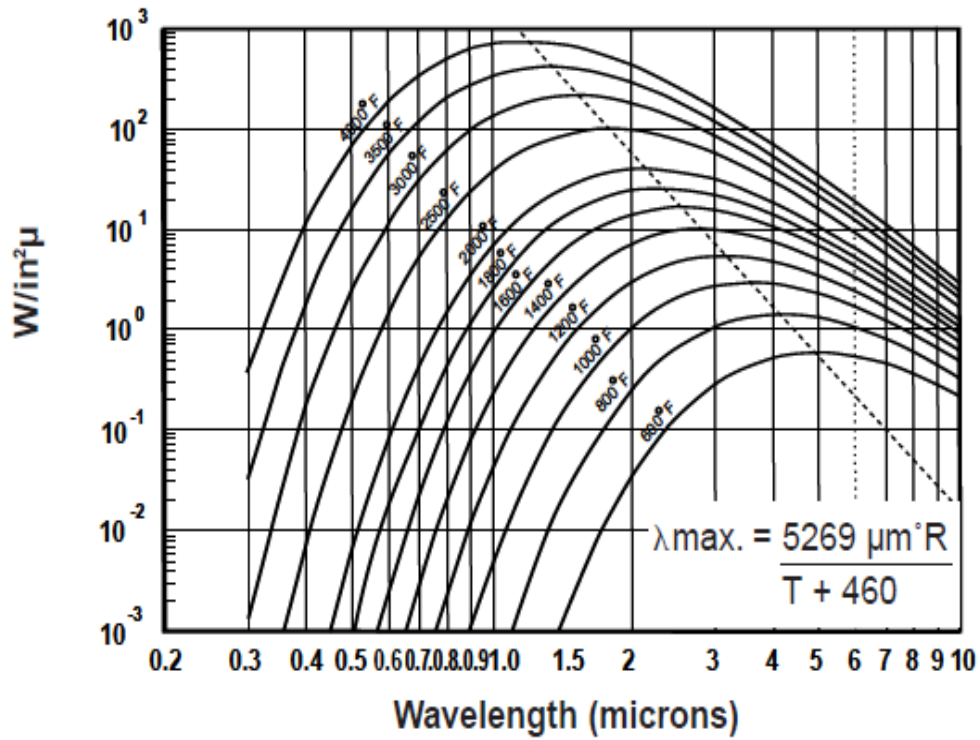


Fig: 3.3 Plank's curve log scale

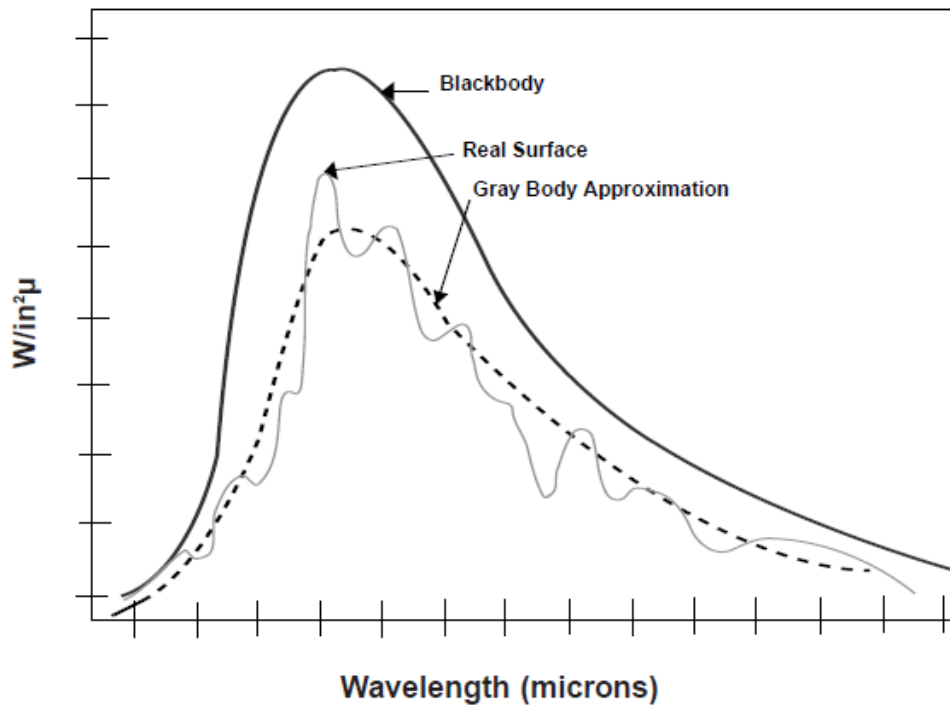


Fig: 3.4 Radiant power vs. wavelength

❖ **Stefan- Boltzmann**

Stefan-Boltzmann Equation is used to calculate the amount of power (watts) radiated by a black body surface of temperature T.

$$\frac{\text{WattRadiated}}{\text{Area}} = \text{Constant} \times (\text{absoluteTemperature})^4$$

From this equation, it can be seen that the watts radiated from the object depend on the absolute temperature of the radiating surface to the fourth power. This means that a small increase in the temperature will produce a large increase in the radiated watts.

❖ **The View factor**

The Stefan- Boltzmann equation calculates the net energy radiated by the heater. It doesn't calculate how much of the radiated energy actually hits the product. There is a geometric relationship between the size of the heater and the product, and the distance between them determines how much of the radiated energy the product intercepts. This relationship is called the view factor.

❖ **Emissivity and Absorptivity**

Not all the radiant energy that reaches the product is absorbed. Some may be reflected, and some transmitted right through. Only absorbed energy will serve to heat the product. These are shown in figure (3.5)

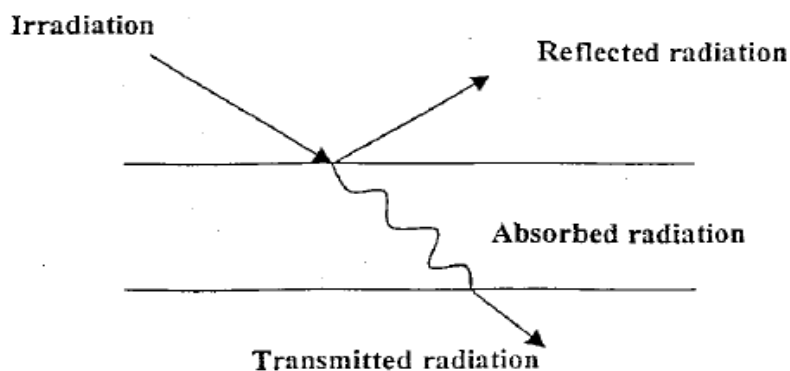


Fig: 3.5 Absorption, Reflection and Transmission by a finite medium

$$r = \frac{\text{Reflected Portion of Irradiation}}{\text{Total Irradiation}}$$

$$\alpha = \frac{\text{Absorbed Portion of Irradiation}}{\text{Total Irradiation}}$$

$$\tau = \frac{\text{Transmitted Portion of Irradiation}}{\text{Total Irradiation}}$$

Relation for the semitransparent surface is considered as:
 Total Incident Energy= Absorbed +Reflected +Transmitted

$$r + \alpha + \tau = 1 \quad (3.2)$$

3.4 Mathematical Model for Infrared Heater

The expression when an electric current is passed through a filament is shown below:

$$i(t) = \frac{U}{R} (1 - e^{-k_1 t}) + C_2 e^{k_2 t} K_{1,2} \quad (3.3)$$

$$= \frac{-1}{2RC} \left(1 \pm \sqrt{1 - \frac{4R^2 C}{L}} \right)$$

Where C_2 is constant

$$k_1 = R/L$$

$$k_2 = \frac{-1}{RC} + \frac{R}{L}$$

A Fourier equation is used to calculate the heating rate:

$$T = T_1 + (T_0 - T_1) e^{-\frac{2N}{\gamma_0} \frac{a^2}{\gamma_0}} \quad (a = C_\rho \gamma \lambda) \quad (3.4)$$

Where a is diffusivity,

T running temperature of the heating surface after T time,

T_0 = initial temperature of the heater

T_1 = temperature of the medium

N = coefficient of heat transfer

γ_0 = penetration depth of heat pulse

The heating element's reliability and stability are determined by the extent to which the heater remains constant over its service life. The relation (3.5) describes the rate of degradation

$$\xi = \xi_0 \exp\left(\frac{-Q}{RT}\right) \quad (3.5)$$

Where ξ_0 is a constant dependent on the composition and method of production of the material of the conducting phase, the electrical Insulator, or the casing; Q is the energy of activation of the aging process, which depends on the ambient conditions and the thermo- mechanical stability of the material of the heater; T is the working temperature of the heater.

3.4.1 Surface Energy Balance

The equation represents the rate of energy transfer from the surface of the heater (E_{out}) to the surface of the target (E_{in}) as being equal (3.6)

$$E_{out} - E_{in} = 0 \quad (3.6)$$

Consider a ceramic heater with a wire resistance of size D and length L having the thermal equilibrium of its surrounding. This equilibrium condition is only distributed when an electric current I flows through the wire. The first law of thermodynamics which is frequently used to determine unknown temperatures, is utilized to create an equation. Relevant terms include heat transfer by convection and radiation due to the electrical current passage through the wire and a change in internal energy storage. Determining the rate of change of temperature and applying the first law of thermodynamics to a system of length L about the wire, it follows:

$$E_g - E_{out} = E_{st} \quad (3.7)$$

Where the energy generation (E_g) due to the electric resistant heating is given by the equation 3.8

$$E_g = I^2 R_e L \quad (3.8)$$

Flow of energy by convection and net radiation is given by the equation:

$$E_{out} = h(\pi DL)(T - T_\infty) + \varepsilon\sigma(\pi DL)(T^4 - T_{sur}^4) \quad (3.9)$$

With the change of temperature, change of energy storage (E_{st}) is expressed as:

$$E_{st} = \frac{du}{dt} = \rho CV \frac{dT}{dt} \quad (3.10)$$

Where ρ is density

C is the specific heat

V is the volume of the wire,

$$V = \left(\frac{\pi D^2}{4}\right) L. \quad (3.11)$$

Substituting the rate equations (3.9) in to energy balance (3.8) and (3.10), it follows

$$I^2 R_e L - h(\pi DL)(T - T_\infty) - \varepsilon\sigma(\pi DL)(T^4 - T_{sur}^4) = \rho C \left(\frac{\pi D^2}{4} \right) L \frac{dT}{dt} \quad (3.12)$$

Rating of wire temperature change is given as:

3.4.2 Resistance Wire (Heating Element)

Material of heating element nickel-chromium (80%Ni-20%Cr) is used due to special mechanical properties in hot state and comparison of different infrared heaters is given below in table (3.1, 3.2)

Table: 3.1 Comparison of different Infrared Heaters

	Metal Sheath	Quartz Tube	Quartz Lamp	Catalytic	Flat Faced Panel	Ceramic
Radiant Efficiency	56 %	61 %	86 %	80 %	88 %	96 %
Physical Strength	High	Low	Very Low	High	Medium	Medium
Heat-Up/ Cool-down	Slow	Fast	Very Fast	Very Slow	Slow	Slow
Temperature	1400°F	1600°F	4000°F	800°F	1600°F	1300°F
Color Sensitivity	Low	Low	High	Low	Low	Low

To calculate resistance of the wire and output power of heater, equations 3.13 and 3.14 are used

$$\text{Resistance } (R) = \rho \left(\frac{l}{A} \right) (\Omega) \quad (3.13)$$

Where,

R= Resistivity, L= length (m), A= Area (m²)

$$\text{Power } (P) = \frac{V^2}{R} (KW) \quad (3.14)$$

Where, V= Voltage (220V single phase), R= Resistance (Ω)

Fig 3.6 shows the rate of change of wire temperature as per equation 3.12

Table: 3.2 Characteristics of commercially used Infrared Heat Sources

Infrared Source	Tungsten Filament		Nickel Chrome Resistance Wire			Wide Area Panels	
	Glass Bulb	T3 Quartz Lamp	Quartz Tube	Metal Sheath	Ceramic	Ceramic Coated	Quartz Face
Source Temperature (°F)	3000 - 4000 °F	3000 - 4000 °F	Up to 1600 °F	Up to 1500 °F	Up to 1600 °F	200 - 1600 °F	Up to 1700 °F
Brightness	Intense white	Intense White	Bright Red to Dull Orange	Dull to Bright Red	Dark to Dull Red	Dark to Cherry Red	Dark to Cherry Red
Typical Configuration	G-30 Lamp	3/8" Dia. Tube	3/8 or 1/2" Tube	3/8 or 1/2" Tube	Various Shapes	Flat Panels	Flat Panels
Type of Source	Point	Line	Line	Line	Small Area	Wide Area	Wide Area
Peak Wavelength (microns)	1.16	1.16	2.55	2.68	3 - 4	2.25 - 7.9	2.5 - 6
Maximum Power Density	1 kW/ft ²	3.9 kW/ft ²	1.3 - 1.75 kW/ft ²	3.66 kW/ft ²	Up to 3.6 kW/ft ²	3.6 kW/ft ²	5.76 kW/ft ²
Watts per Linear Inch	N/A	100	34 - 45	45 - 55	N/A	N/A	N/A
Conversion Efficiency Infrared Energy	86%	86%	40 - 62%	45 - 56%	45 - 50%	45 - 55%	45 - 55%
Response Time Heat/Cool	Seconds	Seconds	1 - 2 Minutes	2 - 4 Minutes	5 - 7 Minutes	5 - 8 Minutes	6 - 10 Minutes
Color Sensitivity	High	High	Medium	Medium	Medium	Low to Medium	Low to Medium
Thermal Shock Resistance	Poor	Excellent	Excellent	Excellent	Good	Good	Good
Mechanical Ruggedness	Poor	Fair	Good	Excellent	Good	Good	Fair
Chromalox Model	—	QR	QRT	RAD, URAD	RCH	CPL, CPLI, CPH	CPHI

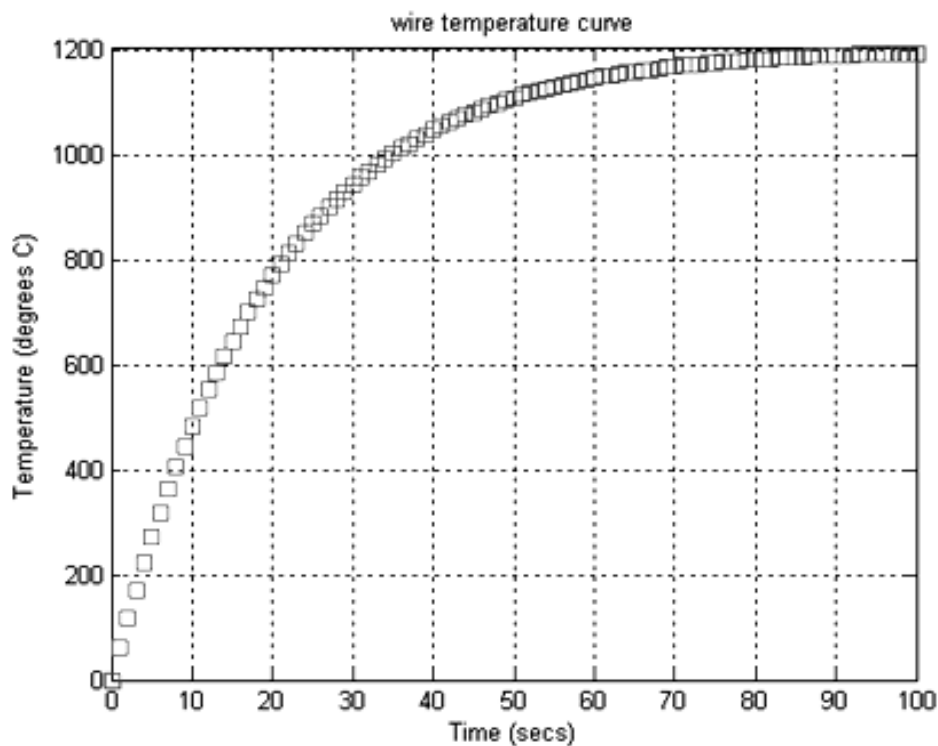


Fig: 3.6 Rate of Change of wire Temperature

3.5 Advantages of using an Infrared Heater

- ❖ It gives instant heating and has reduced operating cost
- ❖ Negligible maintenance: It does not have moving parts to wear out, and no air filters or lubrication are required

- ❖ Clean: It does not give a by-product of Combustion as fossil fuels; it is Safe and Efficient
- ❖ Zero Control flexibility: It can control heat at different zones at different temperatures.

3.6 Features of Ceramic Infrared Heater

- ❖ The efficient heat transfer to the target reduces the processing time and energy cost.
- ❖ The air in the equipment is not heated, and consequently, the ambient temperature may be kept at a normal level.
- ❖ It is possible to design compact and automatic constructions with high Controllability and safety.
- ❖ Heating is more uniform than conventional ovens because surface irregularities on the target have a small effect on the heat transfer rate.

3.7 Specification and Transfer Function

An approximate transfer function by open loop experiment data Using the Zeigler- Nichols process reaction method is expressed by equation (3.15)[32]

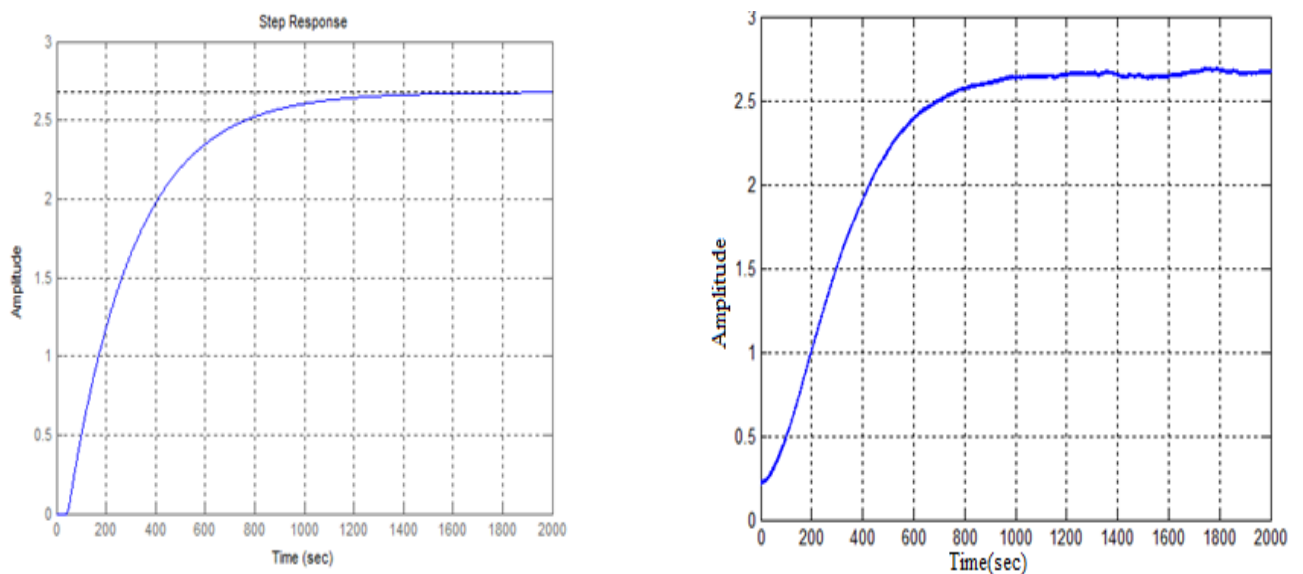


Fig: 3.7 Transfer function approximation using reaction curve method

From figure (3.8) the transfer function is obtained as below

$$G_{IR}(s) = \frac{[2.6770]e^{-46s}}{262s + 1} \quad (3.15)$$

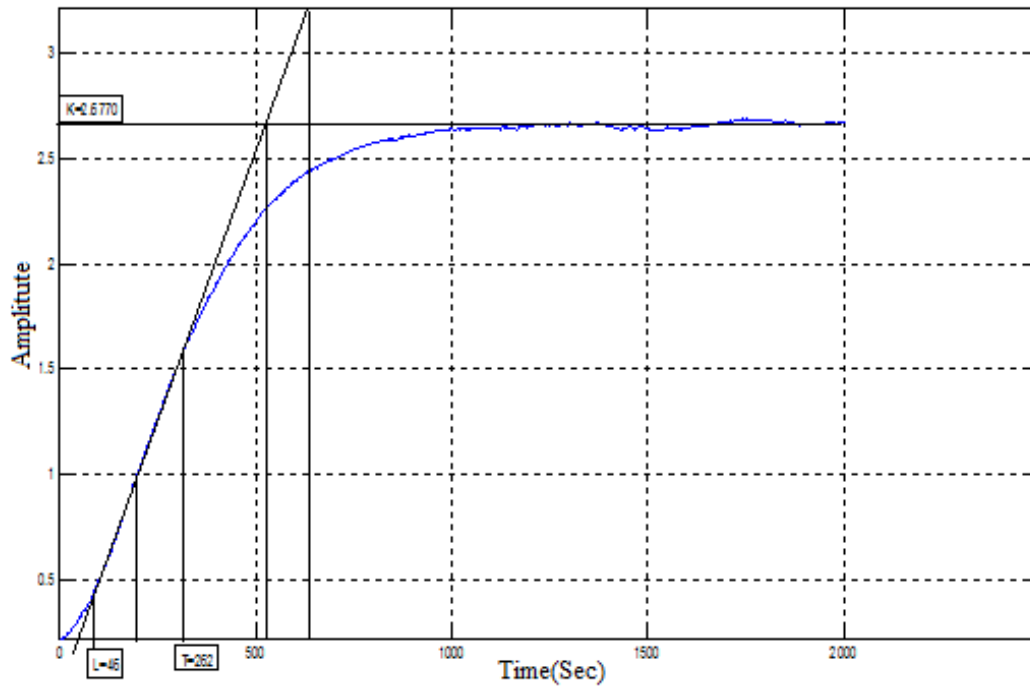


Fig: 3.8 Reaction Curve method for determination for transfer function

3.8 Application of Infrared Heater

- Heating plastic foils and sheets in the thermoforming machine
- Gelling PVC pasty coats on fabrics
- Heating GRP parts during production, Drying plastic emulsions
- Drying Skins, hides, and paint-sprayed leather, Quick- drying gummed paper
- Baking on powder coating, Tempering glass
- Curing epoxy resins, Drying raw tobacco
- Keeping meals worm, Healing processed cheese, Therapeutic medical radiation

3.9 Conclusion

This chapter presents the studies of different types of materials with specifications that are discussed, which helps us design the heating element with more effectiveness for desired applications, features of infrared heaters are also explained. An approximate transfer function by open loop experiment data using the Zeigler- Nichols process reaction method is expressed by the equation for analysis.

CHAPTER 4

CONTROLLER DESIGN

4.1 Introduction

PID Tuning determines the values of a PID controller proportional- integral – derivative gains to achieve desired performance and adhere to design specifications.

Types of Controller tuning methods include the trial and error and process reaction curve methods. The most common classical controller tuning methods are the Zeigler- Nichols, and Cohen- Coon Methods. These methods are often used when the system's mathematical model is unavailable. The Zeigler- Nichols method can be used for both open and closed loop systems, while Cohen- Coon is used for open loop systems. A closed-loop system is a system that uses feedback control. In an open loop system, the output is not compared to the input [50]. The proportional, integral, and derivative values—abbreviated P, I, and D, respectively—are three distinct constant parameters used in the PID controllers' calculation process.

The proportional term is given by:

$$P_{out} = K_p e(\tau) \quad (4.1)$$

For a given change in the error, a high proportional gain causes a significant change in the output.

The integral term is given by:

$$I_{out} = K_i \int_0^t e(\tau) d\tau \quad (4.2)$$

The derivative term is given by:

$$D_{out} = K_d \frac{d}{dt} e(\tau) \quad (4.3)$$

Equation (4.4) below shows the structure of PID Controllers:-

$$U(t) = K_p \left[e(\tau) + \frac{1}{T_i} \int_0^t e(\tau) d\tau + T_d \frac{de(\tau)}{dt} \right] \quad (4.4)$$

Where U = Control Signal, e = is the difference between the current value and set point
 Effect of PID tuning on the system is shown in table (4.1).

Table4.1: Effect of PID Tuning on System

Parameter	Rise Time	Peak Overshoot	Settling Time	Steady State Error
K_p	Decrease	Increase	Small Change	Decrease
K_i	Decrease	Increase	Increase	Decrease Significantly
K_d	Minor Decrease	Minor Decrease	Minor Decrease	No Effect in Theory

4.1.1 The Extremes: Instability or No Response

The loop performance must fall between two extremes. First, the loop must respond to a change in set point and to disturbance, i.e., an error or difference in the process, and the set point must eventually result in the manipulation of the output so that the error is eliminated. If the gain, Integral, and derivative of the loop are turned to zero, there will be no response. The other extreme is instability. An unstable loop will oscillate without a bound. A set point change will cause the loop to start oscillating, the oscillations will continue, and the worst oscillation will grow. Proper tuning of a loop will allow the loop to respond to set point changes and disturbances without causing instability.

Informal methods:

These are several rules of thumb for determining the quality of the tuning of a control loop. Traditionally, quarter wave decay, as shown in figure (4.1) has been considered the optimum decay ratio. This criterion is used by the Zeigler- Nichols tuning method, among others. No single combination of tuning parameters will provide quarter wave decay.

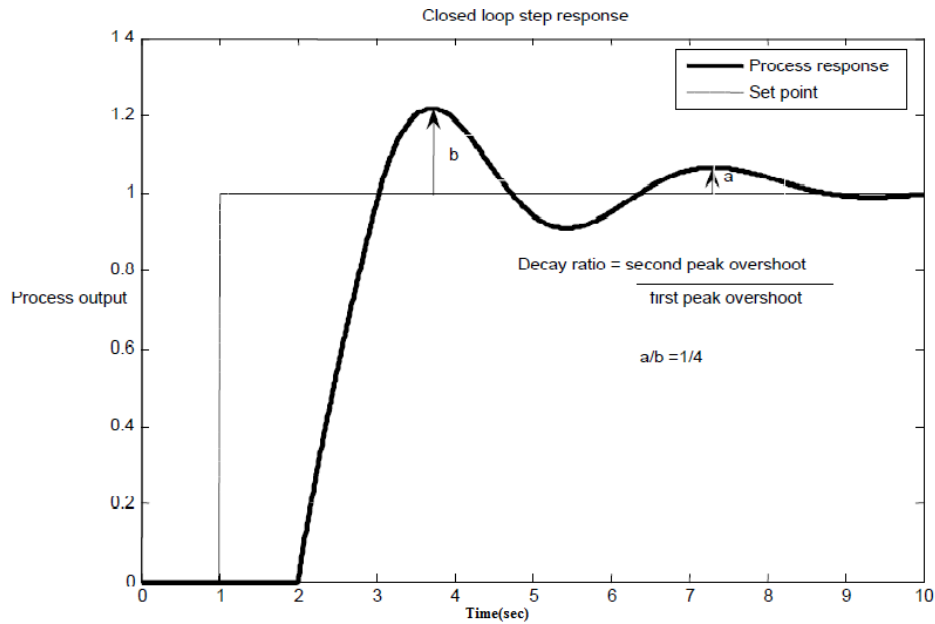


Fig: 4.1 Quarter wave decay

If the gain is increased and the correct amount decreases the reset rate, the decay ratio will remain the same. Quarter wave decay is not necessarily the best tuning for either disturbance rejection or set point response.

4.1.2 Mathematical Criteria- Minimization of Index

There are several criteria for evaluating tuning that is based on integrating the error following a disturbance or set point change. These methods are not used to test control loops in actual plant operation because the usual process noise and random disturbance will affect the outcome. These are used in Control theory education and research using stimulated processes. The indices provide a good way of comparing different Controller tuning methods and Control Algorithm [14].

IAE – Integral of the absolute value of error

$$\int |e| dt$$

ISE – Integral of error squared

$$\int e^2 dt$$

ITAE – Integral of time times the absolute value of error

$$\int t |e| dt$$

ITSE – Integral of time’s error squared

$$\int t e^2 dt$$

Of these methods, the IAE & ISE are the most common.

4.2 Zeigler- Nichols Tuning Methods

Using a tangent line drawn through the steepest portion of the curve (the point of inclination), Zeigler –Nichols presented a graphical method, which is depicted in figure (4.2) [7]. The line continuous below the original process value and the time between the output change and the point at which the tangent line crosses the original process line is called lag. The slope of the line is calculated. The original Zeigler- Nichols formula used the slope or the rate of change rather than the time.

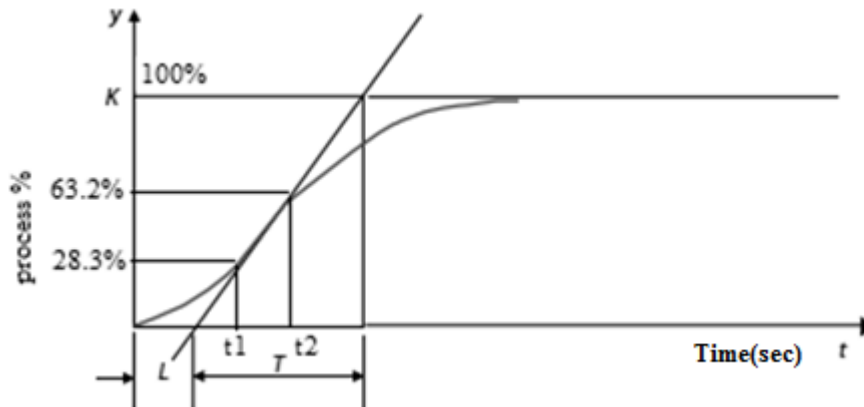


Fig: 4.2 Two Point Method

A point equal to 63.2% of the value between the original and the ultimate process measurement is made on for tangent line. The time between the end of pseudo dead time and the time at which the tangent line goes through the 63.2% point is the processing time constant. This method will give the results when the process is a dead time plus first-order lag. As the minor lag values increase, the tangent and point method provides a shorter time constant.

This technique states that at particular times the change in process by 28.3% (t_1) and 63.2% (t_2) of the overall process change. Then applying two formulas, the pseudo dead time and process time constant are determined.

$$\text{Process- time Constant (T)} = 1.5 (t_2 - t_1)$$

$$\text{Pseudo- dead time (L)} = t_1 - (t_2 - t_1)$$

4.2.1 Zeigler Nichols Open Loop Tuning Method

The first approach is referred to as the "reaction Curve" approach and uses an open loop. The gain K, the pseudo dead time (L), and the processing time constant are calculated using this method to determine the actual values of the assumed process model (T), the gain, integral, and derivative are calculated in table 4.2

Table: 4.2 Ziegler –Nichols open loop tuning values

Controller	Gain(Kp)	Integral Time(Ti)	Derivative time (Td)
PID	$1.2 \left(\frac{T}{K.L} \right)$	2L	$\frac{1}{2}(L)$

4.2.2 Zeigler Nichols Closed Loop Tuning Method

The gain necessary to make the loop oscillate with constant amplitude is established by the closed loop (ultimate gain technique). Most loops will oscillate if the gain is high enough.

The following steps are taken:

1. Put the controller in automated mode with a little gain and no integral or derivative.
2. Gradually increase gain and make minor set point adjustments until oscillation begins.
3. Modify gain to keep oscillations' amplitude constant.
4. Take note of the gain (Ultimate gain Kcr) and period (Ultimate period Pcr) in the figure.

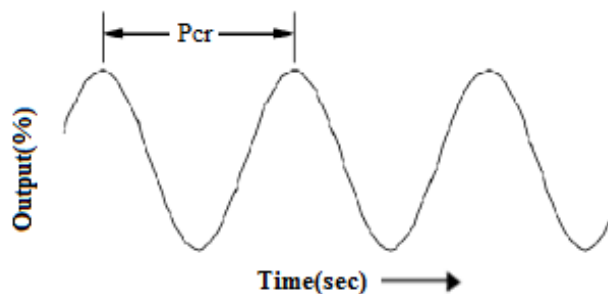


Fig: 4.3 Constant amplitude oscillations

The gain, Integral and derivative are calculated as shown in Table 4.

Table: 4.3 Zeigler Nichols closed loop Tuning Values

Controller	Gain (Kp)	Integral Gain(Ki)	Derivative Gain(Kd)
PID	0.6 Kcr	2/Pcr	Pcr/8

4.3 Cohen- Coon Method

The Cohen- Coon method is similar to Zeigler- Nichols reaction rate method in that it makes use of the First Order plus Delay time (FOPDT) model for developing the tuning parameters. The parameters have more mathematical operations [50]. As can be seen from Table 4.4, the Cohen- Coon method will result in a higher gain than the Zeigler- Nichols method.

4.4 Åström- Hägglund Method

Åström and Hägglund provide a modification to the Zeigler-Nichols approach. They suggest utilizing a relay feedback system. Åström and Hägglund recognized that the Zeigler- Nichols continuous cycling method identifies the point $\left(-1/K_u, 0\right)$ on the Nyquist curve and moves it to a predefined point [56]. With PID Control, it is possible to move a given point on the Nyquist curve to an arbitrary position, as shown in figure 4.4.

Table: 4.4 Cohen-Coon Tuning Values

PID Controller	Gain(Kp)	Integral Time(Ti)	Derivative Time(Td)
PID	$\frac{1}{K} * \left(\frac{T}{L}\right) \left(\frac{4}{3} + \frac{L}{4T}\right)$	$L \left(\frac{32 + 6(L/T)}{13 + 8(L/T)}\right)$	$L \left(\frac{4}{11 + ((2 * L) / T)}\right)$

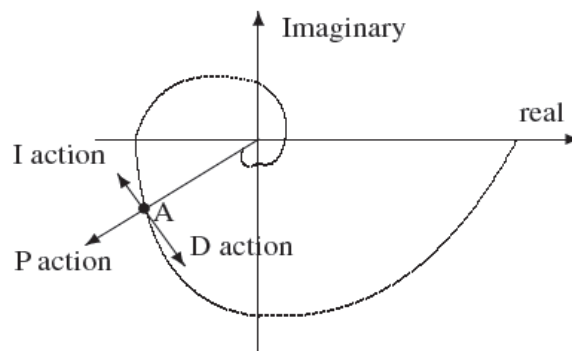


Fig: 4.4 Effect of Changing the PID parameter on the Nyquist plot

By increasing the gain, the arbitrary point (A) moves in the direction of $G(j\omega)$. Changing the I, or D action moves the point in the orthogonal direction.

Let ω be the frequency that corresponds to A. The frequency response of the controller ω is:

$$H_c(j\omega) = K_p \left(1 + \frac{1}{T_i j\omega} + j\omega T_d \right) \quad (4.5)$$

In the Zeigler- Nichols method, point A (denoted as $r_a e^{j(\pi+\phi_a)}$) is initially the point of marginal stability, located at $\left(-1/K_u, 0 \right)$ a frequency $\omega_u = 2\pi/T_u$

When moving from arbitrary point A to a predefined position B, a convenient choice for point A is the ultimate point. Point B can be determined by a desired gain margin and phase margin and is written in polar coordinates as $B = r_b e^{j(\pi+\phi_b)}$. Assuming that the PID controller at frequency ω_0 is $G_c(s) = r_c e^{j(\phi_c)}$. Then,

$$r_b e^{j(\pi+\phi_b)} = r_a \cdot r_c e^{j(\pi+\phi_c+\phi_a)} \quad (4.6)$$

Therefore, $r_c = r_b/r_a$ and $\phi_c = \phi_b - \phi_a$

So, based on the above analysis, PID controllers can be designed as follows

$$K_p = \frac{r_b \cos(\phi_b - \phi_a)}{r_a}, \quad \omega_0 T_d - \frac{1}{\omega_0 T_i} = \tan(\phi_b - \phi_a) \quad (4.7)$$

It is found that, T_i and T_d are not unique. To get a unique PID design, it is usual practice to set $T_d = \alpha T_i$ where α a constant is. Given an α , T_i and T_d can be obtained uniquely from

$$T_i = \frac{1}{2\alpha\omega_0} \left(\tan(\phi_b - \phi_a) + \sqrt{4\alpha + \tan^2(\phi_b - \phi_a)} \right), \quad T_d = \alpha T_i \quad (4.8)$$

By inspection, it is found that Zeigler-Nichols tuning formula is a special case when $\alpha = 1/4$. The Astrom-Hügglund formula for PID controller is given in table 4.5

Table: 4.5 Åström-Hägglund Tuning values

PID Controller	Gain(Kp)	Integral Time(Ti)	Derivative Time(Td)
PID	$k_u r_b \cos(\phi_b)$	$\frac{-T_u}{\pi} \left(\frac{1 + \sin(\phi_b)}{\cos(\phi_b)} \right)$	$\frac{-T_u}{4\pi} \left(\frac{1 + \sin(\phi_b)}{\cos(\phi_b)} \right)$

This method identifies and moves only one point on the Nyquist curve to a desired position.

4.5 Simulation Results

4.5.1 Zeigler Nichols Open Loop Method

By putting up the value of the transfer function of ceramic IR heater having $K = 2.6770$ rad/sec, $L=46$ sec and $T=262$ sec in Table 4.2 for Zeigler Nichols open loop and we calculate the value of parameters K_p , K_i and K_d are found as 2.5532, 0.02775 and 58.7236

So controller value will be as:

$$C_{zno}(s) = 2.5532 + \frac{0.02775}{s} + 58.7326s$$

4.5.2 Zeigler Nichols Closed Loop Method

If we put up the value of the transfer function of ceramic IR heater having $K = 2.6770$ rad/sec, $L=46$ sec, and $T=262$ sec in Table 4.3 for Zeigler Nichols closed loop, the calculated t value will be $K_p=2.15$, $K_i=0.027389$ and $K_d=42.193$

So the value of the controller will be as:

$$C_{znc}(s) = 2.15 + \frac{0.027389}{s} + 42.193s$$

4.5.3 Cohen-Coon Method

When we put the value of the transfer function of ceramic IR heater having gain $K = 2.6770$ rad/sec, $L=46$ sec and $T=262$ sec in Table 4.4 from Cohen-Coon method parameters are calculated, and we get the values of K_p , K_i and K_d as 2.8593, 0.0271 and 46.3487.

So value of the controller will be as:

$$C_{cc}(s) = 2.8593 + \frac{0.0271}{s} + 46.3487s$$

4.5.4 Åström-Hägglund Method

By putting up the value of the transfer function of ceramic IR heater having $K = 2.6770$ rad/sec, $L=46$ sec, and $T=262$ sec in Table 4.5 for Astrom Haggglund method, then we calculate the value of K_p , K_i , and K_d as 0.5184, 0.0038 and 17.7915

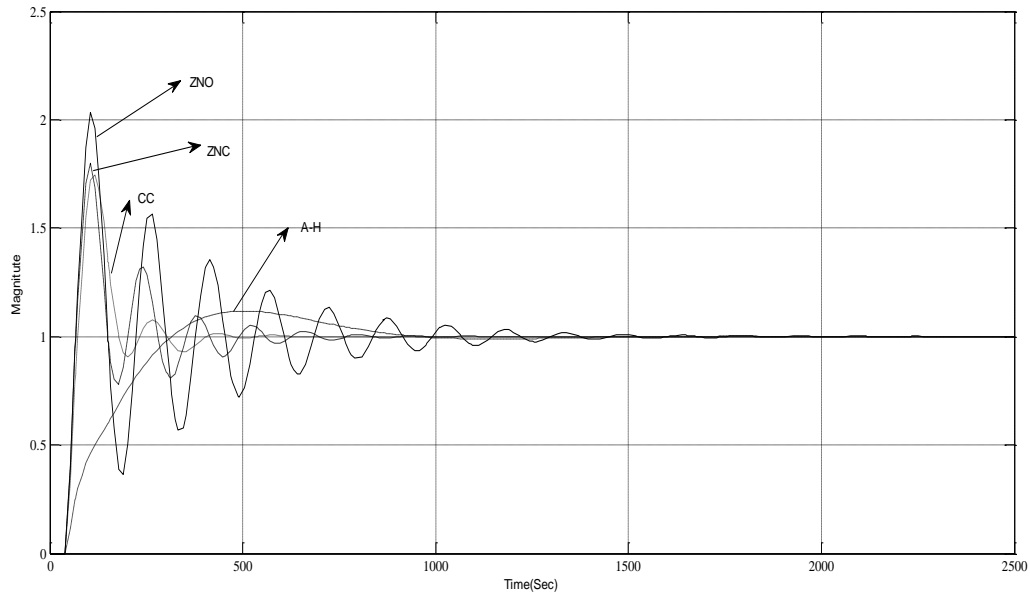


Fig: 4.5 Results of output by using different controllers (ZNO, ZNC, CC, AH)

So the value of the controller as

$$C_{AHM}(s) = 0.5184 + \frac{0.0038}{s} + 17.7915s$$

Using Mat lab simulation, we discovered the results as displayed. in figure 4.5

The analysis of simulation results (rise time, peak time, settling time, peak overshoot) is shown in Table 4.6

Table: 4.6 Performance table of different Conventional PID Controller for Ceramic IR heater control

Performance	Rise Time (T_r)	Peak Overshoot(M_p)	Peak Time (T_p)	Settling Time(T_s)	ISE	IAE
ZNO-PID	21.49	80.11	105.07	675.33	83.4	142.4
ZNC-PID	25.39	74.70	116.93	389.36	80.55	116.4
CC-PID	21.10	103.57	105.07	1270	143.8	269.8
AH-PID	207.91	11.82	504.27	850.55	96.58	183.2

4.6 Integer Order PID Design (IOPID)

It is possible to roughly calculate the plant model's derivatives of amplitude and phase concerning frequency using a new method for PID Controller tuning based on Bode's integrals. Phase and/or gain margins are frequently used to convey specifications. Because they are the measures of robustness together with the cross-over frequency. The slope of the Nyquist curve greatly impacts the performance and resilience of the closed-loop system at the cross-over frequency. [67], the parameters of a PID Controller for a desired phase margin and slope at a given frequency are determined.

4.6.1 Loop Slope Adjustment

Consider the loop transfer $L(j\omega) = C(j\omega)P(j\omega)$

Where

$$C(j\omega) = K_p \left(1 + \frac{1}{j\omega T_i} + j\omega T_d \right) \quad (4.9)$$

The slope of the Nyquist curve of the loop transfer function $L(j\omega)$ at ω_0 defined by ψ is equal to the phase of the derivative of $L(j\omega)$ at ω_0 . The derivative of the loop transfer function with respect to ω is computed as follows

$$\frac{dL(j\omega)}{d\omega} = G(j\omega) \frac{dC(j\omega)}{d\omega} + C(j\omega) \frac{dG(j\omega)}{d\omega} \quad (4.10)$$

Furthermore:

$$\ln G(j\omega) = \ln(|G(j\omega)|) + j\angle G(j\omega)$$

The ideal shape of the open loop transfer functions is of the form:

$$L(s) = \left(\frac{\omega_c}{s} \right)^\gamma, \gamma \in R \quad (4.11)$$

Where ω_c is the gain crossover frequency, that is, $|L(j\omega_c)| = 1$ the parameters γ is the slope of the magnitude curve on a log-log scale, and may assume integer as well non-integer clause? In fact, the transfer function $L(s)$ is a fractional-order differentiator for $\gamma < 0$ and a fractional-

order Integrator $\gamma > 0$. $\gamma = 1$ Both fractional order differentiator and Integrator represent the Integer order controller.

The Bode diagrams $L(s)$ ($1 < \gamma < 2$) are very simple. The amplitude curve is a straight line of a constant slope of -20γ db/decade, and the phase curve is a horizontal line at $-\frac{\gamma\pi}{2}$.

Let us now consider the unity feedback system represented in figure (4.6) with Bode's ideal transfer function $L(s)$ inserted in the forward path. This choice of $L(s)$ gives a closed system with the desirable insensitive property to gain changes. If the gain changes, the crossover frequency ω_c will vary, but the phase margin of the system remains $PM = \pi(1 - \gamma/2)$ rad, independent of the value of the gain [46].

A transfer function $P(s)$ represents the IR heater's mathematical model, with first order plus time delay as:

$$P(s) = \frac{K}{sT + 1} e^{-Ls} \tag{4.12}$$

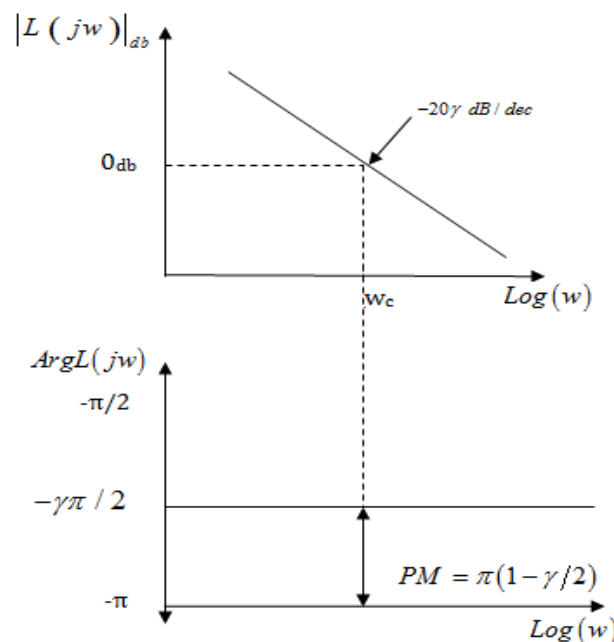


Fig.4.6 Bode diagrams of amplitude and phase of $L(s)$ for $1 < \gamma < 2$.

The frequency response is given as

$$P(j\omega) = \frac{K}{j\omega T + 1} e^{-Lj\omega}$$

$$P(j\omega) = \frac{K}{\sqrt{1+(\omega T)^2}} e^{-(\tan^{-1}(\omega T)+L\omega)} \quad (4.13)$$

The gain and phase of the plant are as follow:

$$P(j\omega) = \frac{K}{\sqrt{1+(\omega T)^2}} \quad (4.14)$$

$$\text{Arg}[P(j\omega)] = -\tan^{-1}(\omega T) - L\omega \quad (4.15)$$

4.6.2 Design Specification for IOPID Controller

Phase Margin & Gain Crossover frequency

Gain and phase margin has always been crucial robustness parameters. The relationship between the phase margin and the system's damping is well recognized. The equations that define the phase margin ϕ_{pm} and gain crossover frequency ω_{cp} are:

$$|G(j\omega_{cp})| = |C(j\omega_{cp})P(j\omega_{cp})|_{dB} = 0 \text{ dB} \quad (4.16)$$

$$\text{Arg}[G(j\omega_{cp})] = \text{Arg}[C(j\omega_{cp})P(j\omega_{cp})] = -\pi + \phi_{pm} \quad (4.17)$$

Where,

PID Controller in the frequency domain with crossover frequency is how $C(j\omega_{cp})$ is expressed, and PID Controller in the frequency domain with a crossover frequency $P(j\omega_{cp})$ is a frequency-domain Infrared Red (FOPID) controller with a crossover frequency? Infrared red (FOPID) controller in the frequency domain with crossover frequency.

The phase bode plot must be flat at a given gain crossover frequency since the plant's gain variation necessitates that the phase directions with respect to frequency be zero...

$$\left(\frac{d(\text{Arg}(G(j\omega)))}{d\omega} \right)_{\omega=\omega_c} = 0 \quad (4.18)$$

According to the PID Controller transfer function, we can get the frequency response for IOPID as:

$$C(j\omega) = K_p + \frac{K_i}{j\omega} + j\omega K_d \quad (4.19)$$

The gain and phase of $C(j\omega)$ are as follow

$$|C(j\omega)| = \sqrt{K_p^2 + \left(K_d\omega - \frac{K_i}{\omega}\right)^2} \quad (4.20)$$

$$\text{Arg}[C(j\omega)] = \tan^{-1}\left(\frac{K_d\omega^2 - K_i}{\omega K_p}\right) \quad (4.21)$$

Then, the open loop frequency responses are as follows;

$$|G(j\omega)| = |C(j\omega)P(j\omega)| \quad (4.22)$$

$$= \frac{K\sqrt{K_p^2 + \left(K_d\omega - \frac{K_i}{\omega}\right)^2}}{\sqrt{1 + \omega^2 T^2}} \quad (4.23)$$

$$\text{Arg}[G(j\omega)] = \tan^{-1}\left(\frac{K_d\omega^2 - K_i}{\omega K_p}\right) - \tan^{-1}(\omega T) - L\omega \quad (4.24)$$

According to the design specification given by equation (4.17), the phase $G(j\omega)$ can be expressed as in the form of ω_{cp} :

$$\text{Arg}[G(j\omega_{cp})] = \tan^{-1}\left(\frac{K_d\omega_{cp}^2 - K_i}{\omega_{cp} K_p}\right) - \tan^{-1}(\omega_{cp} T) - L\omega_{cp} = -\pi + \phi_{pm} \quad (4.25)$$

$$\frac{K_d\omega_{cp}^2 - K_i}{\omega_{cp} K_p} = \tan(-\pi + \phi_{pm} + \tan^{-1}(\omega_{cp} T) + L\omega_{cp}) \quad (4.26)$$

Then,

$$\frac{K_d\omega_{cp}^2 - K_i}{K_p\omega_{cp}} = A_1 \quad (4.27)$$

Where,

$$A_1 = \tan[\tan^{-1}(\omega_{cp} T) + L\omega_{cp} + \phi_{pm}] \quad (4.28)$$

And according to the design specification given by equation (4.18) about the robustness to gain variation in the plant,

$$\left(\frac{d(\text{Arg}(G(j\omega)))}{d\omega}\right)_{\omega=\omega_{cp}} = 0$$

So,

$$\begin{aligned}
&= \frac{d}{d\omega} \left(\tan^{-1} \left(\frac{K_d \omega_{cp}^2 - K_i}{\omega_{cp} K_p} \right) - \tan^{-1}(\omega_{cp} T) - L \omega_{cp} \right) \Big|_{\omega=\omega_{cp}} = 0 \\
&= \frac{1}{1 + \left(\frac{K_d \omega_{cp}^2 - K_i}{\omega_{cp} K_p} \right)^2} \frac{d}{d\omega_{cp}} \left(\frac{K_d \omega_{cp}^2 - K_i}{\omega_{cp} K_p} \right) - \frac{1}{1 + \omega_{cp}^2 T^2} \frac{d}{d\omega_{cp}} (\omega_{cp} T) - L = 0 \\
&= \frac{\omega_{cp}^2 K_p^2}{\omega_{cp}^2 K_p^2 + (K_d \omega_{cp}^2 - K_i)^2} \frac{d}{d\omega_{cp}} \left(\frac{K_d}{K_p} \omega_{cp} - \frac{K_i}{\omega_{cp} K_p} \right) - \frac{T}{1 + \omega_{cp}^2 T^2} - L = 0 \\
&= \frac{\omega_{cp}^2 K_p^2}{\omega_{cp}^2 K_p^2 + (K_d \omega_{cp}^2 - K_i)^2} \left(\frac{K_d}{K_p} + \frac{K_i}{\omega_{cp}^2 K_p} \right) - \frac{T}{1 + \omega_{cp}^2 T^2} - L = 0 \\
&= \frac{\omega_{cp}^2 K_p^2}{\omega_{cp}^2 K_p^2 + (K_d \omega_{cp}^2 - K_i)^2} \left(\frac{\omega_{cp}^2 K_d + K_i}{\omega_{cp}^2 K_p} \right) - \frac{T}{1 + \omega_{cp}^2 T^2} - L = 0 \\
&= \frac{K_p (\omega_{cp}^2 K_d + K_i)}{\omega_{cp}^2 K_p^2 + (K_d \omega_{cp}^2 - K_i)^2} - \frac{T}{1 + \omega_{cp}^2 T^2} - L = 0 \\
&= \frac{K_p (\omega_{cp}^2 K_d + K_i)}{\omega_{cp}^2 K_p^2 + (K_d \omega_{cp}^2 - K_i)^2} = \frac{T}{1 + \omega_{cp}^2 T^2} + L
\end{aligned}$$

Where,

$$B_1 = 1 + \omega_{cp}^2 T^2 \quad (4.29)$$

$$= \frac{K_p (\omega_{cp}^2 K_d + K_i)}{\omega_{cp}^2 K_p^2 + (K_d \omega_{cp}^2 - K_i)^2} = \frac{T}{B_1} + L \quad (4.30)$$

Then, as per the design specification given by equation (4.18), we established an equation about K_p

$$\begin{aligned}
|G(j\omega_{cp})| &= |C(j\omega_{cp})| |P(j\omega_{cp})| = 1 \\
&\Rightarrow \frac{K \sqrt{K_p^2 + \left(K_d \omega_{cp} - \frac{K_i}{\omega_{cp}} \right)^2}}{\sqrt{1 + \omega_{cp}^2 T^2}} = 1 \\
&\Rightarrow \sqrt{K_p^2 + \left(K_d \omega_{cp} - \frac{K_i}{\omega_{cp}} \right)^2} = \frac{\sqrt{1 + \omega_{cp}^2 T^2}}{K}
\end{aligned} \quad (4.31)$$

Squaring on both side,

$$K_p^2 + \left(\frac{K_d \omega_{cp}^2 - K_i}{\omega_{cp}} \right)^2 = \frac{1 + \omega_{cp}^2 T^2}{K^2}$$

Divide both sides by K_p^2

$$1 + \left(\frac{K_d \omega_{cp}^2 - K_i}{\omega_{cp} K_p} \right)^2 = \frac{1 + \omega_{cp}^2 T^2}{K^2 K_p^2}$$

By putting the values of A_1 and B_1

$$1 + A_1^2 = \frac{B_1}{K_p^2 K^2}$$

$$K_p^2 = \frac{1}{K^2} \left(\frac{B_1}{1 + A_1^2} \right)$$

$$K_p = \frac{1}{K} \sqrt{\frac{B_1}{1 + A_1^2}} \quad (4.32)$$

For the determination of K_d

$$\frac{K_d \omega_{cp}^2 - K_i}{K_p \omega_{cp}} = A_1$$

$$K_d \omega_{cp}^2 - K_i = A_1 K_p \omega_{cp} \quad (4.33)$$

By using equation (4.30)

$$K_d \omega_{cp}^2 + K_i = \left(\frac{T}{B_1} + L \right) (K_p \omega_{cp}^2 + K_p A_1^2 \omega_{cp}^2) \quad (4.34)$$

Adding equation (4.33) and (4.34) we get,

$$2K_d \omega_{cp}^2 = \left(\frac{T}{B_1} + L \right) (K_p \omega_{cp}^2 + K_p A_1^2 \omega_{cp}^2) + A_1 K_p \omega_{cp}$$

$$2K_d \omega_{cp}^2 = \omega_{cp}^2 K_p \left(\left(\frac{T}{B_1} + L \right) (1 + A_1^2) + \frac{A_1}{\omega_{cp}} \right)$$

$$2K_d = K_p \left[\left(\frac{T}{B_1} + L \right) (1 + A_1^2) + \frac{A_1}{\omega_{cp}} \right]$$

$$\begin{aligned}
K_d &= \frac{1}{2} K_p \left[\frac{T}{B_1} + \frac{T}{B_1} A_1^2 + L + L A_1^2 + \frac{A_1}{\omega_{cp}} \right] \\
K_d &= \frac{1}{2} \left[K_p \left(\frac{T + B_1 L}{B_1} + A_1^2 \left(\frac{T + L B_1}{B_1} \right) \right) + A_1 \omega_{cp}^{-1} \right] \\
K_d &= \frac{1}{2} \left[K_p \left(\frac{T + B_1 L}{B_1} \right) (1 + A_1^2) + A_1 \omega_{cp}^{-1} \right]
\end{aligned} \tag{4.35}$$

Putting the value of K_p from equation (4.32) in equation (4.35)

$$\begin{aligned}
&= \frac{1}{2} \left[\frac{1}{K} \sqrt{\frac{B_1}{1 + A_1^2}} \left(\frac{T + B_1 L}{B_1} \right) (1 + A_1^2) + \frac{1}{K} \left(\sqrt{\frac{B_1}{1 + A_1^2}} \right) A_1 \omega_{cp}^{-1} \right] \\
&= \frac{1}{2} \left[\frac{1}{K} \sqrt{\frac{1 + A_1^2}{B_1}} (T + L B_1) + K_p A_1 \omega_{cp}^{-1} \right] \\
K_d &= \frac{1}{2K} \left[\sqrt{\frac{1 + A_1^2}{B_1}} (T + L B_1) + A_1 \omega_{cp}^{-1} \sqrt{\frac{B_1}{1 + A_1^2}} \right]
\end{aligned} \tag{4.36}$$

Similarly, K_i can be determined by subtracting equation (4.33) from (4.34)

$$\begin{aligned}
2K_i &= \left(\frac{T}{B_1} + L \right) (K_p \omega_{cp}^2 + K_p A_1^2 \omega_{cp}^2) - A_1 K_p \omega_{cp} \\
2K_i &= \frac{T}{B_1} K_p \omega_{cp}^2 + \frac{T}{B_1} K_p A_1^2 \omega_{cp}^2 + L K_p \omega_{cp}^2 + L K_p A_1^2 \omega_{cp}^2 - A_1 K_p \omega_{cp} \\
2K_i &= K_p \omega_{cp}^2 \left[\frac{T}{B_1} + \frac{T}{B_1} A_1^2 + L + L A_1^2 \right] - A_1 K_p \omega_{cp} \\
2K_i &= K_p \omega_{cp}^2 \left[\left(\frac{T + L B_1}{B_1} \right) + A_1^2 \left(\frac{T + L B_1}{B_1} \right) \right] - A_1 K_p \omega_{cp} \\
2K_i &= K_p \omega_{cp}^2 \left[\left(\frac{1 + A_1^2}{B_1} \right) (T + L B_1) \right] - A_1 K_p \omega_{cp} \\
2K_i &= \frac{1}{K} \sqrt{\frac{B_1}{1 + A_1^2}} \times \left(\frac{1 + A_1^2}{B_1} \right) (T + L B_1) \omega_{cp}^2 - A_1 K_p \omega_{cp}
\end{aligned}$$

$$K_i = \frac{1}{2K} \sqrt{\frac{1+A_1^2}{B_1}} (T\omega_{cp}^2 + LB_1\omega_{cp}^2) - A_1\omega_{cp} \sqrt{\frac{B_1}{1+A_1^2}} \quad (4.37)$$

Thus, we found the values of K_p , K_i and K_d .

According to the Bode and Nyquist plot, the phase margin and gain margin for the process plant are displayed in figure 4.7.

From figure 4.7, we found the value of ω_{cg} and ϕ_{pm} as 0.008 rad/sec and 80° , respectively.

By putting up the value of the transfer function of ceramic IR heater having $K=2.6770$, $L=46$, and $T= 262$ in equations (4.32),(4.36), and (4.37), and the K_p , K_i , and K_d are calculated as 0.9768, 0.0063,25.6246

So the controller will be as:

$$C(s) = 0.9768 + \frac{0.0063}{s} + 25.6246s$$

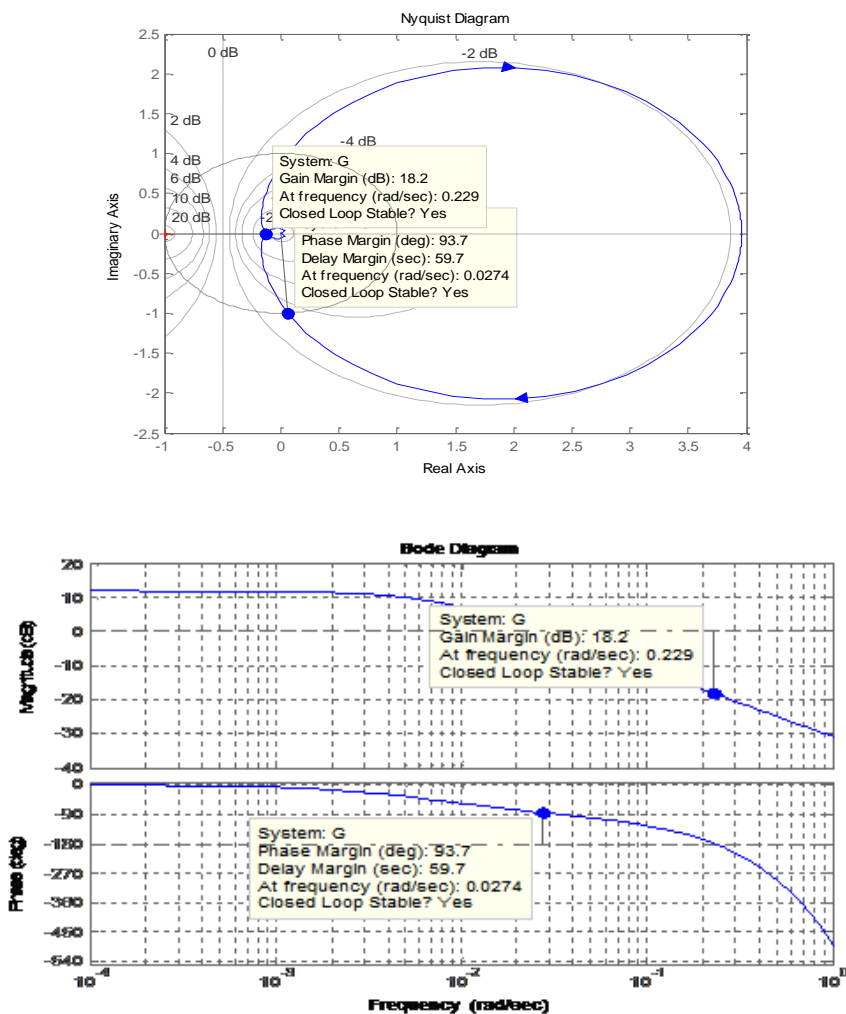


Fig 4.7 Nyquist plot and Bode plot of ceramic IR plant

By using Mat lab simulation, we found the output as shown in figure (4.8)

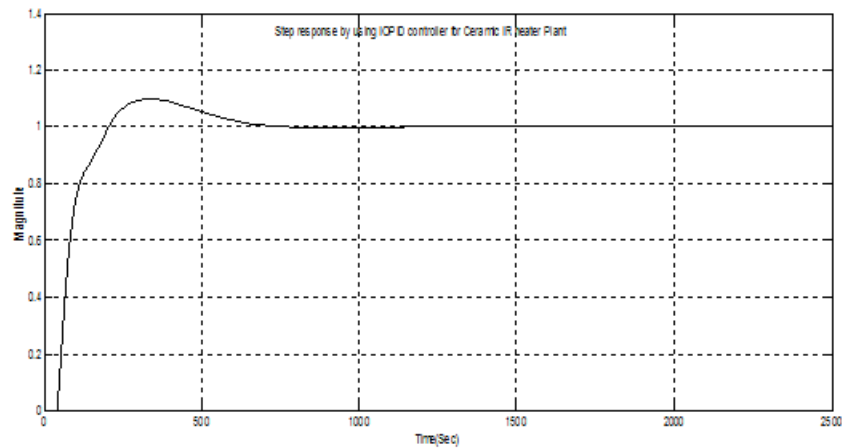


Fig. 4.8 Step response of IOPID controller with Ceramic IR heater Plant

The value of performance parameter is shown in table 4.7

Table: 4.7 Performance table of IOPID Controller for Ceramic IR Heater

Performance	Rise Time (T_r)	Peak Overshoot(M_p)	Peak Time(T_p)	Settling Time(T_s)	ISE	IAE
IOPID	112.41	9.8	341.91	613.86	66.92	114.8

4.7 Fractional Order PID Controller (FOPID)

Fractional order calculus (FOC) is the area of mathematics that deals with differentiation and integration under arbitrary orders of operations, meaning that orders other than integers can be real or even complex numbers. Recent discussions on the real-world applications of Fractional Order Calculus (FOC) have generated significant implications for theoretical research today [63][67]. A fractional order continuous-time live or time-invariant dynamical system can be described by a fractional order differential equation as shown by the equation (4.38).

$$\begin{aligned}
 & a_n D^{\alpha_n} y(t) + a_{n-1} D^{\alpha_{n-1}} y(t) + \dots + a_0 D^{\alpha_0} y(t) \\
 & = b_m D^{\beta_m} u(t) + b_{m-1} D^{\beta_{m-1}} u(t) + \dots + \beta_0 D^{\beta_0} u(t)
 \end{aligned} \tag{4.38}$$

Where $u(t)$ is the input signal, $y(t)$ is the output signal. $D^\gamma \equiv {}_0D_t^\gamma$ represents fractional derivative, a^k with $(k=0, \dots, n)$ and b^k with $(k=0, \dots, m)$ denote constants and α_k with $(k=0, \dots, n)$ and β_k with $(k=0, \dots, m)$ are arbitrary real numbers.

The very first and most important criterion when designing a control system is closed-loop stability. It is well known that a system of integer order continuous time and linear time invariance is stable if and only if all of the roots of its characteristic polynomial have negative real parts.

In other words, the roots must lie in the left half of the complex plane. Investigation of the stability of the fractional order systems represents the more complicated issue.

The stability of compensated fractional Order systems can be analyzed via the theorem of Mitigation or the definition from I. Petras, which describes the way of mapping the poles from s^α -plane into the w - plane. An interesting result is that the poles of the stable fractional order system can be located even in the right half of such a complex plane. This fact is illustrated in figure 4.9 where the stability region for a commensurate fractional order linear time Invariant system with order $0 < \alpha < 1$

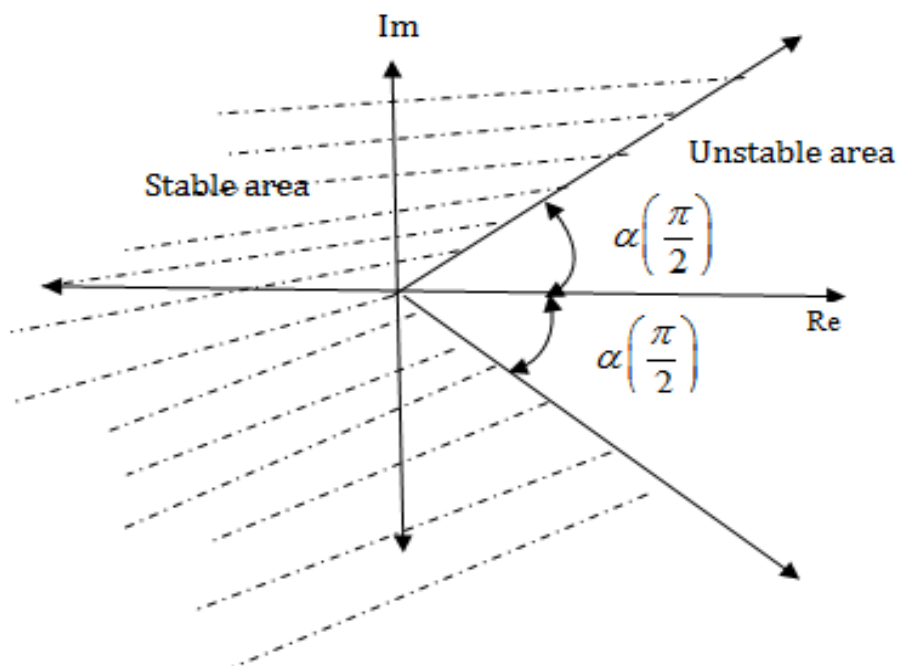


Fig.4.9 Region of stability for the commensurate fractional order system with $0 < \alpha < 1$.

The situation for $\alpha = 1$ is visualized in figure 4.10. In this case, the region of stability corresponds to the classical s- plane.

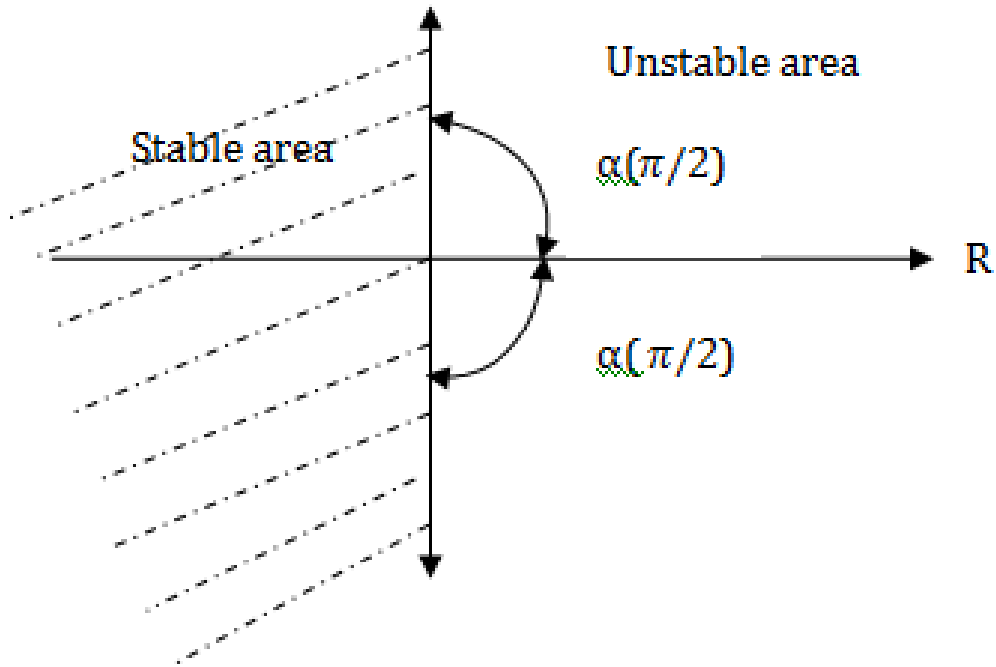


Fig 4.10 Region of stability for the commensurate fractional order system with $\alpha=1$.

Finally, figure 4.11, shows the region of the stability under assumption of $1 < \alpha < 2$.

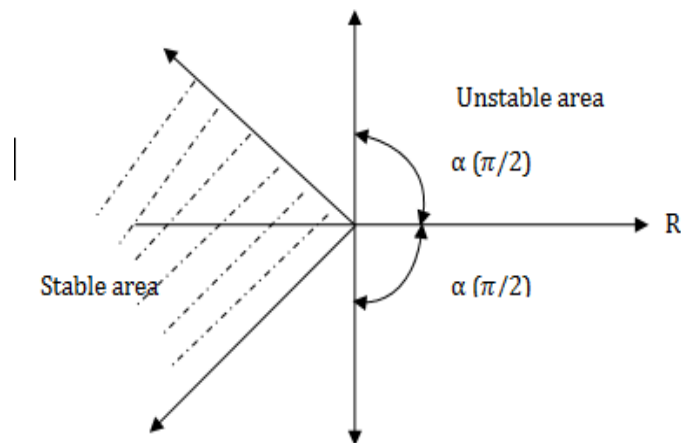


Fig 4.11 Region of stability for the commensurate fractional order system with $1 < \alpha < 2$.

4.7.1 Approximation of Integer Order Fractional Order System

An infinite dimensional LTI filter is mathematically identical to a fractional order linear time-invariant (LTI) system. Therefore, higher-order polynomials with integer order differ-integral operators can be used to approximate a fractional order system. The realization of fractional order differ- integrators in integer order can be carried out in two ways [17].

- Continuous time realization
- Discrete time realization

Using Oustaloup's recursive filter, we employed continuous time realization to convert our fractional order system into an integer order system

4.7.2 Oustaloup's Recursive Filter

Within a selected frequency band, Oustaloup's recursive filter provides a very good fitting to the fractional order elements. Let us assume that the expected fitting range is (ω_l, ω_h) . For filter, it can be written as

$$G_f(s) = K \prod_{-N}^N \frac{s + w'_k}{s + w_k}$$

Where the poles, zeros, and gain of the filter can be evaluated.

$$w'_k = w_b \left(\frac{w_h}{w_l} \right)^{\frac{k+N+1/2(1-\gamma)}{2N+1}}, K = w_h^\gamma; w_k = w_l \left(\frac{w_h}{w_l} \right)^{\frac{k+N+1/2(1+\gamma)}{2N+1}}$$

Where γ is the order of the differentiation,, $2N + 1$ is the order of the filter, and the frequency fitting range is given by (ω_l, ω_h) . The filter can be designed such that it may fit very well within the frequency range of the fractional order differentiator.

$$C(s) = \frac{133.3 s^9 + 4.724e004 s^8 + 3.415e006 s^7 + 3.416e007 s^6 + 7.945e007 s^5 + 2.87e007 s^4 + 3.305e006 s^3 + 1.388e005 s^2 + 1652 s + 4.435}{s^9 + 664.1 s^8 + 1.131e005 s^7 + 2.163e006 s^6 + 1.13e007 s^5 + 6.807e006 s^4 + 1.121e006 s^3 + 2.07e004 s^2 + 98.11 s}$$

4.8 Design of Fractional order PID Controller

The elegant and efficient fractional order modification of Conventional PID Controllers has been introduced by I. Podlubny [8]. They are known as $PI^\lambda D^\mu$ Controllers and can be described by the transfer function given by equation (4.39)

$$C(s) = K_p + K_i s^{-\lambda} + K_d s^\mu \quad (4.39)$$

Where, λ and μ are positive real numbers and K_p, K_i, K_d denote the proportional, integral, and derivative constant, respectively.

A negative unity feedback control system is shown in figure (4.12). The transfer function of the plant is an integer order (first order plus time delay).

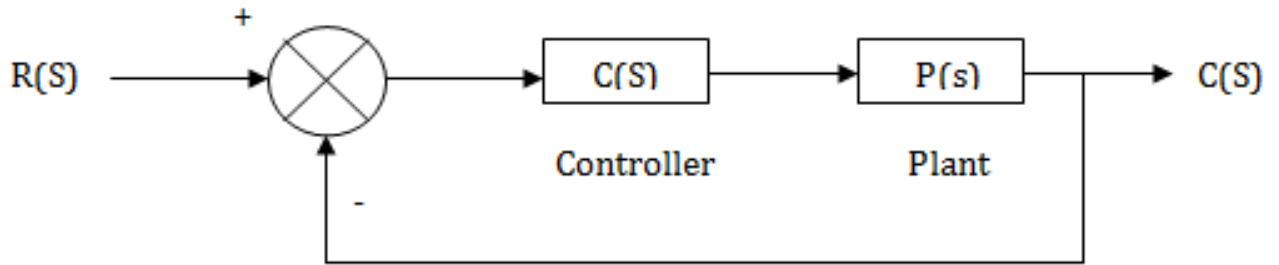


Fig 4.12 Negative feedback control system

Let the ϕ_{pm} be the required phase margin and ω_{cp} be the frequency of the critical point on the Nyquist curve of the plant $P(s)$ as in the design of Integer order PID (IOPID) at which

$$\arg(P(j\omega_{cp})) = -180^\circ \quad (4.40)$$

And the gain margin is:

$$g_m = \frac{1}{|P(j\omega_{cp})|} = K_c \quad (4.41)$$

All parameters of the $PI^\lambda D^\mu$ Controller are calculated to satisfy the robust performance of the plant with parameters uncertainty structure. The method proposed by Monje- Vinagre et.al[8] tuning method for the first order and first order plus time delay with the parameters uncertainly structure considered to design the fractional order PID Controller. Bode Envelopes of the first order and FOPID provide a simple characterization of a process and give valuable information about the dynamics of the process could. Let the FOPID System (IR Plant) can be represented generalized mathematically as:

$$P(s) = \frac{K}{sT + 1} e^{-Ls} \quad (4.42)$$

Where K is the steady state gain, L represents the processing delay, $T>0$ is the time constant. The exact values of these parameters may not be known. But these parameters can be estimated at certain intervals. Therefore modeling of this system as an interval time delay system is a realistic approach. The parameter of the FOPID system with parameter uncertainly structure can be defined as

$$K \in (\underline{K}, \overline{K}), L \in (\underline{L}, \overline{L}), T \in (\underline{T}, \overline{T}) \quad (4.43)$$

Where $\underline{K}, \underline{T}, \underline{L}$ the lower limits are $\overline{K}, \overline{T}, \overline{L}$ are upper limits of the parameters, respectively as per the open loop response of Plant? The fractional order controller is designed to obtain the desired performance for the given interval system.

Owing to the tuning method, Monje, Vinagre and their Colleagues [8] proposed a $PI^\lambda D^\mu$ Controller tuning algorithm for the system to satisfy five design criteria, such as magnitude at the gain crossover frequency, phase margin, robustness to plant uncertainties, high-frequency noise alternation and sensitivity function. Five design criteria of the Monje – Vinagre et.al [8] specification are given as follows:

a. Phase Margin and Gain Crossover Frequency

The gain and phase margins are two important frequency domain specifications and two important measures of robustness. The phase margin is related to the damping of the system. Thus, the following equation should be satisfied

$$|C(j\omega_{cp})P(j\omega_{cp})|_{dB} = 0 \text{ dB} \quad (4.44)$$

$$\left(\arg \left(C(j\omega_{cp})P(j\omega_{cp}) \right) \right) = -\pi + \phi_{pm} \quad (4.45)$$

Where ω_{cp} is the gain crossover frequency and ϕ_{pm} is the required phase margin?

b. Robustness to variation in the gain of the plant

Satisfying the following constraint

$$\left(\frac{d \left(\arg \left(C(j\omega_{cp})P(j\omega_{cp}) \right) \right)}{d\omega} \right)_{\omega=\omega_{cp}} = 0 \quad (4.46)$$

The phase is forced to be flat at ω_{cp} . The phase plot is almost constant within the interval around ω_{cp} . Consequently, the phase plot around the specified frequency ω_{cp} is locally flat, which implies that the system will be more robust to gain variation. Overshoots of the step responses are almost constant within the interval.

c. High-frequency noise Rejection: To satisfy the robustness

To satisfy the robustness due to high-frequency noise, the following condition must be fulfilled

$$\left| T(j\omega_{cp}) = \frac{C(j\omega_{cp})P(j\omega_{cp})}{1 + C(j\omega_{cp})P(j\omega_{cp})} \right|_{dB} \leq A \text{ dB} \quad (4.47)$$

Where A is the desired value of noise alternation for the frequency $\omega_{cp} \geq \omega_t \text{ rad/sec}$.

d. Good output disturbance rejection

To ensure a good output disturbance rejection, the following constraint must be satisfied

$$\left| S(j\omega_{cp}) = \frac{1}{1 + C(j\omega_{cp})P(j\omega_{cp})} \right|_{dB} \leq B \text{ dB} \quad (4.48)$$

Where B is the desired value of the sensitivity function for the frequency $\omega_{cp} \geq \omega_s \text{ rad/sec}$.

The design procedure for a robust $PI^\lambda D^\mu$ Controller to control first order plus time delay (FOPID) system with parametric uncertain structure can be represented as:

$$P(S) = \frac{\left[\frac{K, \bar{K}}{T, \bar{T}} \right] s + 1}{s + 1} e^{-Ls} \quad (4.49)$$

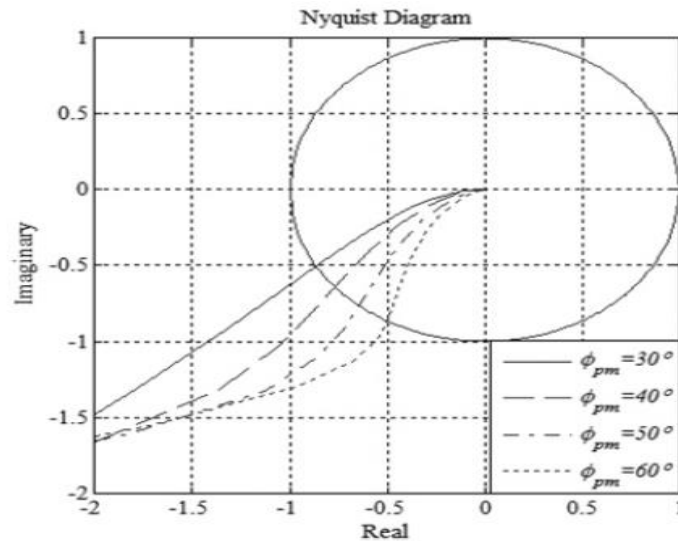


Fig: 4.13 Nyquist plot of system controlled for gain margin

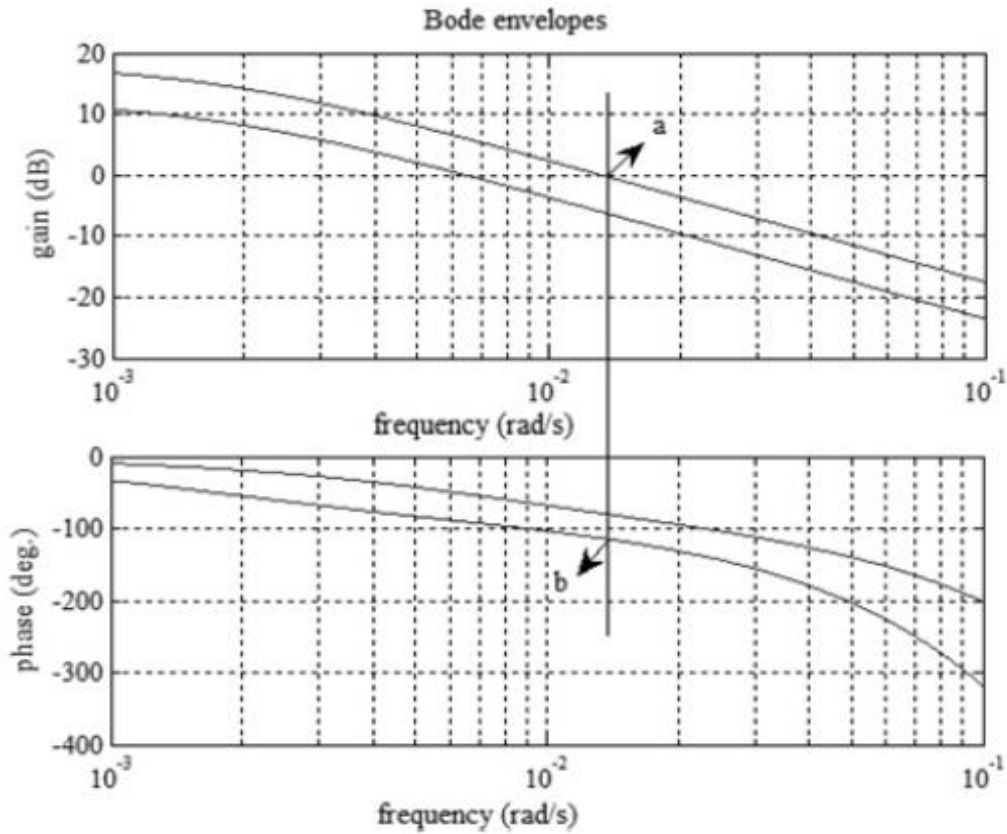


Fig: 4.14 Bode Envelope of a FOPTD plant

The Nyquist plot and Bode envelopes of the FOPID plant to satisfy the robust performance of the system are given in Figures (4.13) and (4.14)

Considering the Bode envelope provided in figure (4.14), minimum and maximum plots of the gain are obtained by the following transfer functions, respectively:

$$P_1(s) = \frac{\underline{K}}{Ts+1} e^{-Ls} \quad P_2(s) = \frac{\overline{K}}{Ts+1} e^{-Ls} \quad (4.50)$$

The delay 'L' does not have any effect on the gain plot of the plant. In order to design a robust $PI^\lambda D^\mu$ Controller, the design criteria should be satisfied with the plant transfer function ($P_1(s), P_2(s)$), namely ω_{cp} & the minimum phase margin must be taken at the point 'a' & 'b' in figure (4.14).

4.8.1 Mathematical Computational for design of FOPID Controller

According to the transfer function of the IR heater, the generalized transfer function described is as:

$$P(S) = \frac{K}{1+Ts} e^{-Ls} \quad (4.51)$$

The frequency response is given as

$$P(j\omega) = \frac{K}{1+j\omega T} e^{-j\omega L} \quad (4.52)$$

$$|P(j\omega)| = \frac{K}{\sqrt{1+\omega^2 T^2}} e^{-(\tan^{-1}(\omega T)+L\omega)} \quad (4.53)$$

The gain and phase of the plant are as follow

$$|P(j\omega)| = \frac{K}{\sqrt{1+\omega^2 T^2}} \quad (4.54)$$

$$\arg(P(j\omega)) = -\tan^{-1}(\omega T) - L\omega$$

According to the fractional order PID Controller transfer function, we can get the frequency form of FOPID as

$$C(j\omega) = K_p + \frac{K_i}{(j\omega)^\lambda} + K_d (j\omega)^\mu \quad (4.55)$$

Frequency domain analysis of Fractional Order Calculus Studies (FOCS) provides the expression for $(j\omega)^\mu$ as

$$(j\omega)^\mu = \omega^\mu \left(\cos\left(\frac{\pi}{2}\mu\right) + j\sin\left(\frac{\pi}{2}\mu\right) \right) \quad (4.56)$$

$$(j\omega)^{-\lambda} = \omega^{-\lambda} \left(\cos\left((-\lambda)\frac{\pi}{2}\right) + j\sin\left((-\lambda)\frac{\pi}{2}\right) \right) \quad (4.57)$$

The gain and phase of $C(j\omega)$ are determined as:

$$C(j\omega) = K_p + K_i (j\omega)^{-\lambda} + K_d (j\omega)^\mu \quad (4.58)$$

$$= K_p + K_i \left(\omega^{-\lambda} \left(\cos\left((-\lambda)\frac{\pi}{2}\right) + j\sin\left((-\lambda)\frac{\pi}{2}\right) \right) \right) + K_d \left(\omega^\mu \left(\cos\left(\frac{\pi}{2}\mu\right) + j\sin\left(\frac{\pi}{2}\mu\right) \right) \right) \quad (4.59)$$

$$= K_p + K_i \omega^{-\lambda} \cos\left(\frac{-\pi}{2}\lambda\right) + K_d \omega^\mu \cos\left(\frac{\pi}{2}\mu\right) + j\omega^{-\lambda} K_i \sin\left(\frac{-\pi}{2}\lambda\right) + j\omega^\mu K_d \sin\left(\frac{\pi}{2}\mu\right) \quad (4.60)$$

$$= K_p + K_i \omega^{-\lambda} \cos\left(\lambda\frac{\pi}{2}\right) + K_d \omega^\mu \cos\left(\mu\frac{\pi}{2}\right) + j \left(K_i \omega^{-\lambda} \sin\left(\lambda\frac{-\pi}{2}\right) + K_d \omega^\mu \sin\left(\mu\frac{\pi}{2}\right) \right) \quad (4.61)$$

Where,

$$\sin\left(\pi\left(-\frac{\lambda}{2}\right)\right) = -\sin\left(\pi\frac{\lambda}{2}\right) \quad \text{And} \quad \cos\left(\pi\left(-\frac{\lambda}{2}\right)\right) = \cos\left(\pi\frac{\lambda}{2}\right)$$

Let

$$R = K_p + \omega^{-\lambda} K_i \cos\left(\lambda\frac{\pi}{2}\right) + K_d \omega^\mu \cos\left(\mu\frac{\pi}{2}\right) \quad (4.62)$$

$$S = -K_i \omega^{-\lambda} \sin\left(\lambda\frac{\pi}{2}\right) + K_d \omega^\mu \sin\left(\mu\frac{\pi}{2}\right) \quad (4.63)$$

$$|C(j\omega)| = \sqrt{\left(K_p + K_i \omega^{-\lambda} \cos\left(\lambda\frac{\pi}{2}\right) + K_d \omega^\mu \cos\left(\mu\frac{\pi}{2}\right)\right)^2 + \left(K_d \omega^\mu \sin\left(\mu\frac{\pi}{2}\right) - K_i \omega^{-\lambda} \sin\left(-\lambda\frac{\pi}{2}\right)\right)^2} \quad (4.64)$$

$$|C(j\omega)| = \sqrt{R^2 + S^2} \quad (4.65)$$

$$\begin{aligned} \arg[C(j\omega)] &= \tan^{-1}\left(\frac{K_d \omega^\mu \sin\left(\mu\frac{\pi}{2}\right) - K_i \omega^{-\lambda} \sin\left(\lambda\frac{\pi}{2}\right)}{K_p + K_i \omega^{-\lambda} \cos\left(\lambda\frac{\pi}{2}\right) + K_d \omega^\mu \cos\left(\mu\frac{\pi}{2}\right)}\right) \\ &= \tan^{-1}\left(\frac{S}{R}\right) \end{aligned} \quad (4.66)$$

According to design specification equation (4.44) and (4.45), the phase of $G(j\omega)$ can be expressed as

$$G(j\omega) = P(j\omega)C(j\omega)$$

$$\arg(G(j\omega)) = \arg[P(j\omega)] + \arg[C(j\omega)] = -\pi + \phi_{pm} \quad (4.67)$$

$$= -\tan^{-1}(\omega T) - L\omega + \tan^{-1}\left(\frac{S}{R}\right) = -\pi + \phi_{pm} \quad (4.68)$$

$$\arg(G(j\omega)) = \tan^{-1}\left(\frac{S}{R}\right) - \tan^{-1}(\omega T) - L\omega = -\pi + \phi_{pm} \quad (4.69)$$

According to specification equation (4.44) and (4.45) the gain of the $G(j\omega)$ can be expressed as:

$$\begin{aligned} |G(j\omega)| &= |P(j\omega)C(j\omega)| \\ &= \left(\frac{K}{\sqrt{1+\omega^2 T^2}}\right) \sqrt{R^2 + S^2} = 0 \text{ dB} \\ |G(j\omega)| &= \left|\frac{K\sqrt{R^2 + S^2}}{\sqrt{1+\omega^2 T^2}}\right|_{dB} = 0 \text{ dB} \end{aligned} \quad (4.70)$$

According to specification equation (4.46), we get.

$$\begin{aligned} \frac{d}{d\omega}(\arg(G(j\omega))) &= 0 \\ \frac{d}{d\omega}\left(\tan^{-1}\left(\frac{S}{R}\right) - \tan^{-1}(\omega T) - L\omega\right) &= \frac{d}{d\omega}(-\pi + \phi_{pm}) \\ \frac{1}{1+(S/R)^2} * \frac{R \frac{d}{d\omega} S - S \frac{d}{d\omega} R}{R^2} - \frac{T}{1+(\omega T)^2} - L &= 0 \end{aligned} \quad (4.71)$$

So

$$\begin{aligned} \frac{d}{d\omega}(S) &= \frac{d}{d\omega}\left(K_d \omega^\mu \sin\left(\mu \pi/2\right) - K_i \omega^{-\lambda} \sin\left(\lambda \pi/2\right)\right) \\ S_u &= K_d \omega^{\mu-1} \mu \sin\left(\mu \pi/2\right) + \lambda K_i \omega^{-\lambda-1} \sin\left(\lambda \pi/2\right) \\ \frac{d}{d\omega}(R) &= \frac{d}{d\omega}\left(K_p + K_i \omega^{-\lambda} \cos\left(\lambda \pi/2\right) + K_d \omega^\mu \cos\left(\mu \pi/2\right)\right) \\ R_u &= -\lambda K_i \omega^{-\lambda-1} \cos\left(\lambda \pi/2\right) + K_d \mu \omega^{\mu-1} \cos\left(\mu \pi/2\right) \\ \frac{d}{d\omega}(\arg(G(j\omega))) &= \frac{1}{1+(S/R)^2} \cdot \frac{R.S_u - S.R_u}{R^2} - \frac{T}{1+\omega^2 T^2} - L = 0 \end{aligned} \quad (4.72)$$

According to specification equation (4.47), high frequency noise rejection expressed as:

$$\left| T(j\omega) = \frac{P(j\omega)C(j\omega)}{1+P(j\omega)C(j\omega)} \right|_{dB} < A \text{ dB}$$

Where $A = -20dB$

So, in Laplace domain function

$$\begin{aligned} T(s) &= \frac{P(s)C(s)}{1+P(s)C(s)} \\ &= \frac{(R+jS)\left(\frac{K}{1+sT}\right)}{1+(R+jS)\left(\frac{K}{1+sT}\right)} \\ &= \frac{(R+jS)K}{\frac{1+sT}{(1+sT)+K(R+jS)}} = \frac{KR+jSK}{1+sT+KR+jKS} \end{aligned}$$

$$\begin{aligned}
&= \frac{KR + jSK}{(1 + KR) + j\omega T + jSK} = \frac{KR + jSK}{(1 + KR) + j(\omega T + SK)} \\
|T(j\omega)| &= \left| \frac{\sqrt{(KR)^2 + (SK)^2}}{\sqrt{(1 + KR)^2 + (\omega T + SK)^2}} \right| \leq -20 \text{ dB} \\
|T(j\omega)| &= \left| \frac{K\sqrt{R^2 + S^2}}{\sqrt{(1 + KR)^2 + (\omega T + SK)^2}} \right| + 20\text{dB} \leq 0
\end{aligned} \tag{4.73}$$

Where $\omega = \omega_i$

According to specification equation (4.48), the good output disturbance rejection expressed as

$$|S(j\omega)| = \left| \frac{1}{P(j\omega)C(j\omega)} \right| \leq B \text{ dB}$$

Where $B = -20\text{dB}$

In Laplace domain function

$$\begin{aligned}
S(s) &= \frac{1}{1 + C(s)P(s)} \\
1 + C(s)P(s) &= 1 + \frac{K(R + jS)}{1 + sT} \\
&= \frac{(1 + sT) + K(R + jS)}{1 + sT} \\
S(s) &= \frac{1 + sT}{(1 + sT) + K(R + jS)} \\
S(j\omega) &= \frac{1 + j\omega T}{(1 + j\omega T) + K(R + jS)} \\
|S(j\omega)| &= \frac{\sqrt{1 + \omega^2 T^2}}{\sqrt{(1 + KR)^2 + (\omega T + KS)^2}} \leq -20\text{dB} \\
S(j\omega) &= \frac{\sqrt{1 + \omega^2 T^2}}{\sqrt{(1 + KR)^2 + (\omega T + KS)^2}} + 20\text{dB}
\end{aligned} \tag{4.74}$$

Where, $\omega = \omega_s$

Equation (as per design result) with the unknown parameter (K_p, K_i, K_d, λ and μ) can be solved to obtain the parameters of $PI^\lambda D^\mu$ for the robust stability of the plant. To solve the five

non-linear equations FMINCON optimization toolbox of Mat Lab is used. Equation (4.70) is taken a main function, and the other equations (4.69), (4.72), (4.73), and (4.74) are taken as non-linear constraints for optimization.

Values of the five unknown parameters (K_p, K_i, K_d, λ and μ) are calculated. Then, $PI^\lambda D^\mu$ Controller to control the plant is obtained in the form of

$$C(S) = K_p + \frac{K_i}{s^\lambda} + s^\mu K_d$$

4.9 Nint Blocks

Ninteger is a toolbox of Mat Lab intended to help developing fractional (or non-integer) order controllers for single input single output (SISO) plants and assess their performance [12].

The toolbox files may be divided into three categories:

The user's accessible files are given a place in the integer folder.

And a separate folder, Cfractions, is provided for these functions that deal with continued fractions, and these may be accessible to the user.

Another separate folder GUI, for the graphical interface only.

A last separate folder, obsolescent, is no longer necessary but is still included to ensure compatibility with older toolbox versions.

The frequency domain transfer function given by the equation is the function that can be used to implement a controller. (4.75)

$$C(S) = K_p + K_d s^{v_D} + \frac{K_i}{S^{v_i}}, \quad v_D, v_i \in R^+ \quad (4.75)$$

By providing both continuous and digital approximations of the controller with this structure are known as fractional P-I-D.

Syntax

Function C= nipid ($K_p, K_d, v_D, K_i, v_i, \text{bandwidth, n, formula,-----},$
expansion, decomposition)

Arguments

A bandwidth specification is based on the following variable formula:

- a. The bandwidth for "Crone" and "Matsuda" must be a two-number vector containing the limits given in *rad/see* of $[\omega_l; \omega_h]$ the frequency range where the approximation is valid.
- b. The frequency indicated in, around which the approximation will be accurate might be thought of as the "Carlson"-bandwidth. It could be a two-number vector that contains a frequency range's bounds.

- c. 'Cfe high'
- d. 'Cfe low.'

The graphical is accessible by typing ninteger at the command prompt. The dialogue, figure (4.15) appears:

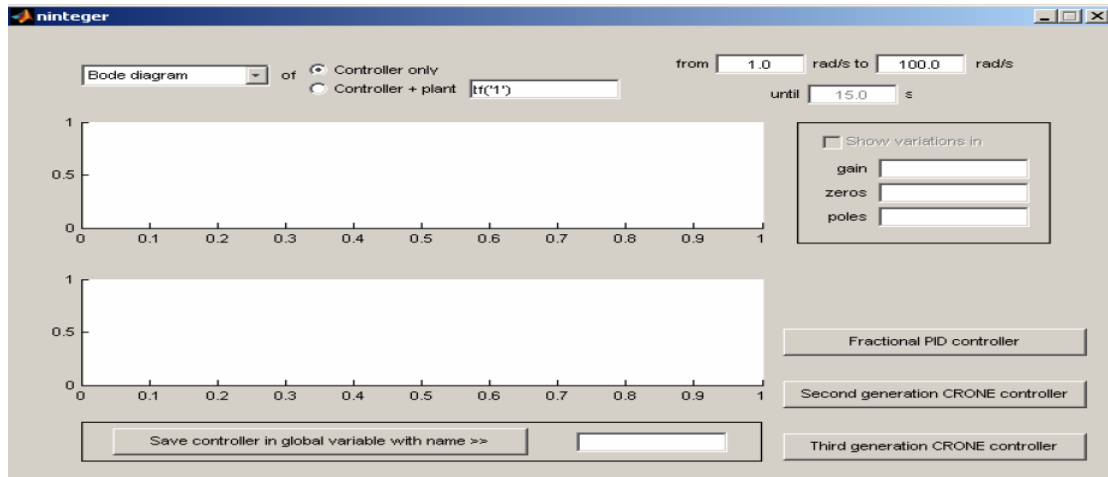


Fig: 4.15 .The main dialog of ninteger before being filled in

This conversation will be used to assess a controller's performance after reckoning it, as may be seen below. Like any other window in your operating system, it can be closed.

4.9.1 Dialogue nipid GUI

When the button of the Fractional order derivative controller is pressed in the main window of ninteger, a dialogue box permits creation of fractional PIDs will appear. With the two pop-up choices in the middle, the type of approximation can be selected. Options matching to the parameter formula of the function nipid are available on the first pop-up menu. The second pop-up menu will become active, and the user will be able to select parameter expansion if a digital controller is selected. With the exception of when option Carlson is selected in the first pop-up menu and the appropriate requirements are met, controllers are always generated using the function nipid.

The dialogue's fields allow you to enter the additional necessary parameters. Only those of them allow for the entry of a value; not all of them are required in all circumstances. In particular:

- ❖ The field that specifies the number of poles and zeros must always be filled out; it always corresponds to the parameter n.

- ❖ The check button offers two parameter decomposition options: "all" if checked and "frac" if not.
- ❖ Values for the gains (K_p , K_i and K_d) and orders (vi and vd) must always be entered. Orders will be rounded to the nearest inverse of an integer (for example, the value 0.3 will be rounded to 1/3) if the Carlson option is selected.
- ❖ When a continuous controller is selected, the fields in the statement from... rad/s to... rad/s must be filled out; they correspond to parameters.
- ❖ . When selecting a digital controller, the sampling time (T_s) needs to be filled.

4.9.2 Performance evaluation in the Main Dialogue

Let us suppose that a Carlson approximation of a fractional controller is devised in the nipid Gui dialogue with the following parameters as in figure (4.16): If nothing was done in the main dialogue prior to pressing OK, Bode diagram of the controller from 1 to 100 rad/s will appear as shown in figure (4.17).

The main dialogue enables visualizing six different controller traits:

- ❖ Bode diagram;
- ❖ Nichols diagram;
- ❖ Nyquist diagram;
- ❖ impulse response
- ❖ step response;
- ❖ The placement of poles and zeros

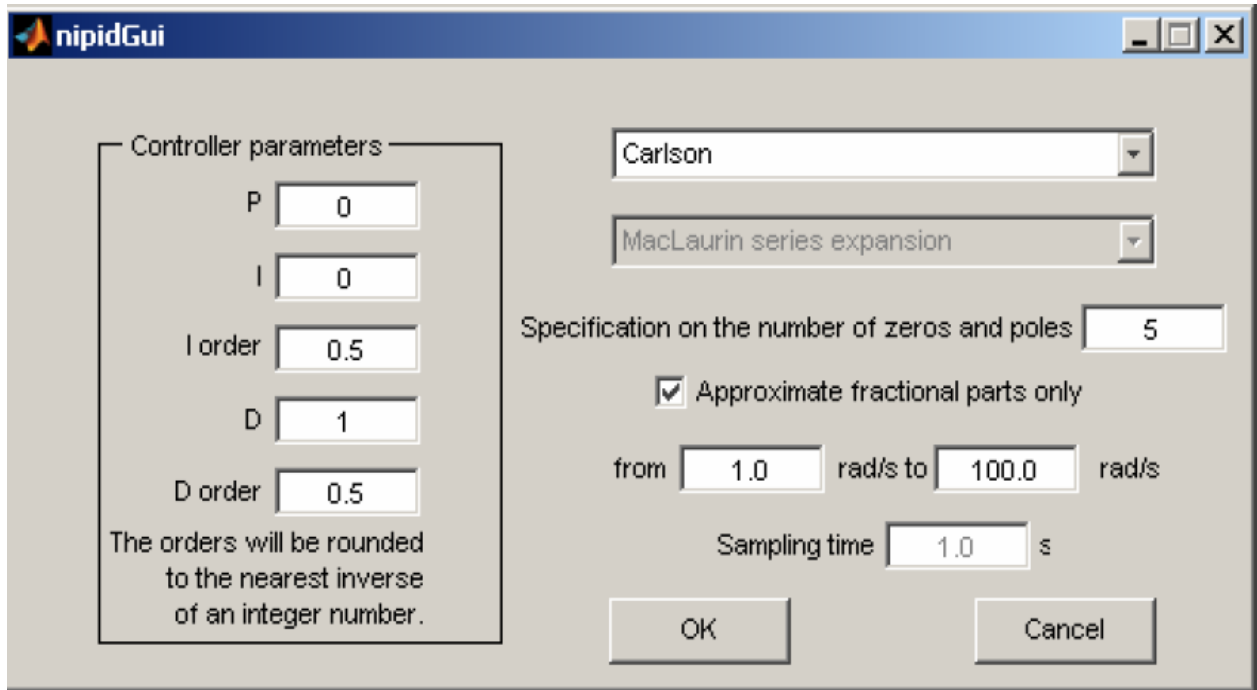


Fig: 4.16 Dialogue nipid Gui filled inside

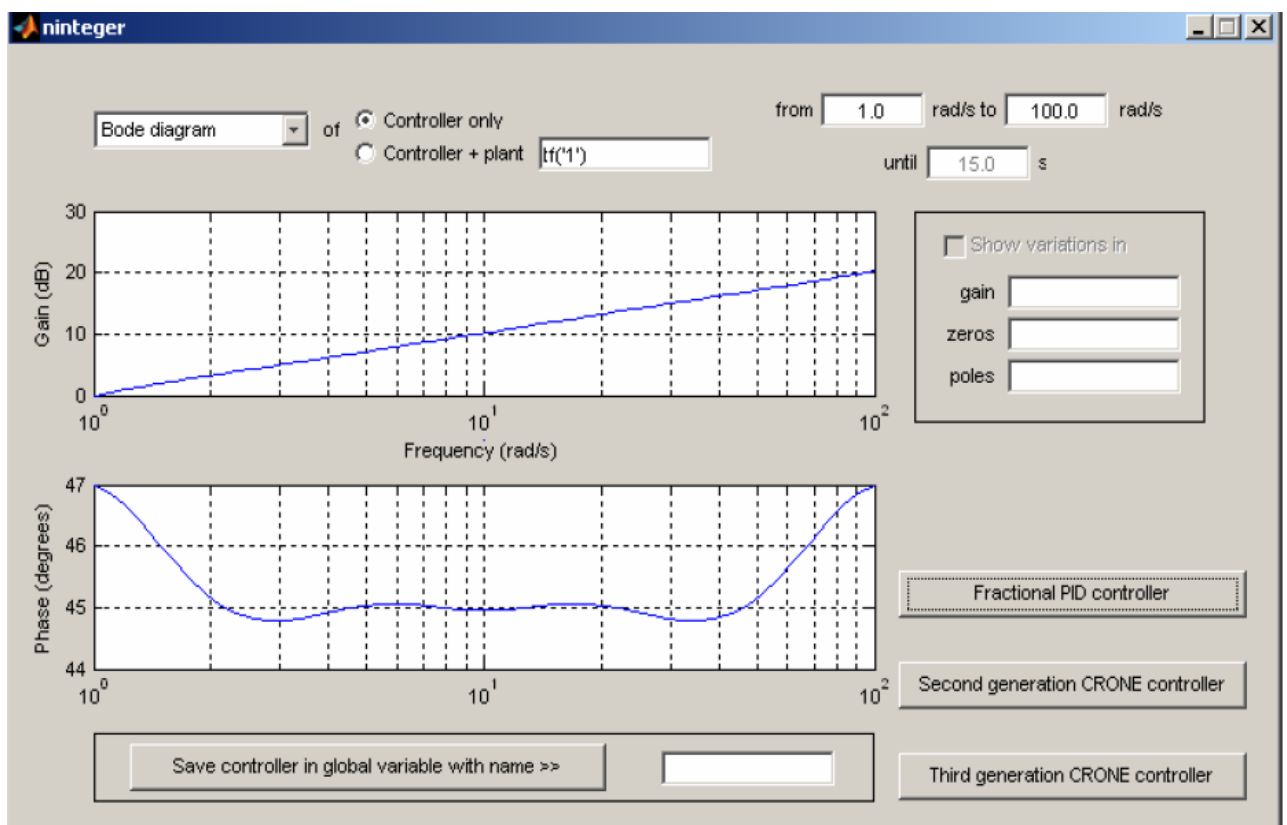


Fig: 4.17, Bode diagram display with main dialogue.

The frequency behavior is sampled at fifty logarithmically spaced frequencies between the values entered in the fields of the phrase from... rad/s to... rad/s, as demonstrated in the Bode,

Nichols, and Nyquist diagrams. The impulse and step functions of Mat Lab determine the number of sampling instants. Time responses are evaluated until the instant provided in the sentence field until... s. When poles and zeros are seen, the former is represented by red crosses, while blue circles represent the latter. A suitable grid is then constructed, and all three of the fields as mentioned above are rendered irrelevant.

It is also feasible to observe the behavior of the open loop created by the controller and the plant for which it was intended, as opposed to only observing what happens with the controller. The plant must then be entered in the field next to the matching radio button in that scenario. After filling the field in, the radio button labeled Controller + plant may be pressed.

4.9.3 Simulink in MatLab

A Simulink library called Nintblocks is provided with two blocks that implement functions nid and nipid as shown in figure (4.18).

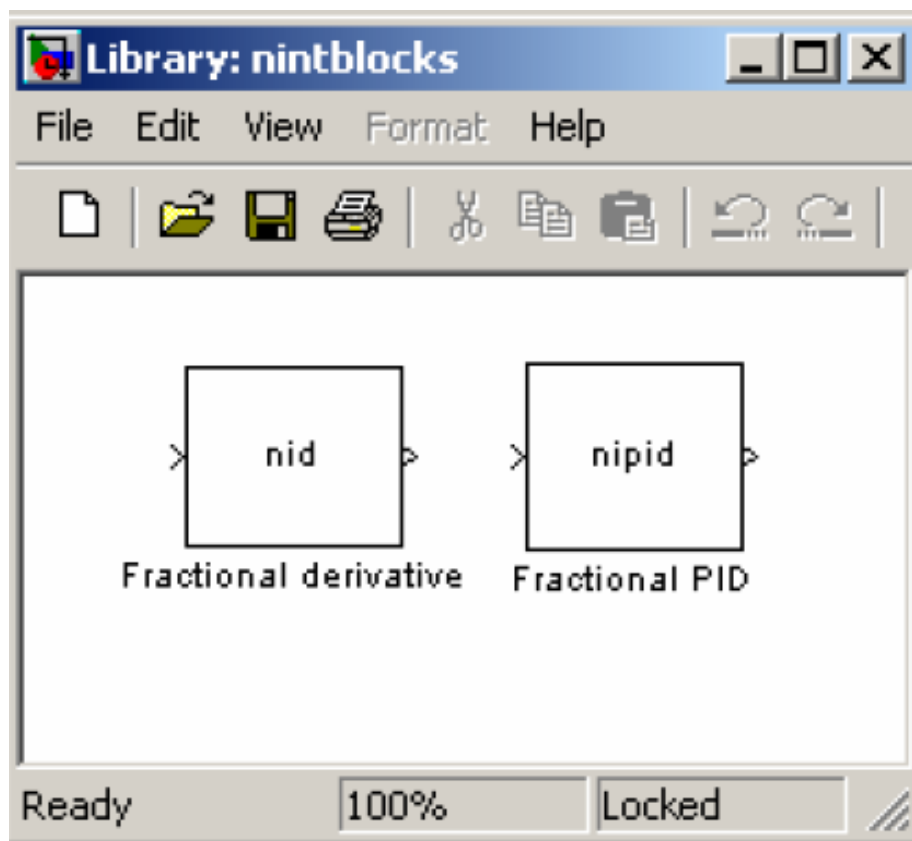


Fig: 4.18 Simulink library

Fractional derivative Block

Function nid is implemented in this block. Through the dialogue shown in figure (4.19):

The following parameters are provided.

This block implements function nid. The parameters are provided by means of the following dialogue as in

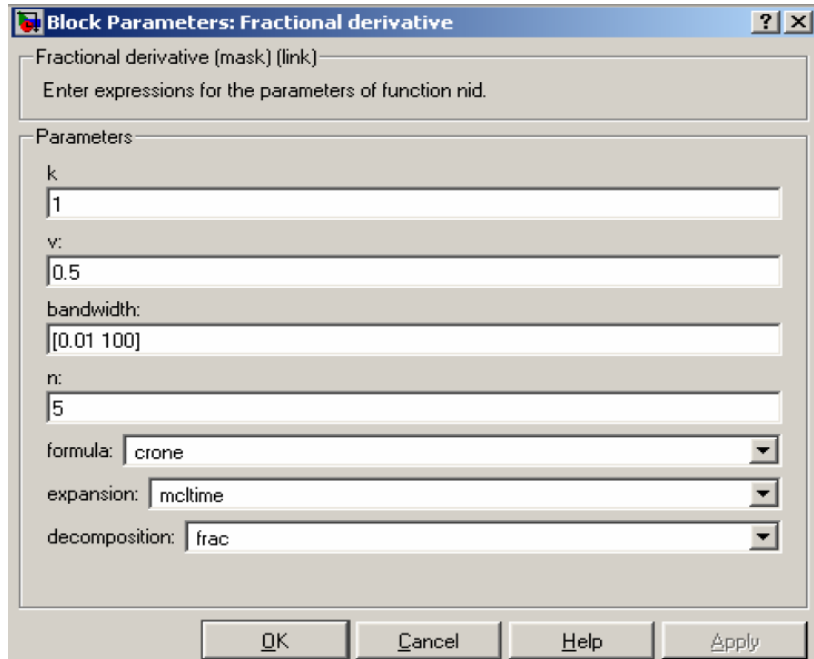


Fig: 4.19 Dialogue of block (Fractional P-D)

Implementation

The block is implemented by an LTI block calling function nid in a masked subsystem. To translate the outcomes of the dialogue's pop-up menus into the strings required by nid, certain lines of code must be added to the Initialization tab of the mask of the subsystem.

Block Fractional PID

This block implements the function nipid shown in figure (4.20). The parameters are provided by means of the following dialogue:

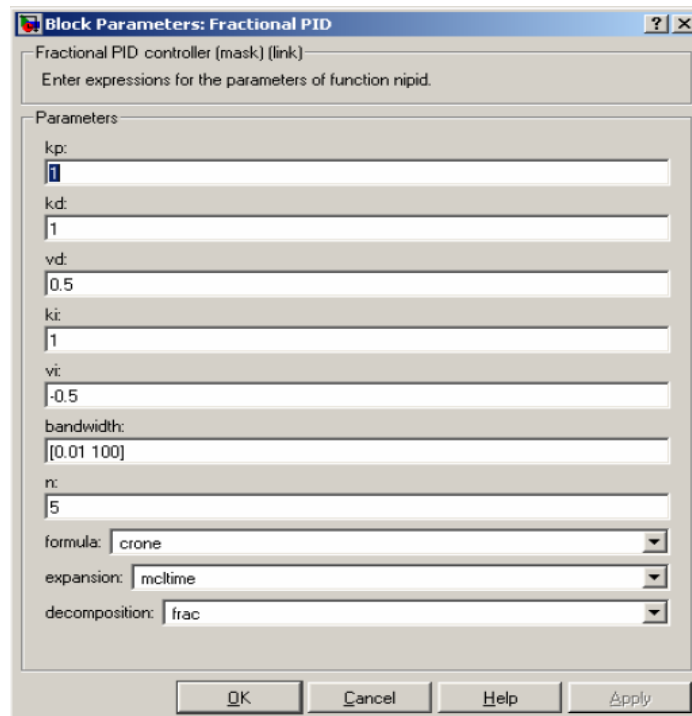


Fig: 4.20 Dialogue of block Fractional PID

Implementation

The block is similar as the above and the function implemented is nipid.

4.10 Implementation of Fractional Order PID Controller on Ceramic Infrared Heater Plant

Based on approximated first order plus time delay transfer function (2.20), a fractional order controller parameter was calculated using the ω_{cg} and ϕ_m as 2.75 rad/sec and 50° . By putting up the value in the equation (4.70), (4.71), (4.73), (4.74), and (4.75), five unknown parameters can be solved by using the FMINCON optimization toolbox of MatLab. Equation (4.71) is considered as a main equation, and other equations are taken as non-linear constraints for optimization. The value of all the five unknown parameters are calculated to obtain the $PI^\lambda D^\mu$ controller to control the ceramic IR heater as $K_p = 0.32033$, $K_i = 0.011387$, $K_d = 2.4855$, $\lambda = 0.9006$, $\mu = 0.17319$ and transfer function of fractional order PID controller given as

$$C(s)_{fopid} = 0.32033 + \frac{0.011387}{s^{0.9006}} + 2.4855s^{0.17319}$$

Ninteger is a toolbox of MatLab intended to help developing fractional (or non-integer) order controllers for single input- single output plant and to access their performance. The step response of the plant with FOPID controller can be obtained by using ‘nintblock’ of Mat Lab developed by Valerio, D [12] shown in figure (4.21).

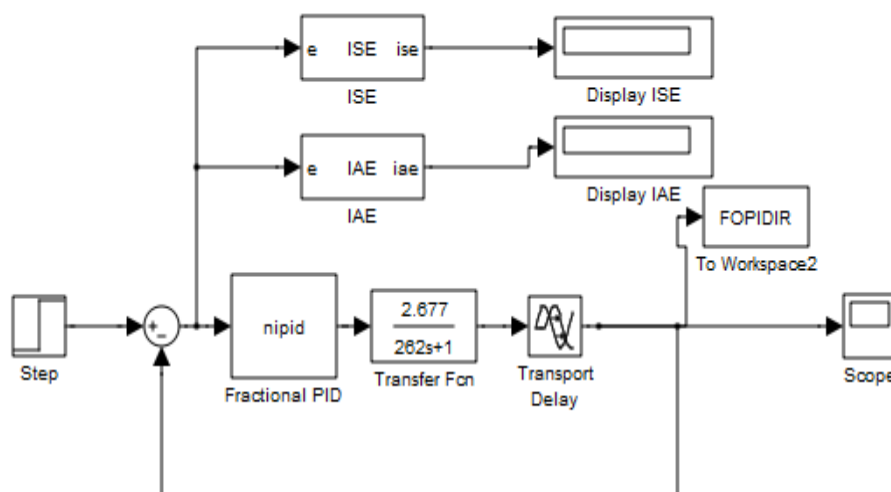


Fig: 4.21 Simulink block diagram of Ceramic IR Heater Control Using $PI^\lambda D^\mu$ Controller

Magnitude plots of High-Frequency Noise Rejection $T(s)$ and output disturbance rejection $S(s)$ of the system obtained in MatLab. It shows that the phase of the system is almost flat and almost constant within an interval around ω_{cp} specified constraints shown in figure (4.22). The step response indicates that the system is more effective and robust to gaining the overshoot of the step responses is almost constant, shown in figure (4.23).

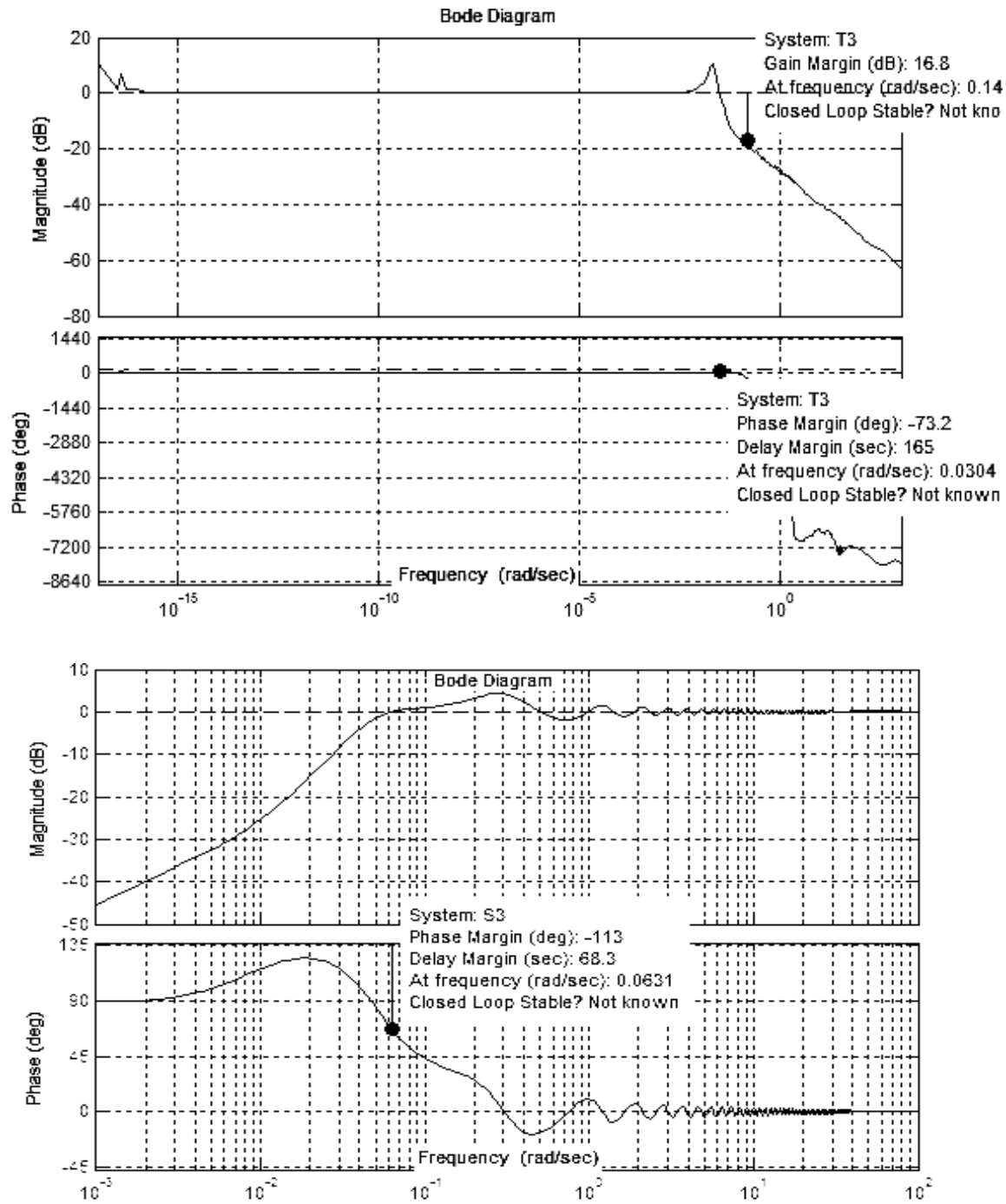


Fig: 4.22 Magnitude of $T(s)$ and $S(s)$ for $C_{FOPID}(s)G(s)$

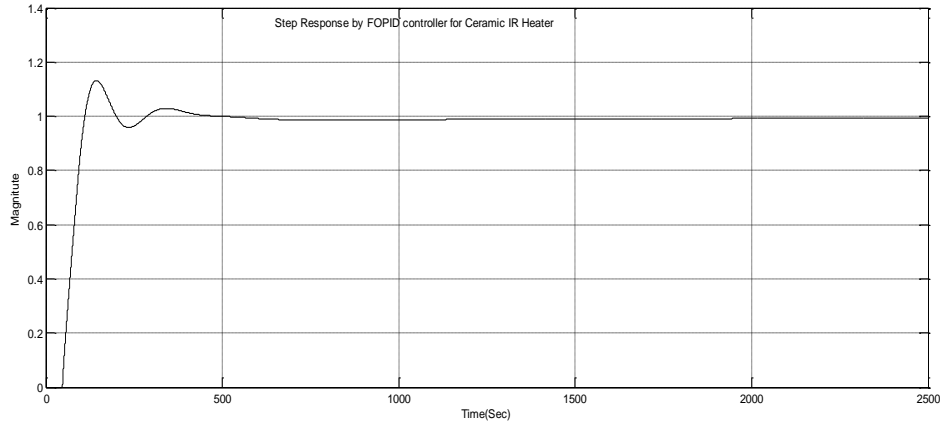


Fig 4.23 step response of the system for CFOPID for phase margin 50 and $\omega_{cp}=2.75\text{rad/sec}$

The simulation's results (peak overshoot, settling time, peak time, and rise time) demonstrate in Fig: 4.23 in which Step response of the system for C_{FOPID} for phase margin (50°) and $\omega_{cp}=2.75 \text{ rad/sec}$ show that the proposed method of the controller has a better response, as shown in Table (4.8)

Table: 4.8 Performance table of FOPID Controller for Ceramic IR heater control

Performance	Rise Time (T_r)	Peak Overshoot(M_p)	Peak Time(T_p)	Settling Time(T_s)	ISE	IAE
FOPID	49.02	14.07	143.13	408.2	64.98	106.2

4.11 Conclusion

Several criteria for designing and evaluating the tuning method are discussed. Zeigler-Nichols presented a graphical two-point method for finding the results when the process is truly a dead time plus first-order lag, parameters are calculated from Zeigler-Nichols open/close loop, Cohen-Coon, Astrom –Hugglund method and simulated. The design and specifications of the Integer order PID Controller are also discussed, and parameters K_P, K_i and K_d are derived. According to Bode and Nyquist plot of ceramic infrared heater displaced. The design of IOPID and FOPID Controllers has been explained by analyzing the tuning parameters to satisfy the robust performance of the plant. Mathematical computational for the design of FOPID has been discussed, and results have been found by using the FMINCON Optimization tool of MatLab.

ARTIFICIAL INTELLIGENCE TECHNIQUES FOR CONTROLLERS DESIGN

5.1 Fuzzy Logic Controller

Fuzzy logic, conceived by Lotfi Zadeh in 1965, is a very human concept, potentially applicable to a wide range of processes and tasks that require human intuition and experience. Fuzzy logic can be applied by means of software, dedicated controllers or fuzzy microprocessors embedded in digital products [26][47].

Proportional Integral Derivative (PID) controller is simple to implement and widely used in industrial applications but exhibits poor performance when applied to a system containing nonlinearities. Fuzzy logic based pre compensator for PID controller has recently yielded a very positive result that it is the best solution for time-varying, nonlinear, dynamic, and ill-understood processes. They have superior performance compared to conventional PID control.

1. It can be configured to fail safely. Therefore, it is naturally robust as it doesn't need exact, noise-free inputs. Despite a wide range of input fluctuations, the output control function is smooth.
2. It is simple to tune and modify to improve or significantly change system performance. By creating the proper regulating principles, new Sensors can be easily added to the system.
3. This makes the sensor inexpensive and imprecise, thus keeping the overall system cost and complexity low.
4. Any reasonable number of inputs (1–8) or more can be processed, and various outputs (1-4 or more) can be produced thanks to the rule-based operation.

5.1.1 Membership Functions

A graphic representation of the degree of each input's participation is the membership function. It defines functional overlap between inputs, assigns weights to each processed input, and eventually produces an output response.

Shape

Triangular is common, but Bell, trapezoidal, and exponential have also been utilized, though triangular is more typical. Greater computational cost is needed to accomplish more sophisticated functions, such as height or magnitude (generally 1), width shouldering Center Points Overlap (N & Z, Z & P normally around 50% of width), etc. By inserting the chosen input parameter (error or error dot) into the horizontal anise and projecting vertically to the upper boundary of the membership function, the Degree of membership (DOM) is obtained (s).

Inferencing

Before being sent to the defuzzification process to develop precise output. There are numerous approaches to inference. The highest rule is chosen using the Max-Min approach, which evaluates the magnitudes of each rule. The result of the MAX- DOT and MAX- PRODUCT technique is the horizontal coordinates of the "fuzzy" Centroid of the composite are under the function (s), which are scaled for each member function to fit under its corresponding peak value. The member functions (s) are essentially shrunk to perform their respective functions (i.e., "Negative," "Zero," and "Positive"). This approach generates a smooth, continuous output by combining the effects of all active rules.

Another strategy that is effective but falls short of increasing the weighting of additional rule votes per output member function is the averaging method. Averaging, for instance, won't take into account the difference between three "Negative" rules and one "Zero" rule that both triggers. Since the sum of the two averages is 0.5. The average of each function is clipped, and the "fuzzy" centroid is calculated

The Root- Sum- Square (RSS) approach calculates the "fuzzy" centroid of the composite region by combining the impacts of all relevant uses, scaling the functions at their respective magnitudes. This approach has more mathematical complexity than alternative approaches

5.1.2 Defuzzification

By merging the inference process's outcomes and then contrasting the area's "fuzzy centroid," it is possible to defuzzify the data and get a clear output. Added after being weighted by the center points of each output membership function.

5.2 Designing of Fuzzy Logic Controller

The fundamental setup of a fuzzy logic controller (FLC) is shown in Figure 5.1. A set of if-then rules of human specialists have accumulated about resolving specific situations are stored in the rule base. It serves as a resource for the fuzzy inference system, which selects the rules most applicable to the circumstances at hand and then implements the actions that these rules recommend. As suggested by its name, the input fuzzifier accepts crisp numerical inputs and transforms them into the fuzzy form required by the fuzzy inference system. The fuzzy inference system's findings are combined and transformed into crisp numeric values as control actions via the defuzzification interface at the output [26].

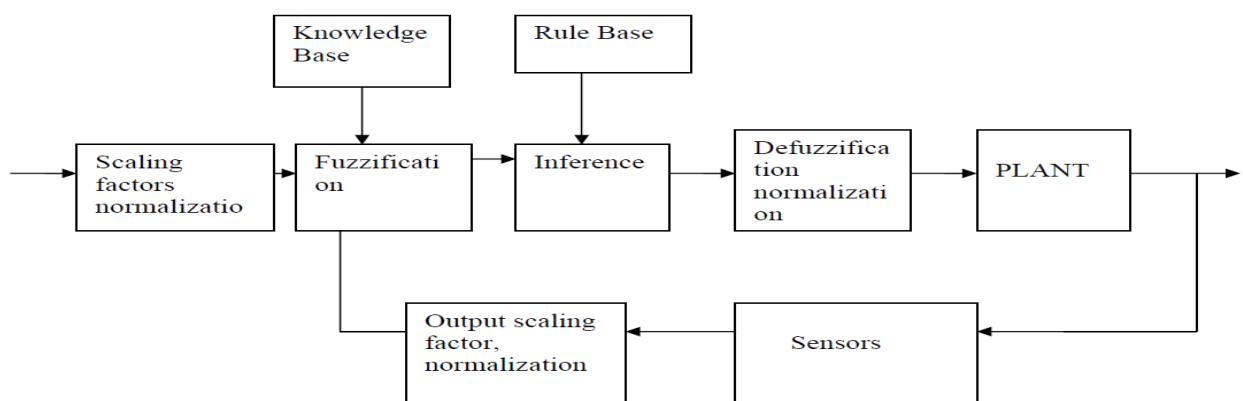


Fig: 5.1 a simple fuzzy logic control system block diagram

5.2.1 Control Structure of Fuzzy Base PID Controller

Figure 5.2 shows the basic control structure. The structure consists of a conventional PID control structure together without a fuzzy structure [73].

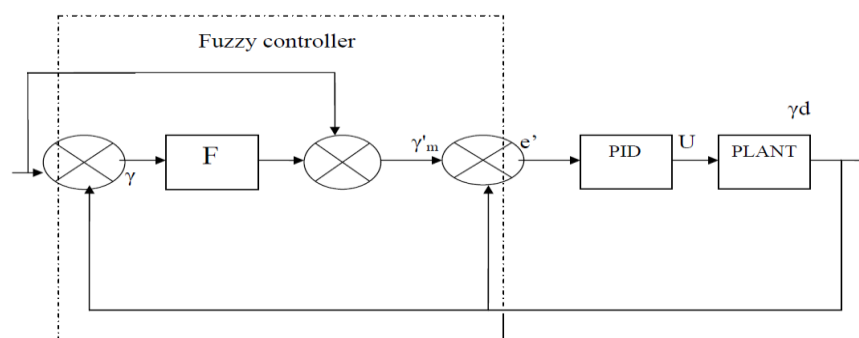


Fig: 5.2 Basic control structure of FLC-based PID Controller

The fuzzy-based controller uses the command input $Y_{m(k)}$ and the plant output Y_p to generate a pre-compensated command signal Y'_m described in the following equations.

$$\begin{aligned}
e(k) &= Y_{m(k)} - Y_{p(k)} \\
\Delta e(k) &= e(k) - e(k-1) \\
\gamma(k) &= F[e(k), \Delta e(k)] \\
Y'_{m(k)} &= Y_{m(k)} + \gamma(k)
\end{aligned}$$

In the above $e(k)$ is the tracking error between the command input $Y_{m(k)}$ and the plant output $Y_{p(k)}$

$\Delta e(k)$ = is the change in the tracking error

$F[e(k), \Delta e(k)]$ = is a non-linear mapping of $e(k)$ and $\Delta e(k)$ on fuzzy logic.

$\gamma(k) \rightarrow F[e(k), \Delta e(k)]$ represents a compensation or correction term so that compensated command signal $Y'_{m(k)}$ is simply the sum of the external command $Y_{m(k)}$ and $\gamma(k)$

F = Fuzzy Controller

The correction term $\gamma(k)$ is based on the error $e(k)$ is the change of error $\Delta e(k)$. The compensated command signal $Y'_{m(k)}$ is applied to a conventional PID Controller.

The equations of governing the PID controller as follows:

$$\begin{aligned}
e'(k) &= y'_m(k) - y'_p(k) \\
\Delta e'(k) &= e'(k) - e'(k-1) \\
U(k) &= U(k-1) + K_p e'(k) + K_i e'(k) + K_d (\Delta e'(k)) - \Delta e'(k-1)
\end{aligned} \tag{5.1}$$

The quantity $e'(k)$ - is the pre-compensated tracking error between the pre-compensated command input $Y'_{m(k)}$ and the plant output $Y_{p(k)}$

$\Delta e'(k)$ - is the change in the pre-compensated tracking error

$U(k)$ - is the command applied input to the plant

The purpose of the fuzzy controller is to modify the command signal to compensate for the overshoot and undershoot present in the output response when the plant has unknown nonlinearities. Such nonlinearities can significantly overshoot and undershoot if a conventional PID control scheme is used.

5.2.2 Fuzzy Logic Tool Box Tools:-

The Fuzzy Logic Toolbox for use with MATLAB is a tool for solving problems with fuzzy logic. Fuzzy logic itself is a valuable engineering tool because it does a good job of trading off between significance and precision—something that humans have been doing for a very long time

1. The Fuzzy Inference System or FIS Editor.
2. The Membership Function Editor: The editor defines the Membership Function to each variable's shapes.

We can display and edit all the membership functions associated with all the input and output variables for the entire fuzzy inference system.

3. The Rule Editor: The Rule Editor is used to modify the list of rules that specify how the system behaves.
4. Rule Viewer: The active rules can be seen in the Rule Viewer, as well as how different membership function shapes impact the outcomes.
5. The Surface Viewer: The Surface Viewer is used to show how one output is dependent on any one or more inputs. Instead of altering the FIS, the Rule Viewer and Surface Viewer are utilized for viewing. These tools are entirely read-only.

These GUIs are dynamically linked, as shown in figures (5.3), (5.4), (5.6), (5.7), and (5.8); any modifications we make to FIS utilizing one of them will have an impact on any open GUIs. For any given system, we can have any or all of them available.

5.2.3 Importing and Exporting from the GUI Tools

When one saves a fuzzy system to disk, one can save it in an ASCII text FIS file representation of that system with the file suffix `.fis`. This text file can be edited and modified and is simple to understand. When one saves his/her fuzzy system to the MATLAB workspace, he/she creates a variable (whose name he/she chooses) that will act as a MATLAB structure for the FIS system. FIS files and FIS structures represent the same system.

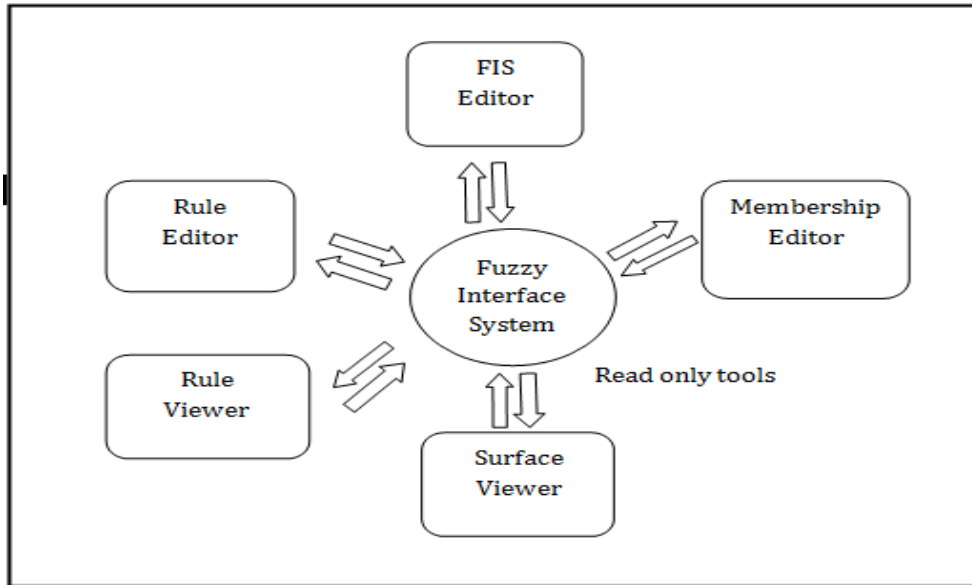


Fig: 5.3 Overview of fuzzy toolbox inference system

The Fuzzy Logic Toolbox includes the following five main GUI tools for creating, editing, and viewing fuzzy inference systems:

These menu items allow you to save, open, or edit a fuzzy system using any of the five basic GUI tools.

Double-click on an input variable icon to open the Membership Function Editor.

Double-click on the system diagram to open the Rule Editor.

The name of the system is displayed here. It can be changed using one of the Save as... menu options.

Double-click on the icon for the output variable, tip, to open the Membership Function Editor.

These pop-up menus are used to adjust the fuzzy inference functions, such as the defuzzification method.

This edit field is used to name and edit the names of the input and output variable.

This status line describes the most recent operation.

Fig: 5.4 The FIS Editor

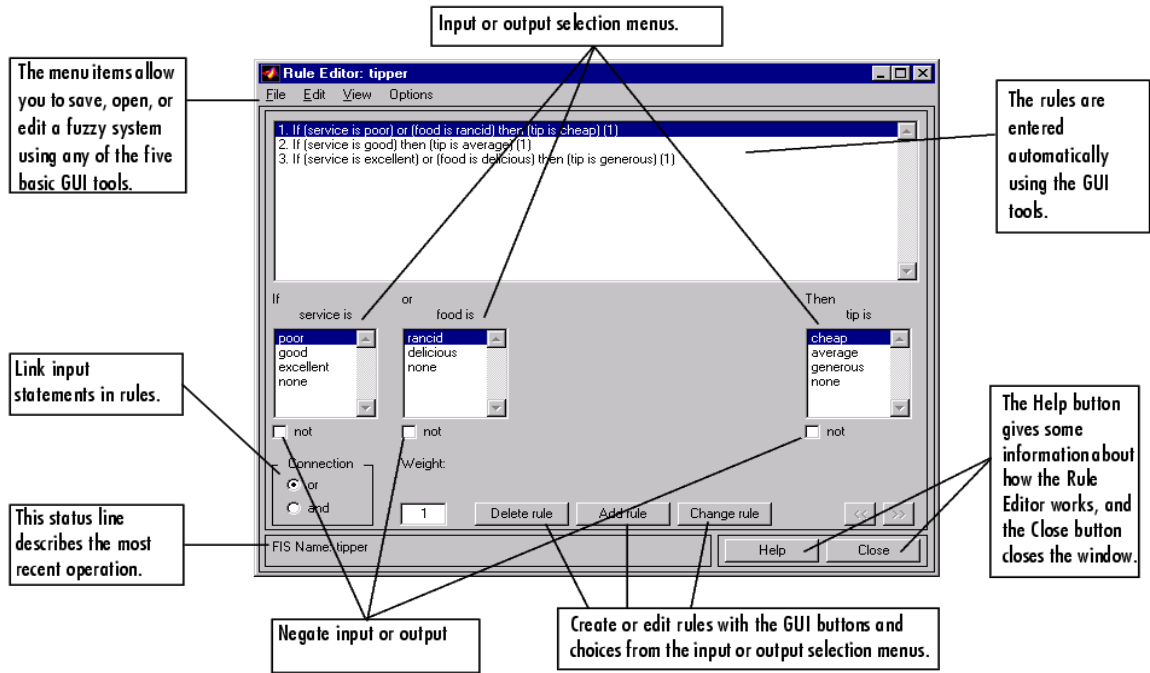


Fig: 5.5 Rule Editor

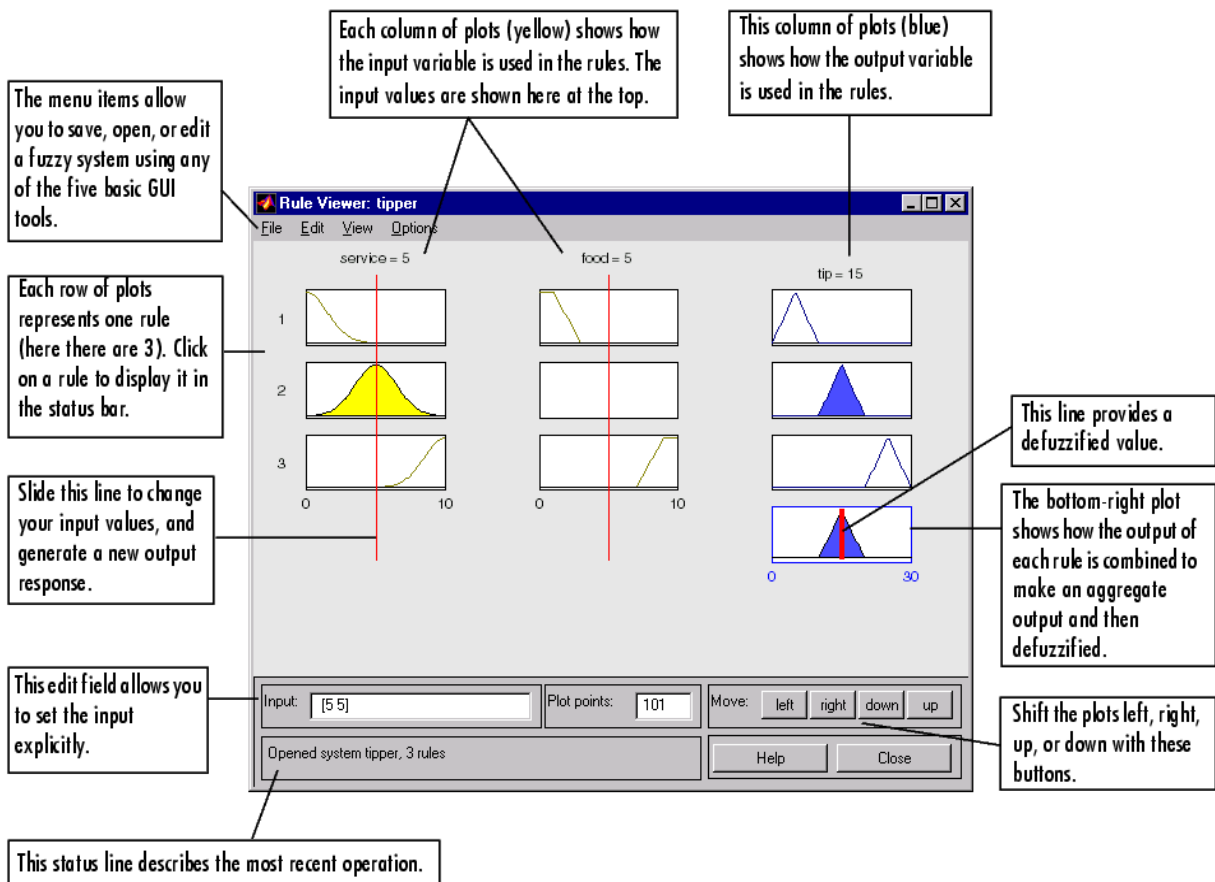


Fig: 5.6 Rule Viewer

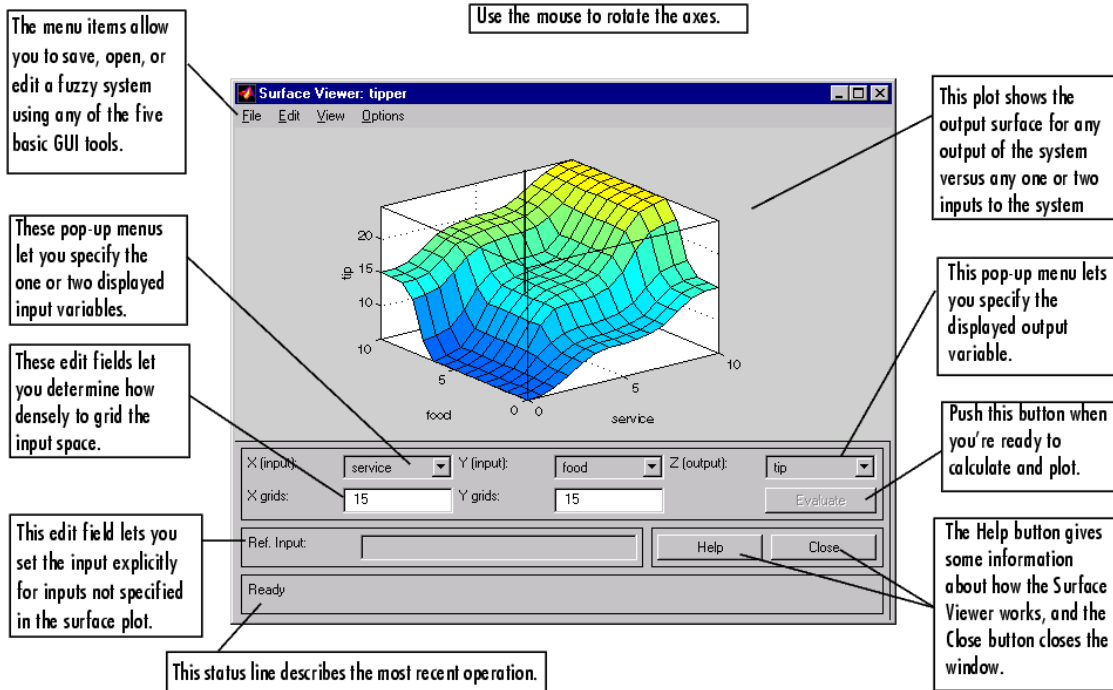


Fig: 5.7 Surface Viewer

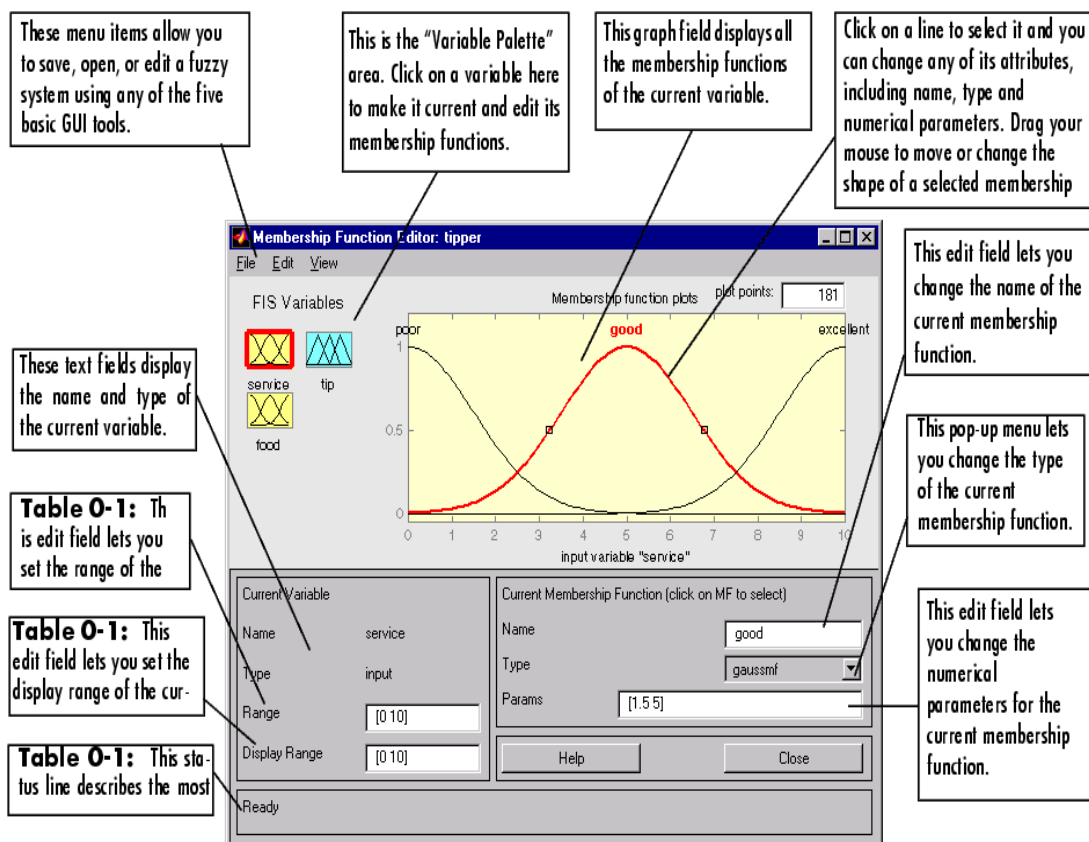


Fig: 5.8 Membership function editor

5.2.4 Rule-Base Matrix of the PID like FLC

In the following, we shall discuss the nature of the rules contained in the PID-like FLC rule base. The typical response of the second-order and third-order systems is shown [26]:

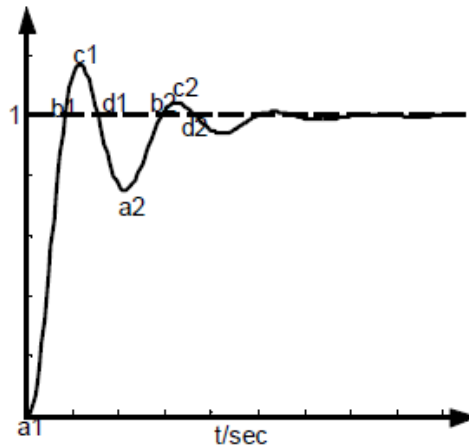


Fig: 5.9 Output response of plant with ZNPID controller for observation of deriving fuzzy control rules.

We can see from the equation of tuning a PID controller using the Zeigler Nichols approach that when the parameter increases, the proportional gain K_c emerges, leading to a significant PID control action. On the other hand, the same results can also be obtained. Therefore, based on the step response (as depicted in Figure 5.9), we may draw the following conclusions about tuning the parameter a : since there is a significant system error at the beginning (point a_1), a more controlled action is needed to provide a quick rising time. According to the relations between tuning the parameter a and the proportional gain K_c , integral gain T_i , and derivative gain T_d , one should give a big value a ; Around the point b_1 in Figure 5.9, a small control action is expected to avoid a large overshoot and a small value a is requested; Along with the decreasing of system error gradually, the control action should go to a steady state. Therefore the tuning parameter should not be regulated again. From the above analysis, the tuning parameter (a) should gradually be reduced from a big value to a small value during the step response. Since the fuzzy method has the ability to reason from the system error and the change of error, it can be utilized online to regulate the parameter properly.

The FLC design is very user-friendly and transparent. Depending on how close the answer is to the set point, the rule base implements the relevant control action (i.e. error and derivative error).

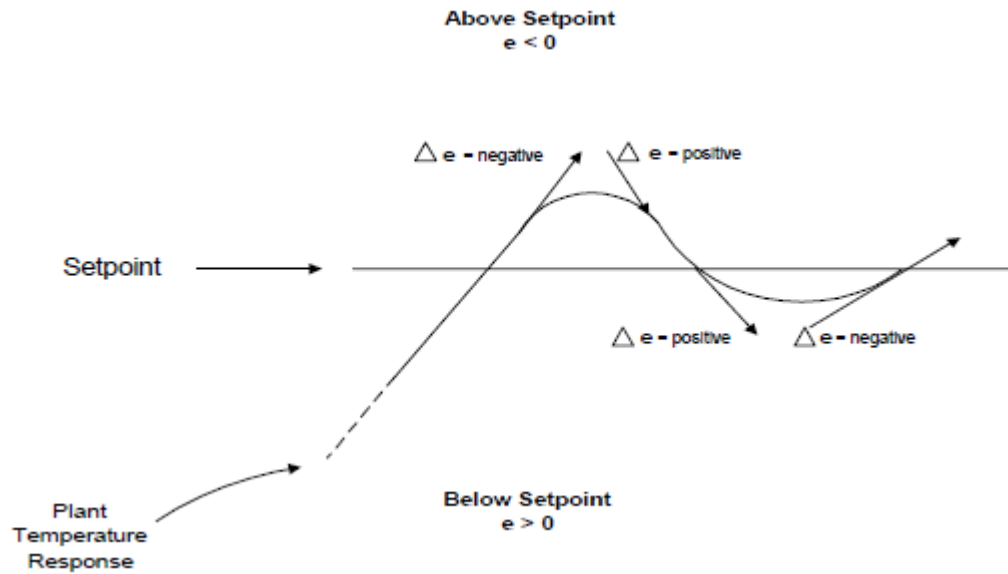


Fig 5.10: The Polarity of the Temperature Vector

For instance, one can consider the polarity and magnitudes of e and \dot{e} as temperature vectors with defined directions and velocities at every k th sampling period. The response is below the set point when the error has a positive polarity and above the set point (or in an overshoot state) when the mistake has a negative polarity, as shown in Figure 5.10. A suitable control action is implemented depending on the plant's velocity of convergence to the set point after determining the relative position from the set point. For instance, the reaction moves very quickly towards the set point when e is negative, and the magnitude is big. A significant negative control action is used to stop and slow the response.

Figure (5.10) above illustrates the effectiveness of having direct control over the error and change of error in driving the temperature to a prescribed set point.

Table:-5.1 Prototype of fuzzy control rules, with term sets

Rule No.	e	\dot{e}	\ddot{e}	Reference Point
1	PB	ZO	PB	a 1
2	PM	ZO	PM	a 2
3	PS	ZO	PS	a 3
4	ZO	NB	NB	b 1
5	ZO	NM	NM	b 2
6	ZO	NS	NS	b 3
7	NB	ZO	NB	c 1
8	NM	ZO	NM	c 2
9	NS	ZO	NS	c 3
10	ZO	PB	PB	d 1
11	ZO	PM	PM	d 2
12	ZO	PS	PS	d 3
13	ZO	ZO	ZO	set point

There are seven phases to the system reaction. 49 rules are split for the fuzzy logic controller presented in table 5.3 depending on whether the output is increasing or decreasing. For a first

order plus time delay system with high static gain, these 49 rules are adequate to address any scenario.

The linguistic variables used in the membership functions are described in Table 5.2

Table: 5.2 Linguistic variables in the fuzzy inference system

Error e(t)		Changes in error $\Delta e(t)$		Controller output u(t)	
NB	Negative Big	NB	Negative Big	PB	Positive Big
NM	Negative Medium	NM	Negative Medium	PB	Positive Big
NS	Negative Small	NS	Negative Small	PM	Positive Medium
ZO	Zero	ZO	Zero	ZO	Zero
PS	Positive Small	PS	Positive Small	NM	Negative Medium
PM	Positive Medium	PM	Positive Medium	NB	Negative Big
PB	Positive Big	PB	Positive Big	NB	Negative Big

Table 5.3: IF-THEN Rules base for fuzzy logic controller

e \ de	NB	NM	NS	ZO	PS	PM	PB
NB	PB	PB	PB	PB	PM	PS	ZO
NM	PB	PB	PM	PM	PS	ZO	NS
NS	PB	PB	PM	PS	ZO	NM	NM
ZO	PB	PM	PS	ZO	NS	NM	NB
PS	PS	PM	ZO	NS	NM	NB	NB
PM	PS	ZO	NS	NM	NM	NB	NB
PB	ZO	NS	NM	NB	NB	NB	NB

Figure (5.11) shows the Simulink representation of temperature control of IR heater using Fuzzy logic controller

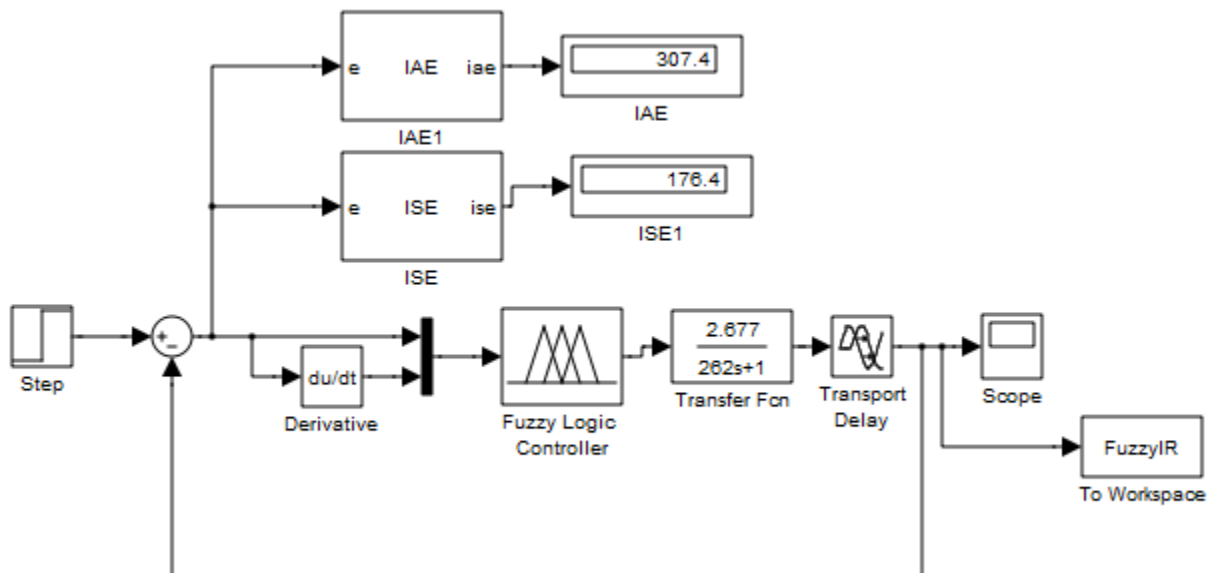


Fig 5.11: Implementation of fuzzy logic controller with plant using Simulink

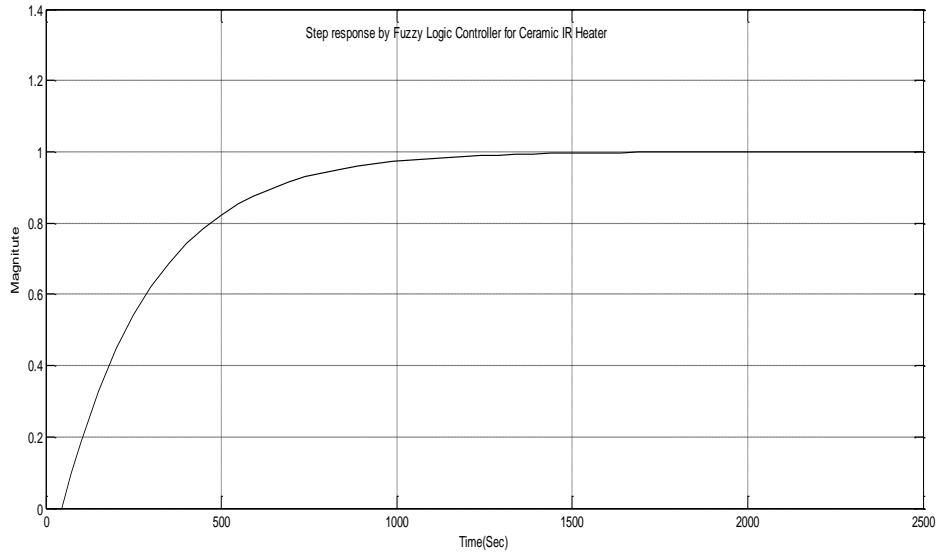


Fig: 5.12 Step response of Fuzzy logic Controller for Ceramic IR Heater

According to the simulation findings (peak overshoot, peak overshoot, settling time, and rise time) the fuzzy logic-based PID controller has a good response.

Table: 5.4 Performance table of Fuzzy Logic based Controller for Ceramic IR heater control

Performance	Rise Time (T_r)	Peak Overshoot(M_p)	Peak Time(T_p)	Settling Time(T_s)	ISE	IAE
FLC based PID	576.47	0	2500	1071	176.4	307.4

5.3 Genetic Algorithm (GA)

A stochastic global search technique called genetic algorithms (GA) imitates the course of natural evolution. One technique for optimization is this one. This approach was initially presented in the United States by John Holland in 1970 at the University of Michigan. Computational systems have improved their performance throughout time, making them desirable for particular types of optimization. The workings of natural selection, in which stronger individuals are probably the victors in a competitive context, are the basis for genetic algorithms. The definition of a genetic algorithm is given in [72]:

The genetic algorithm has three major components. The first component is related to the creation of an initial population of m randomly selected individuals. The initial population

shapes the first generation. The second component input m individuals and gives an output an evaluation for each of them based on an objective function known as the fitness function. This evaluation describes how close to our demands each one of these m individuals is. Finally, the third components are responsible for formulating the next generation. A new era is formed based on the fitness of individuals of the previous one.

Typically, a chromosome—a binary string—or a real-valued number indicates the population or mating pool. The objective function evaluates and measures how successfully a person executes a task. The objective function gives each person a corresponding number called fitness. Each chromosome's fitness is evaluated, and the survival of the fittest principle is used. A genetic algorithm has three primary stages: reproduction, crossover, and mutation.

Every chromosome is evaluated for fitness throughout the reproduction phase. This factor is utilized to create bias in favor of fitter candidates throughout the selection process. Like in natural evolution, a fit chromosome is more likely to be chosen for reproduction. This keeps happening till the selection requirement is satisfied. Thus, an individual's likelihood of being chosen correlates with its fitness level, ensuring that fitter individuals are more likely to have children. The most suitable strings should start to take control after being selected for repetition multiple times.

The crossover algorithm is started after the selection step is finished. In an effort to retain the beneficial aspects of the old chromosomes and produce superior new ones, the crossover procedures swap specific portions of the two selected strings. On the basis of the presumption that, on average, some persons' gene codes generate fitter humans, genetic operators directly alter the features of a chromosome. The crossover probability shows how frequently crossing occurs. There is a 0% chance that the children will resemble their parents exactly. A 100% chance indicates that every generation will be made up completely of brand-new children.

By themselves, selection and crossover will produce a lot of different strings. There are, however, two significant issues with this:

1. The first strings may not have enough diversity to guarantee that the GA explores the whole problem space, depending on the beginning population selected.

2. The GA could converge on sub-optimal strings due to a poor initial population selection. The addition of a mutation operator to the GA might be able to solve these issues. A mutation is a sporadic, random change in a string position's value. In the genetic algorithm, it is regarded as a background operator. Because a high mutation rate would eliminate fit strings and turn the genetic algorithm into a random search, the chance of mutation is typically modest. For example, for a probability of 0.1%, one string out of every thousand will be chosen for

mutation. Mutation probability values of around 0.1% or 0.01% are typical; these values describe the probability that a specific string will be selected for mutation. A string is chosen for mutation after that. The procedure of evaluation of generation N and production of generation N+1 (based on N) is iterated until a performance criterion is met. The creation of offspring based on the fittest individuals of the previous generation is known as breeding. The breeding procedures include three basic genetic operating ones: reproduction, crossover, and mutation.

Reproduction selects probabilistically one of the fittest individuals of generation N and passes it to generation N+1 without applying any changes to it. On the other hand, crossover selects probabilistically two of the fittest individuals of generation N; then in a random way chooses a number of their characteristics and exchanges them in a way that the chosen characteristics of the first individual would be obtained by the second and vice versa. Following their procedures creates two new offspring that both belong to the new generation. Finally the mutation selects probabilistically one of the fittest individuals and changes a number of its characteristics in a random way. The offspring that comes out of this transformation is passed to the next generation.

As it has been stated, each individual has a certain number of characteristics. For these characteristics, the term genes are used. Furthermore, according to the biological paradigm, the set off of an individual's genes forms its chromosome. Thus each individual is fully depicted by its chromosome, and a set of m chromosomes can fully describe each generation.

Comparing genetic algorithms to more conventional search and optimization methods reveals significant differences.

The five main differences are:

1. Unlike conventional algorithms, genetic algorithms scan a population of points concurrently.
2. The only factors that affect the direction of the search in genetic algorithms are the goal function and matching fitness levels. Genetic algorithms do not require derivative information or other auxiliary knowledge.
3. Instead of deterministic rules, genetic algorithms employ probabilistic transition rules.
4. A parameter set's encoding, not the parameter set itself, is what genetic algorithms work on (except where real-valued individuals are used).
5. A number of genetic algorithms may provide the final answer to a particular problem, and the user is free to select one.

The way that a conventional GA works by combining the three components (reproduction, crossover and mutation) described above is depicted in the following flow charts figure (5.13)[43]:

5.3.1 Conventional Genetic Algorithm

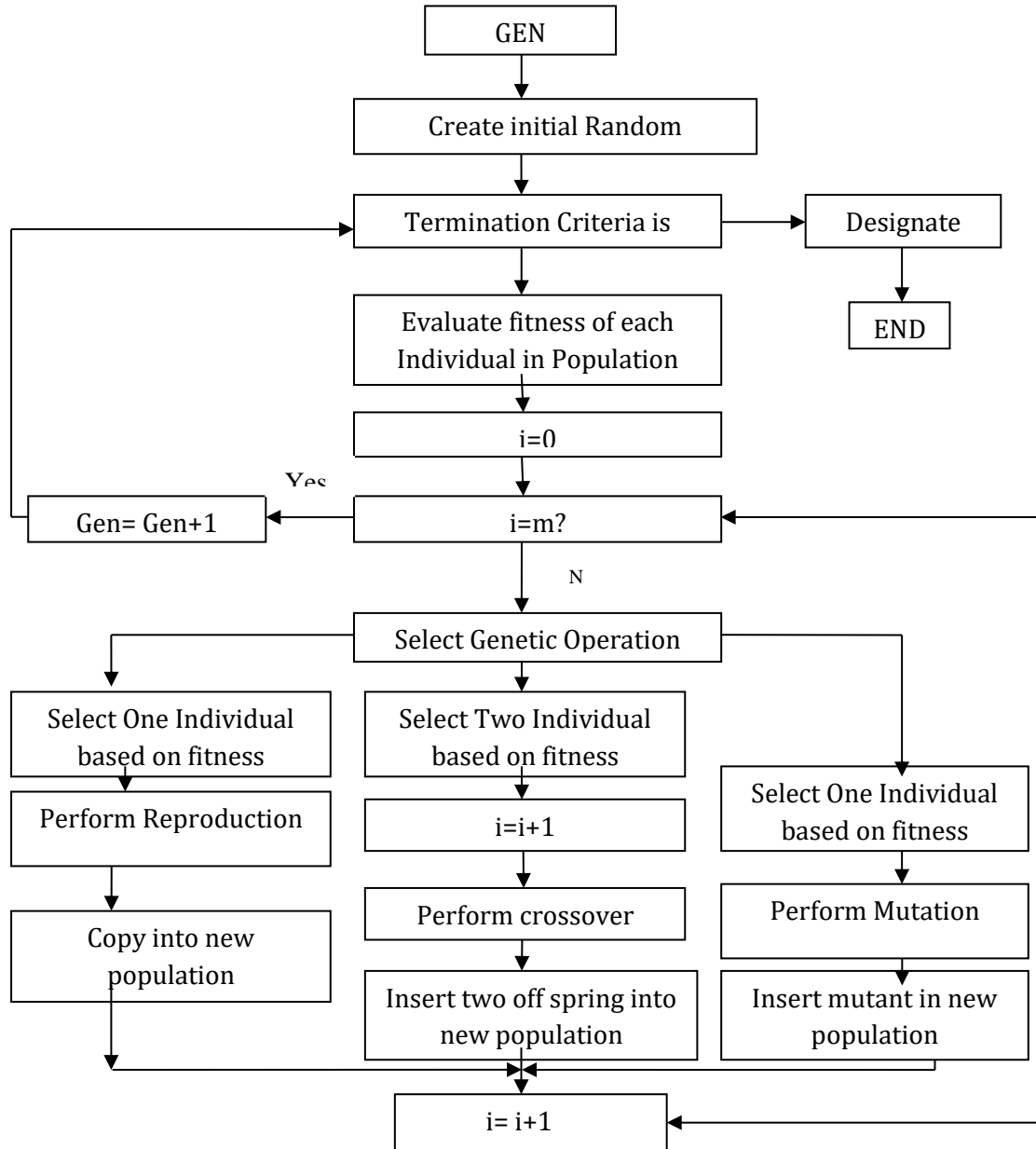


Fig: 5.13 Basic Flow Chart of Genetic Algorithm

The GA's flowchart makes it abundantly evident that every member of a new generation is the result of a reproduction, crossover, or mutation activity. A probabilistic schema is used to select the operation that will be used each time [146]. Each one of the three operations is related with a probability $P_{reproduction}$, $P_{crossover}$ and $P_{mutation}$ in a way that

$$P_{reproduction} + P_{crossover} + P_{mutation} = 1 \quad (5.2)$$

5.3.2 Design of PID Controller using Genetic Algorithm

Drafting the objective function is the most challenging step in developing a genetic algorithm. The optimum PID controller for the system must be evaluated using the objective function, as shown in figure (5.14). An objective function could be developed to identify a PID Controller that provides the smallest overshoot, quickest setting time, or fastest rise time. [39].

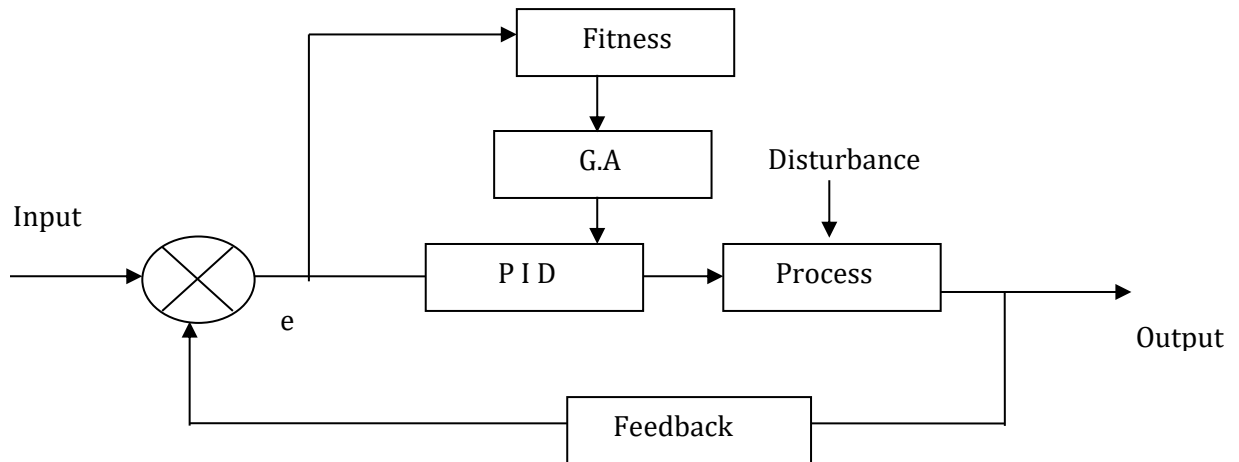


Fig: 5.14 Block diagram of PID tuning using GA

The objective function receives one copy of each chromosome from the population at a time. The chromosomes are then assessed and given a number to represent their fitness; the higher the number, the higher the fitness of the chromosomes. A new population made up of the fittest individuals is created by the genetic algorithm using the fitness value of the chromosomes. The P, I, and D words on each chromosome are made up of three distinct strings. The three terms of the chromosome are separated when it enters the evaluation function. The system transfer function and the newly built PID Controller create a unity feedback loop. As a result, the program's compilation time will be reduced.

5.3.3 Flow Chart of GA for PID Tuning

The flow chart for PID tuning based on GA is shown in figure (5.15).

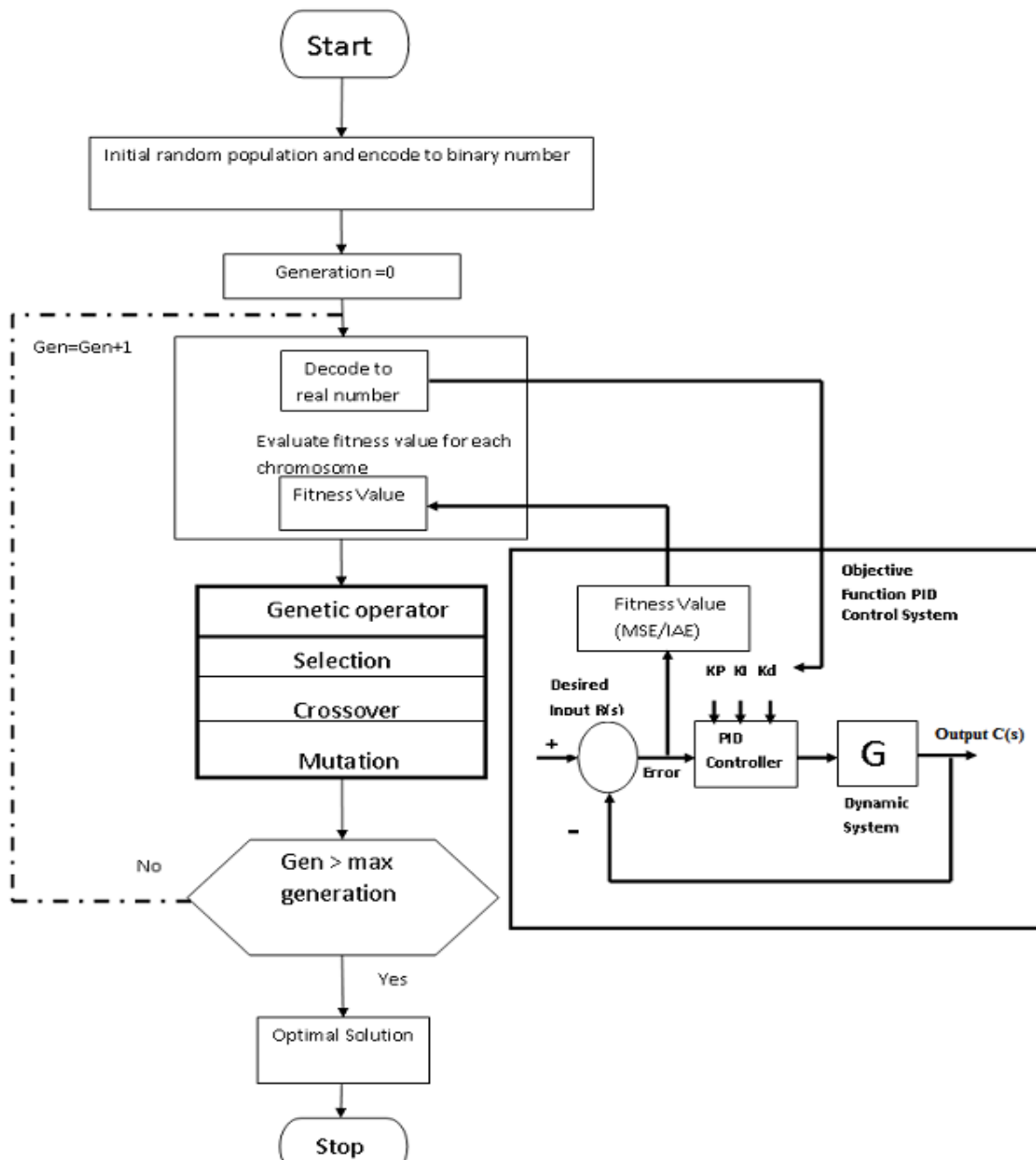


Fig: 5.15 Flow chart of GA for PID Tuning

5.3.4 Performing the Genetic Algorithm

The genetic algorithm is compiled using the command shown below. The function 'ga.m' will evaluate and iterate the genetic algorithm until it fulfills the criteria described by its termination function.

Performing the GA

```
% performing the genetic algorithm
[x,endPop,bPop,traceInfo]=ga(bounds,evalFN,evalOps,startPop,opts,...
    termFN,termOps,selectFN,selectOps,xOverFNs,xOverOps,mutFNs,mutOps);
```

Once the genetic algorithm is completed, the above function will return four variables:

x = the best population found during the GA.

endPop = The GA.s final population.

bestPop = The GA.s best solution tracked over generations.

traceInfo = The best value and the average value for each generation.

For most applications of the genetic algorithm to optimize the problem, the real coding technique is used to represent a solution of a given system. According to control adjectives, three parameters K_p , K_i , and K_d , of a PID controller are required to be designed in this research. The step involved in creating and implementing the programming is as follows:

- a. Generate an initial, random population of the individual for the fixed size.
- b. Evaluate their fitness (to minimize integral absolute error)
- c. Select the fitness members of the population.
- d. Execute mutation operation with low probability
- e. Select the best chromosomes using competition and selection
- f. The process ends if the termination criteria are reached (fitness function).
- g. If the termination criteria not reached, search for another best chromosome.

5.3.5 GA tuning parameters

Table: 5.5 GA tuning parameters

Population Size	100
Fitness Function	IAE
Selection Method	Stochastic Uinorm
Crossover Method	Airthmetic
Crossover Fraction	0.65
Mutation Method	Uniform
Mutation Probability	0.01

Figure (5.18) displays the step response of the GA-based algorithm for the IR heater with unity feedback.

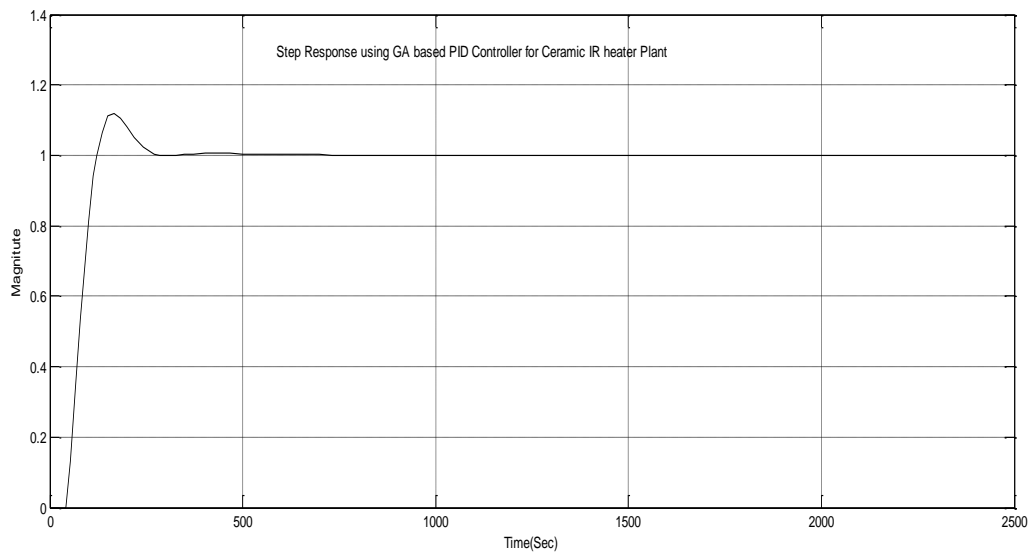


Fig: 5.18 Step response Using GA based PID controller

We observe the output response having overshoot and fast settling time. The PID controller based on GA optimization technique considerably suppress down the undesired overshoot and attain short rise time as well as satisfactory settling time.

The simulation results show how the GA-based PID controller, which is provided, responds in terms of rising time, peak time, settling time, and peak overshoot. in Table 5.6.

Table: 5.6 Performance table of GA based PID controller for Ceramic IR heater control

Performance	Rise Time (T_r)	Peak Overshoot(M_p)	Peak Time(T_p)	Settling Time(T_s)	ISE	IAE
GA based PID	58.45	11.92	166.84	245.71	66.95	89.37

5.4 Particle Swarm Optimization (PSO)

In 1995, Drs. Eberhart and Kennedy created the population-based stochastic optimization method known as particle swarm optimization (PSO), which was motivated by the social behavior of fish schools and bird flocks [30].

Each particle keeps track of the coordinates that are connected to the best solution (fitness) it has so far found to the problem. It is known as this value p_{best} . The best value so far attained by any of the particle's neighbors is another "best" value that the particle swarm optimizer keeps track of. The name of this place is " I_{best} ". A particle's best value is referred to as a global best g_{best} when it uses the entire population as its topological neighbors.

The idea behind particle swarm optimization is to adjust each particle's velocity in the direction of its p_{best} and I_{best} locations at each time step. Separate random numbers are created for acceleration toward and acceleration at sites, and these random numbers are used to weight acceleration.

PSO is based on two fundamental disciplines: social science and computer science. In addition, PSO uses the swarm intelligence concept, which is the property of a system where by the collective behaviors of unsophisticated agents that are in tracking locally with their environment create coherent global functional patterns. Therefore, the common terms of PSO can be described as follows:

1. **Social concept:** - It is known that "human intelligence results from social interaction". Evaluation, companionship, imitation of others, and learning from experience allow humans to adapt to the environment and determine optimal patterns of behavior, attitudes, and suchlike. In addition, a second fundamental social concept indicates that "Culture and Cognition are inspirable consequences of human sociality". Culture is generated when individuals become more similar due to mutual social learning. The sweep of Culture slows individuals to move towards more adaptive behavior patterns.
2. **Swarm intelligence principles:**- Swarm Intelligence can be described by considering five fundamental principles
 - a) **Proximity principles:** The population should be able to carry out simple space and time computations.
 - b) **Quality principles:** The population should be able to respond to quality factors in the environment.
 - c) **Diverse response principle:** The population should not commit its activity along excessively narrow channels.
 - d) **Stability principle:** The population should not change its mode of behavior every time the environment changes.
 - e) **Adaptability principle:** The population should be able to change its behavior mode when it is worth the computational price.

The notion of the particle swarm optimization entails altering the acceleration of each particle towards its p_{best} and g_{best} (for g_{best} version). With distinct random values being created for acceleration toward and places, acceleration is weighted by a random term. The following equation is used by the particle to update its position and velocity after determining the best values.

$$V(id) = v(id) + C1 * r(id) * (p_{best}(id) - x(id)) + C2 * r(id) * (g_{best}(id) - x(id)) \quad (5.3)$$

$$x(id) = x(id) + v(id) \quad (5.4)$$

Where

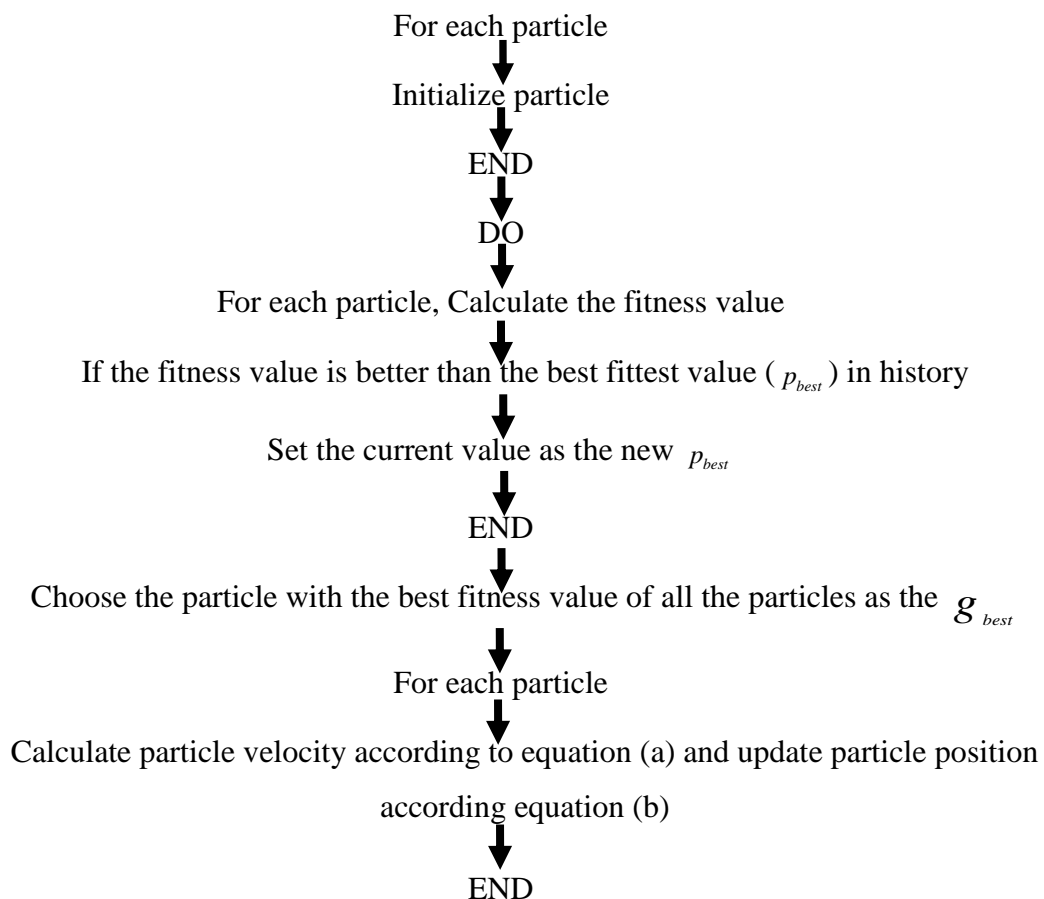
$v(id)$ = Particle- velocity

$x(id)$ = Current- particle

$r(id)$ = random number between (0, 1)

$C1$ & $C2$ = learning factor usually $C1=C2$

The Pseudo code of the procedure is as follows



While maximum interactions or minimum error criteria is not attained. In order to find the new solutions, the swarm of particles traverses the d-dimensional problem space after being initialized with a population of random candidate solutions. The fitness, f : can be estimated as a measure of particular traits. A position represents the position of each particle-vector present (the particle's index is I , and its velocity is represented by a velocity- vector. The best position vector among the swarm is saved in a vector following each interaction. Equation determines the updating of the velocity from the prior velocity to the new velocity vector (5.5). The sum of the prior location and the new velocity is then used in an equation to determine the new position (5.6).

$$velocity_{ij}(new) = w * velocity_{ij}(old) + C_1 * rand_1(p_{best_{ij}}(old)) - present_{ij}(old) + C_2 * rand_2(g_{best_{ij}}(old)) - present_{ij}(old) \quad (5.5)$$

$$present_{ij}(new) = present_{ij}(old) + velocity_{ij}(new) \quad (5.6)$$

Here, w stands for the inertia weight, and the random values are typically selected from $[0, 1]$. C_1 is a positive constant that is referred to as the co-efficient of the self-recognition component. C_2 is also a positive constant that is referred to as the co-efficient of the social component. A particle uses equation (a) to choose where to concentrate its efforts while taking into account both its own experience and the experience of the particle in the swarm that has had the most success. With a range of $[-S, S]$, the particle searches for solutions in the issue space in the particle swarm model (If the range is not symmetrical, it can be translated to the corresponding symmetrical range). The maximum moving distance during one encounter must be limited to the maximum velocity to effectively lead the particles in the search space.

$[-velocity_{max}, velocity_{max}]$ given in equation (5.7):-

$$velocity_{ij} = -Sign(velocity_{ij}) \min(velocity_{ij} / velocity_{max}) \quad (5.7)$$

The value of v_{max} is p s, with $0.1=P=1.0$ and is usually selected to be s , i.e. $p=1$.

5.4.1 Parameters and Tuning of PID in PSO

PSO doesn't require the initialization of many parameters. The initialization procedure is really straightforward. The parameters and initialization procedure for PSO are listed in this section.

The number of particles: The quantity of the particles must be taken into account. A good particle number range for the majority of practical applications is typically $[20, 40]$. 10

particles is often a significant number that is adequate to achieve the best results. When faced with challenging issues, the option of 100 or 200 particles is also available.

Inertia weight: -

In order to encourage broad exploration of the search space, the inertia weight is initially set as a constant, and the parameters are gradually reduced to obtain more optimal solutions. The ideal inertia weight is taken around 1.2, and as the algorithm develops, and value steadily decreases to 0.

Learning factors: Self-recognition and social component parameters and co-efficient are not absolutely necessary for PSO convergence. Adjusting these learning vectors to encourage convergence and lessen local minima is possible. Although it is frequently chosen as the value for these factors, some experimental findings suggest that it might yield even better outcomes.

Range and dimension of particles: -

Based on the optimization problem, the particle dimension and range are chosen. For various particle dimensions, different ranges can be selected.

$velocity_{max}$: - The maximum change by one particle that can be taken during one interaction is defined as the maximum velocity and denoted as $velocity_{max}$. Usually, the range of particles is set to the maximum velocity. For instance, if a particle belongs to the range [-5, 5], then the maximum velocity is 10.

5.4.2 Implementation of PSO- PID Controller

The PID Controller using the PSO algorithm was developed to improve the step transient response of a typical plant. It was also called the PSO- PID Controller. The PSO algorithm was mainly utilized to determine three optimal controller parameters K_p , K_i and K_d such that the controller system could obtain a good step response output [6][34].

Apply the PSO approach next to find the controller parameter; individual k is used in place of particle and population is used to define group. There are three members in an individual because of the three controller parameters K_p , K_i and K_d because of the fact that these members have real values. The dimension of a population is nx3 if there are n individuals in a

population of three. The reduction of performance requirements in the time domain can be achieved with a good step response and a set of good control parameters

5.4.3 Flowchart of PSO for PID Tuning

The flow chart for PID tuning based on PSO is shown in figure (5.19)

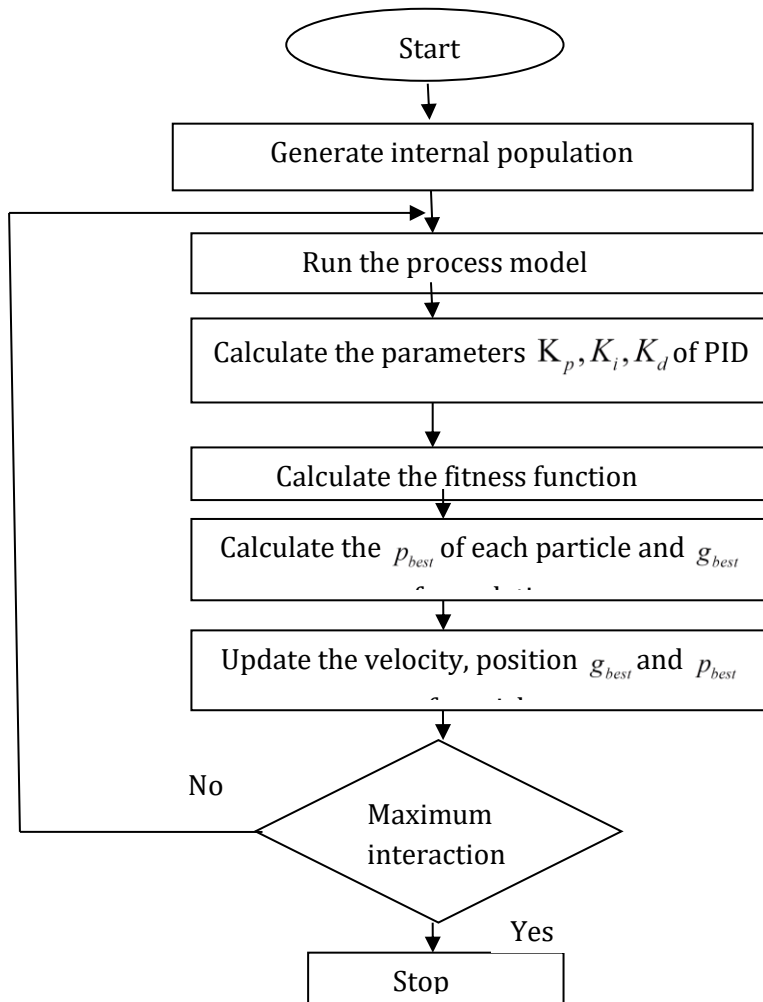


Fig: 5.19 Flow chart of PSO-based PID Controller tuning

5.4.4 PSO Tuning Parameters

Table: 5.7 PSO tuning parameters

Population Size	20
No. of Iteration	50
Velocity Constant, C1	2.5
Velocity Constant, C2	1.6

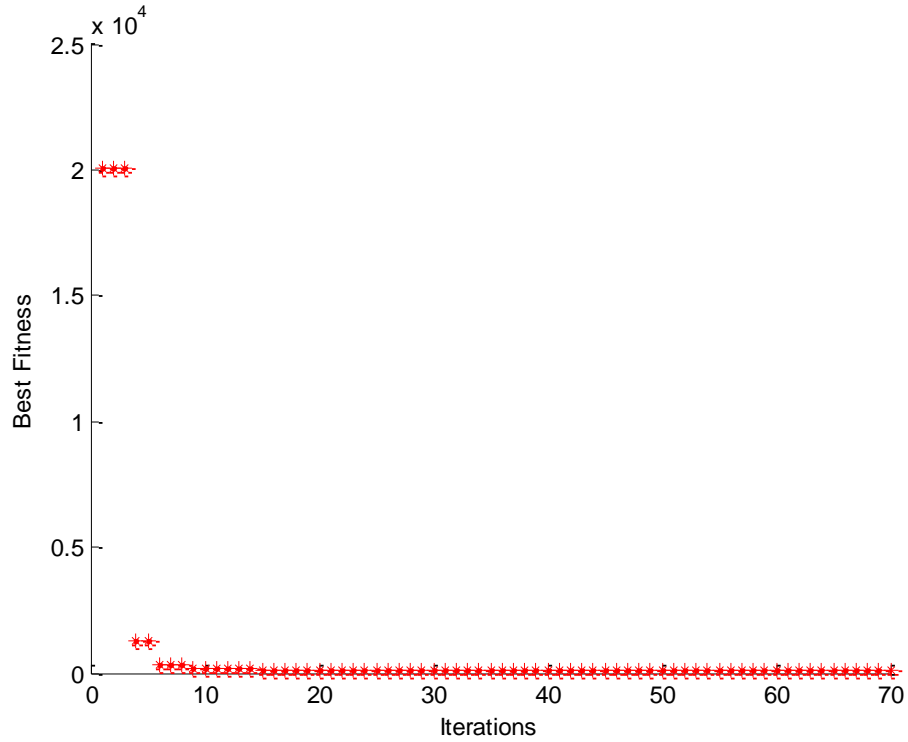


Fig: 5.20 Best Fitness function for the parameter by PSO method

Optimal parameters are designed based on PSO. After 70 generations of genetic operation, the best fitness function is shown in figure(5.20), and the optimal parameters are $K_p = 1.2743$, $K_i = 0.0045$, and $K_d = 6.1043$.

The Simulink module frame utilized for simulation is shown in figure (5.21)

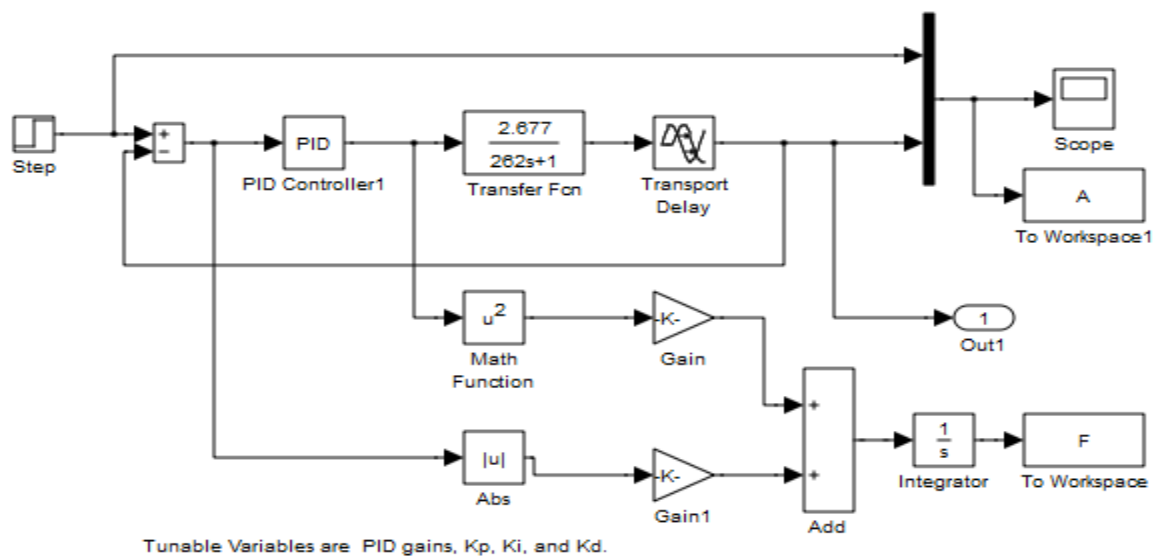


Fig: 5.21 Simulink model for PSO based PID controller

Figure (5.22) displays the step response of the PSO-based algorithm for the IR heater with unity feedback

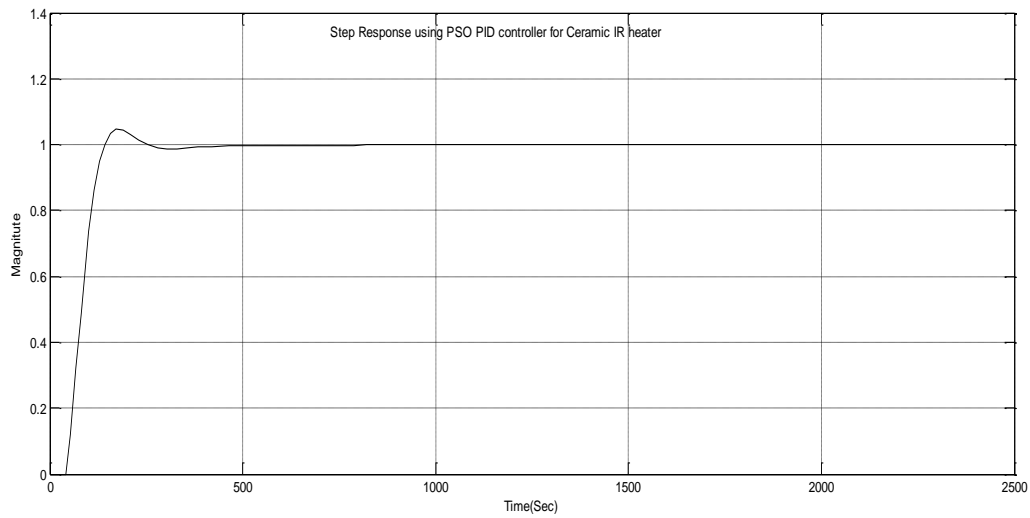


Fig: 5.22 Step response Using PSO-based PID controller

We observe the output response having an overshoot and fast settling time. The PID controller based on the PSO optimization technique considerably suppresses the undesired overshoot and Rising time, peak time, settling time, and peak overshoot simulation results show that the PSO-based PID controller shows response is shown in Table(5.8) to achieve both a quick rise time and a good settle time.

Table: 5.8 Performance table of PSO-based PID controller for Ceramic IR heater control

Performance	Rise Time (T_r)	Peak Overshoot(M_p)	Peak Time(T_p)	Settling Time(T_s)	ISE	IAE
PSO based PID	69.47	4.66	172.2	222.98	68.92	89.3

5.5 Bacterial Foraging Optimization (BFO)

The genuine bacteria move about while foraging thanks to a series of tensile flagella. When a bacteria is foraging, it performs two main tasks: swimming and tossing around, which are made possible by flagella. Each flagellum tugs on the cell when the flagella are rotated in a clockwise

orientation. As a result, the flagella begin to move independently, and the bacteria eventually tumbles less frequently than it would in an unfavorable environment where it would constantly tumble in search of a nutritional gradient. The bacterium can swim incredibly quickly by rotating its flagella in an anticlockwise way. In the algorithm outlined above, bacteria engage in chemotaxis, where they choose to travel in the direction of a gradient of nutrients and avoid an unpleasant environment.

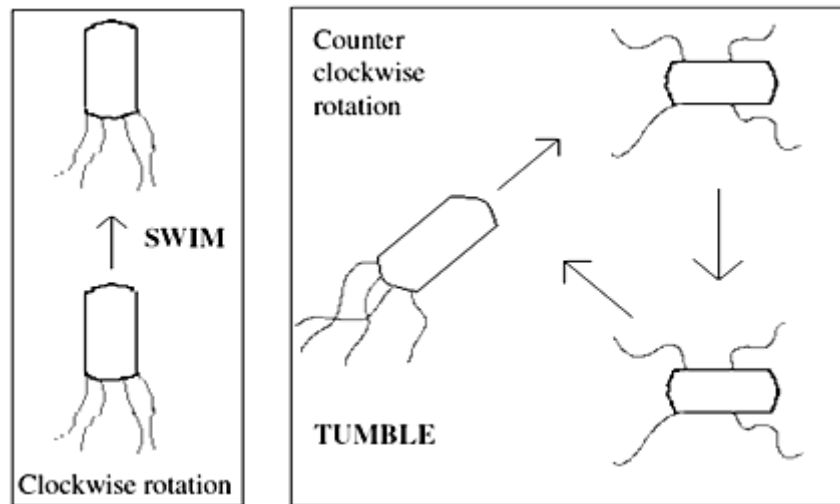


Fig: 5.23, Swim and tumble of a bacterium

When they have enough nourishment, they grow longer and when the temperature is right, they split in half to form an exact duplicate of themselves. Passino developed an event of reproduction in a bacterial foraging optimization algorithm as a result of this phenomena

The whole algorithm's pseudo-code is presented here, with a brief discussion of each step [59].

Chemotaxis

This procedure mimics the swimming and tumbling motion of an E. coli cell via its flagella. E. coli has two ways in which it can migrate biologically. It can swim continuously in one direction for a while, or it can tumble. It can switch between these two actions during its lifetime. Assume that a bacterium is represented by it at the j th chemotactic, k th reproductive, and l th elimination-dispersal steps. is the magnitude of the step in the arbitrary direction indicated by the tumble (run length unit). The movement of the bacteria can then be modeled by computational chemotaxis.

$$\theta^j(j+1, k, l) = \theta^j(j, k, l) + c(i) \frac{\Delta(i)}{\sqrt{\Delta^t(i)\Delta(i)}} \quad (5.7)$$

Where Δ indicates a vector in the random direction whose elements lie in [-1, 1]

Swarming:

When placed amidst a semisolid matrix containing a single nutrient chemo effector, a group of E. coli cells exhibits an intriguing group behavior where they organize themselves into a traveling ring by migrating up the nutrient gradient. When driven by an abundance of succinate, the cells release the attractant aspartate, which aids in group formation and the movement of densely packed swarms of bacteria. The following function may serve as a representation of the cell-to-cell signaling in the E. coli swarm.

$$J_{cc}(\theta, P(j, k, l)) = \sum_{i=1}^S J_{cc}(\theta, \theta^i(j, k, l)) \quad (5.8)$$

$$J_{cc} = \sum_{i=1}^S \left[-d \underset{\text{attractant}}{e^{-w_{\text{attractant}} \sum_{m=1}^P (\theta_m - \theta_m^i)^2}} \right] + \sum_{i=1}^S \left[-h \underset{\text{repellant}}{e^{-w_{\text{repellant}} \sum_{m=1}^P (\theta_m - \theta_m^j)^2}} \right] \quad (5.9)$$

where $J_{cc}(\theta, P(j, k, l))$ is the objective function value to be added to the actual objective function (to be minimized) to present a time-varying objective function, S is the total number of bacteria, p is the number of variables to be optimized, which are present in each bacterium and $\theta = [\theta_1, \theta_2, \theta_3, \dots, \theta_p]$ is the point in p dimensional, search domain.

Reproduction While each of the healthier bacteria (those generating lower values of the objective function) asexually splits into two bacteria, which are subsequently implanted in the same spot, the least healthy bacteria eventually die. This maintains the swarm's size.

Elimination and Dispersal

Various factors, such as a major local temperature rise that wipes out a population of bacteria that is currently living in an area with a lot of nutrient gradients, can cause gradual or abrupt changes in the local environment where a bacterial colony resides. Events may unfold in such a way that they eliminate all the bacteria in a particular area or disperse a population into a different area.

Size of population ‘S’: Increasing S can significantly increase the computational complexity of the algorithm. However, for larger values of S, it is more likely at least some bacteria near an optimum point should be started, and over time, it is then more likely that many bacteria will be in that region due to either chemotaxis or reproduction.

Length of Chemotactic step ‘C(i)’: If C(i) are too large, then if the optimum value lies in a valley with steep edges, the search will tend to jump out of the valley, or it may simply miss possible local minima by swimming through them without stopping. On the other hand, if C(i) are too small, convergence can be slow, but if the search finds a local minimum, it will typically not deviate too far from it. C(i) is a sort of a “step size” for the algorithm.

Chemotactic step ‘Nc’: If the size of Nc is chosen to be too short, the algorithm will generally rely more on luck and reproduction, and in some cases, it could more easily get trapped in a local minimum (premature convergence). Ns creates a bias in the random walk (which would not occur if Ns = 0), with large values tending to bias the walk more in the direction of climbing down the hill.

5.5.1 Algorithm for Bacterial Foraging Optimization-Based Design:

The search procedures of the proposed BFO-PID controller are as follows:-

Step 1)

Initialize parameters S, D, N_s , N_c , N_{re} , N_{ed} , P_{ed} , Δ , C(i), $D_{Attract}$, $W_{Attract}$, $D_{repellant}$ and $W_{repellant}$, where

S: Number of bacteria to be used for searching the total region.

D: Number of parameters to be optimized.

N_s : Swimming length, after which the tumbling of bacteria will be done in a chemotactic step.

N_{re} : Maximum number of reproductions to be undertaken.

N_{ed} : Maximum number of elimination-dispersal events to be imposed over the bacteria.

P_{ed} : Probability with which the elimination-dispersal will continue.

Δ : The location of each bacterium which is specified by random numbers on [0,1]

C(i): This is the chemotactic step size assumed constant for our design.

Step 2)

Elimination-Dispersal loop : l=l+1

Step 3)

Reproduction loop : k = k+1

Step 4)

Chemotaxis loop : $j = j + 1$

a) For $i = 1, 2, 3, 4, \dots, S$, take a chemotactic step for i as bacterium follows.

b) Compute $J(i, j, k, l)$, let $J(i, j, k, l) = J(i, j, k, l) + J_{cc}(\Delta^i(j, k, l), P(j, k, l))$ (i.e. add on the cell-to-cell attractant effect to the nutrient concentration).

c) Let $J_{Last} = J(i, j, k, l)$ to save this value since we may find a better cost via the run.

d) Tumble: Generate a random number vector $\Delta(i) \in R^p$ with each element $\Delta_m(i)$, $m = 1, 2, 3, \dots, D$, a random number on $[-1, 1]$.

e) Move: Let

$$\Delta^i(j+1, k, l) = \Delta^i(j, k, l) + C(i) * \Delta(i) / (\text{sqrt}(\Delta^T(i) * \Delta(i)))$$

This results in a step of size $C(i)$ in the direction of the tumble for bacterium i .

f) Compute $J(i, j, k, l)$, and then let $J(i, j, k, l) = J(i, j, k, l) + J_{cc}(\Delta(j, k, l), P(j, k, l))$

g) Swim : note that we use an approximation since we decide the swimming behavior of each cell as if the bacteria numbered $\{1, 2, \dots, i\}$ have moved and $\{i+1, i+2, i+3, \dots, S\}$ have not; this much is simpler to simulate than simultaneous decisions about swimming and tumbling by all the bacteria at the same time:

- Let $m = 0$ (counter for swim length).

- While $m < N_s$ (if have not climbed down too long)

.Let $m = m + 1$

.If $J(i, j, k, l) < J_{Last}$ (if doing better), let

$$J_{Last} = J(i, j+1, k, l) \text{ and let}$$

$$\Delta^i(j+1, k, l) = \Delta^i(j, k, l) + C(i) * \Delta(i) / (\text{sqrt}(\Delta^T(i) * \Delta(i)))$$

and use this $\Delta^i(j, k, l)$ to compute the new $J(i, j+1, k, l)$ as we did in f).

.Else, let $m = N_s$, this is the end of the while statement.

h) Go to next bacterium ($i+1$) if 'i' is not equal to S (i.e, go to (b)) to process the next bacterium.

Step 5)

If $j < N_c$ go to step 3. In this case, continue chemotaxis, since the life of the bacteria is not over.

Step 6)

Reproduction:

- a) For a given k and l , and for each $i = 1, 2, 3, 4, \dots, S$, let $J_{Health}^i = \sum J(i, j, k, l)$ be the health of bacterium (a measure of how many nutrients it got over its lifetime and how successful it was at avoiding noxious substances). Sort bacteria on chemotactic parameters $C(i)$ in order of increasing cost J_{Health} (higher cost means lower health).
- b) The S_r bacteria with highest J_{Health} values die and the other S_r bacteria with the best values split and the copies that are made are placed at the same location as their parent.

Step 7)

If $k < N_{re}$, go to step 2. In this case, we have not reached the number of specified reproduction steps, so we start the next generation in the next chemotactic step.

Step 8)

Elimination-Dispersal: For $i = 1, 2, 3, 4, \dots, S$, with probability P_{ed} , eliminate and disperse each bacterium (this keeps the number of bacteria in the swarming population constant). To do this, if we eliminate a bacterium, simply disperse one into a random location in the optimization domain.

Step 9)

If $l < N_{ed}$, then go to step 1, otherwise End

The flow chart for PID tuning based on BFO is shown in figure(5.24)

The block diagram for modifying the PID parameters using BFA in conjunction with the SIMULINK model is shown in Figure (5.25). A population of PID should be given to the BFA to start. The specification of the designed BFA technique is shown in Table 5.9.

Table: 5.9 Specification of the BFA

The Number of Bacteria	10
Number of chemotactic steps	5
Limits the length of a swim	4
The number of elimination dispersal events	2
The number of reproduction steps	4

The simulation method combines SIMULINK module and the optimized PID controller using bacteria forging model of the system is shown in Figure (5.26). Bacteria Forging optimization is used to create the PID controller's optimal parameters.

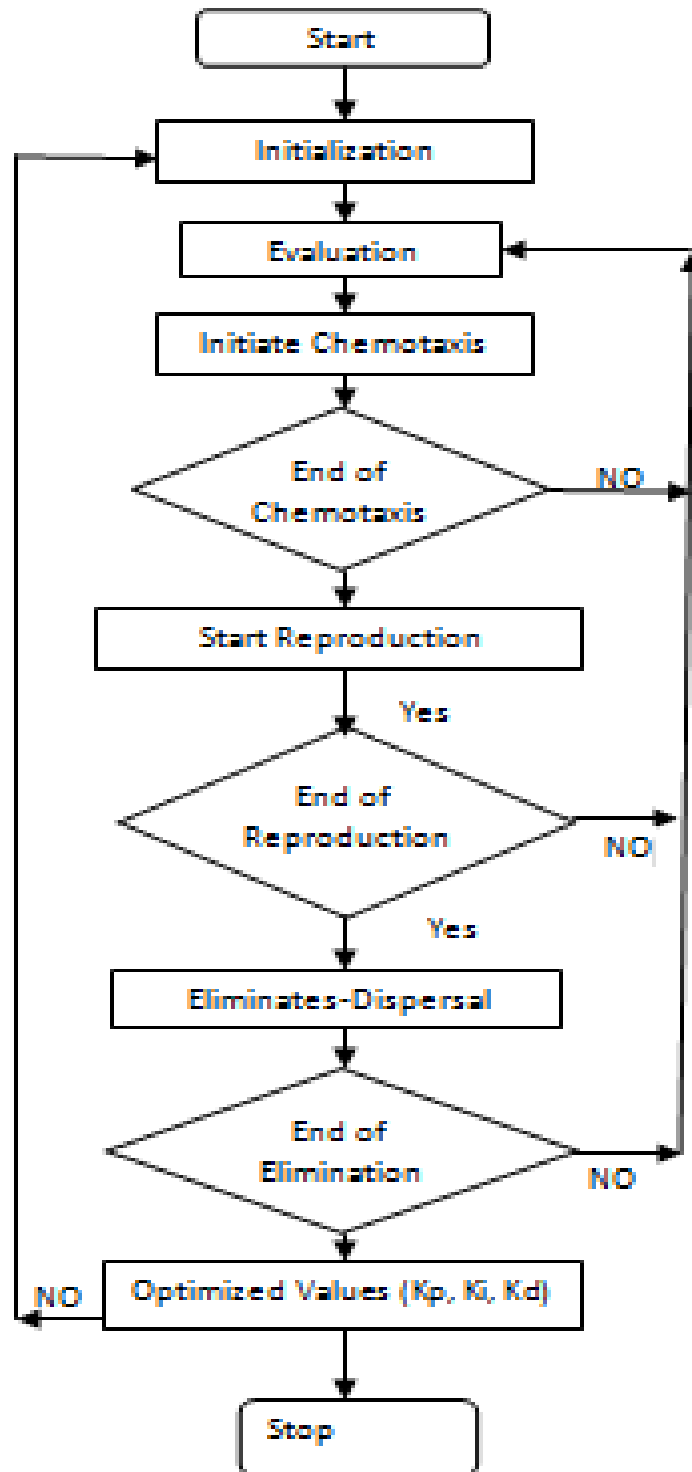


Fig:5.24 BFO flow chart for PID Tuning

After 50 generations of bacteria forging operation, the optimal parameters are $K_p = 1.4652$,

$K_i = 0.0071$, and $K_d = -0.0354$.

The Simulink module frame utilized for simulation is shown in figure (5.26)

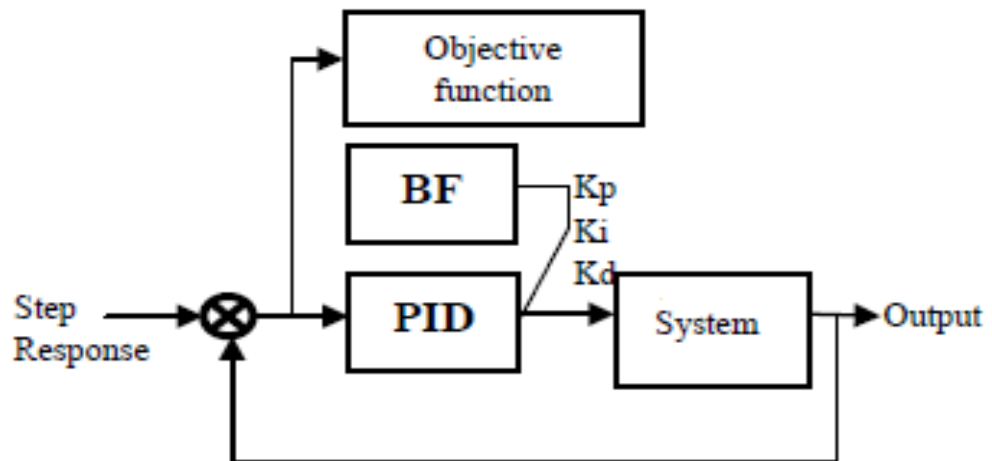


Fig:5.25 Block diagram of BPID to IR Ceramic Thermal Plant

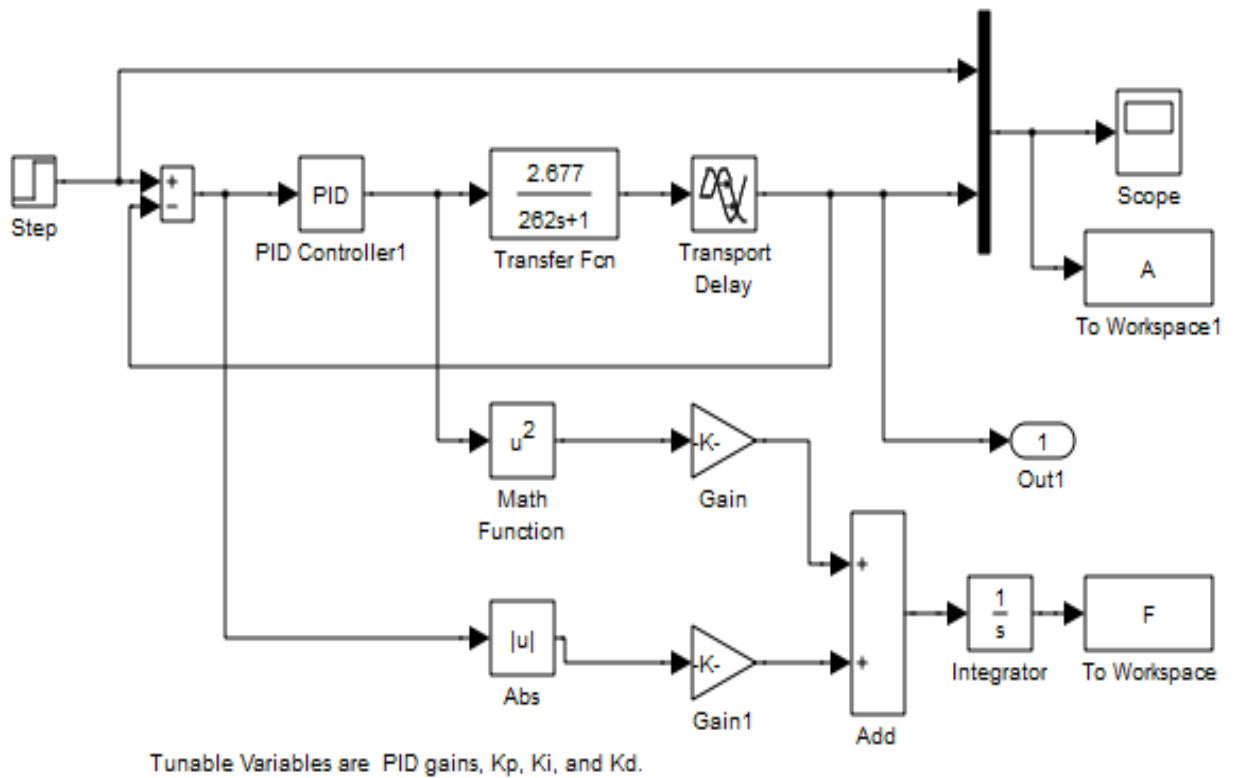


Fig: 5.26 Simulink model for BFO based PID controller

Figure displays the step response of the BFO-based algorithm for the IR heater with unity feedback (5.27)

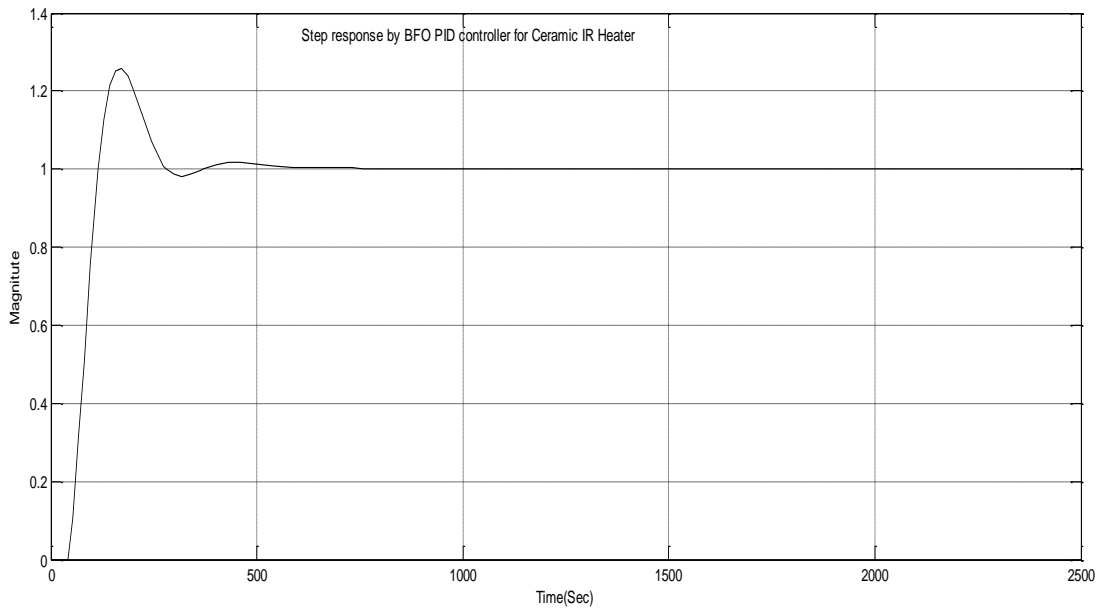


Fig: 5.27 Step response Using BFO based PID controller

We observe the output response having an overshoot and fast settling time. The PID controller based on the BFO optimization technique considerably suppresses the undesired overshoot and attains short rise time as well as good settling time.

Rising time, peak time, settling time, and peak overshoot data from the simulation show that the BFO-based PID controller exhibits the response shown in Table 5.10

Table 5.10 Performance table of BFO-based PID controller for Ceramic IR heater control

Performance	Rise Time (T_r)	Peak Overshoot(M_p)	Peak Time(T_p)	Settling Time(T_s)	ISE	IAE
BFO based PID	54.43	25.9188	172.03	268.16	72.77	107.7

5.6 Ant Colony Optimization (ACO)

Designing meta heuristic algorithms for combinatorial optimization issues using the Ant Colony Optimization (ACO) paradigm. Since 1991, numerous variations of the fundamental concept have been published in the literature, with the first algorithm that can be classified under this framework being described in that year [68]. Combining prior knowledge about a potential solution's structure with knowledge about the structure of successfully acquired good solutions

is the key characteristic of ACO algorithms. Meta heuristic algorithms are those that use some fundamental heuristics to break out of local optima. These include constructive heuristics that start with a null solution and add components to create a good complete solution or local search heuristics that start with a complete solution and iteratively modify them.

ACOs are very well suited for solving various optimization challenges. An artificial ant colony cooperates to solve problems, which is an emergent characteristic of the ants' cooperative interaction. Based on their shared characteristics with natural colonies, Ant algorithms are robust and adaptive. They can be used to solve many optimization problems and several variations of the same problem. Artificial ants borrow many characteristics from their natural counterparts. Artificial ants have two essential characteristics: they live in colonies of cooperative individuals and communicate covertly by leaving behind pheromones. To determine the shortest route from a starting location to a destination point, they use a series of local moves.

To identify the best answer, they just use local knowledge and a stochastic decision procedure. Artificial ants have been enhanced with various new capabilities not present in actual ants, as needed to address a specific optimization challenge. The optimization problem can be solved, or at least partially solved, by each individual ant, but the best solution can only be discovered when several ants cooperate [9][35].

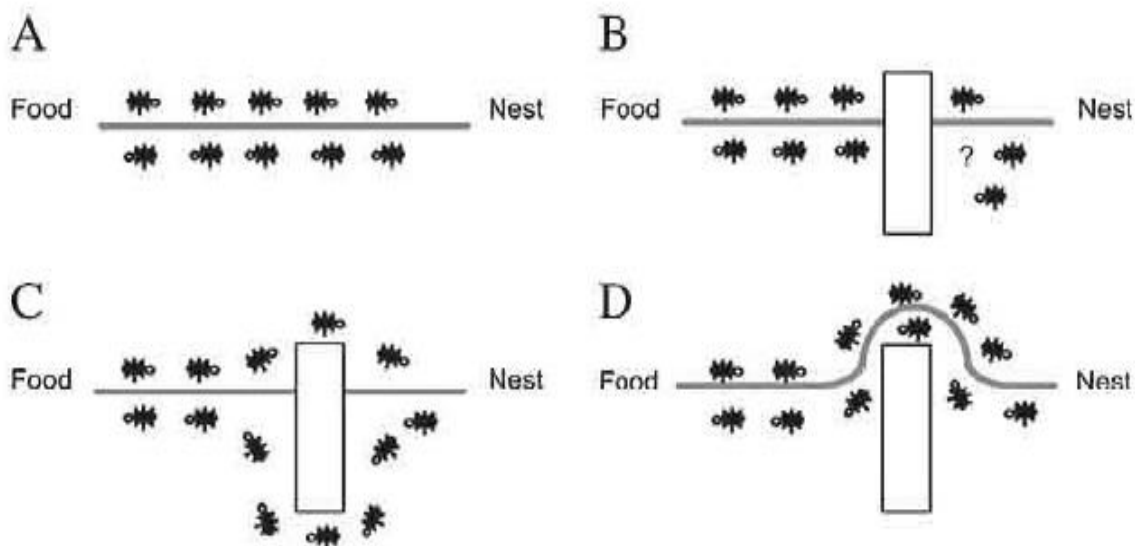


Fig: 5.28 Finding by ants path from nest to food source

It is an emergent outcome of such cooperation since the best answer can only be found by the collective cooperation of all the ants in a colony. The ants use pheromones to change the environment as a means of indirect communication while looking for a solution. An ant is

assigned a beginning state based on a specific problem and travels through a series of surrounding states in an effort to discover the shortest path. It travels using a stochastic local search strategy based on its internal state, pheromone features, and local information stored in the environment. The ants use this private and public information to determine the timing and location of pheromone deposition. The amount of pheromone deposited in the majority of applications is proportionate.

ACO depends upon on the pheromone matrix $\tau = \{\tau_{ij}\}$ for the construction of good solutions.

The initial values of τ are

$$\tau_{ij} = \tau_0 \quad \forall(i, j), \text{ where } \tau_0 > 0 \quad (5.10)$$

The probability $P_{ij}^A(t)$ of choosing a node j at node i is defined by the equation

$$P_{ij}^A(t) = \frac{[\tau_{ij}(t)]^\alpha [n_{ij}]^\beta}{\sum_{ij \in T^A} [\tau_{ij}(t)]^\alpha [n_{ij}]^\beta}; \quad i, j \in T^A \quad (5.11)$$

At each generation of the algorithm, ant constructs a complete solution after each generation starting at the source node

Where

$$n_{ij} = \frac{1}{k_j}, J = [P, i, d] \text{ Represent the heuristic function}$$

α and β = Constant that determines the relative influence of the pheromone values and heuristic values on the decision of the ant.

T^A = the path effect related by ant A at a given time

The quality of the pheromone $\Delta\tau_{ij}$ on each path may be defined as

$$\Delta\tau_{ij}^A = \begin{cases} \frac{L_{\min}}{L_A} & \text{If } i, j \in T^A \text{ Where} \\ 0 & \end{cases} \quad (5.12)$$

L^A = the value of the objective function found by ant A.

L_{\min} = the best solution carried out by the set of ants until the correct iteration.

The pheromone evaporation is a way to avoid an unlimited increase of pheromone traits, and also it allows the forgetfulness of the bad choice

$$\tau_{ij}(t) = P\tau_{ij}(t-1) + \sum_{A=1}^{NA} \Delta\tau_{ij}^A(t) \quad (5.13)$$

Where

NA= number of ants, P= the evaporation rate $0 < P < 1$, Population size= 100, No. of ants= 10, No. of path= 15, Iteration= 100, Fitness function: ISE

5.6.1 Ant Colony Optimization-Based PID Implementation

On the basis of experience and plant behavior, the gains of the controller are adjusted through a trial-and-error process. Gains are optimized using the ACO method, and the numbers are then input into the plant controller. This algorithm's goal is to maximize the PID controller's profits for the specified plant [20][21][24]. The integral derivative gain helps to reduce overshoot and eliminate steady-state error, whereas the proportional gain causes the controller to react to the error. Designing metaheuristic algorithms for combinatorial optimization issues using the ACO paradigm. Since the 1991 presentation of the first algorithm that fits under this classification framework, numerous diverse variations of the fundamental idea have been documented in the literature.

The combination of a priori knowledge about the structure of a potential solution and knowledge about the structure of previously acquired good solutions is the fundamental characteristic of ACO algorithms. A local search heuristic that starts with a complete solution and iteratively improves some of its components is an example of a metaheuristic algorithm. Metaheuristic algorithms are algorithms that, in order to escape from local optima, drive some basic heuristics: either a constructive heuristic starting from a null solution and adding elements to build a good complete one or a local search heuristic. ACO has been used to solve a number of combinatorial issues and is based on how ants communicate indirectly via pheromones while foraging.

The ACO was modeled by how ant colonies naturally identify food sources and carry them back to their nests by creating distinctive path formations. In the ACO algorithm, populations of ants are placed into the d-dimensional search space with randomly chosen places while being

aware of their current best values and location in the d-dimensional space. The distance between each city is modified for both its own pheromone level and that of the neighboring ant.

The conventional fixed gain PID controller is a well-known approach for industrial control processes. The proportional gain (K_p), integral time constant (T_i), and derivative time constant (T_d) are the three key parameters needed to construct this controller [53][69]. On the basis of experience and plant behavior, the gains of the controller are adjusted through a trial-and-error process. The gains are optimized using the ACO algorithm in the proposed ACO-PID controller, and the values are then applied to the plant controller. This algorithm's goal is to maximize the PID controller's gains for the specified plant. The integral derivative gain helps to reduce overshoot and eliminate steady state error, whereas the proportional gain causes the controller to react to the error.

5.6.2 ACO Algorithm Flow Chart for PID Tuning

The flow chart for PID tuning based on ACO is shown in figure (5.29)

Implementation Algorithm

Step I. Initialize randomly potential solutions of the parameters K_p , K_i , K_d by using a uniform distribution. Initialize the pheromone trail and the heuristic value.

Step II. Place the A_{th} ant on the node. Compute the heuristic value associated on the objective (minimize the error).

Step III. Use pheromone evaporation given by equation (5.13) to avoid an unlimited increase of pheromone trails and allow the forgetfulness of bad choices.

Step IV. Evaluate the obtained solutions according to the objectives.

Step V. Display the optimum values of the optimization parameters.

Step VI. Update the pheromone according to the optimum solutions calculated at **step V**. Iterate from step II until the maximum of iterations is reached.

Based on Ant Colony Optimization, the PID controller's ideal parameters are created.

After 100 generations of ant colony optimization operation, the best fitness function is shown in figure (5.30); the optimal parameters are $K_p=1.92$, $K_i=0.01$, and $K_d=19.8$

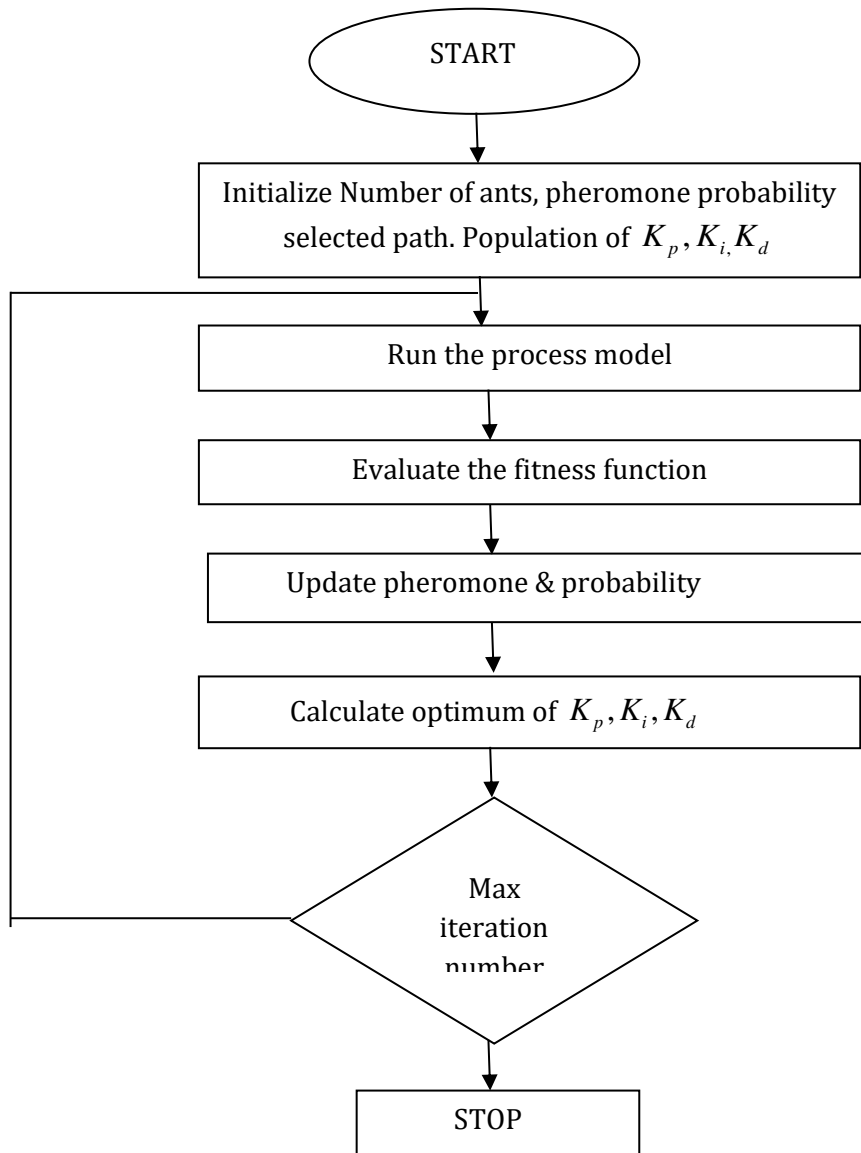


Fig: 5.29 Flow chart of ACO for PID tuning

We observe the output response having an overshoot and fast settling time. The PID controller based on the ACO optimization technique considerably suppresses the undesired overshoot and attains short rise time as well as good settling time. The simulation results (rising time, peak time, settling time, peak overshoot) demonstrate the response of the ACO-based PID controller, which is presented in Table 5.11.

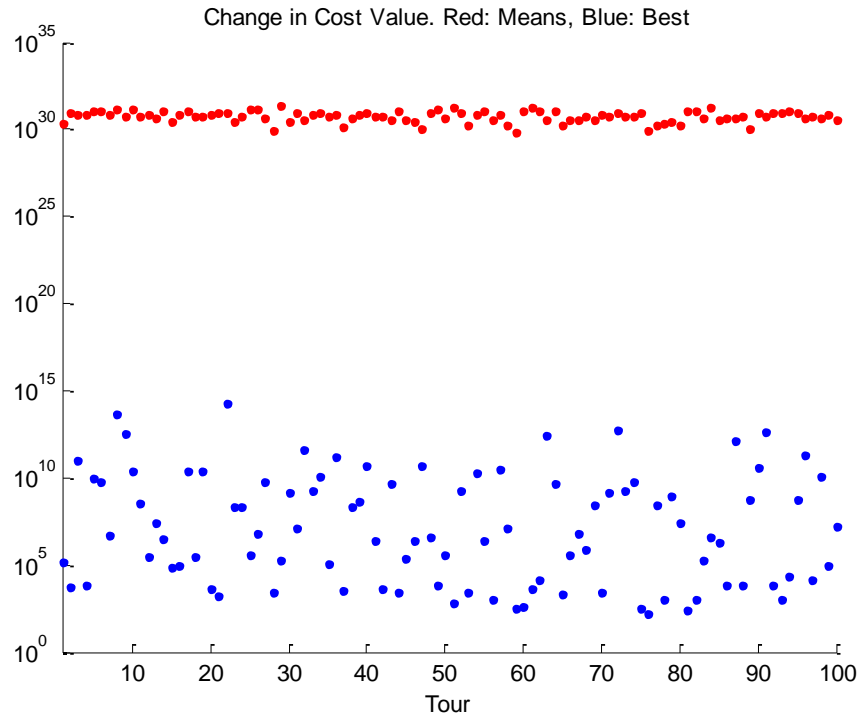


Fig: 5.30 Best Fitness function for the parameter by ACO method

The Simulink module frame utilized for simulation is shown in figure (5.31)

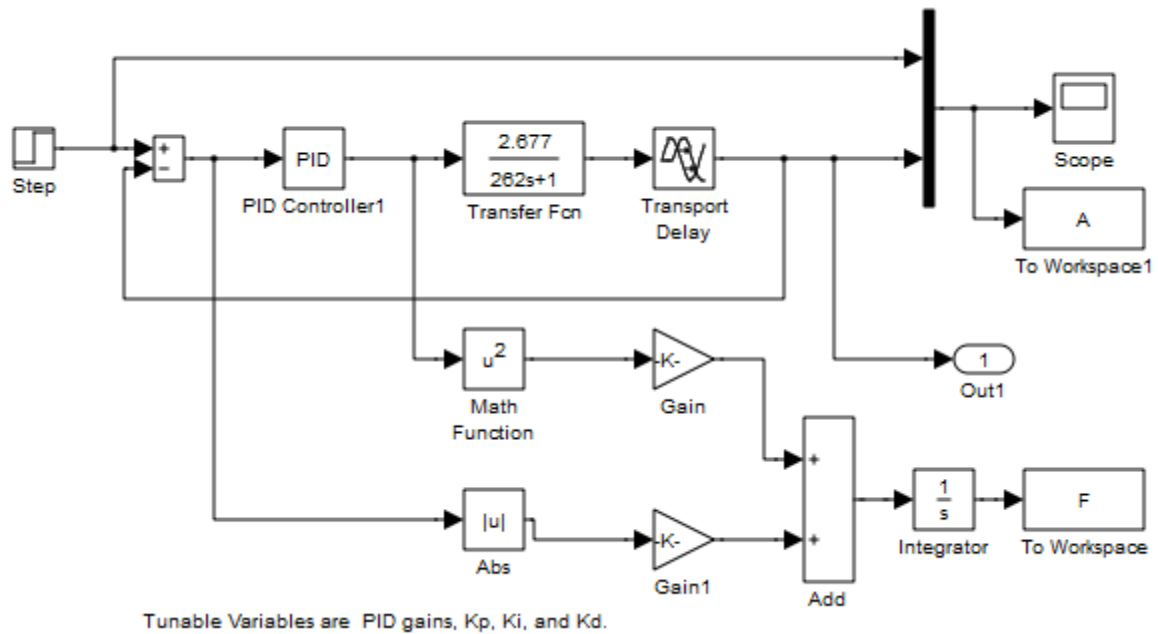


Fig: 5.31 Simulink model for ACO based PID controller

The figure displays the step response of the ACO-based algorithm for the IR heater with unity feedback (5.32)

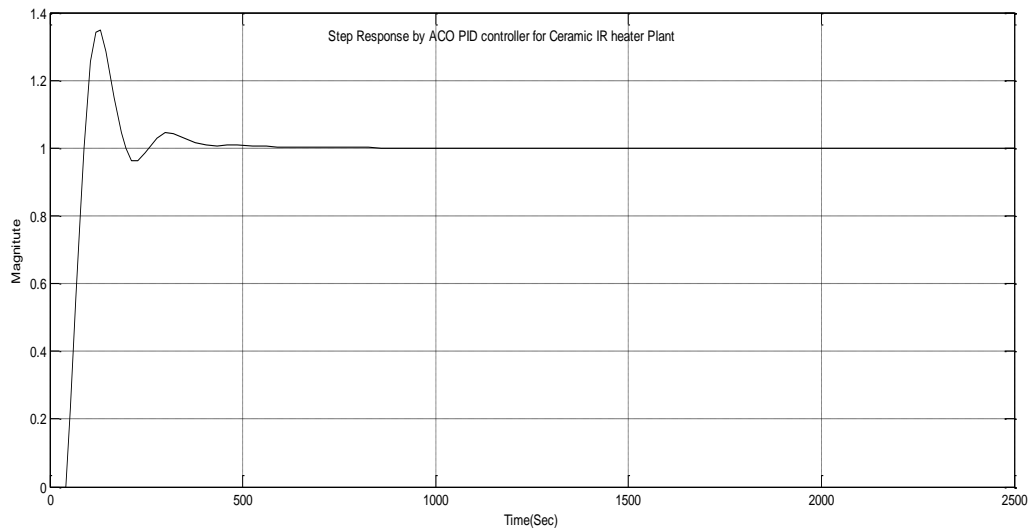


Fig: 5.32 Step response Using ACO-based PID controller

Table: 5.11 Performance table of ACO-based PID controller for Ceramic IR heater control

Performance	Rise Time (T_r)	Peak Overshoot(M_p)	Peak Time(T_p)	Settling Time(T_s)	ISE	IAE
ACO based PID	36.80	34.79	132.28	367.31	63.51	94.28

5.7 Simulation Results

A comparative study has been done using different control techniques to analyze the performance of different controllers. First, the conventional PID controller is implemented as the primary controller.

Table 5.12 Performance of PID, IOPID, Fuzzy Logic Controller, Artificial Intelligence based PID, Bio inspired-based PID controller, and FOPID controllers

Parameter	ZNO	ZNC	AH-PID	CC-PID	IOPID	FOPID	FLC	GA-PID	PSO-PID	ACO-PID	BFO-PID
Rise Time	21.48	25.4	207.9	21.09	112.4	49.02	576.4	58.45	69.47	36.80	54.43
Settling Time	675.3	389.3	850.5	1270	613.8	408.2	1071	245.7	222.9	367.3	268.16
Peak Time	105.0	116.9	504.26	105.1	341.9	143.13	2500	166.8	172.2	132.2	172.03
Peak Overshoot	80.10	74.7	11.82	103.5	9.8	14.07	0	11.92	4.66	34.79	25.91
ISE	83.4	80.55	96.58	143.8	66.92	64.98	176.4	66.95	68.92	63.51	72.77
IAE	142.4	116.4	183.2	269.8	114.8	106.2	307.4	89.37	89.3	94.28	107.7

It has been concluded that the overall performance of FOPID-based controllers is better than other controllers. In real-time implementation, the performance of the process control includes the time required by the heater to be settled on the initial set-up temperature. The real-time controller includes the signal transfer from the temperature sensor for real-time action. The temperature warm-up is slow due to the resistance heating element used in the ceramic infrared heater. The results obtained for simulation with fractional order PID controller show better performance (rise time, settling time, peak time and peak overshoot) than those designed with ceramic infrared HFE systems. This work performs a small-scale test measuring controller performance so that it serves as a platform for future research efforts leading to the real-life implementation of a Ceramic Infrared Heater Temperature control system.

5.8 Conclusion

Artificial intelligence techniques are implemented to find the desired results for the Infrared heater, Simulink model representation for temperature control of IR heater using Fuzzy logic, Genetic Algorithm, and PSO.ACO and BFO are applied in which change in reducing overshoot, rise time, and settling time has been seen.

STABILITY ANALYSIS OF FRACTIONAL ORDER FUZZY CELLULAR NEURAL NETWORKS WITH LEAKAGE DELAY AND TIME-VARYING DELAYS

6.1 Introduction

Fractional-order calculus has a very long history in pure mathematics. The study of fractional calculus can be dated back to 1695; the fractional operator concept was put forward by Leibnitz. Fractional calculus, as an extension of usual calculus dates from the late seventeenth century, and it is regarded as a generalization of derivation and integration of arbitrary order. Over the past few days, the fractional order dynamical system has attracted many researchers in different branches, especially science and engineering. Compared to the traditional integer order dynamical system, the main distinguished influence of fractional order is that infinite Memory and more degrees of freedom because it has nonlocal and weakly singular kernels. For the description of memory and hereditary properties of various materials and processes, fractional order models have been proven to be an excellent instruments in comparison with classical integer order models [109–111]. Actually, the behavior of real world processes generally or most likely is governed by fractional-order systems [112–120]. Moreover, fractional-order systems are more likely to describe most real-world behaviors than integer-order ones because they can provide more practical value and accurate results. Therefore, many researchers have paid close attention to studying the dynamical behaviors of fractional-order systems and have drawn some wonderful results in the literature [121–125]. Stability has been a hot research topic that has drawn much attention from mathematician, physicist, and computer scientists and a large number of research are found in the literature [126].

6.2 Concept of Artificial Neural Networks

The elementary nerve cell, called a neuron, is the fundamental building block of biological neural networks. Its schematic diagram is shown in Figure 6.1. An artificial neuron is a computational model inspired by natural neurons. Natural neurons receive signals through synapses located on the dendrites or membrane of the neuron. When the signals received are strong enough (surpassing a certain threshold), the neuron is activated and emits a signal

through the axon. This signal might be sent to another synapse and might activate other neurons.

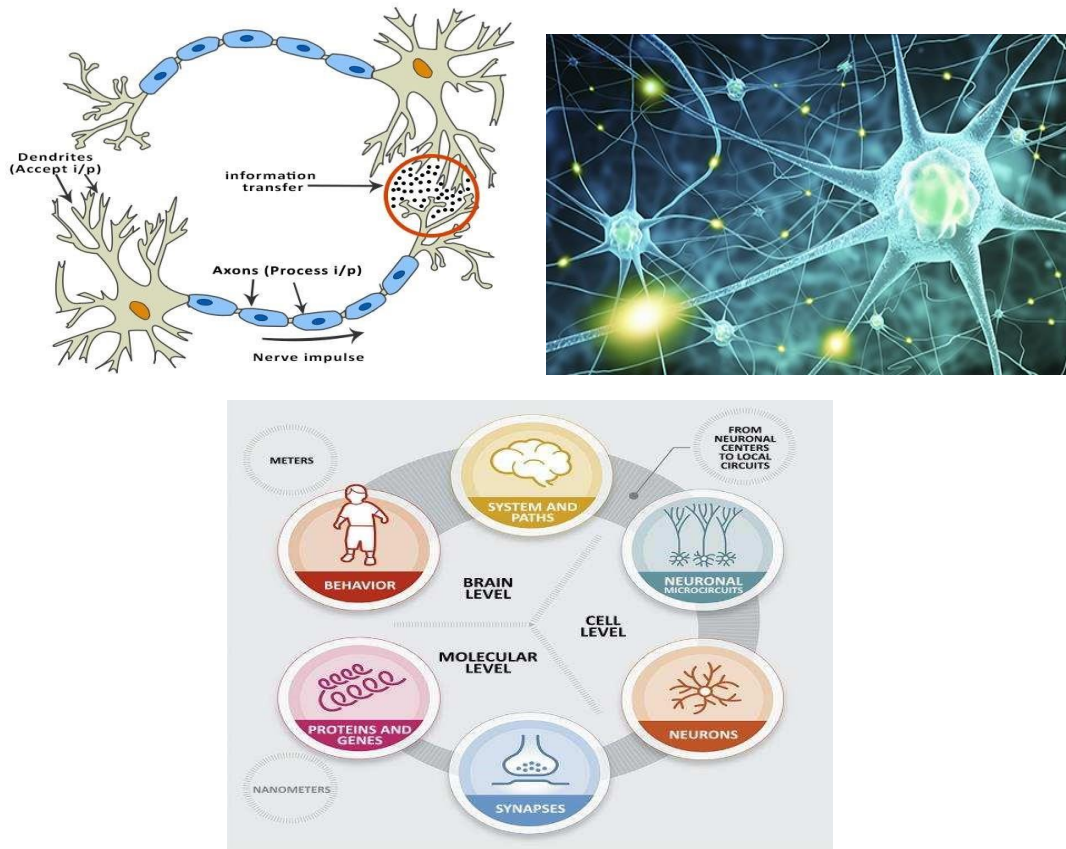


Figure 6.1: Biological neural system

Modern computers cannot equal the cognitive capacities, flexibility, robustness and energy efficiency of the human brain. In fact, compared to computers, the brain works slowly (with spiking frequency signals of the order of hundreds of hertz) and with apparently low precision (individual neural processes). However, the whole brain carries out well-organized computations in parallel (around 10^{16} synaptic operations per second), works in real-time (in continuous interaction with the environment) with closed perception-action loops, and very low energy consumption (approximately 30 W), beating the most powerful computers in certain “biologically relevant tasks”, such as “manipulating objects”, recognizing a scene after having viewed it once, etc. It also provides an elegant degradation of capabilities, self-repair, and modification through learning. These properties inspire scientists and engineers to search for new and disruptive computing Models.

The origin of artificial neural networks was based on trying to mimic how the human brain performs a particular task via the use of simplified mathematical models. The basic concept consists of considering the brain as an information-processing, highly complex, non-linear, parallel computer system.

The most significant features of the domain are:

- (i). The use of massive interconnection networks of simple processing units (neurons)
- (ii). Asynchronous parallel and distributed processing
- (iii). Non-linear dynamics
- (iv). Global interconnection of network elements
- (v). Self-organization
- (vi). High-speed computational capability
- (vii). Modification of the parameters of the network to carry out a specific task or adaptation to its environment via a learning process.

A neural network (NN) has a parallel-distributed architecture with a large number of nodes and connections. Each connection points from one to another and is associated with weight. A neuron is a fundamental unit for the operation of a neural network. Its model is shown in Fig. 6.2. Construction of a neural network involves the following tasks.

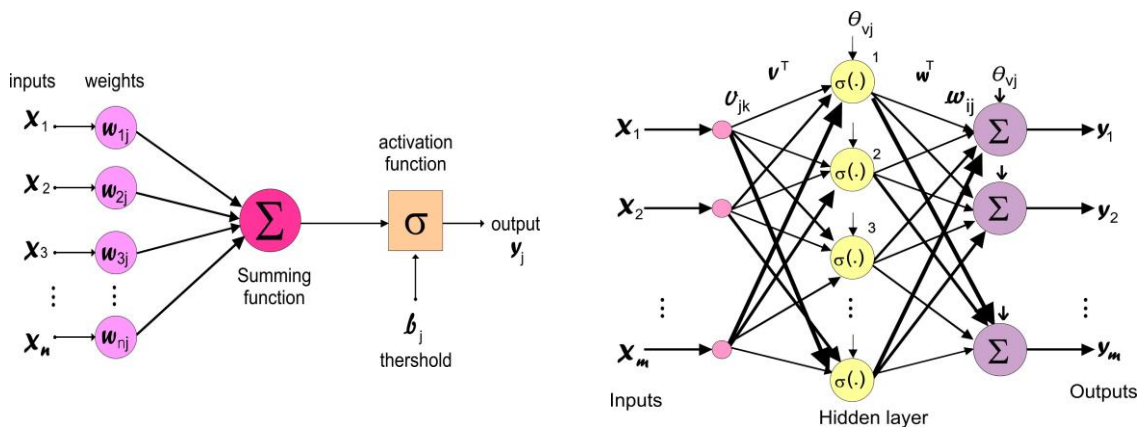


Figure 6.2: A conventional architecture of an artificial neural unit

Determine the network properties: the network topology (connectivity), the types of connections, the order of connections, and the weight range. Determine the node properties: the activation range and the activation (transfer) function. Determine the system dynamics: the weight initialized scheme, the calculating activation formula, and the learning rule. The topology of neural networks refers to its framework as well as its interconnection scheme. The framework is often specified by the number of layers (or slabs) and the number of nodes per layer. The types of layers include:

- The Input Layer: The nodes in it are called input units, which encode the instance presented to the network for processing. For example, each input unit may be designed by an attribute value possessed by the instance.
- The Hidden Layer: The nodes in it are called hidden units, which are not directly observable and hence hidden. They provide non-linearity for the network.

- The Output Layer: The nodes in it are called output units, which encode possible concepts (or values) to be assigned to the instance under consideration. For example, each output unit represents a class of objects.

Input units do not process information, they simply distribute information to other units. According to the interconnection scheme, a neural network can be either a feed-forward network or a recurrent-type network. Their definitions are:

- Feed-forward networks: The feed-forward neural network was the first and arguably most straightforward type of artificial neural network devised. In this work, the information moves in only one direction—forward. From the input nodes, data goes through the hidden nodes (if any) and to the output nodes. There are no cycles or loops in the network. In general, there are two different types of Feed-forward networks.
- Single-Layer Feed-forward networks: The simplest form of a layered network is only an input layer of source nodes and an output layer of target nodes. The main task is to project the input layer onto the output layer and not vice versa.
- Multi-Layer Feed-forward networks: In this type of neural network, there is more than one hidden layer whose processing nodes are called hidden neurons. The function of hidden neurons is to intervene between the external input and the target output layers. The addition of hidden layers gives higher-order statistics to the process of the neural network. This addition of hidden neurons becomes valuable when the number of input neurons are large.

The neural network is a computing model composed of a large number of interconnected nodes (or neurons). The network itself is usually an approximation to some kind of algorithm or function in nature; it may be the expression of a logical strategy. The neural network is a highly nonlinear dynamical system. Although the structure and function of each neuron is not complicated, the dynamic behavior of the neural network is very complex, so using neural networks can express a variety of phenomena in the physical world. In the past ten years, the study of artificial neural networks continued to deepen and merge with wavelet analysis, fuzzy sets, rough sets, and chaos and fractal theory. It has made great progress in pattern recognition, intelligent robot, automatic control, prediction estimate, biology, medicine, economy, and other fields and has successfully solved the practical problems which are difficult for many modern computers, showing good intelligence.

6.2.1 Biology inspired by mathematics and technology

It is interesting from the philosophical point of view that today we observe an inverse merge of technical concepts with the nature of biological systems. Generally, mathematical researchers were inspired by biological systems (neural networks, genetic algorithms, immune-based controllers). However, useful and successful principles have emerged as technology and mathematics advanced further. We can see that the commonly used technique for handling dynamic systems by engineers and

Mathematicians could correspond to how modern researchers look at a biological neuron. A simple case of state-space representation shown in Fig. (6.3) is described by

$$\begin{cases} \frac{dx(t)}{dt} = f(x(t), \mathbf{u}(t)) \\ y(t) = g(x(t)) \end{cases} \quad (6.1)$$

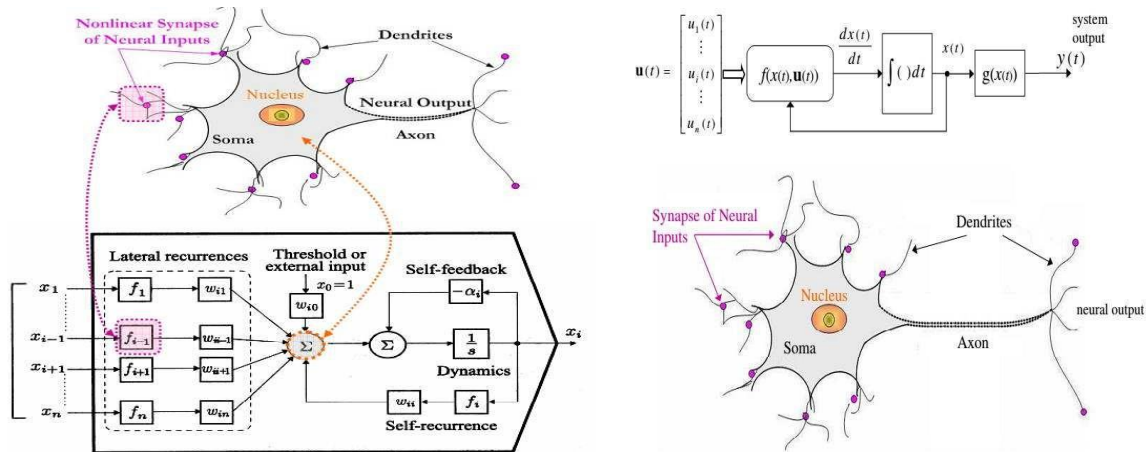


Figure 6.3: Artificial neural network

Where x is the internal state variable, y is the output variable, $f(\cdot)$ and $g(\cdot)$ are static functions, u is a vector of inputs, and t is a continuous variable of time. The complexity of real neurons is highly abstracted when modeling artificial neurons. These basically consist of inputs (like synapses), which are multiplied by weights (strength of the respective signals), and then computed by a mathematical function that determines the activation of the neuron. Another function (which may be the identity) computes the output of the artificial neuron (sometimes in dependence of a certain threshold).

6.2.2 Hopfield-type neural network

The Hopfield-type neural network abstracted from man-brain dynamics is a very important neural model in neurocomputing. The following differential equations describe a continuous-time artificial neural network containing n units:

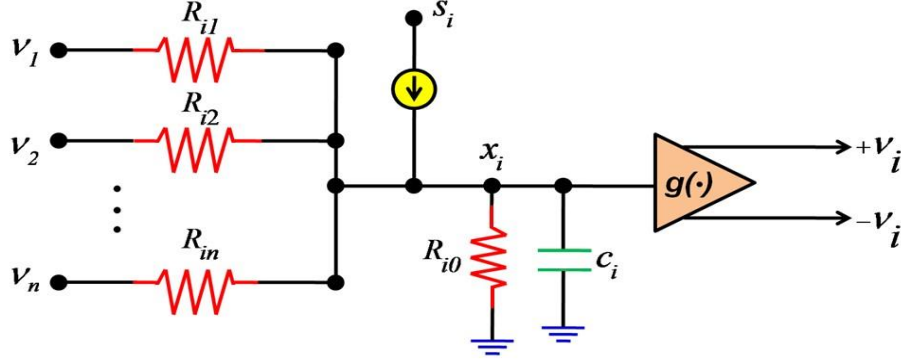


Figure 6.4: Circuit for neuron i in the analog implementation of Hopfield DNN.

$$\begin{cases} C_i \frac{dx_i(t)}{dt} = -\frac{x_i(t)}{R_i} + \sum_{j=1}^n w_{ij} y_j(t) + s_i(t), i = 1, 2, \dots, n, \\ y_j(t) = g_j(x_j(t)). \end{cases} \quad (6.2)$$

This nonlinear system can be implemented by an analog RC (resistance-capacitance) network circuit as shown in Figure 6.4, where $u_i = x_i$ is the input voltage of the i th amplifier, $V_i = g_i(x_i(t))$ is the output voltage of the i th amplifier, where each operational amplifier has two output terminals each providing V_i and $-V_i$, the parameter R_i is defined as

$$\frac{1}{R_i} = \frac{1}{R_i} + \sum_{j=1}^n \frac{1}{R_{ij}}, \quad (6.3)$$

And the weight parameter w_{ij} as

$$w_{ij} = \begin{cases} +\frac{1}{R_{ij}}, R_{ij} \text{ is connected to } V_j \\ -\frac{1}{R_{ij}}, R_{ij} \text{ is connected to } -V_j \end{cases} \quad (6.4)$$

This system can be written in matrix form as

$$\dot{\mathbf{x}}(t) = -\mathbf{A}\mathbf{x}(t) + \mathbf{W}_1 \mathbf{g}(\mathbf{x}(t)) + \mathbf{W}_2 \mathbf{u}, \quad (6.5)$$

where $\mathbf{x}(t) = [x_1(t), \dots, x_n(t)] \in \mathbb{R}^n$ is the neuron state vector, $\mathbf{g}(\mathbf{x}(t)) \in \mathbb{R}^n$ is activation functions, and $\mathbf{u} = [u_1, \dots, u_n]^T$ is a constant input vector.

$$\mathbf{A} = \begin{bmatrix} \frac{1}{R_1 C_1} & 0 & \dots & 0 \\ 0 & \frac{1}{R_2 C_2} & \dots & 0 \\ \vdots & \vdots & \ddots & \vdots \\ 0 & 0 & \dots & \frac{1}{R_n C_n} \end{bmatrix}, \mathbf{W}_1 = \begin{bmatrix} \frac{w_{11}}{C_1} & \frac{w_{12}}{C_1} & \dots & \frac{w_{1n}}{C_1} \\ \frac{w_{21}}{C_2} & \frac{w_{22}}{C_2} & \dots & \frac{w_{2n}}{C_2} \\ \vdots & \vdots & \ddots & \vdots \\ \frac{w_{n1}}{C_n} & 0 & \dots & \frac{w_{nn}}{C_n} \end{bmatrix}, \mathbf{W}_2 = \begin{bmatrix} \frac{1}{C_1} & 0 & \dots & 0 \\ 0 & \frac{1}{C_2} & \dots & 0 \\ \vdots & \vdots & \ddots & \vdots \\ 0 & 0 & \dots & \frac{1}{C_n} \end{bmatrix} \quad (6.6)$$

The product $R_i C_i = \tau_i$, $i = 1, 2, \dots, n$ is often referred to as the time constant of the i th neuron. An identical time constant for each neuron would require $C_i = C$ and $R_i = R$ for all i . In this case, each individual value for τ_i would have to be chosen in such a way that it compensates for

these variations and keeps R_i the same for each neuron. It is also important to note that the time constant τ_i describes the convergence of the neural state x_i . Because of the potentially very high gain of the transfer function, the output v_i might saturate very quickly. Thus, even if state x_i is still far from reaching its equilibrium point, output V_i might appear as if the circuit had converged in merely a fraction of the time Constant τ_i .

Delayed neural network with n neurons

Delay as an objective phenomenon, presents in various engineering, biological and economic systems and often results in poor dynamic network behavior, such as vibration, bifurcation or instability. Therefore research on delayed neural networks (DNNs) dynamic behavior is of great significance. The DNNs are shown by the following differential equations:

$$\frac{dx_i(t)}{dt} = -a_i x_i(t) + \sum_{j=1}^n b_{ij} f(x_j(t)) + \sum_{j=1}^n c_{ij} f(x_j(t - \tau)) + I_i, \quad i = 1, 2, \dots, n, \quad (6.7)$$

Where $a_i = \frac{1}{C_i R_i}$, $b_{ij} = \frac{1}{C_i R_{bij}}$ and $c_{ij} = \frac{1}{C_i R_{cij}}$. As is shown in Fig. 6.5 and DNNs with two neurons can be implemented. According to analyzing the circuit node, system (6.7) with n neurons can be expressed as

$$\begin{aligned} \frac{dx_1(t)}{dt} &= -a_1 x_1(t) + \sum_{j=1}^n b_{1j} f(x_j(t)) + \sum_{j=1}^n c_{1j} f(x_j(t - \tau)) + I_1, \\ \frac{dx_2(t)}{dt} &= -a_2 x_2(t) + \sum_{j=1}^n b_{2j} f(x_j(t)) + \sum_{j=1}^n c_{2j} f(x_j(t - \tau)) + I_2, \\ &\dots = \dots \dots \dots \dots \\ \frac{dx_n(t)}{dt} &= -a_n x_n(t) + \sum_{j=1}^n b_{nj} f(x_j(t)) + \sum_{j=1}^n c_{nj} f(x_j(t - \tau)) + I_n. \end{aligned}$$

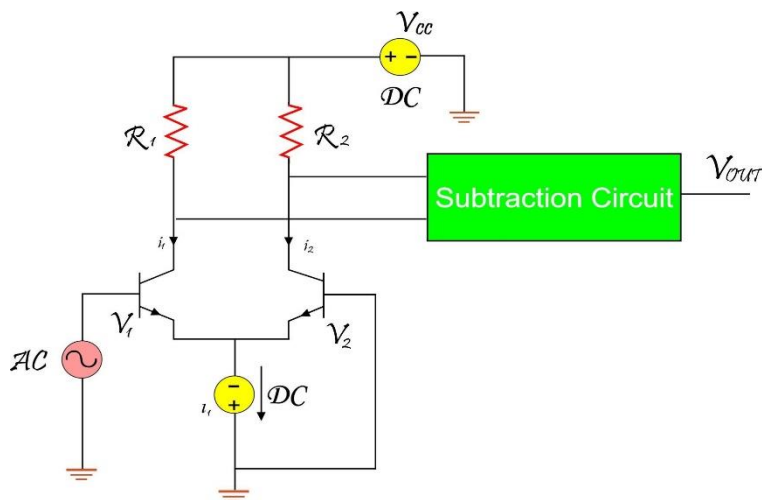


Figure 6.5: Circuit realization of the tangent hyperbolic.

Then the DNNs (6.7) could be rewritten as

$$\dot{x}(t) = -Ax(t) + Bf(x(t)) + Cf(x(t-\tau)) + I, \quad (6.11)$$

6.3 Fractional Order Definitions and Preliminaries

Preliminaries

Definition 1. Suppose that $\beta > 0$ for a function $f(t)$ is defined as

$$J^\beta f(t) = \frac{1}{\Gamma(\beta)} \int_b^t (t-\tau)^{\beta-1} f(\tau) d\tau \quad (6.12)$$

Where $t \geq b, t \in \mathbb{R}, \Gamma(\cdot)$ is the gamma function, given by $\Gamma(\beta) = \int_0^\infty t^{\beta-1} e^{-t} dt$.

Definition 2. The Caputo fractional derivative of order β for a function $f(t)$ is defined as

$$D^\beta f(t) = \frac{1}{\Gamma(n-\beta)} \int_b^t (t-\tau)^{n-\beta-1} f^{(n)}(\tau) d\tau \quad (6.13)$$

In which $t \geq b, t \in \mathbb{R}, n-1 < \beta < n \in \mathbb{N}$

Definition 3. The one-parameter Mittag-Leffler function is defined as

$$E_\varnothing(x) = \sum_{l=0}^{\infty} \frac{x^l}{\gamma(l\varnothing + 1)} \quad (6.14)$$

Definition 4. The two-parameter Mittag-Leffler function is defined as

$$E_{\varnothing,\psi}(x) = \sum_{l=0}^{\infty} \frac{x^l}{\gamma(l\varnothing + \psi)} \quad (6.15)$$

Definition 5. Moreover, the Laplace transform of Mittag-Leffler function in two parameters is

$$\mathbb{L}\{t^{\psi-1} E_{\varnothing,\psi}(-\lambda t^\varnothing)\} = \frac{s^{\varnothing-\psi}}{s^\varnothing + \lambda}, \quad (R(s) > |\lambda|^{\frac{1}{\varnothing}}) \quad (6.16)$$

Where s is the variable in Laplace domain, $R(s)$ denotes the real part of s , $\lambda \in \mathbb{R}$ and \mathbb{L} stands for the Laplace transform,

Lemma 1 Let a vector-value function $p(t) \in \mathbb{R}^n$ is differentiable. Then, for any $t > 0$, one has

$$\frac{1}{2}D^\beta p^2(t) \leq p(t)D^\beta p(t) \quad (6.17)$$

When $0 < \beta < 1$

Lemma 2. Suppose that $x, \in \mathbb{R}^n$ be the two states of the system. Then, one has

$$\left| \bigwedge_{j=1}^n u_{ij} f_j(\vartheta_j) - \bigwedge_{j=1}^n u_{ij} f_j(\zeta_j) \right| \leq \sum_{j=1}^n |u_{ij}| |f_j(\vartheta_j) - f_j(\zeta_j)|$$

$$\left| \bigvee_{j=1}^n v_{ij} f_j(\vartheta_j) - \bigvee_{j=1}^n v_{ij} f_j(\zeta_j) \right| \leq \sum_{j=1}^n |v_{ij}| |f_j(\vartheta_j) - f_j(\zeta_j)|$$

Lemma 3. Let $k_1 > 0, k_2 > 0, k_3 > 1, k_4 > 1$, and $\left(\frac{1}{k_3}\right) + \left(\frac{1}{k_4}\right) = 1$. Then for any $\epsilon > 0$, we have

$$k_1 k_2 \leq \frac{1}{k_3} (k_1 \epsilon)^{k_3} + \frac{1}{k_4} \left(k_2 \left(\frac{1}{\epsilon} \right) \right)^{k_4}$$

The equality holds if and only if $(k_1 \epsilon)^{k_3} = \left(k_2 \left(\frac{1}{\epsilon} \right) \right)^{k_4}$.

Lemma 4. Let $V(t)$ be a continuous function on $[0, \infty)$ satisfying

$$c_{D^\alpha} V(t) \leq -\gamma V(t), \alpha \in (0, 1) \quad (6.18)$$

For some constant γ . Then

$$V(t) \leq V(0) E_\alpha(-\gamma t^\alpha), t \geq 0 \quad (6.19)$$

Lemma 5 Let $u > 0, v > 0, 1 < p < +\infty$, and $\frac{1}{p} + \frac{1}{q} = 1$, then the following relationship holds

$$uv \leq \frac{1}{p} u^p + \frac{1}{q} v^q \quad (6.20)$$

the equality holds if and only if $u = v^{p-1}$

Assumption 1. The neuron activation functions f_j is Lipschitz continuous, that is, there exist positive constants $F_j > 0$:

$$|f_j(\vartheta_j) - f_j(\zeta_j)| \leq F_j |\vartheta_j - \zeta_j|$$

6.4 Main Results

In this, we will derive some criteria from guaranteeing the global Mittag-Leffler stability between the drive system (6.20) and the response system (6.21).

In this paper, we consider the following n-dimensional FCNNs with distributed delay:

$$\begin{aligned}
C_D \alpha_{\zeta_i(t)} = & -d_i \zeta_i(t - \sigma) + \sum_{j=1}^n c_{ij} f_j(\zeta_j(t)) + \sum_{j=1}^n a_{ij} f_j(\zeta_j(t - \tau)) + \sum_{j=1}^n h_{ij} \mu_j \\
& + \bigwedge_{j=1}^n u_{ij} f_j(\zeta_j(t - \tau)) + \bigwedge_{j=1}^n P_{ij} \mu_j \\
& + \bigvee_{j=1}^n v_{ij} f_j(\zeta_j(t - \tau)) + \bigvee_{j=1}^n Q_{ij} \mu_j + I_i, i = 1, 2, \dots, n,
\end{aligned} \tag{6.21}$$

Where ${}^C D \alpha$ is Caputo's fractional derivative and $0 < \alpha < 1$, $d_i > 0$ denotes the rate with which the i th neuron, $\zeta_i(t)$ corresponds to the state variable of the i th unit at time t , c_{ij} , a_{ij} are elements of feedback and feed-forward template h_{ij} is the feed-forward template. u_{ij} , v_{ij} , P_{ij} , Q_{ij} are elements of the fuzzy feedback MIN template and fuzzy feedback MAX template, respectively. \bigwedge and \bigvee denote the fuzzy AND and fuzzy OR operations, respectively. I_i denote the state, input, and bias of the i th neuron, respectively. f_i are the activation functions.

Eqn. (6.20) is considered as a drive system. Now the response system is given as follows:

In this paper, we refer to model (6.20) as the drive system; the response system is given as follows

$$\begin{aligned}
C_D \alpha_{\vartheta_i(t)} = & -d_i \vartheta_i(t - \sigma) + \sum_{j=1}^n c_{ij} f_j(\vartheta_j(t)) + \sum_{j=1}^n a_{ij} f_j(\vartheta_j(t - \tau)) + \sum_{j=1}^n h_{ij} \mu_j \\
& + \bigwedge_{j=1}^n u_{ij} f_j(v_j(t - \tau)) + \bigwedge_{j=1}^n P_{ij} \mu_j \\
& + \bigvee_{j=1}^n v_{ij} f_j(v_j(t - \tau)) + \bigvee_{j=1}^n Q_{ij} \mu_j + I_i + u_i(t),
\end{aligned} \tag{6.22}$$

Where $\vartheta_i(t)$ corresponds to the state variable of the neuron of the response system and $u_i(t)$ indicates the control input.

Suppose that (t) , (t) are arbitrary solutions of system (6.20) and system (6.21), respectively, and let $(t) = (t) - (t)$ for $i \in I$, then from the system (6.20) and system (6.21), the error dynamical system can be derived as

$$\text{Let } \xi_i(t) = v_i(t) - \zeta_j(t) \text{ for } i \in I$$

$$\begin{aligned}
\xi_i(t) = & -d_i \vartheta_i(t - \sigma) + \sum_{j=1}^n c_{ij} f_j(\vartheta_j(t)) + \sum_{j=1}^n a_{ij} f_j(\vartheta_j(t - \tau)) \\
& + \sum_{j=1}^n h_{ij} u_j + \bigwedge_{j=1}^n u_{ij} f_j(\vartheta_j(t - \tau)) + \bigwedge_{j=1}^n p_{ij} u_j + \bigvee_{j=1}^n v_{ij} f_j(\vartheta_j(t - \tau)) \\
& + \bigvee_{j=1}^n q_{ij} u_j + I_i + u_i(t) + d_i \zeta_j(t - \sigma) - \sum_{j=1}^n c_{ij} f_j(\zeta_j(t)) \\
& - \sum_{j=1}^n a_{ij} f_j(\zeta_j(t - \tau)) - \sum_{j=1}^n h_{ij} u_j - \bigwedge_{j=1}^n u_{ij} f_j(\zeta_j(t - \tau)) - \bigwedge_{j=1}^n p_{ij} u_j \\
& - \bigvee_{j=1}^n v_{ij} f_j(\zeta_j(t - \tau)) - \bigvee_{j=1}^n q_{ij} u_j - I_i
\end{aligned} \tag{6.23}$$

$$\begin{aligned}
\xi_i(t) = & -d_i \vartheta_i(t - \sigma) + d_i \zeta_i(t - \sigma) + \sum_{j=1}^n c_{ij} f_j(\vartheta_j(t)) - \sum_{j=1}^n c_{ij} f_j(\zeta_j(t)) \\
& + \sum_{j=1}^n a_{ij} f_j(\vartheta_j(t - \tau)) - \sum_{j=1}^n a_{ij} f_j(\zeta_j(t - \tau)) + \bigwedge_{j=1}^n u_{ij} f_j(\vartheta_j(t - \tau)) \\
& - \bigwedge_{j=1}^n u_{ij} f_j(\zeta_j(t - \tau)) + \bigvee_{j=1}^n v_{ij} f_j(\vartheta_j(t - \tau)) \\
& - \bigvee_{j=1}^n v_{ij} f_j(\zeta_j(t - \tau)) + u_i(t)
\end{aligned}$$

$$\begin{aligned}
\xi_i(t) = & -d_i \xi_i(t - \sigma) + \sum_{j=1}^n c_{ij} [f_j(\vartheta_j(t)) - f_j(\zeta_j(t))] \\
& + \sum_{j=1}^n a_{ij} [f_j(\vartheta_j(t - \tau)) - f_j(\zeta_j(t - \tau))] \\
& + \bigwedge_{j=1}^n u_{ij} [f_j(\vartheta_j(t - \tau)) - f_j(\zeta_j(t - \tau))] \\
& + \bigvee_{j=1}^n v_{ij} [f_j(\vartheta_j(t - \tau)) - f_j(\zeta_j(t - \tau))] + u_i(t)
\end{aligned} \tag{6.24}$$

Now, we introduce the hybrid feedback control are:

$$u_i(t) = u_{1i}(t) + u_{2i}(t)$$

Where,

$$u_{1i}(t) = -\phi_i \xi_i(t) \text{ and } u_{2i}(t) = -\Psi_i \xi_i(t)$$

Where ϕ_i and Ψ_i are feedback gains

$$\begin{aligned}
\xi_i(t) = & -d_i \xi_i(t - \sigma) + \sum_{j=1}^n c_{ij} [f_j(\vartheta_j(t)) - f_j(\zeta_j(t))] \\
& + \sum_{j=1}^n a_{ij} [f_j(\vartheta_j(t - \tau)) - f_j(\zeta_j(t - \tau))] \\
& + \bigwedge_{j=1}^n u_{ij} [f_j(\vartheta_j(t - \tau)) - f_j(\zeta_j(t - \tau))] \\
& + \bigvee_{j=1}^n u_{ij} [f_j(\vartheta_j(t - \tau)) - f_j(\zeta_j(t - \tau))] - \phi_i \xi_i(t) - \Psi_i \xi_i(t)
\end{aligned}$$

Theorem 6.4.1. Given constant $\rho > 0$, the system (6.10) is globally Mittag-Leffler stable if the following conditions hold:

$$\begin{aligned}
& E_1(t) > E_2(t) \\
E_1(t) = & \min_{1 \leq i \leq n} \left[2(d_i + \phi_i(t) + \psi_i(t)) - \sum_{j=1}^n c_{ij} F_j \rho^{-1} - \sum_{j=1}^n c_{ij} F_j \rho - \sum_{j=1}^n c_{ij} F_j \rho^{-1} \right. \\
& \left. + \sum_{j=1}^n |u_{ij}| F_j \rho^{-1} + \sum_{j=1}^n |u_{ij}| F_j \rho^{-1} \right] > 0 \\
E_2(t) = & \max_{1 \leq i \leq n} \left[\sum_{j=1}^n a_{ij} F_i \rho + \sum_{j=1}^n |u_{ij}| F_j \rho + \sum_{j=1}^n |u_{ij}| F_j \rho - d_i \right] > 0
\end{aligned} \tag{6.25}$$

Proof. Let us consider the Lyapunov function is

$$V(t) = \sum_{i=1}^n \frac{1}{2} \xi_i^2(t) \tag{6.26}$$

According to the Caputo fractional-order derivative definition, we have

$$\begin{aligned}
CD_t^\alpha V(t, \xi(t)) &\leq \sum_{i=1}^n \xi_i(t - \sigma)^c D_t^\alpha \xi_i(t) \\
&\leq \sum_{i=1}^n \xi_i(t) \left[-d_i \xi_i(t - \sigma) + \sum_{j=1}^n c_{ij} [f_j(\vartheta_j(t)) - f_j(\zeta_j(t))] \right. \\
&\quad + \sum_{j=1}^n a_{ij} [f_j(\vartheta_j(t - \tau)) - f_j(\zeta_j(t - \tau))] \\
&\quad + \bigwedge_{j=1}^n u_{ij} [f_j(\vartheta_j(t - \tau)) - f_j(\zeta_j(t - \tau))] \\
&\quad \left. + \bigvee_{j=1}^n u_{ij} [f_j(\vartheta_j(t - \tau)) - f_j(\zeta_j(t - \tau))] - \phi_i \xi_i(t) - \Psi_i \xi_i(t) \right] \\
&\leq -\sum_{i=1}^n d_i \xi_i(t) \xi_i(t - \sigma) + \sum_{i=1}^n \sum_{j=1}^n c_{ij} F_j |\xi_i(t)| |v_j(t)| - c_{ij}(t) \\
&\quad + \sum_{i=1}^n \sum_{j=1}^n a_{ij} F_j |\xi_i(t)| |v_j(t - \tau)| - c_{ij}(t - \tau) \\
&\quad + \bigwedge_{j=1}^n u_{ij} [F_j |\xi_i(t)| (\vartheta_j(t - \tau)) - (\zeta_j(t - \tau))] \\
&\quad + \bigvee_{j=1}^n |v_{ij}| F_j |\xi_i(t)| (\vartheta_j(t - \tau)) - \zeta_j(t - \tau) - \phi_i \xi_i^2(t) - \Psi_i \xi_i^2(t) \leq \\
&\leq -\sum_{i=1}^n d_i \xi_i(t) \xi_i(t - \sigma) + \sum_{i=1}^n \sum_{j=1}^n c_{ij} F_j |\xi_i(t)| |\xi_j(t)| \\
&\quad + \sum_{i=1}^n \sum_{j=1}^n a_{ij} F_j |\xi_i(t)| |\xi_j(t - \tau)| + \sum_{i=1}^n \sum_{j=1}^n u_{ij} F_j |\xi_i(t)| |\xi_j(t - \tau)| \\
&\quad + \sum_{i=1}^n \sum_{j=1}^n v_{ij} F_j |\xi_i(t)| |\xi_j(t - \tau)| - \sum_{i=1}^n \phi_i(t) \xi_i^2(t) - \sum_{i=1}^n \Psi_i(t) \xi_i^2(t)
\end{aligned}$$

Using this equation

$$V(t) = \sum_{i=1}^n \frac{1}{2} \xi_i^2(t)$$

$$\begin{aligned}
&\leq -\sum_{i=1}^n d_i \left[\frac{\rho^{-1}}{2} \xi_i^2(t) + \frac{\rho^{-1}}{2} \xi_i^2(t-\sigma) \right] + \sum_{i=1}^n \sum_{j=1}^n c_{ij} F_j \left[\frac{\rho^{-1}}{2} \xi_i^2(t) + \frac{\rho}{2} \xi_j^2(t) \right] \\
&\quad + \sum_{i=1}^n \sum_{j=1}^n a_{ij} F_j \left[\frac{\rho^{-1}}{2} \xi_i^2(t) + \frac{\rho}{2} \xi_j^2(t-\tau) \right] \\
&\quad + \sum_{i=1}^n \sum_{j=1}^n |u_{ij}| F_j \left[\frac{\rho^{-1}}{2} \xi_i^2(t) + \frac{\rho}{2} \xi_j^2(t-\tau) \right] \\
&\quad + \sum_{i=1}^n \sum_{j=1}^n |v_{ij}| F_j \left[\frac{\rho^{-1}}{2} \xi_i^2(t) + \frac{\rho}{2} \xi_j^2(t-\tau) \right] - \sum_{i=1}^n \phi_i(t) \xi_i^2(t) \\
&\quad - \sum_{i=1}^n \psi_i(t) \xi_i^2(t) \\
&\leq -\sum_{i=1}^n d_i \frac{\rho^{-1}}{2} \xi_i^2(t) + d_i \frac{\rho}{2} \xi_j^2(t-\tau) \\
&\quad + \sum_{i=1}^n \sum_{j=1}^n |a_{ij}| F_j \frac{\rho^{-1}}{2} \xi_i^2(t) + \sum_{i=1}^n \sum_{j=1}^n |a_{ij}| F_j \frac{\rho}{2} \xi_i^2(t-\tau) \\
&\quad + \sum_{i=1}^n \sum_{j=1}^n |u_{ij}| F_j \frac{\rho^{-1}}{2} \xi_i^2(t) \\
&\quad + \sum_{i=1}^n \sum_{j=1}^n |u_{ij}| F_j \frac{\rho}{2} \xi_i^2(t-\tau) + \sum_{i=1}^n \sum_{j=1}^n |v_{ij}| F_j \frac{\rho^{-1}}{2} \xi_i^2(t) \\
&\quad + \sum_{i=1}^n \sum_{j=1}^n |v_{ij}| F_j \frac{\rho}{2} \xi_i^2(t-\tau) - \sum_{i=1}^n \phi_i(t) \xi_i^2(t) - \sum_{i=1}^n \psi_i(t) \xi_i^2(t) \\
&\leq -\sum_{i=1}^n d_i \frac{\rho^{-1}}{2} \xi_i^2(t) - \sum_{i=1}^n \phi_i(t) \xi_i^2(t) \\
&\quad - \sum_{i=1}^n \psi_i(t) \xi_i^2(t) \sum_{i=1}^n \sum_{j=1}^n c_{ij} F_j \frac{\rho^{-1}}{2} \xi_i^2(t) + \sum_{i=1}^n \sum_{j=1}^n a_{ij} F_j \frac{\rho^{-1}}{2} \xi_i^2(t) \\
&\quad + \sum_{i=1}^n \sum_{j=1}^n |u_{ij}| F_j \frac{\rho^{-1}}{2} \xi_i^2(t) \\
&\quad + \sum_{i=1}^n \sum_{j=1}^n |v_{ij}| F_j \frac{\rho^{-1}}{2} \xi_i^2(t) + \sum_{i=1}^n \sum_{j=1}^n |a_{ij}| F_j \frac{\rho}{2} \xi_i^2(t-\tau) \\
&\quad + \sum_{i=1}^n \sum_{j=1}^n |u_{ij}| F_j \frac{\rho}{2} \xi_i^2(t-\tau) \\
&\quad + \sum_{i=1}^n \sum_{j=1}^n |v_{ij}| F_j \frac{\rho}{2} \xi_i^2(t-\tau)
\end{aligned}$$

$$\begin{aligned}
&\leq \left[\sum_{i=1}^n [-(d_i + \phi_i(t) + \psi_i(t))] + \sum_{j=1}^n a_{ij} F_j \frac{\rho^{-1}}{2} + \sum_{j=1}^n c_{ij} F_j \frac{\rho^{-1}}{2} \right. \\
&\quad \left. + \sum_{j=1}^n |u_{ji}| F_i \frac{\rho^{-1}}{2} + \sum_{j=1}^n |v_{ij}| F_j \left[\frac{\rho^{-1}}{2} \right] \xi_i^2(t) \right] \\
&\quad \left[\sum_{i=1}^n \left[\sum_{j=1}^n a_{ji} F_j \frac{\rho}{2} + \sum_{i=1}^n |u_{ij}| F_j \left[\frac{\rho}{2} \right] + \sum_{i=1}^n |v_{ij}| F_j \left[\frac{\rho}{2} \right] \xi_i^2(t - \tau) - d_i \xi_i^2(t - \sigma) \right] \right] \\
&\leq -E_1 V(t, \xi(t)) + E_2 \max_{t-\lambda \leq s \leq t} V(s, \xi(s)), \lambda = \max\{\sigma, \tau\}
\end{aligned} \tag{6.27}$$

$$\begin{aligned}
E_1(t) &= \min_{1 \leq i \leq n} \left[2(d_i + \phi_i(t) + \psi_i(t)) - \sum_{j=1}^n c_{ij} F_j \rho^{-1} - \sum_{j=1}^n c_{ij} F_j \rho \right. \\
&\quad \left. - \sum_{j=1}^n c_{ij} F_j \rho^{-1} + \sum_{j=1}^n |u_{ij}| F_j \rho^{-1} + \sum_{j=1}^n |u_{ij}| F_j \rho^{-1} \right] > 0 \\
E_2(t) &= \max_{1 \leq i \leq n} \left[\sum_{j=1}^n a_{ij} F_i \rho + \sum_{j=1}^n |u_{ij}| F_j \rho + \sum_{j=1}^n |u_{ij}| F_j \rho - d_i \right] > 0
\end{aligned} \tag{6.28}$$

From this estimate, for any solution (6.13), which satisfies the Razumichin condition

$$V(s, \xi(s)) \leq V(t, \xi(t)), t - \tau \leq s \leq t$$

We have

$$CD_t^\alpha V(t, \xi(t)) \leq -(E_1 - E_2)V(t, \xi(t)), t \geq 0 \tag{6.29}$$

According to Lemma 5, the claim of Theorem 6.4.1 follows

$$V(t, \xi(t)) \leq V(0, \xi(0))E_\alpha(-\lambda t^\alpha), t \geq 0 \tag{6.30}$$

By Lemma 4 and inequality (6.30), this proves system (6.20) can be achieved globally Mittag-Leffler stabilization under the designed control law.

Hence complete the proof.

Theorem 6.4.2. Given constants, $\delta_0 > 0, \delta_1 > 0, \delta_2 > 0$, and $\omega > 1$, the system (6.20) is globally Mittag-Leffler stable, if the following conditions hold:

$$\bar{E}_1(t) > \bar{E}_2(t)$$

$$\begin{aligned}
\overline{E}_1(t) = \min_{1 \leq i \leq n} & \left[\left(\frac{\omega^{-1}}{\omega} \delta_0 d_i + |\phi_i(t)| + |\Psi_i(t)| \right) - \sum_{j=1}^n |c_{ij}| F_j(\omega - 1) - \sum_{j=1}^n |c_{ij}| F_j \delta_2(\omega - 1) \right. \\
& - \sum_{j=1}^n |c_{ij}| F_j \frac{1}{\delta_1^{\omega-1}} - \sum_{j=1}^n |a_{ij}| F_j \delta_2(\omega - 1) + |u_{ij}| F_j \delta_2(\omega - 1) \\
& \left. + |v_{ij}| F_j \delta_2(\omega - 1) \right] > 0
\end{aligned}$$

Proof. We define a Lyapunov function

$$V(t, \xi(t)) = \sum_{i=1}^n \frac{1}{\omega} |\xi_i(t)|^\omega \quad (6.31)$$

According to the Caputo fractional-order derivative definition, we have

$$\begin{aligned}
CD_t^\alpha V(t, \xi(t)) & \leq |\xi_i(t)|^{\omega-1} \left[-d_i \xi_i(t - \sigma) + \sum_{j=1}^n c_{ij} [f_j(\vartheta_j(t)) - f_j(\zeta_j(t))] \right. \\
& + \sum_{j=1}^n a_{ij} [f_j(\vartheta_j(t - \tau)) - f_j(\zeta_j(t - \tau))] \\
& + \bigwedge_{j=1}^n u_{ij} [f_j(\vartheta_j(s - \tau)) - f_j(\zeta_j(t - \tau))] \\
& + \bigvee_{j=1}^n |v_{ij}| [f_j(\vartheta_j(s - \tau)) - f_j(\zeta_j(t - \tau))] + |\phi_i(t)| |\xi_i(t)| \\
& \left. + |\Psi_i(t)| |\xi_i(t)| \right] \\
& \leq - \sum_{i=1}^n d_i |\xi_i(t)|^{\omega-1} \xi_i(t - \sigma) + |\phi_i(t)| + |\Psi_i(t)| |\xi_i(t)|^\omega \\
& + \sum_{i=1}^n \sum_{j=1}^n |c_{ij}| F_j |\xi_i(t)|^{\omega-1} |\xi_j(t)| \\
& + \sum_{i=1}^n \sum_{j=1}^n a_{ij} F_j |\xi_i(t)|^{\omega-1} |\xi_j(t - \tau)| \\
& + \sum_{i=1}^n \sum_{j=1}^n u_{ij} |F_j| |\xi_i(s)|^{\omega-1} |\xi_j(s - \tau)| ds \\
& + \sum_{i=1}^n \sum_{j=1}^n |v_{ij}| F_j |\xi_i(t)|^{\omega-1} |\xi_j(s - \tau)| ds
\end{aligned} \quad (6.32)$$

From Lemma 3 we have

$$\begin{aligned}
|\xi_i(t)|^{\omega-1}|\xi_j(s-\sigma)| &\leq \frac{\omega-1}{\omega} [|\xi_i(t)|^\omega \delta_0] + \frac{1}{\omega \delta_0^{\omega-1}} |\xi_i(t)|^\omega \\
&= \frac{\omega-1}{\omega} [|\xi_i(t)|^\omega \delta_1] + \frac{1}{\omega} \left| |\xi_i(t)|^\omega \frac{1}{\delta_1^{\omega-1}} \right|^\omega \\
|\xi_i(t)|^{\omega-1}|\xi_j(s-\tau)| &\leq \frac{\omega-1}{\omega} \left[|\xi_i(t)|^{\omega-1} \delta_2^{\frac{\omega-1}{\omega}} \right]^{\frac{\omega-1}{\omega}} + \left[\frac{1}{\omega} |\xi_i(t-\tau)| \delta_2^{-\omega-1} \right]^\omega \\
&= \frac{\omega-1}{\omega} [|\xi_i(t)|^\omega \delta_2] + \frac{1}{\omega} |\xi_i(t-\tau)|^\omega \frac{1}{\delta_2^{\omega-1}}
\end{aligned} \tag{6.33}$$

Now substitute the above values in the above equation we get

$$\begin{aligned}
C_D^\alpha V(t, \xi(t)) &\leq -\sum_{i=1}^n \left(\frac{\omega-1}{\omega} \delta_0 d_i + |\phi_i(t)| + |\Psi_i(t)| |\xi_i(t)|^\omega + \right. \\
&\sum_{i=1}^n \sum_{j=1}^n |c_{ij}| F_j \left[\frac{\omega-1}{\omega} |\xi_i(t)|^\omega \delta_1 + \frac{1}{\omega} |\xi_i(t)|^\omega \frac{1}{\delta_1^{\omega-1}} \right] + \\
&\sum_{i=1}^n \sum_{j=1}^n |a_{ij}| F_j \left[\frac{\omega-1}{\omega} |\xi_i(t)|^\omega \delta_2 + \frac{1}{\omega} |\xi_i(t-\tau)|^\omega \frac{1}{\delta_2^{\omega-1}} \right] + \\
&\sum_{i=1}^n \sum_{j=1}^n |u_{ij}| F_j \left[\frac{\omega-1}{\omega} |\xi_i(t)|^\omega \delta_2 + \frac{1}{\omega} |\xi_i(t-\tau)|^\omega \frac{1}{\delta_2^{\omega-1}} \right] + \\
&\sum_{i=1}^n \sum_{j=1}^n |v_{ij}| F_j \left[\frac{\omega-1}{\omega} |\xi_i(t)|^\omega \delta_2 + \frac{1}{\omega} |\xi_i(t-\tau)|^\omega \frac{1}{\delta_2^{\omega-1}} \right] - \frac{d_i}{\rho \delta_0^{\omega-1}} |\xi_i(t-\tau)|^\omega \leq \\
&-\sum_{i=1}^n \left[\omega \left(\frac{\omega-1}{\omega} \delta_0 d_i + |\phi_i(t)| + |\Psi_i(t)| - \sum_{j=1}^n |c_{ij}| F_j \delta_1 (\omega-1) \right) - \right. \\
&\sum_{j=1}^n |c_{ij}| F_j \frac{1}{\delta_1^{\omega-1}} - \sum_{j=1}^n |a_{ij}| F_j \delta_2 (\omega-1) \left. \right] \frac{|\xi_i(t)|^\omega}{\omega} + \\
&\sum_{i=1}^n \left[\sum_{j=1}^n |a_{ij}| F_j \frac{1}{\delta_2^{\omega-1}} \frac{1}{\omega} |\xi_i(t-\tau)|^\omega + \sum_{i=1}^n \sum_{j=1}^n [|u_{ij}| F_j (\omega-1) \delta_2 + \right. \\
&|v_{ij}| F_j (\omega-1) \delta_2] \frac{1}{\omega} |\xi_i(\tau)|^\omega + \sum_{i=1}^n \sum_{j=1}^n \left[|u_{ij}| F_j \left(\frac{1}{\delta_2^{\omega-1}} \right) + |v_{ij}| F_j \left(\frac{1}{\delta_2^{\omega-1}} \right) \right] \frac{1}{\omega} |\xi_i(t-\tau)|^\omega - \frac{d_i}{\rho \delta_0^{\omega-1}} |\xi_i(t-\tau)|^\omega \\
&\leq -\overline{E}_1(t) V(t, \xi(t)) + \overline{E}_2 \max_{t-\lambda \leq s \leq t} V(s, \xi(t))
\end{aligned}$$

Where

$$\begin{aligned}
\overline{E}_1(t) &= \min_{1 \leq i \leq n} \left[\omega \left(\frac{\omega-1}{\omega} \delta_0 d_i + |\phi_i(t)| + |\Psi_i(t)| \right) - \sum_{j=1}^n |c_{ij}| F_j \delta_1 (\omega-1) \right. \\
&\quad - \sum_{j=1}^n |c_{ij}| F_j \frac{1}{\delta_1^{\omega-1}} - \sum_{j=1}^n |a_{ij}| F_j \delta_2 (\omega-1) + |u_{ij}| F_j \delta_2 (\omega-1) \\
&\quad \left. + |v_{ij}| F_j \delta_3 (\omega-1) \right]
\end{aligned}$$

$$\bar{\mathcal{E}}_2(t) = \max_{1 \leq i \leq n} \left[\sum_{j=1}^n |a_{ij}| F_i \frac{1}{\delta_2^{\omega-1}} \right] + \sum_{j=1}^n |u_{ij}| F_i \frac{1}{\delta_2^{\omega-1}} + \sum_{j=1}^n |v_{ij}| F_i \frac{1}{\delta_2^{\omega-1}} - \frac{d_i}{\rho \delta_0^{\omega-1}} \quad (6.34)$$

From this estimate, for any solution (6.23), which satisfies the Razumichin condition

$$V(s, \xi(s)) \leq V(t, \xi(t)), t - \lambda \leq s \leq t$$

We have

$${}^C D^\alpha V(t, (t)) \leq -(\mathcal{E}_1 - \mathcal{E}_2) V(t, \xi(t)), t \geq 0. \quad (6.35)$$

According to Lemma 5, the claim of Theorem 6.4.2 follows.

$$V(t, (t)) \leq V(0, (0)) E_\alpha(-\gamma t^\alpha), t \geq 0 \quad (6.36)$$

By Lemma 4 and inequality (6.36), this proves the system (6.20) can be achieved globally Mittag-Leffler stabilization under the designed control law. Hence complete the proof.

Theorem 6.4.3. Given constant $\rho > 0$, the system (6.20) is globally Mittag-Leffler stable, if the following conditions holds:

$$\tilde{\mathcal{E}}_1(t) > \tilde{\mathcal{E}}_2(t)$$

$$\begin{aligned} \tilde{\mathcal{E}}_1(t) = \min_{1 \leq i \leq n} & \left[2(d_i + \phi_i + \psi_i) - \sum_{j=1}^n c_{ij} F_j \rho^{-1} - \sum_{j=1}^n c_{ji} F_i \rho - \sum_{j=1}^n a_{ij} F_j \rho^{-1} + \sum_{j=1}^n |u_{ij}| F_j \rho^{-1} \right. \\ & \left. + \sum_{j=1}^n |v_{ij}| F_j \rho^{-1} \right] > 0 \end{aligned}$$

$$\tilde{\mathcal{E}}_2(t) = \max_{1 \leq i \leq n} [\sum_{j=1}^n a_{ji} F_i \rho + \sum_{j=1}^n |u_{ij}| F_j \rho + \sum_{j=1}^n |v_{ij}| F_j \rho - d_i] > 0 \quad (6.37)$$

Proof. Let us consider the Lyapunov function is

$$V(t) = \sum_{i=1}^n \frac{1}{2} \xi_i^2(t) + \sum_{i=1}^n \frac{1}{2q_i} (\phi_i(t) - \phi_i)^2 + \sum_{i=1}^n \frac{1}{2r_i} (\psi_i(t) - \psi_i)^2$$

$${}^C D_t^\alpha \phi_i(t) = q_i \xi_i^2(t), {}^C D_t^\alpha \psi_i(t) = r_i \xi_i^2(t) \quad (6.38)$$

According to the Caputo fractional-order derivative definition, we have

$$\begin{aligned}
c_{D_t^\alpha} V(t, \xi(t)) &\leq \sum_{i=1}^n \xi(t)^C D_t^\alpha \xi_i(t) + \sum_{i=1}^n \frac{1}{q_i} (\phi_i(t) - \phi_i)^C D_t^\alpha \phi_i(t) + \\
\sum_{i=1}^n \frac{1}{r_i} (\psi_i(t) - \psi_i)^C D_t^\alpha \psi_i(t) &\leq \sum_{j=1}^n \xi_i(t) - d_i \xi_i(t) + \sum_{j=1}^n c_{ij} \left[f_j(\vartheta_j(t)) - \right. \\
f_j(\zeta_j(t)) &\left. \right] + \sum_{j=1}^n a_{ij} \left[f_j(\vartheta_j(t - \tau)) - f_j(\zeta_j(t - \tau)) \right] + \sum_{j=1}^n u_{ij} \left[f_j(\vartheta_j(t - \right. \\
\tau) - f_j(\zeta_j(t - \tau)) &\left. \right] + \sum_{j=1}^n |v_{ij}| \left[f_j(\vartheta_j(t - \tau)) - f_j(\zeta_j(t - \tau)) \right] - \phi_i(t) \xi_i(t) - \\
\psi_i(t) \xi_i(t) + \sum_{i=1}^n \frac{1}{q_i} (\phi_i(t) - \phi_i) q_i \xi_i^2(t \leq - \sum_{j=1}^n d_i \xi_i(t) \xi_i(t - \sigma) + \\
\sum_{i=1}^n \sum_{j=1}^n c_{ij} F_j |\xi_i(t)| |\xi_j(t)| + \sum_{i=1}^n \sum_{j=1}^n a_{ij} F_j |\xi_i(t)| |\xi_j(t - \tau)| + \\
\sum_{i=1}^n \sum_{j=1}^n |u_{ij}| F_j |\xi_i(s)| |\xi_j(s - \tau)| + \sum_{i=1}^n \sum_{j=1}^n |v_{ij}| F_j |\xi_i(s)| |\xi_j(s - \tau)| - \\
\sum_{j=1}^n \phi_i \xi_i^2(t) - \sum_{j=1}^n \psi_i \xi_i^2(t) + \sum_{j=1}^n (\phi_i(t) - \phi_i) \xi_i^2(t) + \sum_{j=1}^n (\psi_i(t) - \\
\psi_i) \xi_i^2(t) \\
&\leq - \sum_{i=1}^n (d_i + \phi_i + \psi_i) - \sum_{j=1}^n c_{ij} F_j \frac{\rho^{-1}}{2} - \sum_{j=1}^n c_{ji} F_i \frac{\rho}{2} \\
&- \sum_{j=1}^n a_{ij} F_j \left[\sum_{i=1}^n |u_{ij}| F_j \left[\frac{\rho^{-1}}{2} \right] + \sum_{i=1}^n |v_{ij}| F_j \left[\frac{\rho^{-1}}{2} \right] \right] \xi_i^2(t) \\
&+ \sum_{i=1}^n \left[\sum_{j=1}^n a_{ij} F_j \left[\sum_{i=1}^n |u_{ij}| F_j \left[\frac{\rho^{-1}}{2} \right] + \sum_{i=1}^n |v_{ij}| F_j \left[\frac{\rho^{-1}}{2} \right] \right] \xi_i^2(t) \right. \\
&\left. - \tau) - \xi_i^2(t - \sigma) \right] \\
&\leq -\tilde{\Xi}_1 V(t, \xi(t)) + \tilde{\Xi}_2 \max_{t-\lambda \leq s \leq t} V(s, \xi(s))
\end{aligned} \tag{6.39}$$

Where,

$$\begin{aligned}
\tilde{\Xi}_1(t) &= \min_{1 \leq i \leq n} \left[2(d_i + \phi_i + \psi_i) - \sum_{j=1}^n c_{ij} F_j \rho^{-1} - \sum_{j=1}^n c_{ji} F_i \rho - \sum_{j=1}^n a_{ij} F_j \rho^{-1} \right. \\
&\left. + \sum_{j=1}^n |u_{ij}| F_j \rho^{-1} + \sum_{j=1}^n |v_{ij}| F_j \rho^{-1} \right]
\end{aligned}$$

$$\tilde{\Xi}2(t) = \max_{1 \leq i \leq n} \left[\sum_{j=1}^n a_{ji} F_i \rho + \sum_{j=1}^n |u_{ij}| F_j \rho + \sum_{j=1}^n |v_{ij}| F_j \rho - d_i \right] \quad (6.40)$$

From this estimate, for any solution (6.23), which satisfies the Razumichin condition

$$V(s, \xi(s)) \leq V(t, \xi(t)), t - \lambda \leq s \leq t,$$

We have,

$${}_C D_t^\alpha V(t, \xi(t)) \leq -(\Xi 1 - \tilde{\Xi}2) V(t, \xi(t)), t \geq 0 \quad (6.41)$$

According to Lemma 5, the claim of Theorem 6.4.3 follows.

$$V(t, \xi(t)) \leq V(0, \xi(0)) E\alpha(-\gamma t^\alpha), t \geq 0 \quad (6.42)$$

By Lemma 4 and inequality (6.42), this proves system (6.20) can be achieved globally Mittag-Leffler stabilization under the designed control law.

Hence complete the proof

Remark 6.4.4. In recent days, stability analysis of fuzzy cellular neural networks has been extensively studied by researchers. Stability analysis of fuzzy cellular neural networks with time delay in the leakage term and impulsive perturbations investigated in [172]. Finite-time synchronization of delayed fuzzy cellular neural networks with discontinuous activations is studied (see [173] and references therein). In these works, integer order is considered in our paper fractional order is considered. Great efforts have been made in study of fractional-order neural networks by researchers. See for example, Adaptive control for fractional-order induced chaotic fuzzy cellular neural networks [174], asymptotic stability of delayed fractional-order fuzzy neural networks with impulse effects [175], Mittag-Leffler stability of fractional-order Hopfield neural networks [176], Synchronization of fractional fuzzy cellular neural networks with interactions have been investigated in [177]. Our paper investigates the stability of fractional-order fuzzy cellular neural networks with leakage delay.

6.5 Stability problem- 1

In this section, two examples are given to illustrate the effectiveness of the proposed Global Mittag-Leffler stability schemes.

Example 1. For $n = 2$, consider the following fractional-order fuzzy cellular neural networks,

$$\begin{aligned}
C_D \alpha_{\zeta_i(t)} = & -d_i \zeta_i(t - \alpha) + \sum_{j=1}^2 c_{ij} f_j(\zeta_j(t)) + \sum_{j=1}^2 a_{ij} f_j(\zeta_j(t - \tau)) + \sum_{j=1}^2 h_{ij} \mu_j \\
& + \bigwedge_{j=1}^2 u_{ij} f_j(\zeta_j(t - \tau)) + \bigwedge_{j=1}^2 P_{ij} \mu_j \\
& + \bigvee_{j=1}^n u_{ij} f_j(\zeta_j(s - \tau)) + \bigvee_{j=1}^n Q_{ij} \mu_j + I_i, i = 1, 2,
\end{aligned} \tag{6.43}$$

The parameters of (6.13) error system are assumed that $a_{11} = 0.4$, $a_{12} = 0.6$, $a_{21} = 0.8$, $a_{22} = 0.9$, $c_{11} = 1.5$, $c_{12} = 1.8$, $c_{21} = 2.9$, $c_{22} = 2.8$,

$u_{11} = 0.9$, $u_{12} = 1.2$, $u_{21} = 2.1$, $u_{22} = 3.4$, $v_{11} = 1.8$, $v_{12} = 2.2$, $v_{21} = 0.7$, $v_{22} = 2.7$, $d_1 = 1.3$, $d_2 = 1.2$, $\Psi_1 = 1.7$, $\Psi_2 = 1.6$, $\phi_1 = 1.4$,

$\phi_2 = 1.9$, $\alpha = 0.97$, $(t) = \tanh(t)$. $F_1 = 0.5$, $F_2 = 0.5$, $\rho = 1.2$, the corresponding response system is described by

$$\begin{aligned}
C_D \alpha_{\vartheta_i(t)} = & -d_i \vartheta_i(t - \alpha) + \sum_{j=1}^2 c_{ij} f_j(\vartheta_j(t)) + \sum_{j=1}^2 a_{ij} f_j(\vartheta_j(t - \tau)) + \sum_{j=1}^2 h_{ij} \mu_j \\
& + \bigwedge_{j=1}^2 u_{ij} f_j(\vartheta_j(s - \tau)) + \bigwedge_{j=1}^2 P_{ij} \mu_j \\
& + \bigvee_{j=1}^2 u_{ij} f_j(\vartheta_j(s - \tau)) + \bigvee_{j=1}^2 Q_{ij} \mu_j + I_i + u_i(t),
\end{aligned} \tag{6.44}$$

Where a_{ij} , u_{ij} , v_{ij} , d_i , c_{ij} , and I_i are the same as in system (6.33), and the hybrid feedback controllers is as follows: $u_i(t) = u_{1i}(t) + u_{2i}(t)$, where $u_{1i}(t) = -\phi_i(t) \xi_i(t)$ and $u_{2i}(t) = -\Psi_i(t) \xi_i(t)$ where $\xi_i(t) = \vartheta_i(t) - \zeta_i(t)$ for $i = 1, 2$. The developed idea in Theorem 6.4.1, it asks that

$$\begin{aligned}
\tilde{\Xi}_1(t) = & \min_{1 \leq i \leq n} \left[2(d_i + \phi_i + \Psi_i) - \sum_{j=1}^n c_{ij} F_j \rho^{-1} - \sum_{j=1}^n c_{ji} F_i \rho - \sum_{j=1}^n a_{ij} F_j \rho^{-1} \right. \\
& \left. + \sum_{j=1}^n |u_{ij}| F_j \rho^{-1} + \sum_{j=1}^n |v_{ij}| F_j \rho^{-1} \right] = 7.12 > 0 \\
\tilde{\Xi}_2(t) = & \max_{1 \leq i \leq n} \left[\sum_{j=1}^n a_{ji} F_i \rho + \sum_{j=1}^n |u_{ij}| F_j \rho + \sum_{j=1}^n |v_{ij}| F_j \rho - d_i \right] = 6.60 > 0
\end{aligned} \tag{6.45}$$

Then it follows from Theorem 6.4.1 that system (6.32) and (6.33) can be achieved global Mittag-Leffler stabilization under the designed hybrid feedback control law.

6.6 Stability Problem- 2

Example -2

For $n = 2$, consider the following fractional-order fuzzy cellular neural networks,

$$\begin{aligned}
 C_D \alpha_{\xi_i(t)} = & -d_i \xi_i(t - \alpha) + \sum_{j=1}^2 c_{ij} f_j(\xi_j(t)) + \sum_{j=1}^2 a_{ij} f_j(\xi_j(t - \tau)) + \sum_{j=1}^2 h_{ij} \mu_j \\
 & + \bigwedge_{j=1}^2 u_{ij} f_j(\xi_i(s - \tau)) + \bigwedge_{j=1}^2 P_{ij} \mu_j \\
 & + \bigvee_{j=1}^2 u_{ij} f_j(\xi_j(s - \tau)) + \bigvee_{j=1}^2 Q_{ij} \mu_j + I_i, i = 1, 2,
 \end{aligned} \tag{6.46}$$

where $\alpha = 0.97$, $f(t) = \tanh(t)$ The parameters of (6.13) error system are assumed that $a_{11} = 0.4$, $a_{12} = 0.6$, $a_{21} = 0.8$, $a_{22} = 0.9$, $c_{11} = 1.5$, $c_{12} = 1.8$, $c_{21} = 2.9$, $c_{22} = 2.8$, $u_{11} = 0.9$, $u_{12} = 1.2$, $u_{21} = 2.1$, $u_{22} = 3.4$, $v_{11} = 1.8$, $v_{12} = 2.2$, $v_{21} = 0.7$, $v_{22} = 2.7$, $d_1 = 1.7$, $d_2 = 1.5$, $\Psi_1 = 0.7$, $\Psi_2 = 0.6$, $\phi_1 = 1.4$, $\phi_2 = 1.9$, $\delta_1 = \delta_2 = \delta_3 = 1$ $\omega = 2$.

The corresponding response system is described by

$$\begin{aligned}
 C_D \alpha_{\vartheta_i(t)} = & -d_i \vartheta_i(t) + \sum_{j=1}^2 c_{ij} f_j(\vartheta_j(t)) + \sum_{j=1}^2 a_{ij} f_j(\vartheta_j(t - \tau)) + \sum_{j=1}^2 h_{ij} \mu_j \\
 & + \bigwedge_{j=1}^2 u_{ij} f_j(\vartheta_i(s - \tau)) + \bigwedge_{j=1}^2 P_{ij} \mu_j \\
 & + \bigvee_{j=1}^2 u_{ij} f_j(\vartheta_j(t - \tau)) + \bigvee_{j=1}^2 Q_{ij} \mu_j + I_i + u_i(t),
 \end{aligned} \tag{6.47}$$

where a_{ij} , u_{ij} , v_{ij} , d_i , c_{ij} , and I_i are the same as in system (6.41), and the hybrid feedback controllers is as follows: $u_i(t) = u_{1i}(t) + u_{2i}(t)$, where $u_{1i}(t) = -\phi_i(t)e_i(t)$ and $u_{2i}(t) = -\Psi_i(t)e_i(t)$ where $\xi_i(t) = \vartheta_i(t) - \zeta_i(t)$ for $i = 1, 2$. According to the developed idea in Theorem 6.4.2, it asks that

$$\begin{aligned}
\bar{\mathcal{E}}_1(t) &= \min_{1 \leq i \leq n} \left[\left(\frac{\omega - 1}{\omega} \delta_0 d_i + |\phi_i(t)| + |\Psi_i(t)| \right) - \sum_{j=1}^n |c_{ij}| F_j \delta_1 (\omega - 1) \right. \\
&\quad - \sum_{j=1}^n |c_{ij}| F_j \frac{1}{\delta_1^{\omega-1}} + \sum_{j=1}^n |a_{ij}| F_j \delta_2 (\omega - 1) + |u_{ij}| F_j \delta_2 (\omega - 1) \\
&\quad \left. + |v_{ij}| F_j \delta_3 (\omega - 1) - \frac{d_i}{\rho \delta_0^{\omega-1}} \right] = 5.6 > 0 \\
\bar{\mathcal{E}}_2(t) &= \max_{1 \leq i \leq n} \left[\sum_{j=1}^n |a_{ij}| F_i \frac{1}{\delta_2^{\omega-1}} + \sum_{j=1}^n |u_{ij}| F_i \frac{1}{\delta_2^{\omega-1}} + \sum_{j=1}^n |v_{ij}| F_i \frac{1}{\delta_2^{\omega-1}} \right] = 5.20 > 0 \quad (6.48)
\end{aligned}$$

Then it follows from Theorem 6.4.2 that systems (6.34) and (6.35) can be achieved global Mittag-Leffler stabilization under the designed hybrid feedback control law.

6.7 Conclusion

This chapter addresses the global Mittag-Leffler stability of fractional order fuzzy cellular neural networks with leakage delay and time-varying delays. We proposed the definition of global Mittag-Leffler stability and the fractional Lyapunov direct method, which enriches the knowledge of both the system theory and the fractional calculus. This chapter serves as a first step in presenting sufficient conditions for global Mittag-Leffler stability for a generalized fuzzy cellular fractional-order neural network. The main theoretical finding in this chapter is that sufficient conditions are presented to prove the global Mittag-Leffler stability of the fuzzy cellular neural network. We extend the concept of Lyapunov functions for a fuzzy cellular fractional-order neural network. Under the assumption of Lipschitz continuity of activation functions, we have proved the global Mittag-Leffler stability of the proposed model, which implies a faster convergence rate of the network model than the Lyapunov convergence. Illustrative examples are provided to demonstrate the applicability of the proposed approach.

STABILITY ANALYSIS OF FRACTIONAL ORDER FUZZY CELLULAR NEURAL NETWORK WITH DISTRIBUTED DELAYS VIA HYBRID FEEDBACK CONTROLLER

7.1 Introduction

Stability problems for fractional-order differential systems, including Global stability [177,178], Exponential stability [179], and robust stability [180] have been widely discussed. As we all know, the stability problem is a very important performance measure for any dynamic system. [181] investigated the Mittag-Leffler stability of nonlinear fractional neutral singular systems under Caputo and Riemann–Liouville derivatives. Mittag-Leffler stability is a relatively new concept related deeply to fractional calculus. In [182], conditions on the Stability of fractional-order nonlinear dynamic systems: Lyapunov direct method and generalized Mittag-Leffler stability are established. So far, three basic cellular neural network (CNN) structures have been proposed. The first one is traditional CNN [183], a dynamical and analogical computational network using analog weights, inputs, states, and outputs. The second one is delay-type CNN [184] which introduces delayed weights into the traditional CNN and uses analog weights, inputs, states, and outputs. The last one is discrete-time CNN [189] which uses analog weights, inputs, states, and digital outputs. Unlike the traditional CNNs structure, fuzzy cellular neural networks (FCNN) implement fuzzy logic between its template input and output besides the sum of product operations. Unlike cellular neural networks, fuzzy cellular neural networks integrate fuzzy logic into the structure of customary cell neural systems and keep up nearby connections among cells. Fuzzy cellular neural networks (FCNNs), introduced by Yang et al. [190, 191], such as thinking and reasoning, [192-198] white blood cell detection, [199] and pattern recognition. On the other hand, outer synchronization between two coupled networks has been extensively studied. Similar to traditional CNNs, the stability of the system is very important in the design of FCNNs. We note that several conditions for FCNNs have been proposed [200-208]. Between multiple performance objectives using a single feedback function, whereas hybrid control seeks to achieve multiple performance objectives in a locally adaptive sense by exchanging between individuals from the earlier determined group of input capacities. There are numerous outcomes on half-breed frameworks and cross-breed control in distributed writing. Conferences have been held with published proceedings [209-217], and

special issues of archival publications have been devoted to hybrid systems and control [218, 219].

In addition, the literature on hybrid control systems is very large; a number of references to this literature are identified throughout this paper. Tutorial papers [220–231], a monograph [232,233], and doctoral dissertations that treat hybrid control systems have been written. Examples of hybrid controllers in the automotive field include applications for automated highway systems [234], motion planning [235-239], and so on. Although examining in half-breed control has been the article of an extraordinary and gainful exertion in the ongoing years in the car field, from the best of our knowledge, this is the first time that benefits of both FOC and hybrid control are used for ACC maneuvers.

7.2 Global Mittag-Leffler stability of Fractional order system

The global Mittag-Leffler stability of fractional-order fuzzy cellular neural networks has been studied in this chapter. Stability criteria are derived to ensure the stability of concerned fractional order systems. Moreover, stability has been justified by considering two examples. Further, a novel Lyapunov functional for checking the stability of the fractional order system has been constructed. It has been done with the help of Lemma with Lyapunov function and its sufficient conditions. An effective hybrid feedback controller is applied for the synchronization of master and slave systems [240-243].

7.3 Lyapunov approach for stability

Numerous academics put up the idea of incremental stability as a potent characteristic of dynamical and control systems. Instead of describing the convergence of trajectories with respect to an equilibrium point or specific trajectory, incremental stability explains the convergence of trajectories with respect to one another. Lyapunov functions are crucial in the investigation of incremental stability, just as they are in the research of stability. This chapter presents novel coordinate-independent conceptions of incremental Lyapunov functions that describe incremental stability in terms of the suggested Lyapunov functions [244-247].

7.4 Model Description and Preliminaries

In this chapter, we introduce some basic definitions and the corresponding results will be used later.

Definition 1 ([70]) suppose that $\beta > 0$ for a function $f(t)$ is defined as

$$J^\beta f(t) = \frac{1}{\Gamma(\beta)} \int_t^t (t - \tau)^{\beta-1} f(\tau) d\tau. \quad (7.1)$$

Where $t \geq b, t \in \mathbb{R}, \Gamma_n(-)$ is the gamma function, given by $\Gamma(\beta) = \int_0^\infty t^{\beta-1} e^{-t} dt$.

Definition 2 ([70]) The Caputo fractional derivative of order β for a function $f(t)$ is defined \square

$$D^\beta f(t) = \frac{1}{\Gamma(n-\beta)} \int_b^t (t - \tau)^{n-\beta-1} f^{(n)}(\tau) d\tau \quad (7.2)$$

In which $t \geq b, t \in \mathbb{R}, n - 1 < \beta < n \in \mathbb{N}$.

Definition 3 ([71]) the one-parameter Mittag-Leffler function is defined as

$$E_\phi(x) = \sum_{l=0}^{\infty} \frac{x^l}{\Gamma(l\phi+1)} \quad (7.3)$$

Definition 4 ([71]) the two-parameter Mittag-Leffler function is defined as

$$E_{\phi,\psi}(x) = \sum_{l=0}^{\infty} \frac{x^l}{\Gamma(l\phi+\psi)} \quad (7.4)$$

Definition 5 ([71]) Moreover, the Laplace transform of the Mittag-Leffler function in two parameters is

$$L \cdot [t^{\psi-1} E_{\phi,\psi}(-\lambda t^\phi)] = \frac{s^{\phi-\psi}}{s^\psi + \lambda} \cdot \left(R(s) > |\lambda|^{\frac{1}{\psi}} \right) \quad (7.5)$$

Where s the variable in the Laplace domain is, $R(s)$ denotes the real part of $s, \lambda \in \mathbb{R}$ and L stands for the Laplace transform.

Lemma 1 ([72]) Let a vector-value function $p(t) \in \mathbb{R}^\pi$ is differentiable. Then, for any $t > 0$, one has

$$\frac{1}{2} D^\beta p^2(t) \leq p(t) D^\beta p(t) \quad (7.6)$$

When $0 < \beta < 1$.

Lemma 2 ([248]) Suppose that $x, y \in \mathbb{R}^x$ be the no states of the system (7.7). Then, one has $|N_{j=1}^n u_{ij} f_j(\theta_j) - N_{j=1}^\pi u_{ij} f_j(\zeta_j)| \leq \sum_{j=1}^n |u_{ij}| |f_j(\theta_j) - f_j(\zeta_j)|$,

Lemma 3 ([74]) Let $k_1 > 0, k_2 > 0, k_3 > 0, k_4 > 1$, and $\left(\frac{1}{\pi_3}\right) + \left(\frac{1}{\pi_4}\right) = 1$. Then for any $\epsilon > 0$, we have:

$$k_1 k_2 \leq \frac{1}{k_3} (k_1 \epsilon)^{k_3} + \frac{1}{k_4} \left(k_2 \frac{1}{\epsilon}\right)^{k_4}$$

The equality holds if and only if $(k_1 \epsilon)^{k_3} = \left(k_2 \left(\frac{1}{\epsilon}\right)\right)^{k_4}$.

Lemma 4 ([75]) Let $V(t)$ be a continuous function on $[0, \infty)$ satisfying

$${}^C D^\alpha V(t) \leq -\gamma V(t), \alpha \in (0, 1). \quad (7.7)$$

For some constant γ . Then

$$V(t) \leq V(0) F_\alpha(-\gamma t^\alpha), t \geq 0 \quad (7.8)$$

Lemma 5 ([76]) Let $u > 0, v > 0, 1 < p < +\infty$, and $\frac{1}{p} + \frac{1}{q} = 1$, then the following relationship holds

$$uv \leq \frac{1}{p} u^p + \frac{1}{q} v^q \quad (7.9)$$

The equality holds if and only if $u = v^{p-1}$.

Assumption 1 The neuron activation functions f_j are Lipschitz continuous and satisfy for

$$|f_j(\theta_j) - f_j(\zeta_j)| \leq F_j |\theta_j - \zeta_j|.$$

Positive constants $F_j > 0$.

In this, we will derive some criteria to guarantee the Global Mittag-Leffler stability between drive system (7.10) and response system (7.11).

We consider the following a -dimensional FCNNs with distributed delay:

$${}^C D^\alpha \zeta_i(t) = -d_i \zeta_i(t) + \sum_{j=1}^{\pi} c_{ij} f_j(\zeta_j(t)) + \sum_{j=1}^{\pi} a_{ij} f_j(\zeta_j(t - \tau)) + \sum_{j=1}^{\pi} h_{jj} \mu_j$$

$$\begin{aligned}
& + \Lambda_{j=1}^n u_{ij} \int_0^\infty k_j(s) f_j(\zeta_j(s - \tau)) ds + \prod_{j=1}^n P_{lj} \mu_j \\
& + \prod_{j=1}^n t_{ij} \int_0^\infty k_j(s) f_j(\zeta_j(s - \tau)) ds \\
& + \prod_{j=1}^n Q_{ij} \mu_j + I_{i+i} = 1, 2, \dots, n,
\end{aligned} \tag{7.10}$$

Where, ${}^c D^\alpha$ is the Caputo's fractional derivative and $0 < \alpha < 1, d_t > 0$ denotes the rate with which the i th neuron, $\zeta_i(t)$ corresponds to the state variable of the i th unit at time t , c_{lj}, a_{ij} are elements of feedback and feed-forward template h_{ij} is the feed-forward template. $u_{ij}, v_{ij}, P_{ij}, Q_{ij}$ are elements of fuzzy feedback MIN template, and fuzzy feedback MAX template, respectively. \vee and \wedge denote the fuzzy AND and fuzzy OR operations, respectively. l Denote state, input, and bias of the i th neuron, respectively. f_i is the activation function.

In this paper, we refer to model (7.10) as the drive system; the response system is given as follows

$$\begin{aligned}
& + \prod_{j=1}^\pi u_{lj} \int_0^\infty k_j(s) f_j(\theta_j(s - \tau)) ds + \prod_{j=1}^\pi P_{lj} \mu_j \\
& + \int_{j=1}^\pi v_{lj} \int_0^\infty k_j(s) f_j(\theta_j(s - \tau)) ds \\
& + \int_{j=1}^\pi Q_{lj} \mu_j + I_l + u_l(t).
\end{aligned} \tag{7.11}$$

Where $\theta_1(f)$ corresponds to the state variable of the i th neuron of the response system and $u_L(t)$ indicates the control input.

Suppose that $\zeta_i(t), \nabla_i(t)$ are arbitrary solutions of system (7.10) and system (7.11), respectively. Let $e_1(t) = t_i(t) - \zeta_1(t)$ for $i \in I_+$ then from the system (7.10) and system (7.11), the error dynamical system can be derived as:

$$\begin{aligned}
\xi_l(t) & = -d_l \xi_l(t) + \sum_{j=1}^\pi c_{lj} [f_j(\theta_j(t)) - f_j(\zeta_j(t))] \\
& + \sum_{j=1}^\pi a_{lj} [f_j(\theta_j(t - \tau)) - f_j(\zeta_j(t - \tau))] \\
& + \int_{j=1}^\pi u_{lj} \int_0^\infty k_j(s) [f_j(\theta_j(t - \tau)) - f_j(\zeta_j(t - \tau))] ds \\
& + \int_{j=1}^\pi v_{lj} \int_0^\infty k_j(s) [f_j(\theta_j(t - \tau)) - f_j(\zeta_j(t - \tau))] ds + u_l(t)
\end{aligned} \tag{7.12}$$

Now we introduce the hybrid feedback controls are

$$\begin{aligned}
c^{c^\alpha} \theta_l(t) & = -d_l \theta_l(t) + \sum_{j=1}^n c_{lj} f_j(\theta_j(t)) + \sum_{j=1}^n a_{lj} f_j(\theta_j(t - \tau)) + \sum_{j=1}^n h_{lj} \mu_j \\
& + \Lambda_{j=1}^\pi u_{lj} \int_0^\infty k_j(s) f_j(\theta_j(s - \tau)) ds + \Lambda_{j=1}^\pi P_{lj} \mu_j \\
& + \sqrt{J}_{j=1}^n v_{lj} \int_0^\infty k_j(s) f_j(\theta_j(s - \tau)) ds \\
& + V_{j=1}^\pi Q_{lj} \mu_j + I_l + u_l(t).
\end{aligned} \tag{7.13}$$

Where $t_1(t)$ corresponds to the state variable of the i th neuron of the response system and $u_i(t)$ indicates the control input.

Suppose that $\zeta_i(t), \nabla_i(t)$ are arbitrary solutions of system (7.10) and system (7.11), respectively, and let $e_i(t) = t_1(t) - \zeta(t)$ for $i \in I$, then from the system (7.10) and system (7.11), the error dynamical system can be derived as:

$$\begin{aligned} \xi_i(t) = & -d_i \xi_i(t) + \sum_{j=1}^n c_{ij} [f_j(\theta_j(t)) - f_j(\xi_j(t))] \\ & + \sum_{j=1}^n a_{ij} [f_j(\theta_j(t - \tau)) - f_j(\zeta_j(t - \tau))] \\ & + \Lambda_{j=1}^{\pi} u_{ij} \int_0^{\infty} k_j(s) [f_j(\theta_j(t - \tau)) - f_j(\zeta_j(t - \tau))] ds \\ & + V_{j=1}^{\pi} v_{ij} \int_0^{\infty} k_j(s) [f_j(\theta_j(t - \tau)) - f_j(\zeta_j(t - \tau))] ds + u_i(t) \end{aligned} \quad (7.14)$$

Now we introduce the hybrid feedback controls are

$$\begin{aligned} u_i(t) = & u_u(t) + u_v(t), \quad \text{where} \quad u_{1u}(t) = -\phi_i(t) \xi_i(t) \quad \text{and} \quad u_{2v}(t) = -v_i(t) \xi_i(t). \\ \xi_i(t) = & -d_i \xi_i(t) + \sum_{j=1}^n c_{ij} [f_j(b_j(t)) - f_j(\xi_j(t))] \\ & + \sum_{j=1}^n a_{ij} [f_j(\theta_j(t - \tau)) - f_j(\zeta_j(t - \tau))] \\ & + \int_{j=1}^{\pi} u_{Lj} \int_0^{\infty} k_j(s) [f_j(\theta_j(t - \tau)) - f_j(\zeta_j(t - \tau))] ds \\ & + V_{j=1}^{\pi} v_{ij} \int_0^{\infty} k_j(s) [f_j(\theta_j(t - \tau)) - f_j(\xi_j(t - \tau))] ds - \phi_i(t) \xi_i(t) - v_i(t) \xi_i(t) \end{aligned} \quad (7.15)$$

Remark 7.4.1 Motivated by the success of the applications of the Mittag-Leffler functions in many areas of science and engineering. We present our work here. Applications of Mittag-Leffler functions in certain areas of physical and applied sciences are also very common. Very recently, Chen et al. [248] formulated and investigated the global Mittag-Leffler stability and synchronization of fractional-order memristor NNs. Stamova and Stamov [249] studied the impulsive and linear controllers on Mittag-Leffler synchronization of fractional-order NNs with time-varying delays. To extend the application of fractional calculus in nonlinear systems, we propose the Mittag-Leffler stability and the Lyapunov direct method to enrich the knowledge of both system theory and fractional calculus.

Theorem 7.4.1 Assume that Assumption (1) and Lemma (4) hold, then the system (7.10) is Globally Mittag-Leffler stable, provided the following conditions hold: $\nabla_1(t) > \nabla_2(t)$.

$$\begin{aligned}
\eta_1(t) &= \min_{i \leq l \leq n} [(d_i + \phi_r(t) + \vartheta_i(t)) - \sum_{j=1}^n c_{ij} F_j \rho^{-1} - \sum_{j=1}^n c_j F_l \rho - \sum_{j=1}^n a_{tj} F_j \rho^{-1} \\
&+ \sum_{j=1}^n |u_{ij}| F_j \rho^{-1} + \sum_{j=1}^n |v_j| F_f \rho^{-1}] > 0 \\
\eta_2(t) &= \max_{1 \leq l \leq n} [\sum_{j=1}^n a_j F_{i\rho} + \sum_{j=1}^n |a_{ju}| F_{i\rho} + \sum_{j=1}^n |v_j| F_{i\rho}] > 0
\end{aligned} \tag{7.16}$$

Proof, let us consider the Lyapunov function is

$$V(t) = \sum_{r=1}^m \frac{1}{2} k_i^2(t) \tag{7.17}$$

According to the Caputo fractional-order derivative definition, we have

$$\begin{aligned}
{}^c D^\alpha V(t, \xi_i(t)) &\leq \sum_{l=1}^{\pi} \xi_l(t) {}^c D^2 \xi_l(t) \\
&\leq \sum_{l=1}^{\pi} \xi_l(t) \left[-d_l \xi_l(t) + \sum_{j=1}^n c_{lj} [f_j(t_j(t)) - f_j(\zeta_j(t))] \right. \\
&+ \sum_{i=1}^n \sum_{j=1}^n a_{lj} F_l \left[\frac{\rho^{-1}}{2} \xi_l^2(t) + \frac{\rho}{2} \xi_j^2(t - \tau) \right] \\
&+ \sum_{i=1}^n \sum_{j=1}^n |u_{ij}| \int_0^\infty k_j(s) F_j \left[\frac{\rho^{-1}}{2} \xi_l^2(s) + \frac{\rho}{2} \xi_j^2(s - \tau) \right] ds \\
&+ \sum_{i=1}^n \sum_{j=1}^n |v_{ij}| \int_0^\infty k_j(s) F_j \left[\frac{\rho^{-1}}{2} \xi_l^2(s) + \frac{\rho}{2} \xi_j^2(s - \tau) \right] ds \\
&- \sum_{l=1}^{\pi} \phi_l(t) \xi_l^2(t) - \sum_{l=1}^{\pi} \Psi_l(t) \xi_l^2(t) \\
&\leq -\sum_{l=1}^n d_l \xi_l^2(t) + \sum_{l=1}^n \sum_{j=1}^n c_{lj} F_j \left[\frac{\rho^{-1}}{2} \xi_l^2(t) \right] + \sum_{l=1}^n \sum_{j=1}^n c_{lj} F_j \left[\frac{\rho}{2} \xi_j^2(t) \right] \\
&+ \sum_{i=1}^n \sum_{j=1}^n a_{lj} F_j \left[\frac{\rho^{-1}}{2} \xi_l^2(t) \right] + \sum_{l=1}^n \sum_{j=1}^n a_{ij} F_j \left[\frac{\rho}{2} \xi_j^2(t - \tau) \right] \\
&+ \sum_{i=1}^n \sum_{j=1}^n |u_{ij}| \int_0^\infty k_j(s) F_j \left[\frac{\rho^{-1}}{2} k_l^2(s) \right] ds \\
&+ \sum_{i=1}^{\pi} \sum_{j=1}^n |u_{ij}| \int_0^\infty k_j(s) F_j \left[\frac{\rho}{2} \xi_j^2(s - \tau) \right] ds \\
&+ \sum_{i=1}^{\pi} \sum_{j=1}^n |v_j| \int_0^\infty k_j(s) F_j \left[\frac{\rho^{-1}}{2} k_i^2(s) \right] ds \\
&+ \sum_{i=1}^n \sum_{j=1}^n |t_{ij}| \int_0^\infty k_j(s) F_j \left[\frac{\rho}{2} \xi_j^2(s - \tau) \right] ds \\
&- \sum_{l=1}^n \phi_l(t) \xi_l^2(t) - \sum_{l=1}^n \Psi_l(t) \xi_l^2(t) \\
&\leq -\sum_{l=1}^n d_l \xi_l^2(t) + \sum_{l=1}^n \sum_{j=1}^n c_{lj} F_j \left[\frac{\rho^{-1}}{2} \xi_l^2(t) \right] + \sum_{l=1}^n \sum_{j=1}^n c_{jl} F_l \left[\frac{\rho}{2} \xi_l^2(t) \right]
\end{aligned}$$

$$\begin{aligned}
& + \sum_{l=1}^n \sum_{j=1}^n a_{lj} F_j \left[\frac{\rho^{-1}}{2} \xi_l^2(t) \right] + \sum_{l=1}^n \sum_{j=1}^n a_{jl} F_l \left[\frac{\rho}{2} \xi_l^2(t - \tau) \right] \\
& + \sum_{i=1}^{\pi} \sum_{j=1}^n |u_{ij}| \int_0^{\infty} k_j(s) F_j \left[\frac{\rho^{-1}}{2} k_l^2(s) \right] ds \\
& + \sum_{l=1}^n \sum_{j=1}^n |u_{jl}| \int_0^{\infty} k_j(s) F_l \left[\frac{\rho}{2} \xi_l^2(s - \tau) \right] ds \\
& + \sum_{i=1}^{\pi} \sum_{j=1}^n |t_j| \int_0^{\infty} k_j(s) F_j \left[\frac{\rho^{-1}}{2} k_l^2(s) \right] ds \\
& + \sum_{l=1}^n \sum_{j=1}^n |v_j| \int_0^{\infty} k_j(s) F_l \left[\frac{\rho}{2} k_l^2(s - \tau) \right] ds \\
& - \sum_{i=1}^{\pi} \phi_l(t) \xi_l^2(t) - \sum_{l=1}^{\pi} \Psi_l(t) \xi_l^2(t) \\
& \leq \sum_{l=1}^n I - (d_l + \phi_v(t) + \nabla_l(t)) + \sum_{j=1}^n c_{ij} F_j \frac{\rho^{-1}}{2} \\
& + \sum_{j=1}^n c_j F_i \frac{\rho}{2} + \sum_{j=1}^n a_{ij} F_j \left[\frac{\rho^{-1}}{2} \right]_j^2(t) \\
& + \sum_{l=1}^n \left[\sum_{j=1}^n a_{jl} F_l \left[\frac{\rho}{2} \right] \right] \xi_l^2(f - \tau) + \sum_{l=1}^n \left[\sum_{j=1}^n |u_{lj}| \int_0^{\infty} k_j(s) F_j \left[\frac{\rho^{-1}}{2} \right] ds \right. \\
& \left. + \sum_{j=1}^n |v_j| \int_0^{\infty} k_j(s) F_j \left[\frac{\rho^{-1}}{2} \right] \right] k_j^2(s) ds \\
& + \sum_{i=1}^{\pi} \left[\sum_{j=1}^n |u_{jl}| \int_0^{\infty} k_j(s) F_l \left[\frac{\rho}{2} \right] ds \right. \tag{7.18}
\end{aligned}$$

From this estimate, for any solution (7.13), which satisfies the Razumichin condition We have. According to Lemma 5, the claim of Theorem 7.4.1 follows. By Lemma 4 and inequality (7.19), this proves system (7.10) can be achieved globally Mittag-Leffler stabilization under the designed control law.

Hence complete the proof.

Theorem 7.4.3 Assume that Assumption (1) and Lemma (4) hold, then the system (7.10) is Globally Mittag-Leffler stable, provided the following conditions holds:

$$\begin{aligned}
& + \sum_{j=1}^{\pi} |v_j| \int_0^{\infty} k_j(s) F_l \left[\frac{\rho}{2} \right] \xi_l^2(s - \tau) ds \\
& \leq - \sum_{l=1}^n \left[(d_l + \phi_l(t) + \Psi_l(t)) - \sum_{j=1}^n c_{lj} F_j \frac{\rho^{-1}}{2} - \sum_{j=1}^n c_j F_l \frac{\rho}{2} \right. \\
& \left. - \sum_{j=1}^{\pi} a_{jl} F_j \left[\frac{\rho^{-1}}{2} \right] \right] \xi_l^2(t)
\end{aligned}$$

$$\begin{aligned}
& + \sum_{l=1}^n \left[\sum_{j=1}^n a_{jl} F_l \left[\frac{\rho}{2} \right] \right] \xi_l^2(t - \tau) + \sum_{l=1}^n \left[\sum_{j=1}^n |u_{lj}| \int_0^\infty k_j(s) F_j \left[\frac{\rho^{-1}}{2} \right] ds \right. \\
& + \left. \sum_{j=1}^n |v_{lj}| \int_0^\infty k_j(s) F_j \left[\frac{\rho^{-1}}{2} \right] \right]_{\xi_l^2} (x) ds + \sum_{i=1}^n \left[\sum_{j=1}^n |u_{ij}| \int_0^\infty k_j(s) F_i \left[\frac{\rho}{2} \right] ds \right. \\
& + \left. \sum_{j=1}^n |v_{ij}| \int_0^\infty k_j(s) F_i \left[\frac{\rho}{2} \right] \right] \xi_i^2(s - \tau)(s) ds \\
& \leq -\eta_1 V(t, \xi(t)) + \eta_2 \max_{t-t \leq r \leq t} V(s, \xi(s)). \tag{7.19}
\end{aligned}$$

where,

$$\begin{aligned}
\eta_1(t) &= \min_{1 \leq i \leq e} \left[(d_t + \phi_i(t) + \vartheta_i(t)) - \sum_{j=1}^n c_{ij} F_j \rho^{-1} - \sum_{j=1}^n c_j F_i \rho - \sum_{j=1}^n a_{lj} F_j \rho^{-1} \right. \\
& \quad \left. + \sum_{j=1}^n |u_{ij}| F_j \rho^{-1} + \sum_{j=1}^n |v_{ij}| F_j \rho^{-1} \right] > 0 \\
\eta_2(t) &= \max_{1 \leq i \leq e} \left[\sum_{j=1}^n a_{jl} F_i \rho + \sum_{j=1}^n |u_{jl}| F_i \rho + \sum_{j=1}^n |v_{jl}| F_i \rho \right] > 0
\end{aligned}$$

From this estimate, for any solution (7.13), which satisfies the Razumichin condition

$$V(s, \xi(s)) \leq V(t, \xi(t)), t - \tau \leq s \leq t \tag{7.20}$$

We have

$${}^c D^\alpha V(t, \xi(t)) \leq -(\eta_1 - \eta_2) V(t, \xi(t)), t \geq 0. \tag{7.21}$$

According to Lemma 5, the claim of Theorem 7.4.1 follows.

$$V(t, \xi(t)) \leq V(0, \xi(0)) E_a(-\gamma t^\alpha), t \geq 0 \tag{7.22}$$

By Lemma 4 and inequality (7.19), this proves system (7.10) can be achieved globally Mittag-Leffler stabilization under the designed control law.

Hence complete the proof.

Theorem 7.4.3 Assume that Assumption (1) and Lemma (4) hold, then the system (7.10) is Globally Mittag-Leffler stable, provided the following conditions holds:

$$\theta_1(t) > \theta_2(t)$$

$$\begin{aligned}
\theta_1(t) &= \min_{l \leq l \leq n} \left[\omega(d_l + |\phi_1(t)| + |\Psi_l(t)|) - \sum_{j=1}^n |c_{lj}| F_j \delta_1 (\omega - 1) - \sum_{j=1}^n |c_{jl}| F_l \frac{1}{\delta_1^{\omega-1}} \right. \\
&\quad \left. - \sum_{j=1}^n |a_{ij}| F_j (\omega - 1) \delta_2 + |u_{ij}| F_j (\omega - 1) \delta_3 + |v_{lj}| F_j (\omega - 1) \delta_3 \right] \frac{|\xi_l(t)|^\omega}{\omega} > 0 \\
\theta_2(t) &= \max_{1 \leq l \leq n} \left[\sum_{j=1}^n |a_j| F_l \frac{1}{g_2^{\omega-1}} + \sum_{j=1}^n |u_{jl}| F_l \frac{1}{\delta_3^{\omega-1}} + \sum_{j=1}^n |v_{ju}| F_l \frac{1}{j_3^{av-1}} \right] \frac{|k_l(t - \tau)|^\omega}{a} > 0.
\end{aligned}$$

Proof we define a Lyapunov function

$$V(t, \xi(t)) = \sum_{i=1}^n \frac{1}{\omega} |k_i(t)|^\omega \quad (7.23)$$

According to the Caputo fractional-order derivative definition, we have

$$\begin{aligned}
{}^c D^\alpha V(t, \xi(t)) &\leq \sum_{l=1}^n |\xi_l(t)|^{\alpha-1} [-d_l |k_l(t)| + \sum_{j=1}^n |c_{lj}| |f_j(f_j(t)) - f_j(\zeta_j(t))| \\
&\quad + \sum_{j=1}^n |a_{ij}| |f_j(\theta_j(t - \tau)) - f_j(\zeta_j(t - \tau))| \\
&\quad + \wedge_{j=1}^n |a_{ij}| \int_0^\infty k_j(s) [f_j(\theta_j(s - \tau)) - f_j(\zeta_j(s - \tau))] ds \\
&\quad + \prod_{j=1}^n |v_{jj}| \int_0^\infty k_j(s) [f_j(0_j(s - \tau)) - f_j(\zeta_j(s - \tau))] ds \\
&\quad + |\phi_l(t)| |\xi_l(t)| + |\Phi_l(t)| |\xi_l(t)|] \\
&\leq \sum_{l=1}^n |\xi_l(t)|^{2-1} [-d_l |k_l(t)| + \sum_{j=1}^n |c_{lj}| F_j |\xi_j(t)| + \sum_{j=1}^n |a_{ij}| F_j |k_j(t - \tau)| \\
&\quad + \sum_{j=1}^n |u_{ij}| \int_0^\infty k_j(s) F_j |k_j(s - \tau)| ds \\
&\quad + \sum_{j=1}^n |v_{ij}| \int_0^\infty k_j(s) F_j |F_j(s - \tau)| ds \\
&\quad + |\phi_l(t)| |\xi_l(t)| + |\vartheta_4(t)| |k_l(t)|] \\
&\leq -\sum_{l=1}^n (d_l + |\phi_l(t)| + |\Psi_l(t)|) |\xi_l(t)|^{\omega t} + \sum_{i=1}^n \sum_{j=1}^n |c_{ij}| F_j |k_i(t)|^{\omega-1} |k_j(t)| \\
&\quad + \sum_{l=1}^n \sum_{j=1}^n |a_{ij}| F_j |k_l(t)|^{\omega-1} |\xi_j(t - \tau)| \\
&\quad + \sum_{i=1}^n \sum_{j=1}^n |a_{ij}| \int_0^\infty k_j(s) F_j |k_i(s)|^{\omega-1} |k_j(s - \tau)| ds \\
&\quad + \sum_{l=1}^n \sum_{j=1}^n |v_{lj}| \int_0^\infty k_j(s) F_j |k_l(s)|^{\alpha-1} |\xi_j(s - \tau)| ds
\end{aligned} \quad (7.24)$$

From lemma 3 we have

$$|\xi_1(t)|^{\omega-1} |\xi_j(t)| \leq \frac{\omega - 1}{\omega} [|\xi_1(t)|^{\alpha-1} \delta_1^{\omega-1}]^{\frac{\omega}{\omega v}} + \frac{1}{\omega} [|\xi_j(t)| \delta_1^{\omega-1}]^{\omega t}$$

$$\begin{aligned}
&= \frac{\omega - 1}{\omega} |\xi_1(t)|^\omega \delta_1 + \frac{1}{\omega} |\xi_j(t)|^\omega \frac{1}{\delta_1^{\omega-1}} \\
|\xi_1(t)|^{\omega-1} |\xi_j(t - \tau)| &\leq \frac{\omega - 1}{\omega} [|\xi_1(t)|^{\omega-1} \delta_2^{\omega-1}]^{\frac{\pi}{\omega-1}} + \frac{1}{\omega} \left[|\xi^\omega(t - \tau)|_2^{\frac{\omega-1}{\omega}} \right]^\omega \\
&= \frac{\omega - 1}{\omega} |\xi_1(t)|^\omega \delta_2 + \frac{1}{\omega} |\xi_j(t - \tau)|^\omega \frac{1}{\delta_2^{\omega-1}} \\
&\int_0^\infty |k_l(s)|^{\omega-1} |k_j(s - \tau)| ds \\
&\leq \int_0^\infty \frac{\omega - 1}{\omega} [|\xi_1(s)|^{\omega-1} \delta_3^{\omega-1}]^{\frac{e}{\omega-1}} + \frac{1}{\omega} [|\xi_j(s - \tau)| \delta_3^{\frac{-\omega}{\omega}}]^\omega \\
&= \int_0^\infty \frac{\omega-1}{\omega} |\xi_i(s)|^\omega \xi_3 + \frac{1}{\omega} |k_1(s - \tau)|^\omega \frac{1}{\delta_3^{\omega-1}} \tag{7.25}
\end{aligned}$$

Now substitute the above values in the above equation we get

$$\begin{aligned}
&{}^c D^\alpha V(t, \xi'(t)) \\
&\leq -\sum_{l=1}^n (d_l + |\phi_r(t)| + |\varpi_l(t)|) |\xi_l(t)|^\omega \\
&\quad + \sum_{l=1}^n \sum_{j=1}^n |c_{lj}| F_j \left[\frac{a-1}{\omega} |\xi_l(t)|^{\omega \delta_1} \right. \\
&\quad \left. + \frac{1}{\omega} |\xi_j(t)|^\omega \frac{1}{\delta_1^{\omega-1}} \right] + \sum_{l=1}^n \sum_{j=1}^n |a_{ij}| F_j \left[\frac{\omega-1}{\omega} |k_l(t)|^\omega \delta_2 \right. \\
&\quad \left. + \frac{1}{\omega v} |k_j(t - \tau)|^* \frac{1}{\delta_2^{\omega-1}} \right] \\
&\quad + \sum_{l=1}^n \sum_{j=1}^n |u_{ij}| \int_0^\infty k_j(s) F_j \left[\frac{\omega-1}{\omega} |k_l(s)|^\omega \delta_3 + \frac{1}{\omega'} |k_j(s - \tau)|^\omega \frac{1}{\delta_3^{\omega-1}} \right] ds \\
&\quad + \sum_{i=1}^n \sum_{j=1}^n |t_j| \int_0^\infty k_j(s) F_j \left[\frac{\omega-1}{\omega} |\xi_i(s)|^\omega \delta_3 + \frac{1}{\omega} |k_j(s - \tau)|^\omega \frac{1}{\delta_3^{\omega-1}} \right] ds \\
&\leq -\sum_{l=1}^n |d_l + |\phi_l(t)| + |\Psi_l(t)| | |\xi_l(t)|^\omega + \sum_{l=1}^n \sum_{j=1}^n |c_{lj}| F_j \left[\frac{\omega-1}{\omega} |\xi_l(t)|^{\omega \delta_1} \right] \\
&\quad + \sum_{l=1}^n \sum_{j=1}^n |c_{ij}| F_j \left[\frac{1}{\omega} |\xi_j(t)|^\omega \frac{1}{\delta_1^{\omega-1}} \right] + \sum_{l=1}^n \sum_{j=1}^n |a_{ij}| F_j \left[\frac{\omega-1}{\omega} |\xi_l(t)|^{\omega \delta_2} \right] \\
&\quad + \sum_{i=1}^n \sum_{j=1}^n |a_{ij}| F_j \left[\frac{1}{\omega} |k_j(t - \tau)|^\omega \frac{1}{\delta_2^{\omega-1}} \right] \\
&\quad + \sum_{l=1}^n \sum_{j=1}^n |u_{ij}| \int_0^\infty k_j(s) F_j \left[\frac{\omega-1}{\theta} |k_l(s)|^{\omega^2} \delta_3 \right] ds \\
&\quad + \sum_{l=1}^n \sum_{j=1}^n |u_{ij}| \int_0^\infty k_j(s) F_j \left[\frac{1}{\Delta} |k_j(s - \tau)|^{\omega j} \frac{1}{j_3^{\omega-1}} \right] ds
\end{aligned}$$

$$\begin{aligned}
& + \sum_{i=1}^n \sum_{j=1}^n |v_{ij}| \int_0^\infty k_j(s) F_j \left[\frac{\omega-1}{\omega} |\xi_l(s)|^\omega z_3 \right] ds \\
& + \sum_{i=1}^n \sum_{j=1}^n |v_{ij}| \int_0^\infty k_j(s) F_j \left[\frac{1}{\omega} |k_j(s-\tau)|^\omega \frac{1}{\delta_3^{\omega-1}} \right] ds \\
& \leq - \sum_{l=1}^n \left[d_l + |\phi_l(t)| + |\Psi_l(t)| \right] |\xi_l(t)|^\omega + \sum_{i=1}^n \sum_{j=1}^n |c_{ij}| F_j \left[\frac{\omega-1}{e} |\xi_1(t)|^{\omega \delta_1} \right] \\
& + \sum_{t=1}^n \sum_{j=1}^n |c_j| F_l \left[\frac{1}{\omega} |\xi_l(t)|^\omega \frac{1}{\delta_1^{\omega-1}} \right] \\
& + \sum_{l=1}^n \sum_{j=1}^n |a_{lj}| F_j \left[\frac{\omega-1}{\omega} |k_l(t)|^{\omega \delta_2} \right] \\
& + \sum_{l=1}^n \sum_{j=1}^n |a_{jl}| F_t \left[\frac{1}{\omega} |\xi_i(t-\tau)|^\omega \frac{1}{\delta_2^{\omega-1}} \right] \\
& + \sum_{i=1}^n \sum_{j=1}^n |u_{ij}| \int_0^\infty k_j(s) F_j \left[\frac{\omega-1}{\omega} |k_1(s)|^\omega \delta_3 \right] ds \\
& + \sum_{i=1}^n \sum_{j=1}^n |u_{ij}| \int_0^\infty k_j(s) F_l \left[\frac{1}{\omega} |k_i(s-\tau)|^\omega \frac{1}{\delta_3^{\omega-1}} \right] ds \\
& + \sum_{i=1}^n \sum_{j=1}^n |v_{ij}| \int_0^\infty k_j(s) F_j \left[\frac{\omega-1}{\omega} |\xi_1(s)|^{\omega_3} \right] ds \\
& + \sum_{i=1}^n \sum_{j=1}^n |v_j| \int_0^\infty k_j(s) F_i \left[\frac{1}{\omega} |k_i(s-r)|^\omega \frac{1}{\delta_3^{\omega-1}} \right] ds \\
& \leq \sum_{i=1}^n \left[-a(d_i + |\phi_l(t)| + |\Psi_i(t)|) + \sum_{j=1}^n |c_i| F_j \delta_n(a) - 1 \right] \\
& + \sum_{j=1}^n \left[|c_j| F_i \frac{1}{\delta_1^{\omega-1}} + \sum_{j=1}^n |a_{ij}| F_j \delta_2(\omega-1) \right] \frac{|i(t)|^\omega}{\omega} \\
& + \sum_{i=1}^n \left[\sum_{j=1}^n |a_j| F_i \frac{1}{\delta_2^{\omega-1}} \right] \frac{|E_i(t-\tau)|^\alpha}{\omega} \\
& + \sum_{i=1}^n \sum_{j=1}^n \int_0^\infty k_j(s) |u_{ij}| F_j (\omega-1) \delta_3 + |v_j| F_j (\omega-1) \delta_3 \left| \frac{|\xi_l(s)|^\omega}{\omega} \right. ds \\
& + \sum_{i=1}^n \sum_{j=1}^n \int_0^\infty k_j(s) \left[|u_j| F_l \left(\frac{1}{\delta_3^{\omega-1}} \right) + |v_j| F_l \left(\frac{1}{g_3^{\omega-1}} \right) \right] \frac{|k_l(s-\tau)|^\omega}{\omega} ds \\
& \leq - \sum_{l=1}^n \left[\omega(d_l + |\phi_l(t)| + |\Phi_l(t)|) - \sum_{j=1}^n |c_l| F_j \delta_1(\omega-1) \right. \\
& \left. - \sum_{j=1}^n |c_j| F_i \frac{1}{\delta_1^{\omega-1}} - \sum_{j=1}^n |a_{ij}| F_j \delta_2(\omega-1) \right] \frac{|\xi_1(t)|^\omega}{\omega} \\
& + \sum_{l=1}^n \left[\sum_{j=1}^n |a_{jl}| F_l \frac{1}{\delta_2^{\omega-1}} \right] \frac{|k_l(t-\tau)|^\omega}{\theta} \\
& + \sum_{i=1}^n \sum_{j=1}^n \int_0^\infty k_j(s) |u_{ij}| F_j (\omega-1) \delta_3 + |v_{ij}| F_j (\omega-1) \delta_3 \left| \frac{|k_i(s)|^\omega}{\omega} \right. ds
\end{aligned}$$

$$\begin{aligned}
& + \sum_{l=1}^n \sum_{j=1}^n \int_0^\infty k_j(s) \left[|u_j| F_l \left(\frac{1}{\delta_3^{\omega-1}} \right) + |v_{jl}| F_l \left(\frac{1}{\delta_3^{s-1}} \right) \right] \frac{|k_l(s-\tau)|^\omega}{\omega} ds \\
& \leq -\theta_1(t)V(t, \xi(t)) + \theta_2 \max_{-1 < s \leq t} V(s, \xi(s)). \tag{7.26}
\end{aligned}$$

Where

$$\begin{aligned}
\theta_1(t) &= \min_{1 \leq l \leq n} \left[\omega \left(d_t + |\phi_l(t)| + |\Psi_l(t)| - \sum_{j=1}^n |c_{tj}| F_j \delta_1(\omega-1) - \sum_{j=1}^n |c_j| F_l \frac{1}{\delta_1^{n-1}} \right. \right. \\
&\quad \left. \left. - \sum_{j=1}^n |a_{ij}| F_j (\omega-1) \delta_2 + |u_{lj}| F_j (\omega-1) \delta_3 + |v_{lj}| F_j (\omega-1) \delta_3 \right) \frac{|\xi_l(t)|^\omega}{\omega} \right] \\
\theta_2(t) &= \max_{1 \leq l \leq n} \left[\sum_{j=1}^n |a_{jl}| F_l \frac{1}{\delta_2^{\omega-1}} + \sum_{j=1}^n |u_j| F_l \frac{1}{\delta_3^{a-1}} + \sum_{j=1}^n |v_j| F_l \frac{1}{\delta_3^{\omega-1}} \frac{|\xi_l(t-\tau)|^\omega}{a} \right]
\end{aligned}$$

From this estimate, for any solution (7.13), which satisfies the Razumichin condition

$$V(s, \xi(s)) \leq V(t, \xi(t)), t - \tau \leq s \leq t$$

We have

$${}^c D^\alpha V(t, \xi(t)) \leq -(\eta_1 - \eta_2)V(t, \xi(t)), t \geq 0. \tag{7.27}$$

According to Lemma 5, the claim of Theorem 7.4.2 follows.

$$V(t, \xi(t)) \leq V(0, \xi(0)) E_\alpha(-\gamma t^\alpha), t \geq 0 \tag{7.28}$$

Lemma 4 and inequality (7.25) prove the system (7.10) can be achieved globally Mittag-Leffler stabilization under the designed control law. Hence complete the proof.

Theorem 7.4.4 Assume that Assumption (1) and Lemma (4) hold, then the system (7.10) is globally Mittag-Leffler stable, provided the following conditions hold:

$$\begin{aligned}
& \eta_1(t) > \eta_2(t) \\
\eta_1(t) &= \min_{l \leq l \leq n} \left[(d_l + \phi_l + \vartheta_l) - \sum_{j=1}^n c_{lj} F_j \rho^{-1} - \sum_{j=1}^n c_{jl} F_l \rho - \sum_{j=1}^n a_{lj} F_j \rho^{-1} \right]
\end{aligned}$$

$$\eta_2(t) = \max_{1 \leq l \leq n} \left[\sum_{j=1}^n a_{jl} F_l \rho + \sum_{j=1}^n |u_{jl}| F_l \rho + \sum_{j=1}^n |v_{jl}| F_l \rho \right] > 0$$

Proof: let us consider the Lyapunov function is

$$V(t) = \sum_{i=1}^n \frac{1}{2} \xi_i^2(t) + \sum_{i=1}^n \frac{1}{2q_i} (\phi_i(t) - \phi_i)^2 + \sum_{i=1}^n \frac{1}{2r_i} (\Psi_i(t) - \Psi_i)^2$$

$${}^c D^\alpha \phi_i(t) = q_i \xi_i^2(t), \quad {}^c D^\alpha \Psi_i(t) = r_i \xi_i^2(t)$$

According to the Caputo fractional-order derivative definition, we have

$$\begin{aligned} {}^c D^\alpha V(t, \xi^k(t)) &\leq \sum_{i=1}^n \xi_i(t) {}^c D^\alpha \xi_i(t) + \sum_{i=1}^n \frac{1}{q_i} (\phi_i(t) - \phi_i) {}^c D^\alpha \phi_i(t) \\ &+ \sum_{i=1}^n \frac{1}{r_i} (\Psi_i(t) - \Psi_i) {}^c D^\alpha \Psi_i(t) \\ &\leq \sum_{i=1}^n \xi_i(t) [-d_i \xi_i(t) + \sum_{j=1}^n c_{ij} [f_j(\theta_j(t)) - f_j(\zeta_j(t))] \\ &+ \sum_{j=1}^n a_{tj} [f_j(f_j(t - \tau)) - f_j(\zeta_j(t - \tau))] \\ &+ \Lambda_{j-1}^n |u_{ij}| \int_0^\infty k_j(s) [f_j(f_j(t - \tau)) - f_j(\xi_j(t - \tau))] ds \\ &+ V_{j-1}^n |v_{j}| \int_0^\infty k_j(s) [f_j(\theta_j(t - \tau)) - f_j(\zeta_j(t - \tau))] ds - \phi_i(t) k_i(t) \\ &- \Phi_i(t) \xi_i(t)] + \sum_{i=1}^n \frac{1}{q_i} (\phi_r(t) - \phi_r) q_i \xi_i^2(t) + \sum_{i=1}^n \frac{1}{r_i} (\Psi_i(t) - \Psi_i) r_i \xi_i^2(t) \\ &= -\sum_{i=1}^n d_i \xi_i^2(t) + \sum_{i=1}^n \sum_{j=1}^n c_{ij} F_j |\hat{\xi}_i(t)| |\xi_j(t)| \\ &+ \sum_{i=1}^n \sum_{j=1}^n a_{ij} F_j |k_i(t)| |\xi_j(t - \tau)| \\ &+ \sum_{i=1}^n \sum_{j=1}^n |u_{ij}| \int_0^\infty k_j(s) F_j |k_i(s)| |k_j(s - \tau)| ds \\ &+ \sum_{i=1}^n \sum_{j=1}^n |v_{j}| \int_0^\infty k_j(s) F_j |\xi_i(s)| |\xi_j(s - \tau)| ds \\ &- \sum_{i=1}^n \phi_i(t) \xi_i^2(t) - \sum_{i=1}^n \Phi_i(t) \xi_i^2(t) \\ &+ \sum_{i=1}^n (\phi_i(t) - \phi_i) \xi_i^2(t) + \sum_{i=1}^n (\Psi_i(t) - \Psi_i) \xi_i^2(t) \\ &\leq -\sum_{i=1}^n d_i \xi_i^2(t) + \sum_{i=1}^n \sum_{j=1}^n c_{ij} F_j \left[\frac{\rho^{-1}}{2} k_i^2(t) + \frac{\rho}{2} k_j^2(t) \right] \\ &+ \sum_{i=1}^n \sum_{j=1}^n a_{tj} F_j \left[\frac{\rho^{-1}}{2} \xi_i^2(t) + \frac{\rho}{2} \xi_j^2(t - \tau) \right] \end{aligned}$$

$$\begin{aligned}
& + \sum_{l=1}^n \sum_{j=1}^n |u_{ij}| \int_0^\infty k_j(s) F_j \left[\frac{\rho^{-1}}{2} k_i^2(s) + \frac{\rho}{2} k_j^2(s - \tau) \right] ds \\
& + \sum_{l=1}^n \sum_{j=1}^n |t_{lj}| \int_0^\infty k_j(s) F_j \left[\frac{\rho^{-1}}{2} k_l^2(s) + \frac{\rho}{2} k_j^2(s - \tau) \right] ds \\
& - \sum_{l=1}^n \phi_l(t) \xi_l^2(t) - \sum_{i=1}^n \Psi_i(t) \xi_i^2(t) \\
& + \sum_{l=1}^n \phi_i(t) \xi_i^2(t) - \sum_{l=1}^n \phi_i \xi_i^2(t) + \sum_{l=1}^n \psi_l(t) \xi_l^2(t) - \sum_{l=1}^n \Phi_l \xi_l^2(t) \\
& \leq - \sum_{l=1}^n d_i \xi_l^2(t) + \sum_{l=1}^n \sum_{j=1}^n c_{ij} F_j \left[\frac{\rho^{-1}}{2} \xi_l^2(t) \right] + \sum_{i=1}^n \sum_{j=1}^n c_{ij} F_j \left[\frac{\rho}{2} \xi_j^2(t) \right] \\
& + \sum_{i=1}^n \sum_{j=1}^n a_{ij} F_j \left[\frac{\rho^{-1}}{2} \xi_l^2(t) \right] + \sum_{l=1}^n \sum_{j=1}^n a_{ij} F_j \left[\frac{\rho}{2} \xi_j^2(t - \tau) \right] \\
& + \sum_{l=1}^n \sum_{j=1}^n |u_{lj}| \int_0^\infty k_j(s) F_j \left[\frac{\rho^{-1}}{2} k_l^2(s) \right] ds \\
& + \sum_{l=1}^n \sum_{j=1}^n |u_{ij}| \int_0^\infty k_j(s) F_j \left[\frac{\rho}{2} \xi_j^2(s - \tau) \right] ds \\
& + \sum_{l=1}^n \sum_{j=1}^n |t_{yl}| \int_0^\infty k_j(s) F_j \left[\frac{\rho^{-1}}{2} k_l^2(s) \right] ds \\
& + \sum_{l=1}^n \sum_{j=1}^n |v_{ij}| \int_0^\infty k_j(s) F_j \left[\frac{\rho}{2} \xi_j^2(s - \tau) \right] ds \\
& - \sum_{l=1}^n \phi_l \xi_l^2(t) - \sum_{l=1}^n \Phi_l \xi_l^2(t) \\
& \leq - \sum_{l=1}^n d_i \xi_l^2(t) + \sum_{l=1}^n \sum_{j=1}^n c_{ij} F_j \left[\frac{\rho^{-1}}{2} k_i^2(t) \right] + \sum_{i=1}^n \sum_{j=1}^n c_j F_l \left[\frac{\rho}{2} \xi_l^2(t) \right] \\
& + \sum_{l=1}^n \sum_{j=1}^n a_{lj} F_j \left[\frac{\rho^{-1}}{2} \xi_l^2(t) \right] + \sum_{l=1}^n \sum_{j=1}^n a_j F_l \left[\frac{\rho}{2} \xi_l^2(t - \tau) \right] \\
& + \sum_{l=1}^n (\phi_l(t) - \phi_l) \xi_l^2(t) + \sum_{l=1}^n (\vartheta_l(t) - \downarrow_l) \xi_l^2(t) \\
& \leq - \sum_{l=1}^n d_i \xi_l^2(t) + \sum_{l=1}^n \sum_{j=1}^n c_{ij} F_j \left[\frac{\rho^{-1}}{2} k_i^2(t) + \frac{\rho}{2} k_j^2(t) \right] \\
& + \sum_{l=1}^n \sum_{j=1}^n a_t F_j \left[\frac{\rho^{-1}}{2} \xi_l^2(t) + \frac{\rho}{2} \xi_j^2(t - \tau) \right] \\
& + \sum_{l=1}^n \sum_{j=1}^n |u_{ij}| \int_0^\infty k_j(s) F_j \left[\frac{\rho^{-1}}{2} k_i^2(s) + \frac{\rho}{2} k_j^2(s - \tau) \right] ds \\
& + \sum_{l=1}^n \sum_{j=1}^n |t_{lj}| \int_0^\infty k_j(s) F_j \left[\frac{\rho^{-1}}{2} k_l^2(s) + \frac{\rho}{2} k_j^2(s - \tau) \right] ds \\
& - \sum_{l=1}^n \phi_l(t) \xi_l^2(t) - \sum_{i=1}^n \Psi_i(t) \xi_i^2(t) \\
& + \sum_{l=1}^n \phi_i(t) \xi_i^2(t) - \sum_{l=1}^n \phi_i \xi_i^2(t) + \sum_{l=1}^n \psi_l(t) \xi_l^2(t) - \sum_{l=1}^n \Phi_l \xi_l^2(t)
\end{aligned}$$

$$\begin{aligned}
&\leq -\sum_{l=1}^n d_l \xi_l^2(t) + \sum_{l=1}^n \sum_{j=1}^n c_{lj} F_j \left[\frac{\rho^{-1}}{2} \xi_l^2(t) \right] + \sum_{l=1}^n \sum_{j=1}^n c_{lj} F_j \left[\frac{\rho}{2} \xi_j^2(t) \right] \\
&+ \sum_{l=1}^n \sum_{j=1}^n a_{lj} F_j \left[\frac{\rho^{-1}}{2} \xi_l^2(t) \right] + \sum_{l=1}^n \sum_{j=1}^n a_{lj} F_j \left[\frac{\rho}{2} \xi_j^2(t - \tau) \right] \\
&+ \sum_{l=1}^{\kappa} \sum_{j=1}^n |u_{lj}| \int_0^{\infty} k_j(s) F_j \left[\frac{\rho^{-1}}{2} k_l^2(s) \right] ds \\
&+ \sum_{l=1}^n \sum_{j=1}^n |u_{lj}| \int_0^{\infty} k_j(s) F_j \left[\frac{\rho}{2} \xi_j^2(s - \tau) \right] ds \\
&+ \sum_{l=1}^n \sum_{j=1}^n |t_{lj}| \int_0^{\infty} k_j(s) F_j \left[\frac{\rho^{-1}}{2} k_l^2(s) \right] ds \\
&+ \sum_{l=1}^n \sum_{j=1}^n |v_{lj}| \int_0^{\infty} k_j(s) F_j \left[\frac{\rho}{2} \xi_j^2(s - \tau) \right] ds \\
&- \sum_{l=1}^n \phi_l \xi_l^2(t) - \sum_{l=1}^n \Phi_l \xi_l^2(t) \\
&\leq -\sum_{l=1}^n d_l \xi_l^2(t) + \sum_{l=1}^n \sum_{j=1}^n c_{lj} F_j \left[\frac{\rho^{-1}}{2} k_l^2(t) \right] + \sum_{l=1}^n \sum_{j=1}^n c_{lj} F_l \left[\frac{\rho}{2} \xi_l^2(t) \right] \\
&+ \sum_{l=1}^n \sum_{j=1}^n a_{lj} F_j \left[\frac{\rho^{-1}}{2} \xi_l^2(t) \right] + \sum_{l=1}^n \sum_{j=1}^n a_{lj} F_l \left[\frac{\rho}{2} \xi_l^2(t - \tau) \right] \\
&+ \sum_{l=1}^{\pi} \sum_{j=1}^{\pi} |u_{lj}| \int_0^{\infty} k_j(s) F_j \left[\frac{\rho^{-1}}{2} k_l^2(s) \right] ds \\
&+ \sum_{l=1}^{\pi} \sum_{j=1}^{\pi} |u_{lj}| \int_0^{\infty} k_j(s) F_l \left[\frac{\rho}{2} \xi_l^2(s - \tau) \right] ds \\
&+ \sum_{l=1}^n \sum_{j=1}^{\pi} |v_{lj}| \int_0^{\infty} k_j(s) F_j \left[\frac{\rho^{-1}}{2} \xi_l^2(s) \right] ds \\
&+ \sum_{l=1}^{\pi} \sum_{j=1}^{\pi} |v_{lj}| \int_0^{\infty} k_j(s) F_l \left[\frac{\rho}{2} \xi_l^2(s - \tau) \right] ds \\
&- \sum_{l=1}^n \phi_l k_l^2(t) - \sum_{l=1}^n \Psi_l \xi_l^2(t) \\
&\leq \sum_{l=1}^n \left[-(d_l + \phi_1 + \star_l) + \sum_{j=1}^n c_{lj} F_j \frac{\rho^{-1}}{2} + \sum_{j=1}^n c_{lj} F_l \frac{\rho}{2} \right. \\
&\left. + \sum_{j=1}^{\pi} a_{lj} F_j \left[\frac{\rho^{-1}}{2} \right] \right] \xi_l^2(t) \\
&+ \sum_{l=1}^{\pi} \left[\sum_{j=1}^{\pi} a_{lj} F_l \left[\frac{\rho}{2} \right] \right] \xi_l^2(t - \tau) + \sum_{l=1}^n \left[\sum_{j=1}^{\pi} |u_{lj}| \int_0^{\infty} k_j(s) F_j \left[\frac{\rho^{-1}}{2} \right] ds \right. \\
&\left. + \sum_{j=1}^{\pi} |v_{lj}| \int_0^{\infty} k_j(s) F_j \left[\frac{\rho^{-1}}{2} \right] \right] \xi_l^2(s) ds
\end{aligned}$$

$$\begin{aligned}
& + \sum_{j=1}^{\pi} |v_j| \int_0^{\infty} k_j(s) F_j \left[\frac{\rho^{-1}}{2} \right] \xi_i^2(s) ds \\
& + \sum_{l=1}^{\pi} \left[\sum_{j=1}^{\pi} |u_j| \int_0^{\infty} k_j(s) F_l \left[\frac{\rho}{2} \right] ds \right. \\
& \left. + \sum_{j=1}^n |v v_{ju}| \int_0^{\infty} k_j(s) F_l \left[\frac{\rho}{2} \right] \right] \xi_l^2(s - \tau) ds \\
& \leq - \sum_{l=1}^{\pi} \left[(d_l + \phi_j + \vartheta_l) - \sum_{j=1}^{\pi} c_{lj} F_j \frac{\rho^{-1}}{2} - \sum_{j=1}^n c_{jl} F_l \frac{\rho}{2} \right. \\
& \left. - \sum_{j=1}^{\pi} a_{ij} F_j \left[\frac{\rho^{-1}}{2} \right] \right] \xi_i^2(t) \\
& + \sum_{l=1}^n \left[\sum_{j=1}^n a_j F_l \left[\frac{\rho}{2} \right] \right] \xi_l^2(t - \tau) + \sum_{l=1}^n \left[\sum_{j=1}^n |u_{lj}| i_t t_0^{\infty} k_j(s) F_j \right] \frac{\rho^{-1}}{2} | ds \\
& + \sum_{j=1}^{\pi} |v_{lj}| \int_0^{\infty} k_j(s) F_j \left[\frac{\rho^{-1}}{2} \right] \xi_l^2(s) ds \\
& + \sum_{l=1}^n \left[\sum_{j=1}^n |u_j| \int_0^{\infty} k_j(s) F_l \left[\frac{\rho}{2} \right] ds \right. \\
& \quad \left. + \sum_{j=1}^n |v_{jl}| \int_0^{\infty} k_j(s) F_l \left[\frac{\rho}{2} \right] \right] \xi_l^2(s - \tau) ds \\
& \leq -\eta_1 V(t, \xi^k(t)) + \eta_2 \max_{t-\tau \leq s \leq t} V(s, \xi_s(s))
\end{aligned} \tag{7.29}$$

Where,

$$\begin{aligned}
\eta_1(t) &= \min_{1 \leq l \leq n} \left[(d_l + \phi_v + \Psi_l) - \sum_{j=1}^n c_{lj} F_j \rho^{-1} - \sum_{j=1}^n c_j F_l \rho - \sum_{j=1}^n a_{lj} F_j \rho^{-1} \right. \\
& \left. + \sum_{j=1}^n |u_{lj}| F_j \rho^{-1} + \sum_{j=1}^n |v_{vj}| F_j \rho^{-1} \right] > 0, \\
\eta_2(t) &= \max_{1 \leq s \leq n} \left[\sum_{j=1}^n a_{jl} F_i \rho + \sum_{j=1}^n |u_{jl}| F_i \rho + \sum_{j=1}^n |v_{jt}| F_i \rho \right] > 0
\end{aligned}$$

From this estimate, for any solution (7.13), which satisfies the Razumichin condition

$$V(s, \xi(s)) \leq V(t, \xi(t)), t - \tau \leq s \leq t,$$

We have

$$\begin{aligned}
{}^c D^\alpha V(t, \xi(t)) &\leq -(\eta_1 - \eta_2) V(t, \xi(t)), t \geq 0. \\
(7.30)
\end{aligned}$$

According to Lemma 5, the claim of Theorem 7.4.3 follows.

$$V(t, \xi(t)) \leq V(0, \xi(0)) E_\alpha(-\gamma t^\alpha), t \geq 0 \tag{7.31}$$

By Lemma 4 and inequality (7.31), this proves system (7.10) can be achieved globally Mittag-Leffler stabilization under the designed control law. This completes the proof.

Theorem 7.4.5 Assume that Assumption (1) and Lemma (4) hold, then the system (7.10) is Globally Mittag-Leffler stable, provided the following conditions holds:

$$\theta_1(t) > \theta_2(t)$$

$$\begin{aligned} \theta_1(t) = & \min_{1 \leq l \leq e} \left[\omega(d_l + |\phi_l(t)| + |\Psi_l(t)|) - \sum_{j=1}^n |c_l| F_j \delta_1 (\omega - 1) - \sum_{j=1}^n |c_\mu| F_l \frac{1}{\delta_1^{\omega-1}} \right. \\ & - \sum_{j=1}^n |a_l| F_j (\omega - 1) \delta_2 + |u_{ij}| F_j (\omega - 1) \delta_3 + |v_j| F_j (\omega - 1) \delta_3 \left. \right] \frac{|\xi_l(t)|^\omega}{\omega} \\ & + \min_{l \leq l \leq n} \left[\rho(d_l + |\phi_l(t)| + |\Psi_l(t)|) - \sum_{j=1}^n |c_l| F_j \delta_1 (\rho - 1) - \sum_{j=1}^n |c_{jl}| F_l \frac{1}{\delta_1^{\rho-1}} \right. \\ & - \sum_{j=1}^n |a_{ij}| F_j (\rho - 1) \delta_2 + |u_{ij}| F_j (\rho - 1) \delta_3 + |v_{ij}| F_j (\rho - 1) \delta_3 \left. \right] \frac{1 k_l(t)^\rho}{\rho} > 0. \\ \theta_2(t) = & \max_{1 \leq i \leq s} \left[\sum_{j=1}^n |a_{jt}| F_l \frac{1}{\delta_2^{a_{v-1}}} + \sum_{j=1}^n |u_j| F_l \frac{1}{\delta_3^{\omega-1}} + \sum_{j=1}^n |v_{jt}| F_l \frac{1}{\delta_3^{a-1}} \right] \frac{|\xi_l(t - \tau)|^\omega}{\omega} \\ & + \max_{1 \leq l \leq n} \left[\sum_{j=1}^{\pi} |a_{ju}| F_l \frac{1}{\delta_2^{\rho-1}} + \sum_{j=1}^n |u_{ji}| F_l \frac{1}{\delta_3^{\rho-1}} + \sum_{j=1}^{\pi} |v_{\rho i}| F_l \frac{1}{\delta_3^{\rho-1}} \right] \frac{|\xi_i(t - \tau)|^\rho}{\rho} > 0 \end{aligned}$$

Proof we define a Lyapunov function

$$V(t, \xi(t)) = \sum_{t=1}^n \frac{1}{\omega} |\xi_l(t)|^\omega + \sum_{t=1}^n \frac{1}{\rho} |\xi_t(t)|^\rho \quad (7.32)$$

According to the Caputo fractional-order derivative definition, we have

$$\begin{aligned} & + \sum_{j=1}^{\pi} |a_{ij}| |f_j(0_j(t - \tau)) - f_j(\zeta_j(t - \tau))| \\ & + \wedge_{j=1}^m |u_{ij}| \left| \int_0^\infty k_j(s) |f_j(b_j(s - \tau)) - f_j(\zeta_j(t - \tau))| ds \right. \\ & + \wedge_{j=1}^m |\tau_\gamma| \left| \int_0^\infty k_j(s) |f_j(v_j(s - \tau)) - f_j(\zeta_j(t - \tau))| ds \right. \\ & + |\phi_r(r)| |\xi_1(r)| + |\Phi_u(t)| \|\xi_r(t)\| \\ & + \sum_{i=1}^{\pi} |k_i(t)|^{p-1} [-d_i |\xi_i(t)| + \sum_{j=1}^n |c_{ij}| |f_j(0_j(t)) - f_j(\zeta_j(t))|] \\ & + \sum_{j=1}^{\pi} |a_{ij}| |f_j(0, (t - \tau)) - f_j(\zeta_j(t - \tau))| \\ & + \wedge_{j=1}^m |u_{jj}| \left| \int_0^\infty k_j(s) |f_j(\theta_j(s - \tau)) - f_j(\zeta_j(t - \tau))| ds \right. \\ & \quad \left. + |\phi_r(r)| |\xi_r(t)| + |\psi_l(t)| \|\xi_r(t)\| \right] \end{aligned}$$

$$\begin{aligned}
&\leq \sum_{t=1}^n |\xi_1(t)|^{\omega-1} \left[-d_t |k_t(t)| + \sum_{j=1}^n |c_{ij}| F_j |\xi_j(t)| + \sum_{j=1}^n |a_{ij}| F_j |k_j(t-\tau)| \right. \\
&\quad + \sum_{j=1}^n |u_{ij}| \int_0^\infty k_j(s) F_j |k_j(s-\tau)| ds + \sum_{j=1}^n |v_{ij}| \int_0^\infty k_j(s) F_j |k_j(s-\tau)| ds \\
&\quad + |\phi_l(t)| |k_l(t)| + |\psi_i(t)| |k_i(t)| \\
&\quad \left. + \sum_{i=1}^n |k_i(t)|^{\rho-1} \left[-d_t |\xi_l(t)| + \sum_{j=1}^n |c_{ij}| F_j |k_j(t)| + \sum_{j=1}^n |a_{ij}| F_j |\xi_j(t-\tau)| \right] \right.
\end{aligned}$$

$$\begin{aligned}
&+ \sum_{j=1}^n |u_i| \int_0^\infty k_j(s) F_j |k_j(s-\tau)| ds + \sum_{j=1}^n |v_j| \int_0^\infty k_j(s) F_j |\xi_j(s-\tau)| ds \\
&+ |\phi_T(t)| |\xi_t(t)| + |\Psi_l(t)| |\xi_t(t)| \\
&\leq -\sum_{l=1}^n (d_l + |\phi_l(t)| + |\Phi_l(t)|) |\xi_l(t)|^\omega + \sum_{l=1}^n \sum_{j=1}^n |c_l| |F_j| |\xi_l(t)|^{\otimes-1} |k_j(t)| \\
&+ \sum_{i=1}^n \sum_{j=1}^n |a_i| |F_j| |k_i(t)|^{u-1} |k_j(t-\tau)| \\
&+ \sum_{i=1}^n \sum_{j=1}^n |u_i| \int_0^\infty k_j(s) F_j |k_l(s)|^{\omega-1} |k_j(s-\tau)| ds \\
&+ \sum_{l=1}^n \sum_{j=1}^n |t_l| \int_0^\infty k_j(s) F_j |k_r(s)|^{4-1} |\xi_j(s-\tau)| ds \\
&- \sum_{i=1}^n (d_i + |\phi_i(t)| + |\psi_i(t)|) |\xi_l(t)|^e + \sum_{l=1}^n \sum_{j=1}^n |c_l| |F_j| |k_l(t)|^{e-1} |k_j(t)| \\
&+ \sum_{i=1}^n \sum_{j=1}^n |a_{ij}| |F_j| |k_l(t)|^{e-1} |k_j(t-\tau)| \\
&+ \sum_{i=1}^n \sum_{j=1}^n |u_{ij}| \int_0^\infty k_j(s) F_j |k_l(s)|^{\rho-1} |k_j(s-\tau)| ds \\
&+ \sum_{i=1}^n \sum_{j=1}^n |v_{ij}| \int_0^\infty k_j(s) F_j |k_l(s)|^{e-1} |k_j(s-\tau)| ds
\end{aligned} \tag{7.33}$$

From Lemma 3 we have

$$\begin{aligned}
|\xi_l(t)|^{\omega-1} |\xi_j(t)| &\leq \frac{\omega-1}{\omega} \left[|\xi_1(t)|^{\omega-1} \delta_1^{\frac{\omega-1}{\omega v}} \right]^{\frac{\omega}{\omega-1}} + \frac{1}{\omega} \left[|\xi_j(t)| \delta_1^{\frac{\omega-1}{\Delta}} \right]^{\omega t} \\
&= \frac{\omega-1}{\omega} |\xi_l(t)|^\omega \delta_1 + \frac{1}{\omega} |\xi_j(t)|^\omega \frac{1}{\delta_1^{\omega-1}} \\
|\xi_1(t)|^{\omega-1} |\xi_k(t-\tau)| &\leq \frac{\omega-1}{\omega} \left[|k_t(t)|^{\omega-1} \delta_2^{\frac{\theta-1}{\omega}} \right]^{\frac{\omega}{\omega-1}} + \frac{1}{\omega} \left[|\xi'(t-\tau)| \delta_2^{\frac{\omega-1}{\omega}} \right]^{\omega t} \\
&= \frac{\omega-1}{\omega} |k_t(t)|^\omega \delta_2 + \frac{1}{\omega} |k_j(t-\tau)|^\omega \frac{1}{\delta_2^{\omega-1}} \\
&\int_0^\infty |\xi_l(s)|^{\omega-1} |\xi_j(s-\tau)| ds
\end{aligned}$$

$$\begin{aligned}
&\leq \int_0^\infty \frac{\omega-1}{\omega} \left[|\xi_t(s)|^{\omega-1} \delta_3^{\frac{\omega-1}{\omega}} \right]^{\frac{\omega-1}{\omega}} + \frac{1}{\omega} \left[|\xi_j(s-\tau)| \delta_3^{\frac{\theta-1}{\alpha}} \right]^\omega \\
&= \int_0^\infty \frac{\omega-1}{\omega} |\xi_t(s)|^\omega \delta_3 + \frac{1}{\omega} |\xi_j(s-\tau)|^\omega \frac{1}{\delta_3^{\omega-1}} \\
|\xi_i(t)|^{\rho-1} |\xi_j(t)| &\leq \frac{\rho-1}{\rho} \left[|\xi_1(t)|^{\rho-1} \delta_1^{\frac{\rho-1}{\rho}} \right]^{\frac{\rho}{\rho-1}} + \frac{1}{\rho} \left[|\xi_j(t)| \delta_1^{\frac{-\rho-1}{\rho}} \right]^\rho \\
&= \frac{\rho-1}{\rho} |\xi_d(t)|^\rho \delta_1 + \frac{1}{\rho} |\xi_j(t)|^\rho \frac{1}{\delta_1^{\rho-1}} \\
|\xi_1(t)|^{\rho-1} |\xi_j(t-\tau)| &\leq \frac{\rho-1}{\rho} \left[|\xi_\xi(t)|^{\rho-1} \delta_2^{\frac{\rho-1}{\rho}} \right]^{\frac{\rho}{\rho-1}} + \frac{1}{\rho} \left[|\xi_\xi(t-\tau)| \delta_2^{\frac{-\mu-1}{\rho}} \right]^\rho \\
&= \frac{\rho-1}{\rho} |\xi_t(t)|^\rho \delta_2 + \frac{1}{\rho} |\xi_j(t-\tau)|^\rho \frac{1}{\delta_2^{\rho-1}} \\
\int_0^\infty |kl(s)|^{p-1} |k_j(s-\tau)| ds \\
&\leq \int_0^\infty \frac{\rho-1}{\rho} \left[|\xi_1(s)|^{\rho-1} \delta_3^{\frac{\rho-1}{\rho}} \right]^{\frac{\rho}{\rho-1}} + \frac{1}{\rho} \left[|\xi_j(s-\tau)| \delta_3^{\frac{-\rho-1}{\rho}} \right]^\rho \\
&= \int_0^\infty \frac{\rho-1}{\rho} |k_i(s)|^\rho \delta_3 \\
&\quad + \frac{1}{\rho} |k_j(s-\tau)|^\rho \frac{1}{\delta_3^{\rho-1}} \tag{7.34}
\end{aligned}$$

Now substitute the above values in the above equation we get

$$\begin{aligned}
c^\alpha V(t, D^\alpha(t)) &\leq -\sum_{l=1}^n (d_l + |\phi_l(t)| + |\Phi_l(t)|) |\xi_l(t)|^\omega \\
&\quad + \sum_{l=1}^n \sum_{j=1}^\pi |c_{lj}| F_j \left[\frac{\omega-1}{\omega} |k_l(t)|^\omega \delta_1 \right. \\
&\quad + \frac{1}{\omega} |\xi_j(t)|^\omega \frac{1}{\delta_1^{\omega-1}} \left. + \sum_{l=1}^n \sum_{j=1}^n |a_{ij}| F_j \left[\frac{\omega-1}{\omega} |\xi_1(t)|^{\omega t} \delta_2 \right. \right. \\
&\quad + \frac{1}{\omega} |\xi_j(f-\tau)|^{\omega v} \frac{1}{\delta_2^{\omega-1}} \left. \right] \\
&\quad + \sum_{i=1}^n \sum_{j=1}^\pi |u_{ij}| \int_0^\infty k_j(s) F_j \left[\frac{\omega-1}{\omega} |k_l(s)|^{\omega_3} \right. \\
&\quad + \frac{1}{\omega} |\xi_j(s-\tau)|^\omega \frac{1}{\delta_3^{\omega-1}} \left. \right] ds \\
&\quad + \sum_{l=1}^\pi \sum_{j=1}^\pi |v_{lj}| \int_0^\infty k_j(s) F_j \left[\frac{\omega-1}{\omega} |k_t(s)|^\omega \delta_3 + \frac{1}{\omega^2} |k_j(s-\tau)|^\omega \frac{1}{\delta_3^{\omega-1}} \right] ds
\end{aligned}$$

$$\begin{aligned}
& -\sum_{l=1}^n (d_l + |\phi_l(t)| + |\vartheta_l(t)|) |\xi_l(t)|^e + \sum_{i=1}^n \sum_{j=1}^n |c_{ij}| F_j \left| \frac{\rho-1}{\rho} \right| |\xi_l(t)|^\rho \delta_l \\
& + \frac{1}{\rho} |\xi_j(t)|^\rho \frac{1}{\delta_1^{\rho-1}} + \sum_{i=1}^n \sum_{j=1}^n |a_{ij}| F_j \left[\frac{\rho-1}{\rho} |\xi_i(t)|^\rho \delta_2 \right. \\
& \left. + \frac{1}{\rho} |k_{jj}(t-\tau)|^\rho \frac{1}{\delta_2^{\rho-1}} \right] \\
& + \sum_{l=1}^n \sum_{j=1}^n |u_{lj}| \int_0^\infty k_j(s) F_j \left[\frac{\rho-1}{\rho} |\xi_2(s)|^\rho \delta_3 + \frac{1}{\rho} |k_j(s-\tau)|^\rho \frac{1}{\delta_3^{\rho-1}} \right] ds \\
& + \sum_{l=1}^n \sum_{j=1}^n |v_{lj}| \int_0^\infty k_j(s) F_j \left[\frac{\rho-1}{\rho} |\xi_1(s)|^{\rho_3} \delta_3 + \frac{1}{\rho} |\xi_j(s-\tau)|^\rho \frac{1}{\delta_3^{\rho-1}} \right] ds \\
& \leq -\sum_{l=1}^n \left[d_l + |\phi_l(t)| + |\psi_l(t)| \right] |\xi_l(t)|^\omega + \sum_{i=1}^n \sum_{j=1}^n |c_{ij}| F_j \left[\frac{\omega-1}{\omega} |\xi_t(t)|^{\omega \delta_1} \right] \\
& + \sum_{l=1}^n \sum_{j=1}^n |c_{\mu}| F_l \left[\frac{1}{\omega} |\xi_l(t)|^{\omega t} \frac{1}{g_1^{\omega-1}} \right] \\
& + \sum_{l=1}^n \sum_{j=1}^n |a_{lj}| F_j \left[\frac{\omega-1}{\omega} |\xi_t(t)|^{\omega^2} \delta_2 \right] \\
& + \sum_{l=1}^n \sum_{j=1}^n |a_{jl}| F_l \left[\frac{1}{\omega} |\xi_1(t-\tau)|^\omega \frac{1}{d_2^{\omega t-1}} \right] \\
& + \sum_{l=1}^n \sum_{j=1}^n |u_{lj}| \int_0^\infty k_j(s) F_j \left[\frac{\omega-1}{\omega} |\xi_l(s)|^\omega \delta_3 \right] ds \\
& + \sum_{l=1}^n \sum_{j=1}^n |u_j| \int_0^\infty k_j(s) F_l \left[\frac{1}{\omega} |\xi_l(s-\tau)|^\omega \frac{1}{\delta_3^\omega - 1} \right] ds \\
& + \sum_{l=1}^n \sum_{j=1}^n |v_{lj}| \int_0^\infty k_j(s) F_j \left[\frac{\omega-1}{\omega} |k_j(s)|^{\omega \delta_3} \right] ds \\
& + \sum_{l=1}^n \sum_{j=1}^n |v_{jl}| \int_0^\infty k_j(s) F_l \left[\frac{1}{e^n} |\xi_l(s-\tau)|^\omega \frac{1}{\delta_3^{\omega n-1}} \right] ds \\
& -\sum_{l=1}^n |d_l + |\phi_l(t)| + |\varpi_l(t)| | |\xi_l(t)|^e \\
& + \sum_{l=1}^n \sum_{j=1}^n |c_{ij}| F_j \left[\frac{\rho-1}{\rho} |\xi_t(t)|^\rho g_1 \right] \\
& + \sum_{l=1}^n \sum_{j=1}^n |c_j| F_l \left[\frac{1}{\rho} |k_l(t)|^\Theta \frac{1}{\delta_1^{\rho-1}} \right] \\
& + \sum_{l=1}^n \sum_{j=1}^n |a_{tj}| F_j \left[\frac{\rho-1}{\rho} \left| \xi \right| (t) \right]^\rho \delta_2 \\
& + \sum_{l=1}^n \sum_{j=1}^n |a_{jl}| F_l \left[\frac{1}{\rho} |\xi_s(t-\tau)|^\rho \frac{1}{\delta_2^{\rho-1}} \right]
\end{aligned}$$

$$\begin{aligned}
& + \sum_{l=1}^n \sum_{j=1}^n |u_{\ell}| \int_0^{\infty} k_j(s) F_j \left[\frac{\rho-1}{\rho} |k_j(s)|^{\rho} \delta_3 \right] ds \\
& + \sum_{l=1}^n \sum_{j=1}^n |u_{j\ell}| \int_0^{\infty} k_j(s) F_i \left[\frac{1}{\rho} |\xi_l(s-\tau)|^e \frac{1}{\delta_3^{e-1}} \right] ds \\
& + \sum_{l=1}^n \sum_{j=1}^n |v_{l\ell}| \int_0^{\infty} k_j(s) F_j \left[\frac{\rho-1}{\rho} |\xi_j(s)|^{\rho} \delta_3 + \frac{1}{\rho} |\xi_j(s-\tau)|^{\rho} \frac{1}{\delta_3^{\rho-1}} \right] ds \\
& \leq - \sum_{l=1}^n [d_l + |\phi_l(t)| + |\Psi_l(t)|] |\xi_l(t)|^{\omega} + \sum_{l=1}^n \sum_{j=1}^n |c_{lj}| F_j \left[\frac{\omega-1}{\omega} |\xi_l(t)|^{\omega \xi_1} \right] \\
& + \sum_{l=1}^n \sum_{j=1}^n |c_{\mu}| F_l \left[\frac{1}{\omega} |\xi_l(t)|^{\omega t} \frac{1}{\delta_1^{\omega-1}} \right] \\
& + \sum_{l=1}^n \sum_{j=1}^n |a_{lj}| F_j \left[\frac{\omega-1}{\omega} |\xi_l(t)|^{\omega \delta} \right] \\
& + \sum_{l=1}^n \sum_{j=1}^n |a_{j\ell}| F_l \left[\frac{1}{\omega} |\xi_l(t-\tau)|^{\omega} \frac{1}{\delta_2^{\omega-1}} \right] \\
& + \sum_{l=1}^n \sum_{j=1}^n |u_{\ell}| \int_0^{\infty} k_j(s) F_l \left[\frac{\omega-1}{\omega} |\xi_l(s)|^{\omega \delta_3} \right] ds \\
& + \sum_{l=1}^n \sum_{j=1}^n |u_{j\ell}| \int_0^{\infty} k_j(s) F_i \left[\frac{1}{\omega} |\xi_l(s-\tau)|^{\omega} \frac{1}{\delta_3^{\omega-1}} \right] ds \\
& + \sum_{l=1}^n \sum_{j=1}^n |v_{l\ell}| \int_0^{\infty} k_j(s) F_j \left[\frac{\omega-1}{\omega} |k_l(s)|^{\omega \delta_3} \right] ds \\
& + \sum_{l=1}^n \sum_{j=1}^n |v_{j\ell}| \int_0^{\infty} k_j(s) F_l \left[\frac{1}{\omega} |\xi_l(s-\tau)|^{\omega} \frac{1}{\delta_3^{\omega-1}} \right] ds \\
& - \sum_{l=1}^n [d_l + |\phi_l(t)| + |\Psi_l(t)|] |\xi_l(t)|^e \\
& + \sum_{i=1}^n \sum_{j=1}^n |c_{ij}| F_j \left[\frac{\rho-1}{\rho} |\xi_l(t)|^{\rho g_1} \right] \\
& + \sum_{i=1}^n \sum_{j=1}^n |c_{ju}| F_l \left[\frac{1}{\rho} |k_l(t)|^{\rho} \frac{1}{\delta_1^{\rho-1}} \right] \\
& + \sum_{l=1}^n \sum_{j=1}^n |a_{tj}| F_j \left[\frac{\rho-1}{\rho} |\xi_l(t)|^{\rho} \delta_2 \right] \\
& + \sum_{l=1}^n \sum_{j=1}^n |a_{j\ell}| F_l \left[\frac{1}{\rho} |\xi_l(t-\tau)|^{\rho} \frac{1}{\delta_2^{\rho-1}} \right] \\
& + \sum_{l=1}^n \sum_{j=1}^n |u_{\ell}| \int_0^{\infty} k_j(s) F_j \left[\frac{\rho-1}{\rho} |\xi_t(s)|^e \delta_3 \right] ds \\
& + \sum_{l=1}^n \sum_{j=1}^n |u_{j\ell}| \int_0^{\infty} k_j(s) F_l \left[\frac{1}{\rho} |k_l(s-\tau)|^e \frac{1}{\delta_3^{e-1}} \right] ds \\
& + \sum_{l=1}^n \sum_{j=1}^n |v_{\ell}| \int_0^{\infty} k_j(s) F_j \left[\frac{\rho-1}{\rho} |k_l(s)|^{\rho \delta} \delta_3 \right] ds
\end{aligned}$$

$$\begin{aligned}
& + \sum_{l=1}^n \sum_{j=1}^n |v_{jl}| \int_0^\infty k_j(s) F_l \left[\frac{1}{\rho} |\xi_l(s-\tau)|^e \frac{1}{\delta_3^{e-1}} \right] ds \\
& \leq \sum_{l=1}^n \left[-\omega(d_l + |\phi_l(t)| + |\varpi_l(t)|) + \sum_{j=1}^n |c_l| F_j \delta_1(\omega-1) \right. \\
& \quad \left. + \sum_{j=1}^n |c_{jl}| F_l \frac{1}{\delta_1^{\omega-1}} + \sum_{j=1}^n |a_{ij}| F_j \delta_2(\omega-1) \right] \frac{1 \xi_l(t)^{\omega t}}{\theta} \\
& \quad + \sum_{l=1}^n \left[\sum_{j=1}^n |a_{jl}| F_l \frac{1}{\delta_2^{\omega-1}} \right] \frac{|\xi_l(t-\tau)|^\omega}{\omega} \\
& \quad + \sum_{l=1}^n \sum_{j=1}^n \int_0^\infty k_j(s) [|u_{ij}| F_j(\omega-1) \delta_3 + |v_{ij}| F_j(\omega-1) \delta_3] \frac{|k_l(s)|^\omega}{\omega} ds \\
& \quad + \sum_{l=1}^n \sum_{j=1}^n \int_0^\infty k_j(s) \left[|u_{jl}| F_l \left(\frac{1}{\delta_3^{\omega-1}} \right) + |v_j| F_l \left(\frac{1}{\delta_3^{\omega-1}} \right) \right] \frac{|k_l(s-\tau)|^\omega}{\omega} ds \\
& \quad + \sum_{l=1}^n \left[-\rho(d_l + |\phi_l(t)| + |\Phi_l(t)|) + \sum_{j=1}^n |c_{lj}| F_j \delta_1(\rho-1) \right. \\
& \quad \left. + \sum_{j=1}^n |c_{jl}| F_l \frac{1}{\delta_1^{\rho-1}} + \sum_{j=1}^n |a_{tj}| F_j \delta_2(\rho-1) \right] \frac{|\xi_l(t)|^e}{\rho} \\
& \quad + \sum_{l=1}^n \left[\sum_{j=1}^n |a_{jl}| F_l \frac{1}{\delta_2^{\rho-1}} \right] \frac{|\xi_l(t-\tau)|^e}{\rho} \\
& \quad + \sum_{l=1}^n \sum_{j=1}^n \int_0^\infty k_j(s) \left[|u_{ij}| F_j(\rho-1) \delta_3 + |v_{ij}| F_j(\rho-1) \delta_3 \right] \frac{|k_l(s)|^e}{\rho} ds \\
& \quad + \sum_{l=1}^n \sum_{j=1}^n \int_0^\infty k_j(s) \left[|u_j| F_l \left(\frac{1}{\delta_3^{\rho-1}} \right) + |v_j u| F_l \left(\frac{1}{\delta_3^{\rho-1}} \right) \right] \frac{|\xi_l(s-\tau)|^\rho}{\rho} ds \\
& \leq -\sum_{i=1}^n \left[\omega(d_i + |\phi_i(t)| + |\Psi_i(t)|) - \sum_{j=1}^n |c_{ij}| F_j \delta_1(\omega-1) \right. \\
& \quad \left. - \sum_{j=1}^n |c_{\mu}| F_i \frac{1}{\delta_1^{\omega-1}} - \sum_{j=1}^n |a_{ij}| F_j \delta_2(\omega-1) \right] \frac{|\xi_1(t)|^\omega}{\omega} \\
& \quad + \sum_{l=1}^n \left[\sum_{j=1}^n |a_{jl}| F_l \frac{1}{\delta_2^{\omega-1}} \right] \frac{|F_l(t-\tau)|^\omega}{\omega} \\
& \quad + \sum_{l=1}^n \sum_{j=1}^n \int_0^\infty k_j(s) [|u_{lj}| F_j(\omega-1) \delta_3 + |v_{lj}| F_j(\omega-1) \delta_3] \frac{|k_l(s)|^\omega}{\omega} ds \\
& \quad + \sum_{l=1}^n \sum_{j=1}^n \int_0^\infty k_j(s) \left[|u_{\mu}| F_l \left(\frac{1}{\delta_3^{\omega-1}} \right) + |v_j| F_l \left(\frac{1}{\delta_3^{\omega-1}} \right) \right] \frac{|\xi_l(s-t)|^\omega}{a} ds \\
& \quad - \sum_{t=1}^n \left[\rho(d_t + |\phi_t(t)| + |\downarrow_t(t)|) - \sum_{j=1}^n |c_{lj}| F_j \delta_1(\rho-1) \right. \\
& \quad \left. - \sum_{j=1}^n |c_{jl}| F_l \frac{1}{\delta_1^{\rho-1}} - \sum_{j=1}^n |a_{lj}| F_j \delta_2(\rho-1) \right] \frac{|k_l(t)|^\rho}{\rho} \\
& \quad + \sum_{l=1}^n \left[\sum_{j=1}^n |a_{jl}| F_l \frac{1}{\delta_2^{\rho-1}} \right] \frac{|k_l(t-\tau)|^e}{\rho}
\end{aligned}$$

$$\begin{aligned}
& + \sum_{l=1}^{\pi} \sum_{j=1}^{\pi} \int_0^{\infty} k_j(s) [|u_{lj}| F_j(\rho - 1) \delta_3 + |v_{lj}| F_j(\rho - 1) \delta_3] \frac{|k_t(s)| \rho}{\rho} ds \\
& + \sum_{i=1}^n \sum_{j=1}^{\pi} \int_0^{\infty} k_j(s) \left[|u_{ju}| F_l \left(\frac{1}{s^{\rho-1}} \right) + |v_{ju}| F_l \left(\frac{1}{\delta_3^{\rho-1}} \right) \right] \frac{|\xi_l(s - \tau)| \rho}{\rho} ds \\
& \leq -\theta_1(t) V(t, k(t)) + \theta_2 \max_{t-\tau \leq s \leq t} V(s, \xi(s)). \tag{7.35}
\end{aligned}$$

where

$$\begin{aligned}
\theta_1(t) &= \min_{1 \leq l \leq n} \left[\omega(d_l + |\phi_1(t)| + |\Psi_i(t)|) - \sum_{j=1}^n |c_{lj}| F_j \delta_1 (\omega - 1) - \sum_{j=1}^n |c_{jt}| F_i \frac{1}{\delta_1^{\omega-1}} \right. \\
& - \sum_{j=1}^{\pi} |a_{ij}| F_j (\omega - 1) \delta_2 + |u_{ij}| F_j (\omega - 1) \delta_3 + |\Sigma_{\gamma}| F_j (\omega - 1) \delta_3 \left. \right] \frac{|\xi_1(t)| \omega}{\omega} \\
& + \min_{1 \leq i \leq \pi} \left[\rho(d_l + |\phi_u(t)| + |\Psi_i(t)|) - \sum_{j=1}^{\pi} |c_{lj}| F_j \delta_1 (\rho - 1) - \sum_{j=1}^n |c_j| F_i \frac{1}{g_1^{\rho-1}} \right. \\
& - \sum_{j=1}^{\pi} |a_{ij}| F_j (\rho - 1) \delta_2 + |u_{ij}| F_j (\rho - 1) \delta_3 + |v_j| F_j (\rho - 1) \delta_3 \left. \right] \frac{|k_4(f)|^e}{\rho} \\
\theta_2(t) &= \max_{1 \leq l \leq n} \left[\sum_{j=1}^n |a_j| F_l \frac{1}{\delta_2^{\omega t-1}} + \sum_{j=1}^n |u_{ju}| F_i \frac{1}{\delta_3^{\omega s-1}} + \sum_{j=1}^n |v_j| F_l \frac{1}{\delta_3^{\omega-1}} \frac{|k_u(t - \tau)| \omega}{\omega} \right. \\
& + \max_{1 \leq l \leq \pi} \left[\sum_{j=1}^n |a_{jr}| F_1 \frac{1}{\delta_2^{\rho-1}} + \sum_{j=1}^n |u_j| F_1 \frac{1}{\delta_3^{\rho-1}} + \sum_{j=1}^n |v_j| F_1 \frac{1}{\delta_3^{\rho-1}} \frac{|\xi_l(t - \tau)| \rho}{\rho} \right.
\end{aligned}$$

From this estimate, for any solution (7.13), which satisfies the Razumichin condition

$$V(s, \xi(s)) \leq V(t, \xi(t)), t - \tau \leq s \leq t$$

We have

$${}^c D^\alpha V(t, \xi(t)) \leq -(\eta_1 - \eta_2) V\left(t, \frac{k}{5}(t)\right), t \geq 0 \tag{7.36}$$

According to Lemma 5, the claim of Theorem 7.4.4 follows.

$$V(t, \xi(t)) \leq V(0, \xi(0)) E_a(-\gamma t^\alpha), t \geq 0 \tag{7.37}$$

By Lemma 4 and inequality (7.37), this proves the system (7.10) can be achieved globally Mittag-Leffler stabilization under the designed control law. Hence complete the proof.

Remark 7.4.6. In the FCNNs, the fuzzy minimum feed-forward refers to taking the minimum value of the connection parameters with the fuzzy AND operation, and the fuzzy maximum feed-forward refers to taking the maximum value of the connection parameters with the fuzzy OR operation. The fuzzy minimum feedback refers to taking the minimum value of the delay connection parameter with the fuzzy AND operation, and the fuzzy maximum feedback refers to the maximum value of the delay connection parameter with the fuzzy OR operation. There are many other fuzzy logics, such as fuzzy AND, fuzzy OR, fuzzy NOT, fuzzy NAND, fuzzy

NOR, fuzzy XOR, fuzzy XNOR, complex fuzzy logic and etc. It is worth highlighting that our work can be applied to FCNNs with more complex fuzzy logic. 19

Remark 7.4.7. Neural networks usually have a spatial extension due to the presence of a multitude of parallel pathways with a variety of axon sizes and length and hence there is a distribution of propagation delays over a period of time. It is worth noting that although the signal propagation is sometimes instantaneous and can be modelled with discrete delays, it may also be distributed during a certain time period, so the distributed delays should be incorporated in the model. In other words, it is often the case that the neural network model possesses both discrete and distributed delays. In recent years, the stability of Hopfield neural networks, cellular neural networks and bidirectional associative memory neural networks with distributed delays has been discussed (see [249, 250] and references therein).

Remark 7.4.8. In recent days, stability analysis of fuzzy cellular neural networks have been extensively studied by the researchers. Stability analysis of fuzzy cellular neural networks with time delay in the leakage term and impulsive perturbations investigated in [251]. Finite-time synchronization of delayed fuzzy cellular neural networks with discontinuous activations is studied (see [252] and references there in). In these works integer order is considered in our paper fractional order is considered. Great efforts have been made in study of fractional order neural networks by the researchers. See for example, Adaptive control for fractional order induced chaotic fuzzy cellular neural networks [253], asymptotic stability of delayed fractional-order fuzzy neural networks with impulse effects [250], Mittag-Leffler stability of fractional-order Hopfield neural networks [251,252], Synchronization of fractional fuzzy cellular neural networks with interactions [253] have been investigated. In our paper stability fractional order fuzzy cellular neural networks with hybrid control is investigated.

Remark 7.4.9. In [254], Xu et al. investigated complete synchronization of fractional order complex networks via pinning adaptive and impulsive control strategy. In the past few years, due to the limited theory to deal with finite time stability of fractional order systems, synchronization research of fractional order systems is only the beginning [251] - [258]. In [259], Velmurugan et al. studied synchronization of fractional order neural networks by employing linear feedback control strategy. In [260], Ding et al. designed a novel controller based on feedback control strategy and discontinuous control strategy, and investigated stability of the considered fractional order neural networks. As is known to all, it is more perfect if the designed controller both realize the network synchronization objective and reduce the corresponding control cost. Motivated by the above discussions, we designed a novel hybrid

feedback controller, which is based on a simple discontinuous control strategy and study stability problem of fractional order cellular neural networks.

Remark 7.4.10. It is well known that every control strategy has its own advantages and disadvantages. Therefore, in some cases, hybrid control strategies are necessary to control some complex systems to achieve synchronization or other properties. Since fuzzy cellular neural networks may experience instantaneous perturbation or abrupt changes at certain instances, hybrid impulsive and other control strategies could be used to control them to the synchronous state. However, to authors' knowledge, there have few research achievements on the stability of fuzzy cellular neural networks by means of hybrid control strategies at present. It is still an open problem that deserves further investigation, which motivated our research in this paper.

7.5 Results and Discussion

in this section, two examples are given to illustrate the effectiveness of proposed Global Mittag-Leffler stability schemes.

7.5.1 Stability problem-1

Example 1 For $n=4$, consider the following fractional-order fuzzy cellular neural networks,

$$\begin{aligned}
{}^{cD} \zeta_i(t) &= -d_i \zeta_i(t) + \sum_{j=1}^2 c_{ij} f_j(\zeta_j(t)) + \sum_{j=1}^2 a_{ij} f_j(\zeta_j(t - \tau)) + \sum_{j=1}^2 h_{ij} \mu_j \\
&+ \wedge_{j=1}^2 u_{ij} \int_0^\infty k_j(s) f_j(\zeta_j(s - \tau)) ds + \wedge_{j=1}^2 p_{yj} \mu_j \\
&+ \int_{j=1}^\pi v_{jj} \int_0^\infty k_j(s) f_j(\zeta_j(s - \tau)) ds \\
&+ \int_{j=1}^2 Q_{ij} \mu_j + I_i, i \\
&= 1.2.
\end{aligned} \tag{7.38}$$

The parameters of (7.13) error system are assumed that $a_{11} = 0.4, a_{12} = 0.6, a_{13} = 0.9, a_{14} = 1.1.2, a_{21} = 0.8, a_{22} = 0.9, a_{23} = 2.3, a_{24} = 1.5, a_{31} = 0.7, a_{32} = 1.8, a_{33} = 0.5, a_{34} = 0.7, a_{41} = 1.3, a_{42} = 0.5, a_{43} = 0.2, a_{44} = 0.9, c_{11} = 1.5, c_{12} = 1.8, c_{13} = 0.7, c_{14} = 1.3, c_{21} = 2.9, c_{22} = 2.8, c_{23} = 0.9, c_{24} = 0.7, c_{31} = 1.8, c_{32} = 1.5, c_{33} = 0.7, c_{34} = 0.9, c_{41} = 2.8, c_{42} = 2.9, c_{43} = 0.7, c_{44} = 1.3, u_{11} = 0.9, u_{12} = 1.2, u_{13} = 2.1, u_{14} = 3.4, u_{21} = 2.1, u_{22} = 3.4, u_{23} = 1.2, u_{24} = 0.9, u_{31} = 2.1, u_{32} = 1.2, u_{33} = 0.9, c_{34} = 1.7, u_{41} = 1.7, u_{42} = 1.7, u_{43} = 1.2, u_{44} = 0.9, v_{11} = 1.8, v_{12} = 2.2, v_{13} = 0.7, v_{14} = 2.7, v_{21} = 2.2, v_{22} = 0.9, v_{23} = 0.5, v_{24} = 1.2, v_{31} = 1.7, v_{32} = 2.2, v_{33} = 0.7, v_{34} = 0.9, v_{41} = 0.9, v_{42} = 0.5, v_{43} = 1.8, v_{44} = 1.7, d_1 = 5, d_2 = 7, d_3 = 7, d_4 = 5, v_1 = 0.6, v_2 = 0.7, V_3 = 0.5, V_4 = 0.4, \phi_1 = 1.4, \phi_2 = 3.1, \phi_3 = 2.7, \phi_4 = 3.7, \alpha = 0.97. f(t) = fanh(t).$

The corresponding response system is described by

$${}^{cD} \hat{D}_i(t) = -d_i v_l(t) + \sum_{j=1}^2 c_{ij} f_j(\hat{\theta}_j(t)) + \sum_{j=1}^2 a_{ij} f_j(\hat{D}_j(t - \tau)) + \sum_{j=1}^2 h_{ij} \mu_j$$

$$\begin{aligned}
& + N_{j=1}^2 u_{ij} \int_0^\infty k_j(s) f_j(j_j(s - \tau)) ds + N_{j=1}^2 p_j \mu_j + \int_{j=1}^2 v_{lj} \int_0^\infty k_j(s) f_j(\theta_j(s - \tau)) ds \\
& + \int_{j=1}^2 Q_{(j)} \mu_j + I_l + u_i(t)
\end{aligned} \tag{7.39}$$

Where $a_{tj}, u_{tj}, t_j, d_t, c_{ij}$, and I_l are the same as in system (7.39), and the hybrid feedback controllers is as follows: $u_l(t) = u_u(t) + u_U(t)$, where $u_u(t) = -\phi_x(t)\xi_2(t)$ and $u_{2i}(t) = -\Psi_i(t)\xi_i(t)$. Where $\xi_l(t) = \theta_t(t) - \zeta_1(t)$ for $i = 1, 2$. According to the developed idea in Theorem 4.1, it asks that (Fig. I)

$$\begin{aligned}
\eta_1(t) = \min_{1 \leq l \leq n} [(d_f + \phi_v(t) + \Psi_i) - \sum_{j=1}^n c_{lj} F_j \rho^{-1} - \sum_{j=1}^n c_{jt} F_l \rho - \sum_{j=1}^n a_{ij} F_j \rho^{-1} \\
+ \sum_{j=1}^n u_{lj} F_j \rho^{-1} + \sum_{j=1}^n v_{jj} F_j \rho^{-1}] = 12.33 > 0.
\end{aligned}$$

$$\nabla_2(t) = \max_{1 \leq l \leq n} [\sum_{j=1}^n a_{ju} F_l \rho + u_{j1} F_l \rho + \sum_{j=1}^n v_j F_l \rho] = 12.18 > 0.$$

Then it follows from Theorem 7.4.1 that system (7.38) can be achieved global Mittag-Leffler stabilization under the designed hybrid feedback control law (Fig.7 2).

7.5.2 Stability problem-2

Example 2 For $n = 2$, consider the following fractional-order fuzzy cellular neural networks,

$$\begin{aligned}
& + \Lambda_{j=1}^2 u_{lj} \int_0^\infty k_j(s) f_j(\zeta_j(s - \tau)) ds + \Lambda_{j=1}^2 p_{ij} \mu_j + \int_{j=1}^n t_{ij} \int_0^\infty k_j(s) f_j(\zeta_j(s - \tau)) ds + \\
& V_{j=1}^2 Q_{ij} \mu_j + I_i, i = 1, 2
\end{aligned} \tag{7.40}$$

Where $\alpha = 0.97, f(t) = \tanh(t)$

The parameters of (7.13) error system are assumed that $a_{11} = 0.9, a_{12} = 0.8, a_{13} = 0.4,$
 $a_{14} = 0.6, a_{21} = 0.4, a_{22} = 0.8, a_{23} = 0.7, a_{24} = 0.3, a_{31} = 0.3, a_{32} = 0.7, a_{33} = 0.7,$
 $a_{34} = 0.5, a_{41} = 0.5, a_{42} = 0.8, a_{43} = 0.3, a_{44} = 0.5, c_{11} = 0.4, c_{12} = 0.5, c_{13} = 0.4. c_{14} =$
 $1.3, c_{21} = 0.7, c_{22} = 0.8, c_{23} = 0.5, c_{24} = 0.7, c_{31} = 0.4, c_{32} = 0.7, c_{33} = 0.9, c_{34} = 0.3, c_{41} =$
 $0.3, c_{42} = 0.8, c_{43} = 0.5, c_{44} = 0.7, u_{11} = 0.9, u_{12} = 1.1, u_{13} = 1.3, u_{14} = 0.7, u_{21} =$
 $1.3, u_{22} = 0.9, u_{23} = 0.8, u_{24} = 1.2, u_{31} = 1.2, u_{32} = 0.7, u_{33} = 1.1. u_{34} = 1, u_{41} =$
 $1.3, u_{42} = 1, u_{43} = 0.5, u_{44} = 0.3, v_{11} = 0.7, v_{12} = 1.1, v_{13} = 1, v_{14} = 1.3, v_{21} = 1, v_{22} =$
 $0.3, v_{23} = 0.7, v_{24} = 0.2, v_{31} = 0.4, v_{32} = 0.8, v_{33} = 0.9. v_{34} = 1.2, v_{41} = 1.1, v_{42} =$
 $0.2, v_{43} = 0.7, v_{44} = 1.2, d_1 = 9, d_2 = 9, d_3 = 7, d_4 = 7. \psi_1 = 2.7, v_2 = 3.1, v_3 = 4.5, v_4 =$
 $2.5, \phi_1 = 5.3, \phi_2 = 4.7, \phi_3 = 5.3, \phi_4 = 5.1, \alpha = 0.97. f(t) = 1 \tanh(t).$
 $\omega = 2, \delta_1 = \delta_2 = \delta_3 = 1, F_l = 1. (i = 1, 2, 3, 4).$

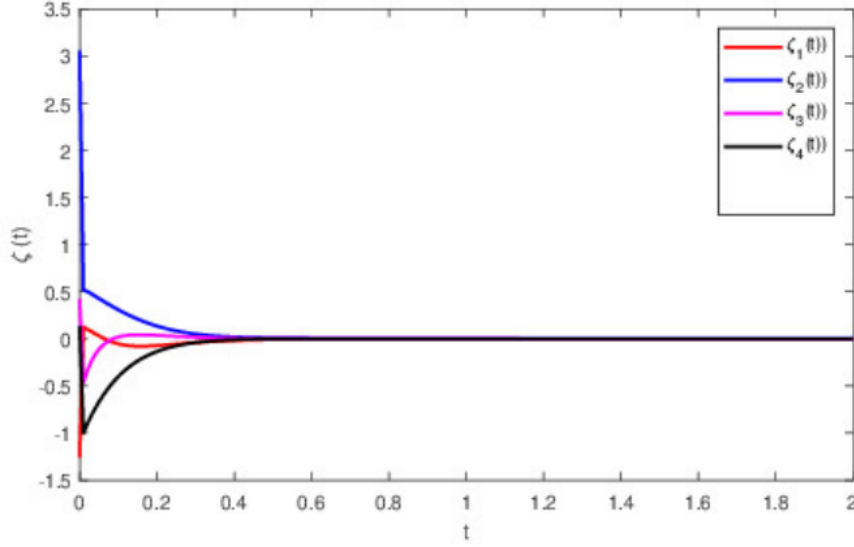


Fig. 7.1 State trajectories of the FCNN system from Example I

The corresponding response system is described by

$$\begin{aligned}
c_{D^2} \hat{v}_i(t) = & -d_l \theta_l(t) + \sum_{j=1}^2 c_{lj} f_j(\theta_j(t)) + \sum_{j=1}^2 a_{ij} f_j(\theta_j(t - \tau)) + \sum_{j=1}^2 h_{jj} \mu_j \\
& + \prod_{j=1}^2 u_{ij} \int_0^\infty k_j(s) f_j(\theta_j(s - \tau)) ds + N_{j-1}^2 p_{lj} \mu_j + V_{j=1}^2 v_{dj} \int_0^\infty k_j(s) f_j(v_j(s - \tau)) ds \\
& + \sum_{j=1}^2 Q_{ij} \mu_j + I_l + u_i(t)
\end{aligned} \tag{7.41}$$

Where $a_{lj}, u_{lj}, t_{yj}, d_l, c_{lj}$, and I_l are the same as in system (7.4I), and the hybrid feedback controllers is as follows: $u_l(t) = u_u(t) + u_u(t)$, where $u_u(t) = -\phi_l(t)e_l(t)$ and $u_{2u}(t) = -\Psi_i(t)e_l(t)$. Where $\xi_L(t) = \theta_l(t) - \zeta_i(t)$ for $i = 1, 2$. According to the developed idea in Theorem 3.2, it asks that

$$\begin{aligned}
\theta_1(t) = & \min_{1 \leq i \leq n} \left[(d_l + |\delta_l(t)| + |\Phi_l(t)|) - \sum_{j=1}^n |c_{ij}| F_j \delta_1(\omega - 1) - \sum_{j=1}^n |c_{jd}| F_l \frac{1}{\delta_1^{\omega-1}} \right. \\
& \left. + \sum_{j=1}^n |a_{lj}| F_j(\omega - 1) \delta_2 + |u_{ij}| F_j(\omega - 1) \delta_3 + |v_{lj}| F_j(\omega - 1) \delta_3 \right] = 10.40 > 0. \\
\theta_2(t) = & \max_{1 \leq i \leq n} \left[\sum_{j=1}^n |a_{jl}| F_l \frac{1}{\delta_2^{\omega-1}} + \sum_{j=1}^n |u_{jl}| F_l \frac{1}{\delta_3^{\omega-1}} + \sum_{j=1}^n |v_{jl}| F_l \frac{1}{\delta_3^{\omega-1}} \right] = 10 > 0.
\end{aligned}$$

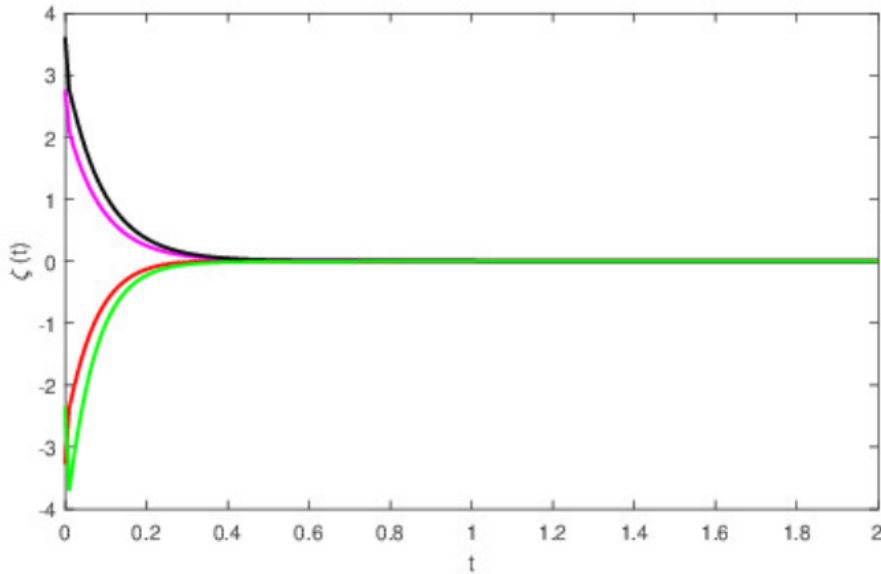


Fig. 7.2 State trajectories of the FCNN system from example 2

Then it follows from Theorem 7.4.2 that system (7.40) can be achieved global Mittag-Leffler stabilization under the designed hybrid feedback control law.

7.6 Conclusion

In this chapter, Global Mittag-Leffler stability of fractional order fuzzy cellular neural networks with distributed delays via hybrid feedback controllers has been addressed. We proposed the definition of Global Mittag-Leffler stability and the fractional Lyapunov direct method, which enriches the knowledge of both the system theory and the fractional calculus. This chapter serves as a first step in presenting sufficient conditions for global Mittag-Leffler stability for a generalized fuzzy cellular fractional-order neural network with distributed delay. The main theoretical findings in this chapter are that hybrid feedback control law. We extend the concept of Lyapunov functions for a fuzzy cellular fractional-order neural network. Under the assumption of Lipschitz continuity of activation functions, we have proved the Global Mittag-Leffler stability of the proposed model, which implies faster convergence rate of the network model than the Lyapunov convergence.

CHAPTER 8

CONCLUSION AND FUTURE SCOPE

The performance of new FO-PID controller was compared to the integer order proportional integral Derivative/proportional integral derivative (IOPID/PID) controller. Our observation was that since the Ceramic Infrared systems have very small relative dead time they do not need a full integrator for their control. FO-PID controller gives a strong competition to IOPID controller tuned by new analytical method for some cases. For FO- PID method introduced, the resulting closed-loop system has the desirable feature of being robust to gain variations with step responses exhibiting an iso-damping property. Extensive simulation results are included to illustrate the simple yet practical nature of the developed new tuning rules.

This thesis work discusses a process control case study taking temperature control of Ceramic Infrared HFE. First of all temperature control HFE system of Ceramic Infrared Heater is developed and a conventional PID controller is implemented in it. In what concerns fractional PID, another possible improvement would be the development of additional tuning rules. Rules similar to the second Ziegler-Nichols rule (making use of a closed-loop response of the plant) are certainly possible. Rules specific for non-minimum phase plants may also be of interest. All the classical approaches (Åström-Hägglund, Cohen-Coon) urge to decrease the integral action when the actuator saturates. But, the correction is taken through a feedback. It delays its effect.

A comparative study is done using different control techniques for the primary control of different controller. First, the conventional PID controller is implemented as primary controller. The PID controller gives a high overshoot and high settling time. So artificial intelligence principles in the controller architecture are proposed and implemented. Then the fuzzy PID, Genetic Algorithm, Ant Colony and Bacteria forging based PID controller is implemented and it gives a better response than the conventional PID controller. Then the IOPID with high gain based on Bode and Nyquist based stability margin and fractional PID controller is used and unit step responses are shown for different values of integral order and derivative order. It is found out that the fractional PID controller has the better response than both conventional and fuzzy PID Genetic Algorithm, Ant Colony and Bacteria forging based PID controller.

The recommendations on the conclusion of this study acknowledges that Ceramic IR Heater process, whether it be heating or drying, is still a modest researched area. Much work remains to be done concerning the investigation of the effects of infrared radiation on various materials.

This work performs a small-scale test measuring controller performance, so that it serves as a platform for future research efforts leading to real-life implementation of a Ceramic Infrared Heater Temperature control system.

Stability problem have been proved with examples considering the sufficient conditions for global Mittag-Leffler stability for a generalized fuzzy cellular fractional-order neural network with distributed delay. The main theoretical findings in these chapters are that hybrid feedback control law. We extend the concept of Lyapunov functions for a fuzzy cellular fractional-order neural network. Under the assumption of Lipschitz continuity of activation functions, we have proved the Global Mittag-Leffler stability of the proposed model, which implies faster convergence rate of the network model than the Lyapunov convergence.

Future Scope

With the use of the controller developed in this thesis, the study of IR and its effects on many materials is now possible. A summary of the potential applications and improvements of the controller is presented below:

- A further comparative study using an auto-tuning PID controller, that automatically recalculates the parameters of the process as the load demand changes, is a consideration.
- The enlargement of the buffer used to store the list of temperatures for plotting needs to be increased so as to provide a clearer picture of the complete temperature profile.
- Increase the heating capacity of the infrared heaters i.e. increases the power densities of the heaters, by mounting an arrangement of heaters on a panel. This is a more useful and practical way to study the effect on industrial processes.
- Also, may be performed experiments to determine the spectral radiation densities of different heaters and various heater arrangements. The research conducted for this dissertation serves as a basis for more intensive study of the many aspects of infrared processing. With an amplified heating capacity that an arrangement of many infrared heaters offers, a more worthwhile exportation of IR heating is possible. A modification of the power electronics components in

this study would make this controller a more functionally competent unit for industrial purposes.

Stability of fractional order fuzzy cellular neural network with other sufficient conditions with the help of considering Mittag-Leffler function and Lyapunov function with examples may be investigated.

REFERENCES

- [1] Abdollah Homaifar and Ed McCormick; “Simultaneous Design of Membership Function and Rule Sets for Fuzzy Controllers Using Genetic Algorithm”, IEEE Transactions on Fuzzy Systems, Vol.3,1995.
- [2] Amjad J. Humaidi ; “Tuning of PID Controller Based on Foraging Strategy for Pneumatic Position Control System”; IJCCE ,Vol-10,No. 1, ,2010.
- [3] Antonio Visioli; “Fuzzy Logic Based Set Point Weight Tuning of PID Controllers”, IEEE Transactions on Systems, Man and Cybernetics , Vo. 29,1999.
- [4] Anuj Narang , Sirish L.Shah and Tongwen Chen ; “ Tuning of fractional PI Controller for fractional order system models with and without time delay”, American Control Conference ,2010.
- [5] B.Nagaraj and N. Muruganath; “A Comparative Study of PID Controller Tuning Using GA, EP, PSO and ACO”,ICCCCT, IEEE-2010.
- [6] B.Nagaraj and N.Muruganath ; “ Soft Computing – Based Optimum Design of PID Controller for a Position Control of a DC Motor”, Mediamira Science Publisher,2010
- [7] C R Madhuranthakam , A. Elkamel and H.Budman ; “ Optimal Tuning of PID controllers for FOPTD,SOPTD and SOPTD with lead processes”, Journal of Chemical Engineering and Processing , ELSEVIER,2008.
- [8] C.Yeroglu and N Tan ; “ Note on Fractional Order Proportional Integral Differential Controller Design”, IET Control Theory , Vol. 5, 2011.
- [9] Christian Blum; “Ant Colony Optimization: Introduction and Hybridizations”; Seventh International Conference on Hybrid Intelligent Systems, IEEE, 2007.
- [10] Chunna Zhao, Dingyu and YangQuan Chen; “A fractional Order PID Tuning Algorithm for A Class of Fractional order Plants”, International Conference on Mechatronics and Automation, 2005.
- [11] Deepyaman Maiti, Ayan Acharya, Mithun Chakraborty, Amit Konar and Ramadoss Janarthanan ; “ Tuning PID and $PI\lambda D\delta$ Controllers using the Integral Time Absolute Error Criterion”,ICIAFS, IEEE, 2008.
- [12] Duarte Valério and José Sá da Costa; “Tuning of Fractional PID controllers with Ziegler – Nichols – type rules”, Journal of Signal Processing , Science Direct, 2006.
- [13] Emine Dogru Bolat ; “ Implementation of Matlab-SIMULINK based Real Time Temperature Control for Set Point Changes”, International Journal of Circuit , Systems and Signal Processing ,2007.
- [14] Fernando G. Martins ; “ Tuning PID Controllers using the ITAE Criterion”, International Journal of Engineering, Vol.21,2005.

- [15] Hamideh Hamidian and Ali Akbar Jalali ; “ Calculation of PID Controller Parameters for Unstable First Order Time Delay Systems”,IJSER,Vol.2,2011.
- [16] Hongbo Xin , Xiaoyu Liu,Tinglei Huang and Xiangjiao Tang ; “ Temperature Control System based on Fuzzy Self Adaptive PID Controller”, International Conference on Genetic and Evolutionary Computing , IEEE,2009.
- [17] HongSheng Li, Ying Luo and YangQuan Chen ; “ A Fractional order Proportional and Derivative (FOPD) Motion Controller: Tuning Rule and Experiments”, IEEE Transactions on Control Systems Technology, Vol-18, 2010.
- [18] Hu Sheng , Yan Li and YangQuan Chen ; “ Application of numerical inverse Laplace transform algorithms in fractional calculus” , Journal of the Franklin Institute ,Science Direct , 2011.
- [19] Hung-Cheng Chen and Sheng-Hsiung Chang ; “ Genetic Algorithms based Optimization Design of a PID Controller for an Active Magnetic Bearing”, International Journal of Computer Science and Network Security, Vol. 6,2006.
- [20] Hung-Ching Lu , His-Kuang Liu and Lian – Fue Yang ; “PID Controller Parameter Estimator Using Ant Colony System”; IEEE International Conference on System Science and Engineering, IEEE,2013.
- [21] Huseyin Atakan Varol and Zafer Bingul; “A New PID Tuning Technique Using Ant Algorithm”; American Control Conference, 2004.
- [22] Hyo-Sung Ahn, Varsha Bhambhani and YangQuan Chen ; “ Fractional order integral and derivative controller for temperature profile trackling”, Indian Academy of Sciences , Oct-2009.
- [23] I.Santi Prabha, K Durga Rao and D Siva Rama Krishna ; “ Fuzzy Logic based Intelligent Controller design for an Injection Mould Machine Process Control”,IJAEST,2011.
- [24] Ibtissem Chiha, Noureddine Liouane and Pierre Borne ; “Tuning PID Controller Using Multiobjective Ant Colony Optimization ”; Applied Computational Intelligence and Soft Computing ,Hindawi Publishing Corporation,Vol. 2012 .
- [25] Ivo Petráš, Ľubomir Dorčák and Imrich Košťal; “ Control Quality Enhancement by Fractional Order Controllers” Acta Montanistica Slovaca ,1998
- [26] Jianming Zhang, Ning Wang and Shuqing Wang; “ A Developed Method of Tuning PID Controllers with Fuzzy Rules for Integrating Processes”, American Control Conference , Boston,2004
- [27] Jin-Sung Kim, Jin-Hwan Kim, Ji-Mo Park , Sung-Man Park and Won-Yong Choe ; “ Auto Tuning PID Controller based Improved Genetic Algorithm for Reverse Osmosis Plant”, World Academy of Science Engineering and Technology,2008

- [28] Lasse M. Eriksson and Heikki N. Koivo ; “ Comparison of Low complexity Controller in varying Time delay systems”, SICE Journal of control , Measurement and System Integration, Vol.1, pp. 111-119, 2008.
- [29] Leehter Yao and Chin-Chin Lin; “Design of Gain Scheduled Fuzzy PID Controller”, World Academy of Science, Engineering and Technology, 2005.
- [30] Li Xu-zhou, Yu Fei and Wang You-bo ; “ PSO Algorithm based online Self Tuning of PID Controller”, International Conference on Computational Intelligence and Security , IEEE, 2007
- [31] Liu Yijian and Fang Yanjun ; “Optimization Design of PID Controller Parameters Based on Improved E. Coli Foraging Optimization Algorithm”; International Conference on Automation and Logistics , IEEE, 2008.
- [32] M Adonis and M T E Khan; “Analysis of the efficiency of a simplified infrared energy management system”, Journal of Energy in Southern Africa, Vol. 19 No. 2 , May 2008.
- [33] M Adonis and M T E Khan; “PID Control of Infrared Radiative Power Profile for Ceramic Emitters”, International conference on Control Theory and Application, IEEE, 2001
- [34] Mahmud Iwan Solihin , Lee Fook Tack and Moey Leap Kean ; “ Tuning of PID Controller using Particle Swarm Optimization(PSO)”, International Conference on Advance Science , Engineering and Information Technology , Malaysia, 2011
- [35] Marco Darigo, Naure Birattari and Thomas Stützle; “ Ant Colony Optimization”, IEEE Computational Intelligence Magazine , Nov. 2006.
- [36] Mendes N, Oliveira G H C and Araujo H X; “Building Thermal Performance Analysis by using Matlab / Simulink ” , IBPSA Conference, Brazil, 2001.
- [37] Mendes N, Oliveira G H C, Araujo H X and Coelho L S ; “ A Matlab- Based Simulation tool for Building Thermal Performance Analysis” , IBPSA Conference, Netherland, 2003.
- [38] Mohammad Ali Nekoui , Mohammad Ali Khameneh and Mohammad Hosein Kazemi ; “ Optimal Design of PID Controller for a CSTR System Using Particle Swarm Optimization”, International Power Electronics and Motion Control Conference, 2010.
- [39] Muhammet Ünal , Hasan Erdal and Vedat Topuz ; “Trajectory Tracking Performance Comparison between Genetic Algorithm and Ant Colony Optimization for PID Controller Tuning on Pressure Process”; Wiley Periodicals Inc. , January 2010; pp. 518-528.
- [40] Nazlia Omar, Mohd. Faizal Ismail , Rozli Zulkifli and Rosilah Hassan ; “ Development of a Real-Time Temperature and Voltage Monitoring System for Semiconductor Devices”, European Journal of Scientific Research , Vol. 34, pp.168-177, 2009.
- [41] NS Izuegbu and ML Adonis ; “ Simulation and Modelling of Energy Efficient Design of a Ceramic Infrared Heater”, Industrial and Commercial Use of Energy, IEEE 2011.

- [42] P.Poongodi and S. Victor; “Genetic algorithm based PID controller design for LTI system via reduced order model”, International conference on Instrumentation, Control and Automation,2009.
- [43] P.Wang and D.P.Kwok; “Auto-Tuning of Classical PID Controllers Using An Advanced Genetic Algorithm”, IEEE, 1992.
- [44] Podlubny I., Dorcak L and Kostial I.; “On fractional Derivative, Fractional Order Dynamic Systems and PI λ D μ -controllers”, IEEE,1994.
- [45] R.Padma Sree and M.Chidambaram ; “ Simple Method of Tuning PI Controllers for Stable Inverse Response Systems”, Journal of Indian Institute of Science,2003.
- [46] Ramiro S. Barbosa , Manuel F . Silva and J A Tenreiro Machado, “Tuning and Application of Integer and Fractional Order PID Controllers” Intelligent Engineering Systems and Computational Cybernetics , Springer Science , 2009.
- [47] S R Vaishnav and Z J Khan ; “ Design and Performance of PID and Fuzzy Logic Controller with smaller Rule set for Higher Order System”, World Congress on Engineering and Computer Science 2007,USA,2007.
- [48] S.M.Giriraj Kumar, Deepak Jayaraj and Anoop R. Kishan ; “ PSO based Tuning of a PID Controller for a High Performance Drilling Machine”, International Journal of Computer Application , Vol. 1,2010.
- [49] S.M.GiriRaj Kumar, K.Ramkumar , and Sanjay Sarma O.V ; “Real Time Application of Ants Colony Optimization”; International Journal of Computer Application , Vol. 3-2010.
- [50] Saeed Tavakoli and Mahdi Tavakoli ; “ Optimal Tuning of PID Controllers for First order plus Time delay model using Dimensional Analysis”, International Conference on Control and Automation , Canada,IEEE,2003.
- [51] Sing-Fu Lee, Hung-Ching Lu and Ta-Hsiung Hung; “Optimal design GA Based Fuzzy PID Controllers”, IEEE, 2002.
- [52] Sofiane Bououden , Salim Filali , and Mohammed Chadli,Fouad Allouani ; “Using Ant Colony Optimization Algorithm For Enhancing an Optimal PI Controller ”; IJ-STA, Vol - 5,Dec 2011; pp. 1648-1659.
- [53] Duan Hai-Bin, Wang Dao-Bo and Yu Xie-Fen; “Novel Approach to Nonlinear PID Parameter Optimization Using Using Ant Colony Optimization Algorithm ”; Journal of Bionic Engineering , Science Direct ,2006.
- [54] Song Chaohong, Luo Qiang and Shi Feng; “Genetic Algorithms for Optimization of Complex Nonlinear System”, International Conference on Computer Science and Software Engineering, IEEE, 2008.
- [55] T. Hägglund and K J Åström ; “ Revisiting the Zeigler – Nichols Tuning rules for PI Control- The Frequency Response Method”, Asian Journal of Control ,Vol. 6, pp. 469-482,2004.

- [56] T. Hägglund and K J Åström; “Revisiting the Zeigler – Nichols step response method for PID control”, *Journal of Process Control*, ELSEVIER, pp. 635-650,2004.
- [57] T.Suksri , V.Boonpranchoo , V.Kongratana ,V. Tipsuwanporn and N.Numsumran ; “ Design of Temporal Controller for Small Oven Process Using STM32F103RE”,*World Congress on Engineering and Computer Science* , Vol. 2, 2011.
- [58] Truong Nguyen Luan Vu and Moonyong Lee ; “ Analytical Design of fractional order proportional integral controllers for time delay processes”, *ISA Transactions* , ELSEVIER, 2013.
- [59] V.Rajinikanth and K.Latha; “Controller Parameter Optimization for Nonlinear Systems Using Enhanced Bacteria Foraging Algorithm”; *Applied Computational Intelligence and Soft Computing*, Hindawi Publishing Corporation 2012.
- [60] Wael M. Korani , Hassen Taher Dorrah and Hassan M. Emara ; “Bacterial Foarging Oriented by Particle Swarm Optimization Strategy for PID Tuning,GECCO,2008.
- [61] Wen Tan, Jizhen Liu,Tongwen Chen and Horacio J. Marquez ; “ Comparison of some well-known PID Tuning formulas”, *Journal of Computers and Chemical Engineering*, ELSEVIER,2006.
- [62] Y.Jin , Y-Q. Chen and D.Xue , “ Time- constant robust analysis of a fractional order [proportional derivative] controller , *IET Control Theory and Application* , Vol.5, 2011.
- [63] YangQuan Chen , Ivo Petras and Dingyu Xue , “ Fractional Order Control – A Tutorial”, *American Control Conference* , 2009.
- [64] YangQuan Chen , Tripti Bhaskaran and Dingyii Xue; “ Practical Tuning Rule Development for Fractional Order Proportional and Integral Controllers” *Journal of Computational and Nonlinear Dynamics*, ASME ,Vol. 3, April 2008.
- [65] Yanhai Chen and Weixing Lin ; “An Improved Bacterial Foraging Optimization”; *International Conference on Robotics and Biomimetics* , IEEE ,2009.
- [66] Ying Luo , ChunYang Wang and YangQuan Chen ; “ Tuning Fractional Order Proportional Integral Controllers for fractional Order Systems”, *IEEE*,2009.
- [67] Ying Luo , YangQuan Chen , Chun Yang Wang and You Guo Pi ; “ Tuning fractional order proportional integral controllers for fractional order systems”, *Journal of Process Control* , Science Direct , 2010.
- [68] Ying Pei, Wenbo Wang and Song Zhang ; “Basic Ant Colony Optimization”, *International Conference on Computer Science and Electronic Engineering* ,IEEE,2012.
- [69] Ying Tung Hsiao, Cheng-Long Chuang and Cheng- Chih Chien; “Ant Colony Optimization for Designing of PID Controllers”, *IEEE*, 2004, *International Symposium on Computer Aided Control System Design*; pp. 321-326.

- [70] Yung K.Lee and John M. Watkins ; “ Determination of All Stabilizing Fractional Order PID Controllers” ,American Control Conference , 2011.
- [71] Zaid Amin Abduljabar; “ Simulation and Design of Fuzzy Temperature Control for Heating and Cooling Water System’ , International Journal of Advancements in computing Technology, Vol.3,2011.
- [72] Zhenyu Yang and Gerulf Pederson ; “ Automatic Tuning for a 1-D Levitation System using a Genetic a Genetic Algorithm – A Real Case Study”, International Symposium on Intelligent Control , IEEE, 2006.
- [73] Zhiqiang Gao, Thomas A.Trautzsch and James G.Dawson ; “ A Stable Self Tuning Fuzzy Logic Control System for Industrial Temperature Regulation”,IEEE,2002
- [74] Zhou Ying,Zhang Lie, Wang Gui-li and Yang Qian ; “ A Nonlinear PID Controller Based on an Adaptive Genetic Algorithm”, International Conference on Intelligent Networks and Intelligent Systems, IEEE,2009.
- [75] Maiti, Deepyaman, et al. "Tuning PID and $PI/\lambda D \delta$ controllers using the integral time absolute error criterion." *2008 4th International Conference on Information and Automation for Sustainability*. IEEE, 2008.
- [76] Luo, Ying, et al. "Tuning fractional order proportional integral controllers for fractional order systems." *Journal of Process Control* 20.7 (2010): 823-831.
- [77] GirirajKumar, S. M., Deepak Jayaraj, and Anoop R. Kishan. "PSO based tuning of a PID controller for a high performance drilling machine." *International Journal of Computer Applications* 1.19 (2010): 12-18.
- [78] Yeroglu, Celaleddin, and Nusret Tan. "Note on fractional-order proportional–integral–differential controller design." *IET control theory & applications* 5.17 (2011): 1978-1989.
- [79] Narang, Anuj, Sirish L. Shah, and Tongwen Chen. "Tuning of fractional PI controllers for fractional order system models with and without time delays." *Proceedings of the 2010 American Control Conference*. IEEE, 2010.
- [80] Nagaraj, B., and N. Murugananth. "Soft computing-based optimum design of PID controller for a position control of DC motor." *ACTA Electrotechnica* 51.1 (2010): 21-24.
- [81] Luo, Ying, et al. "Tuning fractional order proportional integral controllers for fractional order systems." *Journal of Process Control* 20.7 (2010): 823-831.
- [82] Lee, Yung K., and John M. Watkins. "Determination of all stabilizing fractional-order PID controllers." *Proceedings of the 2011 American Control Conference*. IEEE, 2011.

- [83] Guo, Wei, et al. "A novel model algorithmic controller with fractional order PID structure." *Proceedings of the 10th World Congress on Intelligent Control and Automation*. IEEE, 2012.
- [84] Das, Saptarshi, et al. "Improved model reduction and tuning of fractional-order PI λ D μ controllers for analytical rule extraction with genetic programming." *ISA transactions* 51.2 (2012): 237-261.
- [85] Aguila-Camacho, Norelys, and Manuel A. Duarte-Mermoud. "Fractional adaptive control for an automatic voltage regulator." *ISA transactions* 52.6 (2013): 807-815.
- [86] Turner, Laura E. "The Mittag-Leffler Theorem: The origin, evolution, and reception of a mathematical result, 1876–1884." *Historia Mathematica* 40.1 (2013): 36-83.
- [87] Pakhira, Anindya, et al. "Symbolic representation for analog realization of a family of fractional order controller structures via continued fraction expansion." *ISA transactions* 57 (2015): 390-402.
- [88] Liu, Lu, Feng Pan, and Dingyu Xue. "Fractional-order controller design for oscillatory fractional time-delay systems based on the numerical inverse Laplace transform algorithms." *Mathematical Problems in Engineering* 2015 (2015).
- [89]. Zamani, Abbasali, S. Masoud Barakati, and Saeed Yousofi-Darmian. "Design of a fractional order PID controller using GBMO algorithm for load–frequency control with governor saturation consideration." *ISA transactions* 64 (2016): 56-66.
- [90] Yumuk, E., et al. "Design of an integer order PID controller for single fractional order pole model." *2015 IEEE Conference on Systems, Process and Control (ICSPC)*. IEEE, 2015.
- [91] Tepljakov, Aleksei, et al. "Incorporation of fractional-order dynamics into an existing PI/PID DC motor control loop." *ISA transactions* 60 (2016): 262-273.
- [92] Rabah, Karima, Samir Ladaci, and Mohamed Lashab. "A novel fractional sliding mode control configuration for synchronizing disturbed fractional-order chaotic systems." *Pramana* 89.3 (2017): 1-13.
- [93] Yakoub, Z., et al. "Model-based fractional order controller design." *IFAC-Papers On Line* 50.1 (2017): 10431-10436.
- [94] Sánchez, Helem Sabina, et al. "Tuning rules for robust FOPID controllers based on multi-objective optimization with FOPDT models." *ISA transactions* 66 (2017): 344-361.
- [95] Zhang, Lei, Qiankun Song, and Zhenjiang Zhao. "Stability analysis of fractional-order complex-valued neural networks with both leakage and discrete delays." *Applied Mathematics and Computation* 298 (2017): 296-309.

- [96] Tepljakov, Aleksei, et al. "FOPID controllers and their industrial applications: a survey of recent results." *IFAC-PapersOnLine* 51.4 (2018): 25-30.
- [97] Wu, Zhenlong, et al. "Tuning for fractional order PID controller based on probabilistic robustness." *IFAC-PapersOnLine* 51.4 (2018): 675-680.
- [98] Liping Chen , Jinde Cao , Ranchao Wu, J.A. Tenreiro Machado , António M. Lopes , and Hejun Yang," Stability and synchronization of fractional-order memristive neural networks with multiple delays", Elsevier, 22 June 2017.
- [99] Helem Sabina Sánchez , Fabrizio Padula , Antonio Visioli and Ramon Vilanova," Tuning rules for robust FOPID controllers based on multi-objective optimization with FOPDT models", ISA Transactions , Elsevier, 18 September, 2016.
- [100] Erdal Cokmez , Serdal Atiç, Fuat Peker and Ibrahim Kaya," Fractional-order PI Controller Design for Integrating Processes Based on Gain and Phase Margin Specifications ",Elsevier, IFAC (International Federation of Automatic Control) , 2018.
- [101] Tushar Verma and Akhilesh Kumar Mishra Comparative Study of PID and FOPID Controller Response for Automatic Voltage Regulation Article in IOSR Journal of Applied Physics · September 2014'.
- [102] Ardak Kashkynbayev, Jinde Cao and Zhaksybek Damiyev ," Stability analysis for periodic solutions of fuzzy shunting inhibitory CNNs with delays", Advances in Difference Equations ,springer journal , 2019.
- [103] Swapnil W. Khubalkar, and Anjali S. Junghare. "Modeling and control of fractional order PID controller fed rotary inverted pendulum." 2018 International Conference on Power, Instrumentation, Control and Computing (PICC). IEEE, 2018.
- [104] M. Syed Ali¹, M. Hymavathi¹, Bandana Priya, Syeda Asma Kauser³ and Ganesh Kumar Thakur ⁴" Stability analysis of stochastic fractional-order competitive neural networks with leakage delay" AIMS Mathematics, 6(4): 3205–3241. DOI:10.3934/math.2021193 Received: 04 October 2020 Accepted: 31 December ,2020.
- [105] Hongyun Yan, Yuanhua Qiao ,Lijuan Duan, and Ling Zhang Global Mittag–Leffler Stabilization of Fractional-Order BAM Neural Network State Feedback Controllers, Hindawi Mathematical Problems in Engineering Volume 2020.
- [106] Jia Jia, Xia Huang , Yuxia Li , Jinde Cao and Ahmed Alsaedi Global Stabilization of Fractional-Order Memristor-Based Neural Networks With Time Delay, 998 IEEE Transactions On Neural Networks And Learning Systems, Vol. 31, No. 3, March 2020.

- [107] Ibrahim' Avcı, Numerical Simulation of Fractional Delay Differential Equations Using the Operational Matrix of Fractional Integration for Fractional-Order Taylor Basis, *Fractal Fract.* 2022, 6, 10.
- [108] M. Syed Ali, M. Hymavathi , Bandana Priya , Syeda Asma Kauser and Ganesh Kumar Thakur, Stability analysis of stochastic fractional-order competitive neural networks with leakage delay *AIMS Mathematics*, 6(4): 3205–3241.
- [109] F. Liu, M. Meerschaert, S. Momani, N. Leonenko, W. Chen, O. Agrawal, Fractional differential equations, *Int. J. Differ. Equ. Appl.* 2013 (2010).
- [110] H. Haubold, A. Mathai, *An Introduction to Fractional Calculus, An Introduction to Fractional Calculus*, 2017.
- [111] M. Dalir, Applications of fractional calculus, *Appl. Math. Sci.* 4 (2010) 1021–1032.
- [112] P. Arena, R. Caponetto, L. Fortuna, D. Porto, Bifurcation and chaos in non-integer order cellular neural networks, *Int. J. Bifurcation Chaos* 8 (1998) 1527–1539.
- [113] B.S. Chen, J.J. Chen, Global asymptotical ω -periodicity of a fractional order non-autonomous neural networks, *Neural Netw.* 68 (2015) 78–88.
- [114] M. Syed Ali, L. Palanisamy, J. Yogambigai, L. Wang, Passivity-based synchronization of Markovian jump complex dynamical networks with time-varying delays, parameter uncertainties, reaction–diffusion terms, and sampled-data control, *J. Comput. Appl. Math.* 352 (2019) 79–92.
- [115] M. Syed Ali, J. Yogambigai, S. Saravanan, S. Elakkia, Stochastic stability of neutral-type Markovian-jumping BAM neural networks with time varying delays, *J. Comput. Appl. Math.* 349 (2019) 142–156, 10 2019.
- [116] M. Syed Ali, J. Yogambigai, Extended dissipative synchronization of complex dynamical networks with additive time-varying delay and discrete-time information, *J. Comput. Appl. Math.* 348 (2019) 328–341.
- [117] J.J. Chen, Z.G. Zeng, P. Jiang, Global Mittag-Leffler stability and synchronization of memristor-based fractional-order neural networks, *Neural Netw.* 51 (2013) 1–8.
- [118] E. Kaslik, S. Sivasundaram, Nonlinear dynamics and chaos in fractional order neural networks, *Neural Netw.* 32 (2012) 245–256.
- [119] I. Stamova, Global Mittag-Leffler stability and synchronization of impulsive fractional-order neural networks with time-varying delays, *Nonlinear Dynam.* 77 (2014) 1251–1260.

- [120] H.Q. Li, X.F. Liao, M.W. Luo, A novel non-equilibrium fractional-order chaotic system and its complete synchronization by circuit implementation, *Nonlinear Dynam.* 68 (2012) 137–149.
- [121] C. Yin, Y. Cheng, Y.Q. Chen, B. Stark, S.M. Zhong, Adaptive fractional-order switching-type control method design for 3D fractional order nonlinear systems, *Nonlinear Dynam.* 82 (2015) 39–52.
- [122] C. Yin, S.M. Zhong, W. Chen, Design of sliding mode controller for a class of fractional-order chaotic systems, *Commun. Nonlinear Sci. Numer. Simul.* 17 (2012) 356–366.
- [123] B.S. Chen, J.J. Chen, Global asymptotical ω -periodicity of a fractional-order non-autonomous neural networks, *Neural Netw.* 68 (2015) 78–88.
- [124] L.P. Chen, Y. Chai, R.C. Wu, T.D. Ma, H.Z. Zhai, Dynamic analysis of a class of fractional-order neural networks with delay, *Neurocomputing* 111 (2013) 190–194.
- [125] Z. Quanxin, S. Shiyun, T. Tianren, Mean square exponential stability of stochastic nonlinear delay systems of, *Internat. J. Control* 90 (2017) 2384–2393.
- [126] SM. Lee, OM. Kwon, SH. Lee, Improved stability criteria for sampled-data systems using modified free weighting matrix, *J. Frankl. Inst.* 356 (2019) 2198–2211.
- [127] Rakesh Kumar, Subir Das, Yang Cao, Effects of infinite occurrence of hybrid impulses with quasi-synchronization of parameter mismatched neural networks, *Neural Netw.* 122 (2020) 106–116.
- [128] Yang Cao, Liangyin Zhang, Chanying Li, Michael Z.Q. Chen, Observer-based consensus tracking of nonlinear agents in hybrid varying directed topology, *IEEE Trans. Cybern.* 47 (8) (2017) 2212–2222.
- [129] Yang Cao, R. Sriraman, R. Samidurai, Stability and stabilization analysis of nonlinear time-delay systems with randomly occurring controller gain fluctuation, *Math. Comput. Simulation* 171 (2020) 36–51.
- [130] Z.-S. Lv, C.-P. Zhu, P. Nie, J. Zhao, H.-J. Yang, Y.-J. Wang, C.-K. Hu, Exponential distance distribution of connected neurons in simulations of two-dimensional in vitro neural network development, *Front. Phys.* 12 (2017) 128902.
- [131] H.-L. Zeng, C.-P. Zhu, S.-X. Wang, Y.-D. Guo, Z.-M. Gu, C.-K. Hu, Scaling behaviors and self-organized criticality of two-dimensional small-world neural networks, *Physica A* 540 (2020) 123191.

- [132] M. Syed Ali, S. Saravanan, L. Palanisamy, Stochastic finite-time stability of reaction–diffusion cohen-grossberg neural networks with time-varying delays, *Chinese J. Phys.* 57 (2019) 314–328.
- [133] R. Vadivel, M. Syed Ali, F. Alzahrani, Robust H-infinity synchronization of Markovjump stochastic uncertain neural networks with decentralized event-triggered mechanism, *Chinese J. Phys.* 60 (2019) 68–87.
- [134] P. Balasubramaniam, M. Syed Ali, Robust stability of uncertain fuzzy cellular neural networks with time-varying delays and reaction diffusion terms, *Neurocomputing* 74 (2010) 439–446.
- [135] X. Li, S. Song, Impulsive control for existence, uniqueness and global stability of periodic solutions of recurrent neural networks with discrete and continuously distributed delays, *IEEE Trans. Neural Netw. Learn. Syst.* 24 (2013) 868–877.
- [136] Y. Du, S. Zhong, N. Zhou, K. Shi, J. Cheng, Exponential stability for stochastic cohen-grossberg BAM neural networks with discrete and distributed time-varying delays, *Neurocomputing* 127 (2014) 144–151.
- [137] M. Syed Ali, N. Gunasekaran, ME. Rani, Robust stability of hopfield delayed neural networks via an augmented LK functional, *Neurocomputing* 234 (2017) 198–204.
- [138] S. Liu, XY. Li, W. Jiang, XF. Zhou, Mittag–Leffler Stability of nonlinear fractional neutral singular systems, *Commun. Nonlinear Sci. Numer. Simul.* 17 (2012) 3961–3966.
- [139] Y. Li, Y.Q. Chen, I. Podlubny, Stability of fractional-order nonlinear dynamic systems: Lyapunov direct method and generalized Mittag-Leffler stability, *Comput. Math. Appl.* 24 (2010) 1429–1468.
- [140] L.O. Chua, L. Yang, Cellular neural networks: Theory, *IEEE Trans. Circuits Syst.* 35 (1988) 1257–1272.
- [141] T. Roska, L.o. Chua, Cellular neural networks with nonlinear and delay-type template elements and nonuniform grids, *Int. J. Circuit Theory Appl.* 20 (1992) 469–481.
- [142] H. Harrer, J.A. Nossek, Discrete-time cellular neural networks, *Int. J. Circuit Theory Appl.* 20 (1992) 453–467.
- [143] T. Yang, LB. Yang, CW. Wu, LO. Chua, Fuzzy cellular neural networks: theory, *Int. J. Circuit Theory Appl.* (1996) 181–186.
- [144] T. Yang, LB. Yang, CW. Wu, LO. Chua, Fuzzy cellular neural networks: applications, in: *Fourth IEEE International Workshop on Cellular Neural Networks and their Applications Proceedings*, 1996, pp. 225–230.

- [145] Z.D. Huang, Almost periodic solutions for fuzzy cellular neural networks with multi-proportional delays, *Int. J. Mach. Learn. Cybern.* 78 (2016) 1323–1331.
- [146] S.T. Wang, M. Wang, A new detection algorithm based on fuzzy cellular neural networks for white blood cell detection, *IEEE Trans. Inf. Technol. Biomed.* 10 (2006) 5–10.
- [147] W.Y. Ma, C.P. Li, Y.J. Wu, Impulsive synchronization of fractional Takagi–Sugeno fuzzy complex networks, *Chaos* 26 (2016) 084311.
- [148] H. Shen, F. Li, H. Yan, H.R. Karimi, H.K. Lam, Finite-time event-triggered H_∞ control for T-S fuzzy Markov jump systems, *IEEE Trans. Fuzzy Syst.* 26(2018) 3122–3135.
- [149] H. Shen, F. Li, Z. Wu, J.H. Park, Victor. Sreeram, Victor sreeram fuzzy-model-based non-fragile control for nonlinear singularly perturbed systems with semi-Markov jump parameters, *IEEE Trans. Fuzzy Syst.* 26 (2018) 3428–3439.
- [150] M.S. Branicky, *Introduction to Hybrid Systems*, Springer, 2005, pp. 91–116.
- [151] R. Alur, T. Henzinger, E. Sontag, *Hybrid Systems III*, Vol. 1066, Springer, 1996.
- [152] P.J. Antsaklis, W. Kohn, A. Nerode, S. Sastry, *Hybrid Systems V*, Vol. 1273, Springer, 1997.
- [153] C.J. Tomlin, R. Greenstreet, *Hybrid Systems: Computation and Control*, Vol. 2289, Springer, 2002.
- [154] A.S. Morse, *Control Using Logic-Based Switching*, Springer, 1997, pp. 1–276.
- [155] P.J. Antsaklis, Special issue on hybrid systems: Theory and applications - A brief introduction to the theory and applications of hybrid systems, *Proc. IEEE* 88 (2000) 879–887.
- [156] Y. Wardi, M. Egerstedt, B. Lennartson, P. Tabuada, *Hybrid systems*, *Nonlinear Anal.* (2019).
- [157] M. Syed Ali, J. Yogambigai, Synchronization of complex dynamical networks with hybrid coupling delays on time scales by handling multitude Kronecker product terms, *Appl. Math. Comput.* 291 (2016) 244–258.
- [158] A. Feuer, G.C. Goodwin, M. Salgado, Potential benefits of hybrid control for linear time invariant plants, in: *Proceedings of the 1997 American Control Conference*, Vol. 5 (1997) pp. 2790–2794.
- [159] N.H. McClamroch, C. Rui, I. Kolmanovsky, M. Reyhanoglu, Hybrid closed loop systems: A nonlinear control perspective, in: *Proceedings of the 36th IEEE Conference on Decision and Control*, Vol. 1 (1997) pp. 114–119.

- [160] A.J. van der Schaft, J.M. Schumacher, An introduction to hybrid dynamical systems, Springer 251 (1999) 1–174.
- [161] J. Lygeros, D. Godbole, S. Sastry, Verified hybrid controllers for automated vehicles, *IEEE Trans. Automat. Control* 43 (1998) 522–539.
- [162] E. Frazzoli, Robust hybrid control for autonomous vehicle motion planning, in: *Proceedings of the IEEE Conference on Decision and Control*, Vol. 1 (2000) pp. 821–826.
- [163] E. Frazzoli, M.A. Dahleh, E. Feron, A maneuver-based hybrid control architecture for autonomous vehicle motion planning, *Inf. Technol. Dyn. Syst.* (2005) 299–323.
- [164] A. Balluchi, P. Soueres, A. Bicchi, Hybrid feedback control for pathtracking with a bounded-curvature vehicle, in: *Proceedings of the Fourth International Workshop on Hybrid Systems*, (2001) pp. 133–146.
- [165] K. Diethelm, N.J. Ford, Analysis of fractional differential equations, *J. Math. Anal. Appl.* 265 (2002) 229–248.
- [166] C. Li, F. Zhang, A survey on the stability of fractional differential equations, *Eur. Phys. J. Spec. Top.* 193 (2011) 27–47.
- [167] M.A. Duatte-Mermoud, N. Aguila-Camacho, J.A. Gallegos, R. Castro-Limares, Using general quadratic Lyapunov functions to prove Lyapunov uniform stability for fractional order systems, *Commun. Nonlinear Sci. Numer. Simul.* 22 (2015) 650–659.
- [168] S.H. Maboobi, M. Shahrokhi, H.N. Pishkenari, Observer-based control design for three well-known chaotic systems, *Chaos Solitons Fractals* 29 (2006) 381–392.
- [169] A. Wu, Z. Zeng, Global Mittag-Leffler stabilization of fractional-order memristive neural networks, *IEEE Trans. Neural Netw. Learn. Syst.* 28 (2015) 1–12.
- [170] J. Chen, Z. Zeng, P. Jiang, Global Mittag-Leffler stability and synchronization of memristor-based fractional-order neural networks, *Neural Netw.: Off. J.Int. Neural Netw. Soc.* 51 (2013) 1–8.
- [171] J. Kuang, *Applied Inequalities*, Shandong Science and Technology Press, 2004.
- [172] S. Long Q. Song, X. Wang D. Li, Stability analysis of fuzzy cellular neural networks with time delay in the leakage term and impulsive perturbations, *J. Franklin Inst. B* 349 (7) (2012) 2461–2479.
- [173] L. Duan, H. Wei, L. Huang, Finite-time synchronization of delayed fuzzy cellular neural networks with discontinuous activations, *Fuzzy Sets Syst.* 361 (2019) 56–70.

- [174] P. Mani, R. Rakkiyappan, S. Lakshmanan, Y.H. Joo, Adaptive control for fractional order induced chaotic fuzzy cellular neural networks and its application to image encryption, *Inform. Sci.* 491 (2019) 74–89.
- [175] J. Chen, C. Li, X. Yang, Asymptotic stability of delayed fractional-order fuzzy neural networks with impulse effects, *J. Franklin Inst. B* 355 (15) (2018) 7595–7608.
- [176] S. Zhang, Y. Yu, H. Wang, Mittag-Leffler Stability of fractional-order hopfield neural networks, *Nonlinear Anal. Hybrid Syst.* 16 (2015) 104–121.
- [177] W. Ma, C. Li, Y. Wu, Y. Wu, Synchronization of fractional fuzzy cellular neural networks with interactions, *Chaos* 27 (2017) 103106.
- [178] Shahri ESA, Balochian S (2015) Analysis of fractional-order linear systems with saturation using Lyapunov's second method and convex optimization. *Int J Autom Comput* 12(4):440–447.
- [179] Arena P, Caponetto R, Fortuna L, Porto D (1998) Bifurcation and chaos in non-integer order cellular neural networks. *Int J Bifurc Chaos* 8:1527–1539.
- [180] Syed AliM, Palanisamy L, Yogambigai J, Wang L (2019) Passivity-based synchronization of Markovian jump complex dynamical networks with time-varying delays, parameter uncertainties, reaction–diffusion terms, and sampled-data control. *J Comput Appl Math* 352:79–92.
- [181] Syed AliM, Yogambigai J, Saravanan S, Elakkia S (2019) Stochastic stability of neutral-type Markovian jumping BAM neural networks with time varying delays. *J Comput Appl Math* 349:142–156.
- [182] Syed Ali M, Yogambigai J (2019) Extended dissipative synchronization of complex dynamical networks with additive time-varying delay and discrete-time information. *J Comput Appl Math* 348:328–341.
- [183] Stamova I (2014) Global Mittag-Leffler stability and synchronization of impulsive fractional-order neural networks with time-varying delays. *Nonlinear Dyn* 77:1251–1260.
- [184] Li HQ, Liao XF, Luo MW (2012) A novel non-equilibrium fractional-order chaotic system and its complete synchronization by circuit implementation. *Nonlinear Dyn* 68:137–149.
- [185] Chen LP, Chai Y, Wu RC, Ma TD, Zhai HZ (2013) Dynamic analysis of a class of fractional-order neural networks with delay. *Neurocomputing* 111:190–194.
- [186] Quanxin Z, Shiyun S, Tianren T (2017) Mean square exponential stability of stochastic nonlinear delay systems of. *Int J Control* 90:2384–2393.

- [187] Li X, Yang X, Huang T (2019) Persistence of delayed cooperative models, Impulsive control method. *Appl Math Comput* 342:130–146.
- [188] Li X, Shen J, Rakkiyappan R (2018) Persistent impulsive effects on stability of functional differential equations with finite or infinite delay. *Appl Math Comput* 329:14–22.
- [189] Syed Ali M, Narayanana G, Sevgen S, Shekher V, Arik S (2019) Global stability analysis of fractional order fuzzy BAMneural networks with time delay and impulsive effects. *Commun Nonlinear Sci Numer Simul* 78, Article ID 104853.
- [190] Yucel E, Syed Ali M, Gunasekaran N, Arik S (2017) Sampled-data filtering of Takagi-Sugeno fuzzy neural networks with interval time-varying delays. *Fuzzy Sets Syst* 316:69–81.
- [191] Ozcan N, Syed AliM, Yogambigai J, Zhu Q, Arik S (2018) Robust synchronization of uncertain Markovian jump complex dynamical networks with time-varying delays and reaction–diffusion terms via sampled data control. *J Franklin Inst* 355(3):1192–1216.
- [192] Song C, Fei S, Cao J, Huang C (2019) Robust synchronization of fractional-order uncertain chaotic systems based on output feedback sliding mode control. *Mathematics* 7(7):599.
- [193] Yang X, Wen S, Liu Z, Li C, Huang C (2019) Dynamic properties of foreign exchange complex network. *Mathematics* 7:832.
- [194] Wang F, Yao Z (2016) Approximate controllability of fractional neutral differential systems with bounded delay. *Fixed Point Theory* 17:495–507.
- [195] Rajchakit G, Pratap A, Raja R, Cao J, Alzabut J, Huang C (2019) Hybrid control scheme for projective lag synchronization of Riemann-Liouville sense fractional order memristive BAM neural networks with mixed delays. *Mathematics* 7(8):759.
- [196] Yang X, Wen S, Liu Z, Li C, Huang C (2019) Dynamic properties of foreign exchange complex network. *Mathematics* 7:832.
- [197] Huang C, Wen S, Huang L (2019) Dynamics of anti-periodic solutions on shunting inhibitory cellular neural networks with multi-proportional delays. *Neurocomputing* 357:4752.
- [198] Zhang J, Huang C (2020) Dynamics analysis on a class of delayed neural networks involving inertial terms. *Adv Differ Equ* 120.
- [199] Qian C, Hu Y (2020) Novel stability criteria on nonlinear density-dependent mortality Nicholson’s blowflies systems in asymptotically almost periodic environments. *J Inequal Appl* Article number: 13.

- [200] Zhang J, Huang C (2020) Dynamics analysis on a class of delayed neural networks involving inertial terms. *Adv Differ Equ* Article number: 120.
- [201] ShiM, Guo J, Fang X, Huang C (2020) Global exponential stability of delayed inertial competitive neural networks. *Adv Differ Equ* Article number: 87.
- [202] Cao Q, Wang G, Qian C (2020) New results on global exponential stability for a periodic Nicholson's blowflies model involving time-varying delays. *Adv Differ Equ* Article number:43.
- [203] HuangC, SuR,HuY(2020) Global convergence dynamics of almost periodic delay Nicholson's blowflies systems. *J Biol Dyn* 14:633–655.
- [204] HuangC, SuR,HuY(2020) Global convergence dynamics of almost periodic delay Nicholson's blowflies systems. *J Biol Dyn* 14:633–655.
- [205] Wang J, Chen X, Huang L (2019) The number and stability of limit cycles for planar piecewise linear systems of node-saddle type. *J Math Anal Appl* 469(1):405–427.
- [206] Wang J, Huang C, Huang L (2019) Discontinuity-induced limit cycles in a general planar piecewise linear system of saddle-focus type. *Nonlinear Anal Hybrid Syst* 33:162–178.
- [207] WangW(2018) Finite-time synchronization for a class of fuzzy cellular neural networks with time-varying coefficients and proportional delays. *Fuzzy Sets Syst* 338:40–49.
- [208] Huang C, Zhang H (2019) Periodicity of non-autonomous inertial neural networks involving proportional delays and non-reduced order method. *Int J Biomath* 12(2):1950016.
- [209] Yang H (2021) Weighted pseudo almost periodicity on neutral type CNNs involving multi-proportional delays and D operator. *AIMS Math* 6:1865–1879.
- [210] Huang C, Yang L, Cao J (2020) Asymptotic behavior for a class of population dynamics. *AIMS Math* 5:3378–3390.
- [211] Huang C, Long X, Huang L, Fu S (2020) Stability of almost periodic Nicholson's blowflies model involving patch structure and mortality terms. *Can Math Bull* 63(2):405–422.
- [212] Huang C,Wang J, Huang L (2020) Asymptotically almost periodicity of delayed Nicholson-type system involving patch structure. *Electron J Differ Equ* 61:1–17.
- [213] Hu H, Yi T, Zou X (2020) On spatial-temporal dynamics of a Fisher-KPP equation with a shifting environment. *Proc. Am. Math. Soc.* 148:213–221.

- [214] Hu HJ, Yuan XP, Huang LH, Huang CX (2019) Global dynamics of an SIRS model with demographics and transfer from infectious to susceptible on heterogeneous networks. *Math. Biosci. Eng.* 16(5):5729–5749.
- [215] Hu H, Zou X (2017) Existence of an extinction wave in the Fisher equation with a shifting habitat. *Proc Am. Math. Soc.* 145:4763–4771.
- [216] Lee SM, Kwon OM, Lee SH (2019) Improved stability criteria for sampled-data systems using modified free weighting matrix. *J Franklin Inst* 356:2198–2211.
- [217] Balasubramaniam P, Syed Ali M (2010) Robust stability of uncertain fuzzy cellular neural networks with time-varying delays and reaction diffusion terms. *Neurocomputing* 74:439–446.
- [218] Li X, Song S (2013) Impulsive control for existence, uniqueness and global stability of periodic solutions of recurrent neural networks with discrete and continuously distributed delays. *IEEE Trans Neural Netw Learn Syst* 24:868–877.
- [219] Du Y, Zhong S, Zhou N, Shi K, Cheng J (2014) Exponential stability for stochastic Cohen-Grossberg BAM neural networks with discrete and distributed time-varying delays. *Neurocomputing* 127:144–151.
- [220] Syed Ali M, Gunasekaran N, Rani ME (2017) Robust stability of hopfield delayed neural networks via an augmented LK functional. *Neurocomputing* 234:198–204.
- [221] Liu S, Li XY, Jiang W, Zhou XF (2012) Mittag-Leffler stability of nonlinear fractional neutral singular systems. *Commun Nonlinear Sci Numer Simul* 17:3961–3966.
- [222] Li Y, Chen YQ, Podlubny I (2010) Stability of fractional-order nonlinear dynamic systems: Lyapunov direct method and generalized Mittag-Leffler stability. *Comput Math Appl* 24:1429–1468.
- [223] Chua LO, Yang L (1988) Cellular neural networks: theory. *IEEE Trans Circuits Syst* 35:1257–1272.
- [224] Roska T, Chua LO (1992) Cellular neural networks with nonlinear and delay-type template elements and nonuniform grids. *Int J Circuit Theory Appl* 20:469–481.
- [225] Harrer H, Nossek JA (1992) Discrete-time cellular neural networks. *Int J Circuit Theory Appl* 20:453–467.
- [226] Yang T, Yang LB, Wu CW, Chua LO (1996) Fuzzy cellular neural networks: theory. *Int J Circuit Theory Appl* 181–186.

- [227] Yang T, Yang LB, Wu CW, Chua LO (1996) Fuzzy cellular neural networks: applications. In: Proceedings of fourth IEEE international workshop on cellular neural networks and their applications, pp 225–230.
- [228] Huang ZD (2016) Almost periodic solutions for fuzzy cellular neural networks with multi-proportional delays. *Int J Mach Learn Cybern* 78:1323–1331.
- [229] Wang ST, Wang M (2006) A new detection algorithm based on fuzzy cellular neural networks for white blood cell detection. *IEEE Trans Inf Technol Biomed* 10:5–10.
- [230] Ma WY, Li CP, Wu YJ (2016) Impulsive synchronization of fractional Takagi-Sugeno fuzzy complex networks. *Chaos* 26:084311.
- [231] Antsaklis PJ (2000) Special issue on hybrid systems: theory and applications—a brief introduction to the theory and applications of hybrid systems. *Proc IEEE* 88:879–887.
- [232] Li X, Shen J, Akca H, Rakkiyappan R (2015) LMI-based stability for singularly perturbed nonlinear impulsive differential systems with delays of small parameter. *Appl Math Comput* 250:798–804.
- [233] Li X, O'Regan D, Akca H (2015) Global exponential stabilization of impulsive neural networks with unbounded continuously distributed delays. *IMA J Appl Math* 80(1):85–99.
- [233] Li X, Caraballo T, Rakkiyappan R, Han X (2015) On the stability of impulsive functional differential equations with infinite delays. *Math Methods Appl Sci* 38(14):3130–3140.
- [234] Syed Ali M, Yogambigai J (2016) Synchronization of complex dynamical networks with hybrid coupling delays on time scales by handling multitude Kronecker product terms. *Appl Math Comput* 291:244–258.
- [235] Feuer A, Goodwin GC, Salgado M (1997) Potential benefits of hybrid control for linear time invariant plants. In: Proceedings of the 1997 American control conference, vol 5, pp 2790–2794.
- [236] McClamroch NH, Rui C, Kolmanovsky I, Reyhanoglu M (1997) Hybrid closed loop systems: a nonlinear control perspective. In: Proceedings of the 36th IEEE conference on decision and control, vol 1, pp 114–119.
- [237] van der Schaft AJ, Schumacher JM (1999) An introduction to hybrid dynamical systems. *Springer* 251:1–174.
- [238] Lygeros J, Godbole D, Sastry S (1998) Verified hybrid controllers for automated vehicles. *IEEE Trans Autom Control* 43:522–539.

- [239] Frazzoli E (2000) Robust hybrid control for autonomous vehicle motion planning. Proc IEEE Conf Decis Control 1:821–826.
- [240] Frazzoli E, Dahleh MA, Feron E (2005) A maneuver-based hybrid control architecture for autonomous vehicle motion planning. In: Information technology for dynamical systems, pp 299–323.
- [241] Balluchi A, Soueres P, Bicchi A (2001) Hybrid feedback control for path tracking with a bounded-curvature vehicle. In: Proceedings of the fourth international workshop on hybrid systems, pp 133–146.
- [242] Diethelm K, Ford NJ (2002) Analysis of fractional differential equations. J Math Anal Appl 265:229–248.
- [243] Li C, Zhang F (2011) A survey on the stability of fractional differential equations. Eur Phys J Special Top 193:27–47.
- [244] Duatte-Mermoud MA, Aguila-Camacho N, Gallegos JA, Castro-Limares R (2015) Using general quadratic Lyapunov functions to prove Lyapunov uniform stability for fractional order systems. Commun Nonlinear Sci Numer Simul 22:650–659.
- [245] Maboobi SH, Shahrokhi M, Pishkenari HN (2006) Observer-based control design for three well-known chaotic systems. Chaos Solitons Fractals 29:381–392.
- [246] Wu A, Zeng Z (2015) Global Mittag-Leffler stabilization of fractional-order memristive neural networks. IEEE Trans Neural Netw Learn Syst 28:1–12.
- [247] Chen J, Zeng Z, Jiang P (2013) Global Mittag-Leffler stability and synchronization of memristor-based fractional-order neural networks. Neural Netw Off J Int Neural Netw Soc 51:1–8.
- [248] Kuang J (2004) Applied inequalities. Science and Technology Press, Shandong 77.
Chen J, Zeng Z, Jiang P (2014) Global Mittag-Leffler stability and synchronization of memristor-based fractional-order neural networks. Neural Netw 51:1–8.
- [249] Stamoiva I, Stamoiv G (2017) Mittag-Leffler synchronization of fractional neural networks with timevarying delays and reaction–diffusion terms using impulsive and linear controllers. Neural Netw 96:22–32.
- [250] Long S, Song Q, Wang X, Li D (2012) Stability analysis of fuzzy cellular neural networks with time delay in the leakage term and impulsive perturbations. J Franklin Inst 349(7):2461–2479.
- [251] Duan L, Wei H, Huang L (2019) Finite-time synchronization of delayed fuzzy cellular neural networks with discontinuous activations. Fuzzy Sets Syst 361:56–70.

- [252] Mani P, Rakkiyappan R, Lakshmanan S, Joo YH (2019) Adaptive control for fractional order induced chaotic fuzzy cellular neural networks and its application to image encryption. *Inf Sci* 491:74–89.
- [253] Chen J, Li C, Yang X (2018) Asymptotic stability of delayed fractional-order fuzzy neural networks with impulse effects. *J Franklin Inst* 355(15):7595–7608.
- [254] Zhang S, Yu Y, Wang H (2015) Mittag-Leffler stability of fractional-order Hopfield neural networks. *Nonlinear Anal Hybrid Syst* 16:104–121.
- [255] Ma W, Li C, Wu Y, Wu Y (2017) Synchronization of fractional fuzzy cellular neural networks with interactions. *Chaos* 27:103106.
- [256] Li H, Hu C, Jiang Y, Wang Z, Dong Z (2016) Pinning adaptive and impulsive synchronization of fractional order complex dynamical networks. *Chaos Solitons Fract* 92:142–149.
- [257] Wang L, Song Q, Liu Y, Zhao Z, Alsaadi F (2017) Finite-time stability analysis of fractional-order complex-valued memristor-based neural networks with both leakage and time-varying delays. *Neurocomputing* 245:86–101.
- [258] Xiao J, Zhong S, Li Y, Xu F (2017) Finite-time Mittag-Leffler synchronization of fractional-order memristive BAM neural networks with time delays. *Neurocomputing* 219:431–439.
- [259] Velmurugan G, Rakkiyappan R, Cao J (2016) Finite-time synchronization of fractional order memristor based neural networks with time delays. *Neural Netw* 73:36–46.
- [260] Ding Z, Zeng Z, Wang L (2018) Robust finite-time stabilization of fractional-order neural networks with discontinuous and continuous activation functions under uncertainty. *IEEE Trans Neural Netw Learn Syst* 29:1477–1490.

List of Publication

1. **Singh A**, Rai JN. Stability analysis of fractional order fuzzy cellular neural networks with leakage delay and time varying delays. *Chinese Journal of Physics*. 2021 Oct 1; 73:589-99. (ELSEVIER), Indexing: SCI, Impact Factor=3.957.
<https://doi.org/10.1016/j.cjph.2021.07.029>.
2. **Singh A**, Rai JN. Stability of fractional order fuzzy cellular neural networks with distributed delays via hybrid feedback controllers. *Neural Processing Letters*. 2021 Apr; 53(2):1469-99. (SPRINGER), Indexing: SCI, Impact Factor= 2.565.
<https://doi.org/10.1007/s11063-021-10460-7>.
3. A. Choudhary, V. Kumar, V. Aggarwal, J. N. Rai and **A. Singh**, "Adaptive Partial PID Controller For Speed Control of Induction Motor," 2021 2nd International Conference for Emerging Technology (INCET), Belagavi, India, 2021, pp. 1-6, [doi: 10.1109/INCET51464.2021.9456169](https://doi.org/10.1109/INCET51464.2021.9456169).
4. Rai JN, **Singh A**. Robust Fractional Order PID Controller for Speed Control of DC Motor using FOMCON Toolbox for MATLAB. *International Electrical and Electronics Engineering Conference (IEEEEC-2021)*.
5. V. Shekher, **A. Singh** and J. N. Rai, "Design and Experimental analysis of Integer Order PID Controller for Ceramic IR heating system," 2018 2nd IEEE International Conference on Power Electronics, Intelligent Control and Energy Systems (ICPEICES), Delhi, India, 2018, pp. 993-999, [doi: 10.1109/ICPEICES.2018.8897417](https://doi.org/10.1109/ICPEICES.2018.8897417).
6. Rai JN, **Singh A**. Comparative study of PID and Fuzzy logic controller for steam Temperature control in Thermal power Plant. *1st International conference on New Frontiers in engineering Science and Technology 2018*.

BIODATA

Name: AJENDRA SINGH

Father's Name: Dr. Ramswaroop Singh

Mother's Name: Smt. Malti Devi

Address: 20D, Jhang CGHS Rohini, Sector -13 Delhi-110085

Email ID: ajendrasingh25@gmail.com

Education: Ph.D. (Electrical Engineering 2016): Pursing from August 2016 Contd., with course work 80.33%.

M.Tech (Control System 2006-2009): Passed from Delhi College of Engineering, University of Delhi with 73.70% Marks.

B.Tech (Electrical Engineering 1999-2003): Passed from Delhi College of Engineering, University of Delhi with 71.03% Marks.

Diploma in Electrical Engineering with honors 1985-1988: Passed from Aligarh Muslim University Aligarh with 78.26% distinction (Hons.)

Experience:

- (i) (1989-1997) 8½ years Industrial experience to manage a process control plant in General Engineering Works Faridabad, Haryana.
- (ii) (2004-2006, 2011-2013) 5-year teaching experience in Delhi College of Engineering/ Delhi Technological University.
- (iii) (1997- continued) 13½ years' experience as a Foreman, Group B, class II post in Electrical Engineering Department, Delhi Technological University, Delhi.

Technical Training

- Participated in National conference at Maharaja Agrasen Institute of Technology NC-ECC Feb 2-4, 2006.
- Attended program on **motivation and orientation for faculty members** of engineering Institution August 22nd-23rd 2008 at Delhi College of Engineering.
- Attended program on **knowledge power in the world of learning** in Delhi College of Engineering August 25-26, 2008.
- Attended and presented a paper in NEEC-2011 in Delhi Technological University 16-17, 2011.
- Attended two weeks AICTE sponsored **staff development program on Recent Advance in Electrical power & Energy Systems 9-22, Dec-2011.**
- Attended –AICTE sponsored staff development program on **Flexible AC transmission systems and power system voltage stability recent advances, July 11-22, 2011** in Delhi Technological University (Formerly DCE).

- Attended **one week Quality improvement program on Applications on solar Energy and Photovoltaics in IIT, Delhi 12-DEC. 12-18,2012**, AICTE Govt. of India.
- Attended and presented a paper in 2012 IEEE. Fifth India International conference on power Electronics (**IICPE 6th -8th Dec.-2012**)
- Attended **one-week UGC sponsored short term training program** in Electrical Engineering Department, Delhi Technological University, Delhi-42 9th-13th Dec. 2013.
- Participated program on **new knowledge Age future perspectives** and Action plan 5-6 ,2013 sponsored by ISTE, Delhi section.
- Attended one-week TEQIP- II sponsored Faculty Development Program on Renewable Energy and Alternative Fuels (REAF-2014) **from June 16-20,2014** Organized Delhi Technological University.
- Attended two weeks UGC sponsored short term training program on Integrating Renewable Energy sources into Emerging Electrical Power System organized by Department of Electrical Engineering, Delhi Technological University, Delhi. During **8th-19th Dec.-2014**.
- Attended one-week TEQIP- II Faculty Development Program on “Recent Trends in Switchgear and Protection” during July 21-25 2014.
- Participated in the National workshop on Power Electronics (NWPE-2015) organized by Department of Electrical Engineering, Delhi Technological University, Delhi. During **6th-7th November 2015**.
- Participated in MHRD sponsored one week GIAN course on challenges and opportunities in Renewable Energy. Role of the smart grid organized by Department of Electrical Engineering, Delhi Technological University, Delhi. During **June 3-8,2016**.
- Participated in TEQIP- II sponsored one-week short term Program on **PLC, HMI SCADA and AC drives**, organized by Electrical Engineering Department of Delhi Technological University, Delhi. During **June 13-17, 2016**.
- Participated in MHRD sponsored GIAN course on **Photovoltaic Array to utility interface power converters** organized by Department of Electrical Engineering, Delhi Technological University, Delhi. During **August 22-27, 2016**.
- Participated in MHRD sponsored one week GIAN course on **smart power Flow controller for smart Grid Applications** organized by department of Electrical Engineering, Delhi Technological University, Delhi. During **DECEMBER. 18th-23rd, 2017 A Grad**.
- Attended Skill Development Program on Focus on **Power Sector in India and Energy Management Strategies from 20.01.2017 to 22.01.2017** in Electrical Engineering department Delhi Technological University, Delhi.
- Attended one-day **personality development workshop** organized by Delhi Technological University held on **JAN.12 2017**.
- Participated in one-week sponsored GIAN Course on **Recent Trends in power system Reliability Evaluation models, statistical Methods and Applications** organized by department of Electrical Engineering, Delhi Technological University, Delhi. During **October 9th -13th , 2017 ‘A’ Grad**.

- Participated in MHRD sponsored one week GIAN course on **Emerging Cutting –Edge Technologies in Advanced Electrical Machines and drives. Design and performance issues, Fault Diagnosis, Failure, Prognosis and Milligan**, organized by department of Electrical Engineering, Delhi Technological University, Delhi. During **November 6th -10th, 2017**.
- Participated as organizer and presented a paper in the 2018, IInd IEEE, International Conference on **power Electronics, Intelligent control and Energy system (ICPEICES-2018) held during 22-24 October 2018**, organized by department of Electrical Engineering, Delhi Technological University, Delhi.
- Successfully Completed, one day joint workshop on **Patent Filing procedure**. Conducted by Rajiv Gandhi National Institute of Intellectual Property Management (RGNIPM) Nagpur and Delhi Technological University, Delhi on 28 may 2018.
- Participated in the **short term training Program on Electric Transportation from 20-24th Aug.2018** organized by department of Electrical Engineering, Delhi Technological University, Delhi.
- Participated one week MHRD sponsored GIAN Course on **Recent Trends in protection of Micro grid with high DER penetration Issues, Challenges and mitigation 12-16,2018 ‘A’ Grad**.
- Participated **one week faculty Development Program** under TEQIP II on Recent Advance and challenges in power & energy for sustainable growth held during **June 1-5, 2015**.
- Attended one day work shop on **sensitization of University Administration Gender, Disabilities and social inclusion** on July 2019 organized by Delhi Technological University, Delhi.
- Participated five days Faculty Development Program on **Emerging technological on Electrical and Allied Engineering (ETEAE-2022)** organized by department of Electrical Engineering BIT Sindhri, Dhandad from 27.01.22 to 31.01.2022.
- Participated **five days faculty Development program** on recent advancement in Electrical and Allied Engineering (RAEAE-2021) by collaboration with TEQIP- III from **12th July-16th July 2021** in BIT, Sindhri, Dhanbad.

Achievement

Awarded (**for two Research paper**) February 2022, by Delhi Technological University, Delhi.